INVESTIGATIONS ON MULTI-PORT ANTENNA SYSTEMS FOR BETTER SPECTRUM UTILIZATION EFFICIENCY IN COGNITIVE RADIO APPLICATIONS

Submitted in partial fulfilment of the requirements

for the award of the degree of

Doctor of Philosophy

by

D Srikar

(Roll No. 717025)

Supervisor

Dr. S. Anuradha

Associate Professor, Dept. of ECE

Department of Electronics & Communication Engineering
NATIONAL INSTITUTE OF TECHNOLOGY WARANGAL – 506004, T.S, INDIA
July-2021

APPROVAL SHEET

This thesis entitled "**Investigations on Multi-Port Antenna Systems for Better Spectrum Utilization Efficiency in Cognitive Radio Applications**" by Mr. **D Srikar** is approved for the degree of **Doctor of Philosophy**.

Examiners

_____

_____

Supervisor

_____

Dr. S. Anuradha

Associate Professor, Electronics and Communication Engineering Department,

NIT WARANGAL

Chairman

_____

Prof. L. Anjaneyulu

Head, Electronics and Communication Engineering Department,

NIT WARANGAL

Date:

Place:

DECLARATION

This is to certify that the work presented in the thesis entitled "**Investigations on Multi-Port Antenna Systems for Better Spectrum Utilization Efficiency in Cognitive Radio Applications**" is a bonafide work done by me under the supervision of **Dr. S. Anuradha**, Department of Electronics and Communication Engineering, National Institute of Technology Warangal, and was not submitted elsewhere for the award of any degree.

I declare that this written submission represents my ideas in my own words and where others' ideas or words have been included, I have adequately cited and referenced the original sources. I also declare that I have adhered to all principles of academic honesty and integrity and have not misrepresented or fabricated or falsified any idea/date/fact/source in my submission. I understand that any violation of the above will be cause for disciplinary action by the institute and can also evoke penal action from the sources which have thus not been properly cited or from whom proper permission has not been taken when needed.

D Srikar

Roll No: 717025

Date:

Place: Warangal

Department of Electronics and Communication Engineering
National Institute of Technology
Warangal – 506 004, Telangana, India

CERTIFICATE

This is to certify that the dissertation work entitled **"Investigations on Multi-Port Antenna Systems for Better Spectrum Utilization Efficiency in Cognitive Radio Applications"**, which is being submitted by Mr. D Srikar (Roll No.717025), is a bonafide work submitted to National Institute of Technology Warangal in partial fulfilment of the requirement for the award of the degree of *Doctor of Philosophy in Electronics and Communication Engineering*.

To the best of our knowledge, the work incorporated in this thesis has not been submitted elsewhere for the award of any degree.

Dr. S. Anuradha
Supervisor
Department of ECE
National Institute of Technology
Warangal – 506004

Dedicated to My

Family, Gurus, & Friends

Contents

ACKNOWLEDGEMENTS

I am grateful to many people who made this work possible and helped me during my Ph.D studies. I am greatly indebted to my research supervisor Dr. S. Anuradha for giving me excellent support during my research activity at NIT Warangal. She encouraged me in choosing my research topic, her vision in my research area leads to successful investigations. I am very much thankful for giving research freedom and guidance, support in non-academic matters and for the humanity shown to me. With her inimitable qualities as a good teacher, she chiseled my path towards perfection. Ever since I met her, she has been an eternal source of motivation, inspiration, encouragement and enlightenment. She is responsible for making the period of my research work as an educative and enjoyable learning experience. The thesis would not have seen the light of the day without her insistent support and cooperation.

I am also grateful to Prof. L. Anjaneyulu, Head of the Department, Dept. of Electronics and Communication Engineering, for his valuable suggestions and support that he shared during my research tenure.

I take this privilege to thank all my Doctoral Scrutiny Committee members, Prof. Y. N. Reddy, Mathematics Department, Prof. L. Anjaneyulu, Professor, Department of Electronics and Communication Engineering, Dr. J. Ravi Kumar, Associate Professor, Department of Electronics and Communication Engineering for their detailed review, constructive suggestions and excellent advice during the progress of this research work.

I am grateful to the former Head of the ECE department Prof. N. Bheema Rao for his continuous support and encouragement. I would also appreciate the encouragement from teaching, non-teaching members and fraternity of Dept. of E.C.E. of N.I.T. Warangal. They have always been encouraging and supportive.

I take this opportunity to convey my regards to my closest friends for being always next to me. Thanks to M. Ranjeeth, K. Shri Ramtej, and Ch. Vijaya Durga Department of Electronics and Communication Engineering for their motivation and support throughout my work.

I acknowledge my gratitude to all my teachers and colleagues at various places for supporting and cooperating me to complete this work.

I would like to thank my family members (D. Dora Kumar Reddy, D. Sree Lakshmi, and D. Srisruja) for giving me mental support and inspiration. They have motivated and helped me to complete my thesis work successfully.

Finally, I thank God for filling me every day with new hopes, strength, purpose and faith.

D Srikar

ABSTRACT

The channels in the licensed spectrum are in an idle state for many of the times because of their inefficient utilization. Consequently, the spectrum utilization efficiency is degraded. In order to solve the wastage of the spectrum problem, these idle channels can be effectively used for other applications. So, the cognitive radio (CR) technology is employed to utilize the unused channels (licensed). It is assumed that the primary users, who generally do not use their channels fully, own the licensed spectrum. Therefore, in order to detect the spectrum holes (white spaces), the radio environment is monitored continuously. Whenever a spectrum hole is detected, the respective channel can be used by the secondary user for other applications until the primary users demand it.

Normally, printed monopole antennas are used for spectrum sensing and reconfigurable narrow band antennas are used for communicating in white spaces. Two varieties of antennas are widely used for cognitive radio applications. One is the dual port antenna system that has a printed monopole wideband sensing antenna and a reconfigurable narrowband (NB) antenna integrated on the same substrate and the other one is single port antenna system that has a reconfigurable wideband (WB) sensing/ narrowband antenna. However, to improve the spectrum utilization efficiency effectively, multiport integrated WB and multiple wideband/narrowband antenna systems are very advantageous when multiple white spaces are identified.

In this thesis, we firstly present the design of a super wideband (SWB) antenna for spectrum sensing applications. This SWB antenna utilizes the Apollonius fractal with nested Apollonius circles and is useful for both ultra wideband (UWB) and SWB applications. Since multi-input-multi-output (MIMO) systems have been the most promising systems to overcome multipath fading problems and MIMO antennas with polarization diversity enhance the channel capacity in both line-of-sight (LOS) and non-line-of-sight (NLOS) propagations, integrated wideband and multiple frequency reconfigurable WB/NB antenna system for CR MIMO applications is presented. Finally, as integrated UWB and multiple WB/NB antenna systems enhance the spectrum utilization efficiency by performing multiple communication tasks, integrated UWB and multiple WB/NB antenna systems for CR and CR MIMO applications are also presented to overcome the drawbacks of reconfigurable antennas.

List of Figures

List of Tables

Nomenclature

4G	4th Generation
5G	5th Generation
BBDR	Broadband Disaster Relief
BDR	Bandwidth Dimension Ratio
CCL	Channel Capacity Loss
CPW	Coplanar Waveguide
CR	Cognitive Radio
CST	Computer Simulation Technology
DG	Diversity Gain
DRIVE	Development of Robust and Innovative Vaccine Effectiveness
ECC	Envelope Correlation Coefficient
FBW	Fractional Bandwidth
FCC	Federal Communication Committee
FET	Field Effect Transistor
GaAs	Gallium Arsenide
GPR	Ground Penetrating Radar
GSM	Global System for Mobile Communication
IEEE	Institute of Electrical and Electronics Engineers
ISM	Industrial Scientific and Medical
LOS	Line of Sight
MEMS	Micro-Electro-Mechanical System
MIMO	Multi Input Multi Output
NB	Narrowband
NLOS	Non Line of Sight
OFDM	Orthogonal Frequency Division Multiplexing
PAM	Pulse Amplitude Modulation
PIN	P-type Intrinsic N-type
PMA	Printed Monopole Antenna
PPM	Pulse Position Modulation

PSK	Phase Shift Keying
QoS	Quality of Service
RF	Radio Frequency
RLAS	Radio Local Area Network Systems
SDR	Software Defined Radio
SMA	Sub Miniature version A
SNG	Satellite News Gathering
SRR	Split Ring resonator
SWB	Super Wideband
UWB	Ultra Wideband
VSAT	Very Small Aperture Terminal
VSWR	Voltage Standing Wave Ratio
WB	Wideband
Wi-Fi	Wireless Fidelity
WPAN	Wireless Personal Area Networks

Chapter-1

Introduction

1.1. Introduction

The channels in the licensed spectrum are in idle state for many of the times because of their inefficient utilization. As a result, the spectrum utilization efficiency is degraded. However, in order to solve the wastage of spectrum problem, these idle channels can be effectively used for other applications. Federal Communication Committee (FCC) came up with several solutions to improve the spectrum utilization efficiency in 2002. Also, a classification among these solutions is done based on how the licensed spectrum channels in the idle state are utilized. The proposed solutions are spectrum reallocation, spectrum sharing and spectrum leasing [1-4].

The spectrum sharing is divided into three categories. They are open spectrum sharing, hierarchical spectrum sharing and dynamic spectrum allocation. Depending on the maximum transmit power level, hierarchical spectrum sharing is further divided into two categories which are named as spectrum underlay and spectrum overlay (spectrum interweave). The cognitive radio technology is employed in spectrum overlay to utilize the licensed spectrum channels (unused). In spectrum overlay approach, it is assumed that the primary users, who generally do not fully utilize their channels, own the licensed spectrum. Therefore, in order to detect the spectrum holes, the radio environment is monitored continuously. Whenever a spectrum hole is detected, the respective channel can be used by the secondary user for other applications till the primary users demand it. When the primary users want to utilize the channels being used by secondary users then the secondary users must switch to other unused licensed channels.

Normally, printed monopole antennas, which produce omnidirectional patterns, are used for spectrum sensing and a reconfigurable narrow band antenna is used for communicating in white spaces. In all cognitive radio applications, planar monopole antennas are extensively employed due to their many advantages such as low cost, light weight, easy integration with planar structures, small size and easy fabrication. The ultra-wideband (UWB) antennas employed for the purpose of spectrum sensing operation in the frequency range, which was unlicensed by FCC in 2002, i.e., 3.1-10.6 GHz [5], but from one country to other country this frequency range varies within 3.1-10.6 GHz [6]. The frequency reconfigurable antennas used in cognitive radio applications must switch their operating frequencies rapidly depending on the frequency of the spectrum holes identified.

1.2. Integrated UWB and Multiple WB/NB Antenna System Model for CR Applications

The basic model of the integrated UWB and multiple wideband (WB)/NB antenna system is shown in Fig. 1. As shown in Fig. 1.1, P1 is the port associated with UWB sensing antenna and P2, P3, P4, P5,…..,Pn are the ports associated with WB/NB antennas for communication. All antennas are maintained in such a way that good isolation is maintained among the antennas.

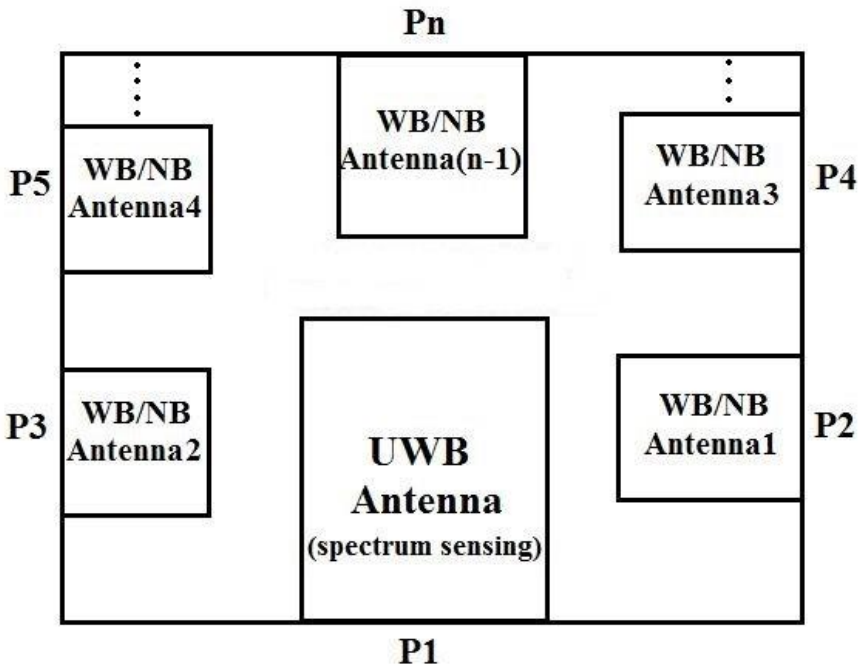

Fig. 1.1. Integrated UWB and multiple wideband (WB)/NB antenna system

1.3. Motivation

As there is a need of compact UWB/super wideband (SWB) antennas for spectrum sensing in cognitive radio applications, a SWB antenna using fractal is presented in this thesis. All of the existing reconfigurable antennas for CR applications can perform only one communication operation at a time irrespective of the number of spectrum holes identified. So, to perform multiple communication tasks simultaneously, this thesis presents an integrated wideband and multiple frequency reconfigurable WB/NB antenna system that also acts as a dynamic n-element MIMO antenna system, where 'n' is a variable that depends on the number spectrum holes identified.

The existing reconfigurable mechanisms have several disadvantages like usage of additional hardware, biasing line effects, power consumption and non-linear effects of switches. Sometimes, motors or extra biasing circuitry might be required to implement the reconfigurable mechanisms. However, the reconfigurable antennas have been adapted for cognitive radio applications to reduce the space, cost and for fast tuning. Also, these reconfigurable mechanisms are very hard to implement in practice. Therefore, in order to overcome the difficulties in implementing the reconfigurable mechanisms and to get all the benefits in low profile planar antennas, integrated UWB and multiple wideband (WB)/NB antenna system is considered as the best alternative to avoid the complex reconfigurable mechanisms.

Spectrum utilization efficiency, which is the primary motive of CR technology, also can be improved significantly by performing multiple communication operations at a time when detected multiple spectrum holes match with the operating frequencies of WB/NB antennas for communication. This has motivated us to present integrated UWB and multiple wideband (WB)/NB antenna systems for CR and CR MIMO applications in this thesis.

1.4. Research Objectives

The objectives of the proposed work for CR and CR MIMO applications are:

1. To design and develop a SWB antenna for spectrum sensing in cognitive radio applications.

2. To design and develop an integrated wideband and multiple frequency reconfigurable WB/NB antenna system for cognitive radio MIMO applications.
3. To design and develop integrated UWB and multiple wideband (WB)/NB antenna system for cognitive radio applications.
4. To design and develop integrated UWB and multiple wideband (WB)/NB antenna systems for cognitive radio MIMO applications.

1.5. Thesis Organization

The thesis is organized into seven chapters. This section gives the summary of all chapters.

Chapter 1: Gives the introduction, background, and reasons for choosing the problem.

Chapter 2: Provides the literature review, and also gives brief outline of the thesis.

Chapter 3: Presents the design of a low profile nested Apollonius circles based super wideband fractal antenna for UWB and SWB Applications. Also, time domain analysis of the proposed SWB antenna is also presented

Chapter 4: Describes the design of nine-port reconfigurable antenna for cognitive radio MIMO applications. To evaluate the diversity characteristics of the reconfigurable CR MIMO antenna, the crucial parameters such as envelope correlation coefficient (ECC) and diversity gain (DG) are calculated.

Chapter 5: Comprises the designs of integrated UWB and multiple wideband (WB)/NB antenna systems for CR applications to avoid the complexities involved in reconfigurable antennas and enhance the spectrum utilization efficiency.

Chapter 6: Illustrates the designs of Integrated UWB and multiple wideband (WB)/NB antenna systems for CR MIMO applications to avoid the difficulties involved in reconfigurable antennas and increase the spectrum utilization efficiency. To evaluate the diversity characteristics of the CR MIMO antennas, the crucial parameters such as envelope correlation coefficient (ECC) and diversity gain (DG) are calculated.

Chapter 7: Provides the conclusion and a brief discussion on the future scope of the thesis.

Chapter-2

Literature Survey

2.1. Introduction

In this chapter, the literature background of basics of an antenna, different parameters of an antenna, microstrip antenna, printed monopole antenna, UWB technology, SWB technology, CR technology, and types of antenna systems needed for CR MIMO antenna are reported.

2.2. Basics of an Antenna

An antenna is an inevitable building block in all wireless communication systems and no wireless communication is imagined without having an antenna. It is a normal metallic device (typically a rod or wire) used for either radiating radio waves or receiving radio waves according to Webster's dictionary. As per IEEE standard 145-1983, it is defined as "a source that is meant for radiating radio waves or receiving radio waves" [7]. As depicted in Fig. 2.1, the transmission line (guiding device) transports the electromagnetic energy to the antenna from the transmitting source. Finally, electrical signals are converted to electromagnetic waves by the antenna. At the receiving end, the antenna behaves as a sensor to capture the electromagnetic waves.

As illustrated in Fig. 2.2, a sinusoidal voltage source, which has a peak voltage V, is fed to an antenna. The internal resistance and reactance of the source are R_s and X_s, respectively. R_l, R_r, and X_a represent loss resistance, radiation resistance, and reactance of the antenna, respectively.

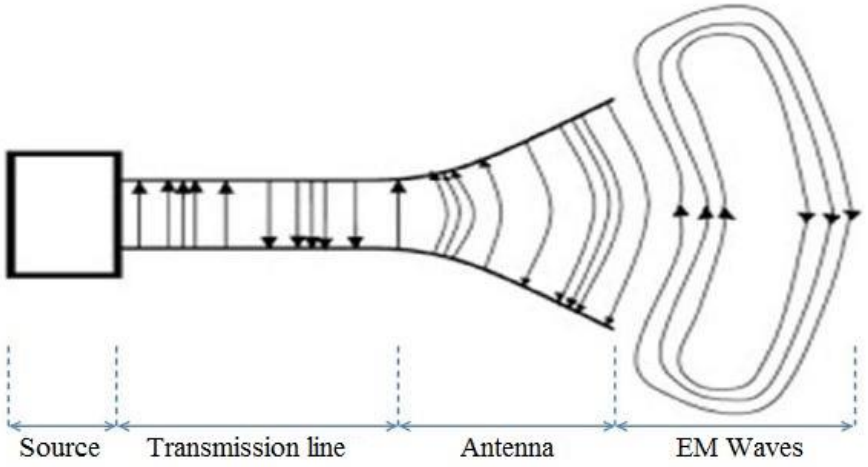

Fig. 2.1. Antenna as a transition device [8]

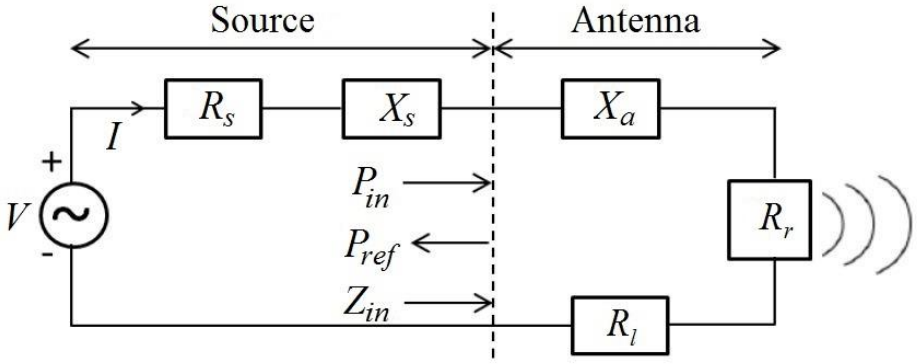

Fig. 2.2. Equivalent circuit of an antenna [8]

Several parameters of the antenna are defined as follows:

2.2.1. Input Impedance

An antenna's input impedance is described as the ratio of the voltage to current at the terminals of the input. If V_a is the voltage and I is the current fed to antenna then the mathematical expression of the input impedance is defined as

$$Z_{in} = \frac{V_a}{I} \tag{2.1}$$

If R_a is the antenna's resistance and X_a is the antenna's reactance then the input impedance of antenna is given as

$$Z_{in} = R_a + \mathrm{j}X_a \tag{2.2}$$

R_a can be expressed as sum of antenna's loss resistance R_l and antenna's radiation resistance R_r.

$$R_a = R_l + R_r \tag{2.3}$$

All conductor losses and dielectric losses are accounted in case of loss resistance R_l. For maximum power transfer to the antenna, impedance of the source Z_s and input impedance of the antenna Z_{in} must match properly. So, impedance of the antenna must be equal to the conjugate of the impedance of the source for perfect impedance matching according to the maximum power transfer theorem.

$$Z_{in} = Z_s^* \tag{2.4}$$

$$\text{So, } R_a = R_s \text{ and } X_a = -X_s \tag{2.5}$$

Generally, the internal resistance and internal reactance are 50 Ohms and 0 Ohms, respectively, for all microstrip antennas. Therefore, the input impedance of the antenna must be equal to 50 Ohms for perfect impedance matching.

2.2.2. Reflection Coefficient

Reflection coefficient Γ is a crucial parameter to find out how much incident power is reflected to source. It is a measure of mismatch between the antenna and source and is defined as the ratio of the reflected power P_{ref} to the incident power P_{in}.

$$\Gamma = \frac{P_{ref}}{P_{in}} \tag{2.6}$$

When it is expressed in dB, the mathematical expression for the reflection coefficient is given as

$$\Gamma \text{ (dB)} = 10 \log \left(\frac{P_{ref}}{P_{in}}\right) \tag{2.7}$$

Return loss is also a parameter of antenna similar to reflection coefficient. It is also expressed in dB and given as

$$\text{Return loss (dB)} = -\Gamma \text{ (dB)} \tag{2.8}$$

A reflection coefficient of -15 dB indicates a return loss of 15 dB. So, return loss is always a positive quantity since reflection coefficient is a negative quantity. Generally, reflection

coefficient of less than -10 dB is preferred for an antenna. Reflection coefficient of -10dB indicates that one-tenth of the incident power is reflected.

2.2.3. VSWR

Voltage standing wave ratio (VSWR) is an important parameter to find out how much incident power is reflected to source. The acceptable VSWR for an antenna is less than 2. VSWR is used to find out the reflected power in another way and can be found out from the mathematical expression given below.

$$\text{VSWR} = \frac{1 + |\Gamma|}{1 - |\Gamma|} \tag{2.9}$$

2.2.4. Bandwidth

The bandwidth of an antenna is normally nothing but the range of frequencies, where the antenna works properly. The characteristics of an antenna such as polarization, input impedance, reflection coefficient, beam width, radiation efficiency, gain, etc., are within their acceptable value in the bandwidth of an antenna. Two types of bandwidths are generally used to express the bandwidth of an antenna. They are absolute bandwidth (ABW) and fractional bandwidth (FBW). The absolute bandwidth is nothing but the difference between the upper cut-off frequency and lower cut-off frequency. Whereas the fractional bandwidth is considered as the percentage difference between the upper cut-off frequency and lower cut-off frequency over centre frequency f_C. The mathematical expressions of absolute bandwidth and fractional bandwidth are given as

$$\text{FBW (\%)} = \frac{f_H - f_L}{f_C} \times 100 \tag{2.10}$$

where

$$f_C = \frac{f_L + f_H}{2} \tag{2.11}$$

The fractional bandwidth percentage for wideband antennas and UWB antennas should be more than 10% and 20%, respectively, as per FCC. In case of narrowband antennas, it is less than 10%. Impedance bandwidth is mostly considered for any antenna. Normally, impedance bandwidth is considered most of the times for any antenna. However, depending on the application for which the antenna is used, it is considered. Generally, the range of frequencies over which the return loss is less than 10 dB is considered as the impedance bandwidth.

2.2.5. Polarization

The plane in which the electric field exists determines the orientation of radio wave. This orientation of the radio wave is nothing but the polarization of the antenna. In general, three different types of polarization (linear, circular, and elliptical polarizations) are generally possible for an antenna. The concept of axial ratio is used to find out the polarization. The ratio of the orthogonal components of the electric field gives the axial ratio. Axial ratio is unity for a circularly polarized antenna since orthogonal components of the electric field are equal in magnitude. It is greater than 1 in case of an elliptically polarized antenna, whereas it is infinity in case of a perfect linearly polarized antenna.

2.2.6. Directivity and Gain

The directivity of an antenna is described as "the ratio of the radiation intensity U from the antenna in a specific direction to the radiation intensity of an isotropic source U_0" as per the *IEEE Standard Definition of Terms for Antennas*. The radiation intensity U_0 is $\frac{P_{rad}}{4\pi}$ for an isotropic source. The mathematical expression of directivity is shown below.

$$\text{Directivity} = \frac{U}{U_0} = \frac{U}{\frac{P_{rad}}{4\pi}} = \frac{4\pi U}{P_{rad}} \tag{2.12}$$

Gain is also a crucial parameter to describe the antenna's radiation performance. The directivity of the antenna and radiation efficiency of the antenna are taken into account in case of antenna gain. Antenna gain in a specific direction is described as "the ratio of the radiation intensity in a specific direction $U\ (\theta, \phi)$ that is achieved if the power, which is fed to the antenna, is equally radiated in all directions. If P_{in} is the total input power or power fed to antenna then the radiation intensity of the power radiated equally in all directions is $\frac{P_{in}}{4\pi}$. The antenna gain is given as

$$\text{Gain} = \frac{radiation\ intensity}{\frac{total\ input\ power}{4\pi}} = 4\pi\ \frac{radiation\ intensity}{total\ input\ power} = 4\pi\ \frac{U\ (\theta,\ \phi)}{P_{in}} \tag{2.13}$$

Normally, antenna's reported gain is considered in most of the cases. It is described as "the power gain of the antenna in a specific direction to the power gain of an antenna that is considered as reference in its referenced direction. Both of the antennas must be fed with same input power in this case. Typically, dipole antennas, horn antennas, etc., for which their gains are known, are taken as reference antennas. The reference antennas in most of the cases are

lossless isotropic sources. The mathematical expression for the antenna relative gain is given as

$$\text{Gain} = 4\pi \ \frac{U\ (\theta,\ \phi)}{P_{in}\ (lossless\ isotropic\ source)} \tag{2.14}$$

The expression for gain in terms of directivity and radiation efficiency is given as

$$\text{Gain} = \text{Directivity} \times \text{Radiation Efficiency} \tag{2.15}$$

where the radiation efficiency ρ_{rad} is described as the ratio of radiated power to the power fed to the antenna (input power). Its mathematical expression is shown below.

$$\rho_{rad} = \frac{P_{rad}}{P_{in}} = \frac{R_r}{R_r + R_l} \tag{2.16}$$

2.2.7. Radiation Pattern

Radiation pattern, which is also known as antenna pattern, is a graphical representation of the radiation properties of the antenna as a function of space coordinates or a mathematical function according to IEEE std 145-1983. It is found out in the far-field region in most of the cases and is demonstrated as a function of the directional coordinates.

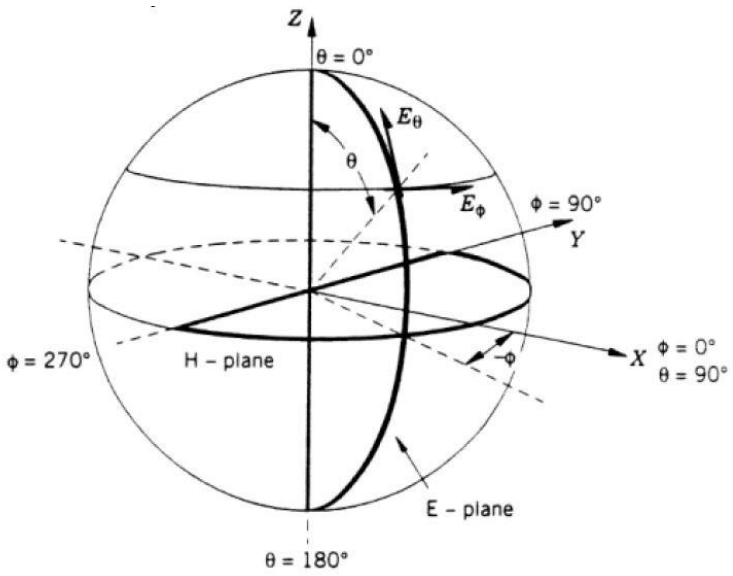

Fig. 2.3. Three dimensional spatial distribution of an antenna [8]

The radiation properties comprise field strength, power flux density, directivity, radiation intensity, phase or polarization. Typically, the radiation pattern is spatial distribution of the electromagnetic energy radiated. The spatial distribution is either two dimensional or three

dimensional. Fig. 2.3 shows the three dimensional coordinate system in terms of θ and ϕ in space. A combination of several two dimensional antenna radiation patterns gives a three dimensional antenna radiation pattern.

Antenna's radiation performance is demonstrated with reference to two patterns in principal planes (E-plane and H-plane) in case of linearly polarized antennas. The E-plane and the H-plane are defined as "the plane that comprises the electric field vector and the maximum radiation's direction" and "the plane that comprises the magnetic field vector and the maximum radiation's direction", respectively. Radiation patterns are classified into three types as per the radiation behaviour of the antenna. The first type, the second type, and third type are isotropic, directional, and omnidirectional, respectively. An isotropic radiation pattern, which does not exist in practice, is a lossless antenna radiation pattern in which same radiation exists in any direction.

The directive properties of antennas that are under test are described by taking an isotropic antenna as reference. But the isotropic is an ideal antenna that is not physically realizable. In case of antenna that has directional radiation pattern, radiation or reception of electromagnetic energy occurs more in some specific directions than other directions. If the maximum directivity of an antenna is more than that of directivity of a normal dipole antenna then the pattern of that antenna will be directional. If the radiation pattern of an antenna is non-directional in one plane and directional in orthogonal planes then the antenna pattern is said to be omnidirectional.

2.3. Microstrip Antenna

Despite many varieties of antennas, such as linear wire antennas, loop antennas, horn antennas, lens antennas, reflector antennas etc., are being utilized for different applications in wireless communication systems, microstrip antennas have grabbed more attention due to their advantages, such as light weight, compactness, inexpensive, easy manufacturability with modern printed circuit technology, simple integration with planar structures, and conformable to nonplanar surfaces as well. However, the microstip antennas have disadvantages like narrow bandwidth, low efficiency, high quality factor, low power, spurious feed radiation, etc. Microstrip antennas are often called as patch antennas.

Even though the microstrip antenna was discovered in 1953, it has grabbed good attention in 1970s. Since then, rigorous research in microstrip antennas has been going on for

different applications. The structure of the basic patch antenna is shown in Fig. 2.4. As depicted in Fig. 2.4, it comprises a dielectric substrate of thickness h and has two conducting layers at the front and back portions of the substrate. Typically, copper is used for conducting layers.

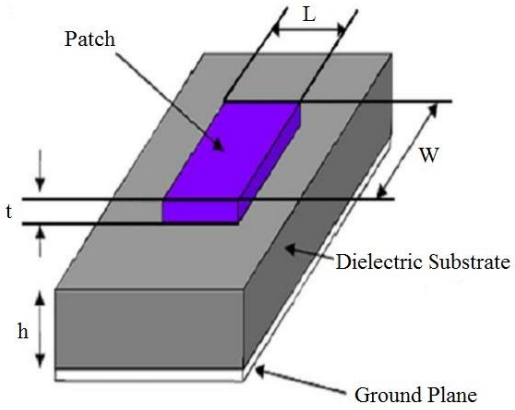

Fig. 2.4. Structure of basic patch antenna [7]

The upper and lower conducting layers are referred as radiating patch and ground plane, respectively. Rectangular and circular radiating patches are normally more preferred in practice. Depending on the requirements, other shapes can also be used. Various complex structures have also been investigated in the literature as they can be simulated easily with the help of some advanced simulators. Some shapes of the radiating patches are displayed in Fig. 2.5.

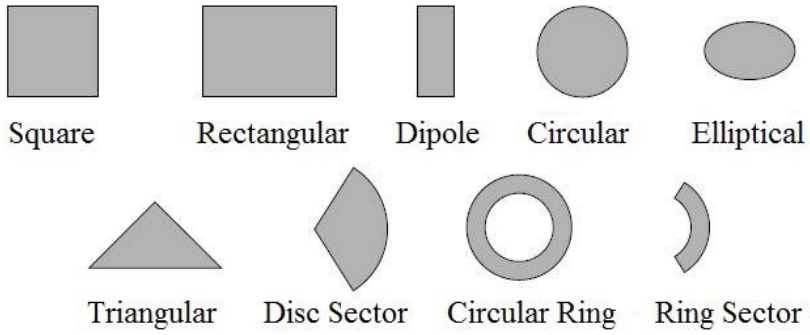

Fig. 2.5. Different shapes of the radiating patches [7]

In order to feed microstrip antenna, many feeding techniques are used. Some of them [9, 10] are the microstrip line feed [11, 12], coaxial probe feed [13], proximity coupling and aperture coupling. Microstrip line feed is the simplest technique among them since its fabrication is easy and impedance matching between the radiating patch and the microstrip feed line can be done easily [14]. The microstrip line feed patch antenna is displayed in Fig. 2.6.

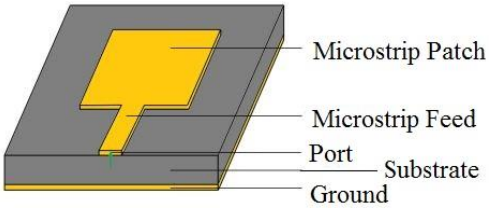

Fig. 2.6. Microstrip line fed patch antenna [15]

The mathematical equations for finding out the dimensions of the radiating patches with different shapes are given in [7]. The conventional radiating patches produce single resonating band with narrow bandwidth. So, to generate multiband, slots are incorporated in the radiating patches as incorporation of slots in patch leads to multiple resonating paths. Also, incorporation of slots in ground plane can also produce multiple resonant frequencies. When some portion of the ground plane is etched, perturbations in the current distributions occur. The perturbations in the ground plane generated by slots and the energy coupling that exists between the slots generate multiple resonant frequencies.

2.4. Printed Monopole Antenna

The conventional microstrip antennas, microstrip fed slot antennas, and microstrip antennas with defected ground structures have narrow operating bandwidths. Since the world has been witnessing enormous development in modern wireless communication systems, antennas with wide bandwidth are of great demand. Also, single antenna with wide bandwidth covers many applications. Nowadays, printed monopole antennas (PMAs) are widely being used as they have wide impedance bandwidth. So, they are considered to be the one of the promising candidates for UWB technology due to their omnidirectional radiation pattern in azimuthal plane and wide impedance bandwidth. The radiation pattern of the conventional microstrip antenna is directional, whereas it is similar to that of radiation pattern of a dipole antenna in case of printed monopole antenna. Integration with other components can be done easily in case of printed monopole antennas since they have reduced size and no backing of ground plane is required. Moreover, these printed monopole antennas are very easy to fabricate. For all of the UWB technology based low cost systems, cost effective printed monopole antennas, which are generally fabricated on a low cost FR-4 substrate, are mostly preferred.

The main thing to be kept in mind while designing an antenna that has an impedance bandwidth ratio of 3.42:1 for VSWR ≤ 2 with a large impedance bandwidth is the antenna must

have multiple resonances. This can be realized so easily by printed monopole antennas. Unlike conventional dipole antennas, conventional monopole antennas, and conventional microstrip antennas that have single resonance, some modified design considerations have to be followed. So, in case of printed monopole antennas, the lower band edge frequency and bandwidth are the crucial design parameters to be considered. The maximum height of the printed monopole mainly decides the lower band edge frequency. Whereas the proper impedance matching between microstrip line and impedance of various modes decides the total bandwidth of the printed monopole antenna.

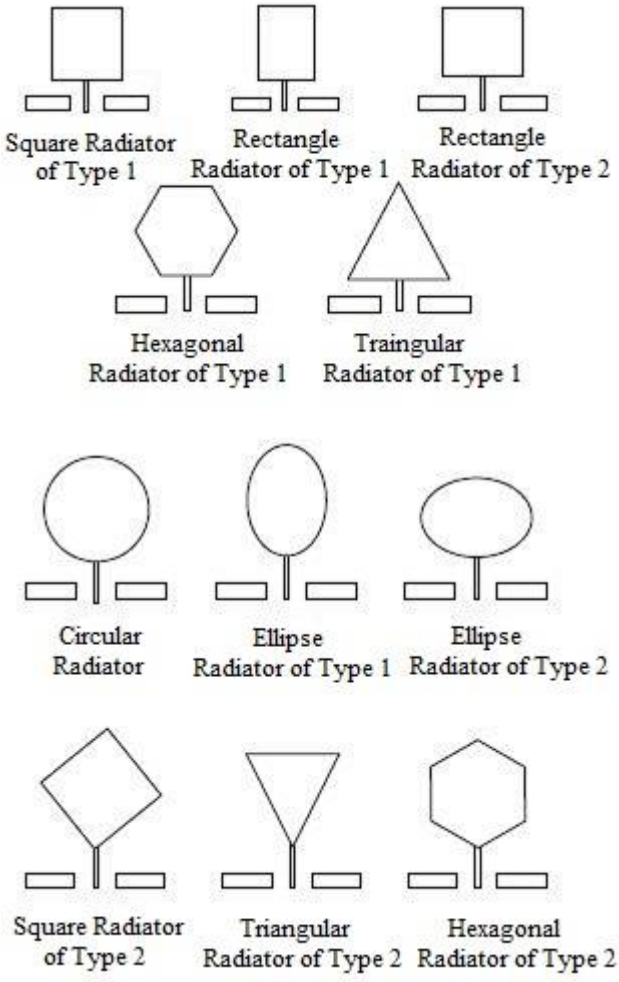

Fig. 2.7. PMAs with various shaped radiators [16]

The printed monopole antenna achieves good azimuthal radiation pattern with very wide impedance bandwidth. The reasons can be demonstrated in two ways. The PMA can be treated as microstrip antenna configuration, whose location of the backing ground plane is at infinity. As it is known that a radiating patch is normally located on a dielectric substrate (typically

FR4), we assume that air, which is a thick dielectric substrate and has a relative permittivity of 1, exists above the substrate. This kind of microstrip antenna configuration with a thick dielectric substrate of relative permittivity close to 1 produces large impedance bandwidth.

On the other hand, PMAs can be viewed as vertical monopole antennas. Normally, a monopole antenna comprises a vertical cylindrical wire that is mounted over its ground plane. As its diameter increases, bandwidth also increases. A cylindrical monopole antenna, which has a large effective diameter, can be equated to a PMA. The lower band edge frequencies can be determined using this analogy for all regular shapes of PMAs for various feed configurations. The PMAs with various shapes are depicted in Fig. 2.7. The shapes of the radiator of PMA include square, rectangle, hexagon, triangle, circle, and ellipse for different feed positions, as illustrated in Fig. 2.7. The mathematical equation to calculate the lower band edge frequency of PMA with any regular shape is given in [16].

2.5. UWB Technology

Nowadays, there has been a huge demand for advanced wireless communication services in modern communication systems. These advanced wireless communication services are needed to supply high bandwidth and high data rates for applications, such as live video streaming, data access and data transfer in portable wireless communication systems. Since current services are facing some issues, such as limited bandwidth and limited speed in data rate, they are not appropriate for the above applications. Therefore, some new and efficient technologies are necessary for the modern communication users to get their requirements fulfilled. UWB technology is a promising technology and an attractive one for the above said applications.

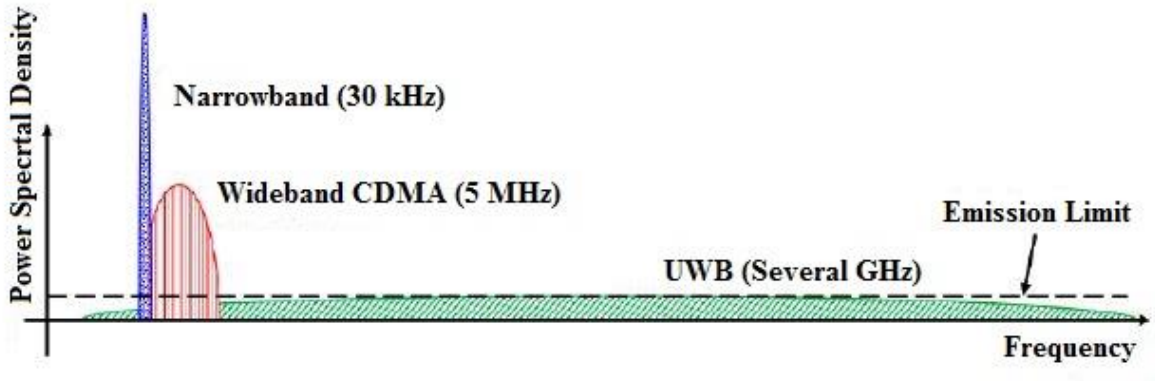

Fig. 2.8. Power spectral density of various signals [17]

A radio spectrum, which has an absolute bandwidth of more than 500 MHz or a 20% minimum fractional bandwidth, is nothing but the UWB spectrum according to the rules of FCC. The term UWB signal mentions baseband, carrier-free, wide relative bandwidth radio signal, time domain, impulse, orthogonal function, and non- sinusoidal signal. In this UWB technology, low power pulses, whose duration is very small, are transmitted. Also, over small distances, high data rates are yielded through this UWB technology.

Power spectral density of various signals is depicted in Fig. 2.8. Maximum data rates of up to hundreds of Mbps or sometimes even up to Gbps are possible with this UWB technology at distances ranging from 1 meter to 10 meters. Different technologies have different data rates as displayed in Fig. 2.9. As illustrated in Fig. 2.9, maximum data rates of up to 1 Mbps and 100 Kbps are achieved for maximum distances of 10 meters in Bluetooth technology and above 10 km in GSM technology, respectively.

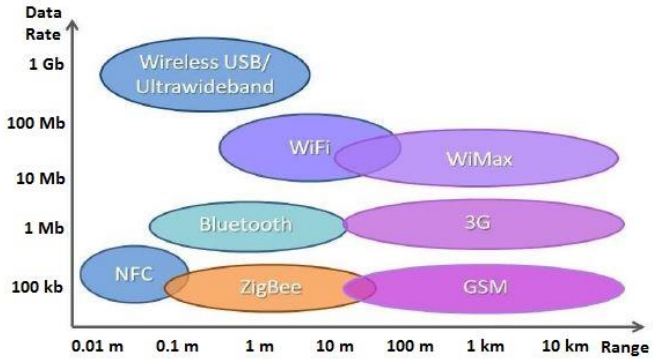

Fig. 2.9. Data rates for several technologies [19]

System performance can be comfortably optimized by changing different parameters such as power, data rate, range, and quality of service since substantial flexibility is possible with UWB technology. Without using any extra hardware, only one system is able to provide wireless communication services for different wireless communication applications. For an instance, high data rate and low power can be attained for short distance applications. The benefits of UWB signals are accurate ranging, low power transmission, superior obstacle penetration, multicarrier modulation, resistance to jamming, robustness against eavesdropping, coexistence with narrow bandwidth systems, no up/down conversion, excellent time resolution, covert operation, high temporal resolution, and interference rejection [18].

Despite the power levels of the transmitted UWB signals are low and are below a noise floor, the quality of communication is guaranteed. Since the power levels of the transmitted

UWB signals are low and are below a noise floor, detection of UWB signals is very difficult. Long battery life can be attained as UWB systems have an advantage of this low power feature. Moreover, the UWB signals are hardly visible to the other wireless signals that are being operated. Therefore, the chances of interference issue with other wireless services are very less. Thus, secure and reliable communications are possible with these UWB systems. Elimination of UWB signals by noise signals is also not possible since the shape of UWB signal is specific, whereas the noise signal does not have any particular shape. Also, the inference of noise signals with the UWB signals has to be uniform all over the spectrum. Despite this interference exists, UWB signals can be successfully recovered. Hence, UWB signals are very promising and are helpful in providing secure and reliable communications. UWB systems normally do not need modules, such as filters, additional oscillators, amplifiers, mixers, etc., since modulation and demodulation of UWB signals are not needed. So, the complexity, size, and cost of the devices decrease significantly. Also, with the help of these narrow pulses, modulation schemes such as PAM, PPM, and PSK can be executed.

Multicarrier modulation, which is another striking feature of UWB signals, can be useful in OFDM technique. The problems, which normally exist in high data rate wireless communication, can be easily solved by UWB technology. The UWB technology is used in many applications, such as spectrum sensing in cognitive radio, ground penetrating radar, surveillance systems, wireless personal area networks, wireless body area networks, vehicular radar, wireless telemetry, medical imaging, telemedicine, 4G, vehicular radar, RF energy harvesting, and radar imaging.

2.6. Super Wideband Technology

In recent years, modern wireless communication systems have noticed enormous developments. Since the technology is developed, there is a huge demand for both short range and long range communications. Even though Ultra Wide Band (UWB) technology is a strong candidate for short range communications, it is not able to cover long range communications. Now a days, in order to cover both short range and long range transmission, the users of Wireless Personal Area Networks (WPAN) are strongly demanding extremely large bandwidth for future UWB communications. A Super Wideband (SWB) technology is required to fulfil the above demands. Moreover, due to the advantages of its high data rates and very large operating bandwidth, this SWB technology is gaining more importance in modern wireless

communication systems. Super wideband antennas have bandwidth dimension ratio (BDR) of 10 to 1.

Some of the applications, where SWB antennas are used, are mobile applications, radio determination applications, wideband high-definition television, broadband disaster relief (BBDR), defence systems, satellite applications, ISM applications, Doppler navigation aids, satellite news gathering (SNG)/ very small aperture terminal (VSAT), short range radar, wireless access systems (WAS)/ radio local area network systems (RLANS), radio astronomy, aeronautical radio navigation, etc.

2.7. Cognitive Radio Technology

Radio spectrum congestion problem occurs in a densely populated scenario due to the rapid growth in wireless communication standards. As there is no uniform distribution in spectrum occupancy, over-crowdedness occurs in some parts of the spectrum, whereas the remaining parts of the spectrum are rarely used. Therefore, there exists an unbalanced usage of the spectrum. To address this problem, cognitive radio system was proposed [20]. Thus, for future wireless communication systems, this cognitive radio system is considered as a potential solution. Federal Communication Committee (FCC) proposed so many solutions to improve the spectrum utilization efficiency in licensed spectrum in 2002, as illustrated in Fig. 2.10. The interference that exists among the signals can be avoided with the help of these solutions when the spectrum channels are in utilization. Moreover, the issue of availability of limited spectrum is also mitigated by these solutions to certain extent by making the use of the unused channels for other wireless communication applications.

A classification among these solutions is done based on the utilization of the licensed spectrum channels in the idle state. The proposed three categories of solutions are spectrum leasing, spectrum reallocation and spectrum sharing. Reorganization of allocated frequency bands to various wireless communication services is done in spectrum reallocation in accordance with the utility of the spectrum that is allocated previously. For an instance, cognitive radio operation is allowed in IEEE 802.22 standard. In spectrum leasing approach, the other parties are granted the licensed spectrum on lease depending on the spectrum's availability and time. The spectrum reallocation and the spectrum leasing are the two approaches to access the spectrum statically. Whereas the allocated frequency bands are shared

by the users either dynamically or simultaneously with a few restrictions in spectrum sharing approach.

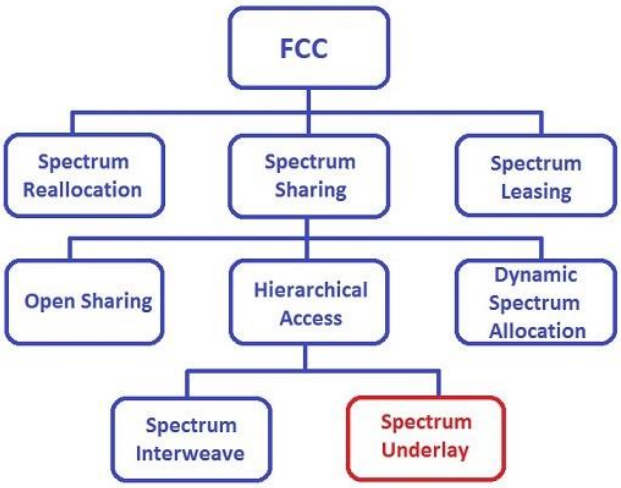

Fig. 2.10. Solutions proposed by FCC [2]

In the recent years, there has been a tremendous research in spectrum sharing approach by carrying out some activities such as RF circuit design, antenna design, implementation of reconfiguration algorithm, sensing, etc. This spectrum sharing approach is sometimes called as dynamic spectrum access. It is further divided into three types as open spectrum sharing, hierarchical spectrum sharing and dynamic spectrum allocation. In open spectrum sharing approach, all users share the spectrum at the same time with some restrictions on the power of the transmitted signal. The restrictions on the transmitted signal power are always in accordance with rules and regulations of models that are already used. An example for this IEEE 802.11 ISM bands such as Bluetooth and Wi-Fi.

In dynamic spectrum allocation approach, spectrum utilization efficiency is enhanced by allocating the frequency bands to various other wireless communication services dynamically in accordance with their spatial and temporal stats. A European project, which was named as DRIVE, is an example for this approach. Hierarchical spectrum sharing is classified based on the maximum transmitted power level and the interaction with the radio environment. The classified two models are spectrum underlay and spectrum overlay. Spectrum overlay approach, which is also referred as spectrum interweave, is well known as opportunistic spectrum access. Each of the two models has its own way of accessing the channels in licensed spectrum as well as in unlicensed spectrum. In case of licensed spectrum, the primary users and

the secondary users are generally called as licensed users and unlicensed users, respectively. The primary users, who own the licensed spectrum, do not utilize their channels fully. The secondary users can also access the licensed spectrum without having an effect on the primary user's quality of service. In case of unlicensed spectrum, any user can access the spectrum and there exists no primary and secondary users.

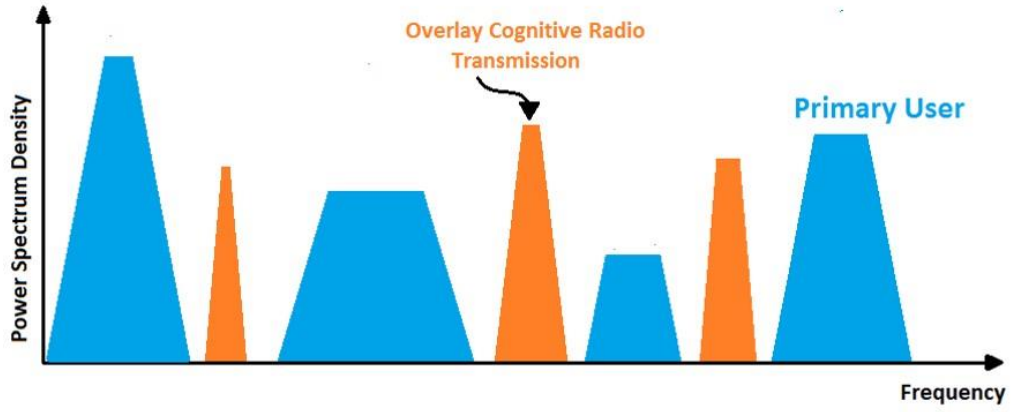

(a)

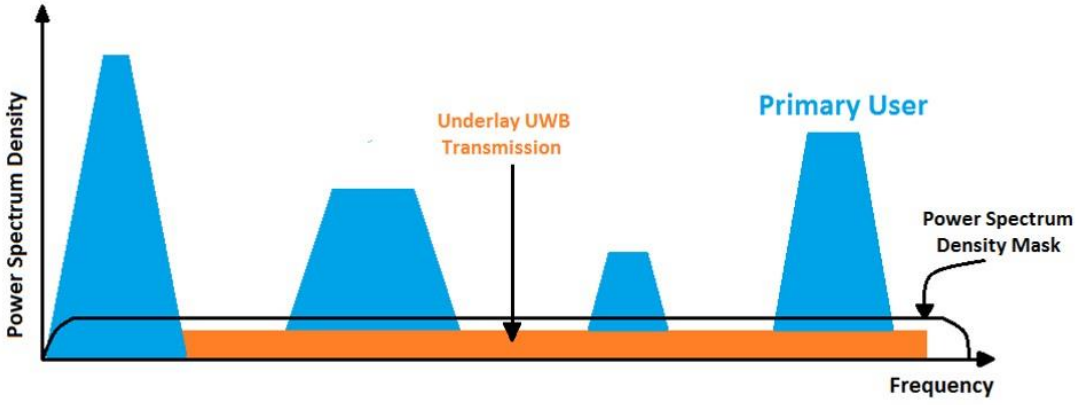

(b)

Fig. 2.11. Hierarchical access (a) spectrum overlay (b) spectrum underlay [3]

A spectrum hole, which is also called as white space, is an empty channel that exists in a distinct location at a particular time. These spectrum holes are detected by the spectrum contenders by means of appropriate sensing algorithms in spectrum overlay approach. With the help of sensing mechanism, the unused frequencies (i.e., spectrum holes) can be known. Moreover, interference that exists among the signals can be avoided when there is utilization of spectrum channels. In

case any spectrum hole is identified then that respective channel can be exploited for other wireless communication services irrespective of the transmitted power, as depicted Fig. 2.11a. When the spectrum is licensed, the secondary users are the spectrum contenders. In this case, the QoS of the primary users (licensed users) is not affected by the secondary users. The unutilized channels can be made available for secondary users until the primary users access them. When primary users demand those licensed channels, the secondary users must switch to other free channels for maintaining the proper communication. In case there are no other free channels, the secondary users must terminate communication. Otherwise, as discussed in spectrum underlay approach, the secondary users can share the licensed spectrum while maintaining low level of transmitted power without affecting the QoS of the both of the users. On opportunistic basis, all users share the spectrum when the spectrum is unlicensed. So, whoever among all the users senses the unused channel first can access that unused channel. This opportunistic basis is normally called as "first-sense-first-use". When the channel is utilized by one user, rest of the users have to either wait until that channel becomes vacant or sense any other spectrum holes.

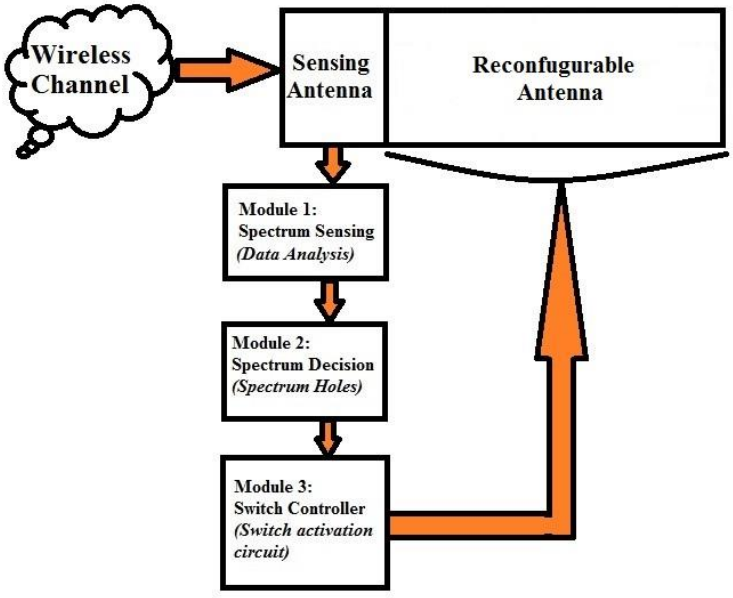

Fig. 2.12. Work flow of cognitive radio

The spectrum can be shared by all the spectrum contenders simultaneously in spectrum overlay approach by ensuring that the transmitted signal power is very low. The transmitted power level must not exceed a noise floor, which is acceptable for all the other users, as illustrated in Fig. 2.11b. Therefore, the spectrum contenders, who share the spectrum simultaneously, are not

visible to the other users. When the spectrum is licensed, the secondary users are able to share the licensed spectrum with the primary users simultaneously. A best example that falls in this category is maintaining the transmitted power level of less than -41.3 dBm/MHz in 3.1 GHz-10.6 GHz, (i.e., UWB). When the spectrum is unlicensed, all users share the spectrum with the users who have already occupied the channels at the same time on an opportunistic basis called as "first-sense-first-use".

In case of spectrum overlay approach, one antenna is required for sensing the spectrum and the other antenna is required for the purpose of communication. Whereas only one antenna is required for communication in case of spectrum underlay approach. Normally, frequency reconfigurable antenna is mostly used for the purpose of communication since it is able to change its operating frequency according to the detected frequency of the spectrum hole.

The cognitive radio model is defined as the process of monitoring the radio environment (spectrum sensing), making the decision, performing communication task, and changing its radio parameters in accordance with the information that is sensed. The work flow of the cognitive radio model is illustrated in Fig. 2.12. With the help of the cognitive radio technology, the system collects the information about the spectrum holes by monitoring the status of the radio environment continuously and reconfigures its radio parameters such as bandwidth and frequency dynamically for communication. Moreover, as the availability of spectrum is also limited, this problem can be mitigated to some extent with the help of this cognitive radio technology by using the free channels for any other wireless communication applications. In 1998, Joseph Mitola coined the idea of cognitive radio technology. Also, he published an article in 1999. He added some additional capabilities like monitoring the radio environment (spectrum sensing), making the decision, performing communication task, and changing its radio parameters dynamically to software defined radio platform. Therefore, cognitive radio model can be viewed as SDR with some extra hardware and capabilities. FCC gave the definition of cognitive radio as "a radio that is able to change the parameters of its transmitter based on the environment in which it operates" [21].

The three major functionalities of cognitive radio are as follows:

- Spectrum sensing
- Decision making
- Spectrum management

The process of sensing the radio environment for spectrum holes continuously is called as spectrum sensing. The process of identifying the channels effectively for transmission is termed as decision making. The process that involves performing communication tasks and updating the parameters of communication for maintaining quality of service is called as spectrum management.

2.8. Cognitive Radio Technology in UWB

In 2001, FCC made a frequency band (3.1 GHz - 10.6 GHz) unlicensed for UWB applications since UWB technology has numerous advantages. However, for UWB applications, some countries dedicated a few frequency bands [22]. Since 2002, this UWB spectrum has been witnessing a huge demand for various UWB applications in educational institutions, industries, and many government organizations. Hence, it is crucial to implement cognitive radio technology due to two reasons. The first reason is to enhance the spectrum utilization effectively when free spectrum channels are available. The second reason is to avoid the interference that exists among the signals when spectrum channels are in utilization. It is always possible to implement underlay mechanism in the UWB spectrum as discussed previously with a restriction on the power level of the transmitted signal. Therefore, underlay mechanism can be used in case the overlay mechanism is not possible.

Cognitive radio technology uses planar UWB monopole antennas to sense the spectrum holes in radio environment in the frequency band that ranges from 3.1 GHz and 10.6 GHz in UWB systems as planar UWB antennas cover complete UWB spectrum. It uses narrowband antennas to perform communication tasks since NB antennas are more efficient and have better performance than planar UWB antennas. To perform communication tasks, mostly frequency reconfigurable antennas are normally used since they have capability to change their operating frequencies dynamically according to the updated frequencies of the spectrum holes.

The requirements of the UWB antennas and frequency reconfigurable NB antennas are as follows:

- Return loss must be greater than 10 dB in the UWB and in the required band for UWB antennas and frequency reconfigurable NB antennas, respectively.
- Omnidirectional radiation patterns are required for both UWB antennas and frequency reconfigurable NB antennas.

- Gains must be stable throughout the operating bandwidth of UWB antennas and frequency reconfigurable antennas.
- Moreover, UWB antennas and frequency reconfigurable NB antennas must be compact enough to be compatible with modern portable wireless devices.

2.9. Types of Antenna Systems Needed for Cognitive Radio

Three varieties of antenna systems are normally used for cognitive radio applications. The first one is using two separate antennas in which one wideband antenna is meant for sensing and the other frequency reconfigurable NB antenna is meant for communication. The second one is the dual port antenna system that has a printed monopole WB sensing antenna and a reconfigurable narrowband communication antenna integrated on the same substrate. The third one is single port antenna system that has a reconfigurable WB sensing/ narrowband antenna. But this antenna system must have a proper switching mechanism to switch between sensing and communication modes. Among these antenna systems, dual port antenna systems have grabbed more attention in the recent years. However, to improve the spectrum utilization efficiency effectively, multiport integrated WB sensing antenna and multiple wideband/narrowband antenna systems are very advantageous when multiple white spaces are identified.

To enhance the spectrum utilization efficiency effectively, this thesis proposes antenna systems that consist of UWB sensing antenna and multiple WB/NB antennas for CR applications.

2.10. Cognitive Radio MIMO Antennas

The high data rates wireless devices with efficient spectrum utilization are grabbing more attention as they have become crucial in the present day wireless communication. MIMO systems have been the most promising systems to overcome multipath fading problems. Moreover, MIMO antennas with polarization diversity enhance the channel capacity in both line-of-sight (LOS) and non-line-of-sight (NLOS) propagations. As MIMO systems provide high data rates and CR technology utilizes the spectrum efficiently, MIMO systems with CR technology are treated as promising systems to attain high data rates and utilize the spectrum efficiently.

To enhance the spectrum utilization efficiency effectively and attain high data rates, this thesis proposes an antenna system that consists of wideband sensing antenna and multiple

frequency reconfigurable WB/NB antennas for CR MIMO applications. Also, antenna systems that consist of WB sensing antenna and multiple WB/NB antennas for CR MIMO applications are proposed in this thesis.

2.11. Literature Review

Till now, many works have been presented on UWB/SWB antennas for spectrum sensing in CR applications and also antennas for CR and CR MIMO applications [23-166]. Some of them are as follows:

Pourahmadazar *et al*., (2011) proposed a monopole antenna that uses Pythagorean tree fractal structure [23]. A modified Pythagorean tree fractal is inserted in the conventional T-shaped radiator. Additional resonances are generated by increasing the fractal iterations, thus resulting in wide impedance bandwidth.

Roshna *et al*., (2014) presented a very small novel coplanar stripline-fed antenna for UWB applications [24]. The presented antenna, which is printed on a FR-4 substrate, comprises a staircase shaped patch, which is shorted with a strip. Its volume is $25 \times 7 \times 1.6$ mm^3. Despite the active patch does not comprise any metamaterial structures and fractal geometries, compactness is achieved because of its optimized structure.

Tripathi *et al*., (2014) proposed a hexagonal fractal UWB antenna using Koch fractal geometry [25]. Koch fractal geometry is incorporated in the radiator of the monopole as well as in the ground plane, so multiple resonances are generated. As a result, the fractional bandwidth percentage of the antenna increases till 122%. Also, stable radiation patterns are also possible due to the fractal geometry.

Pandey *et al*., (2014) presented a compact metamaterial based microstrip antenna for UWB applications [26]. The presented antenna comprises π-shaped slots on the active patch and crossed shaped slots on the ground plane. Due to these two layers of metamaterials, series capacitance and shunt inductance are developed, thus leading to the left-handed behaviour of the metamaterial.

Guo *et al*., (2010) presented a new design approach to achieve wide bandwidth [27]. The proposed UWB antenna achieves compactness due to the quasi self-complementary structure of the ground plane along with a tapered radiating slot.

Islam *et al*., (2015) proposed a metamaterial UWB antenna that comprises four metamaterial unit cells, which are able to show both the characteristics of negative permeability and negative permittivity on the triangle-shaped radiator and three rectangular slots on the ground plane [28]. The 10 dB return loss bandwidth of the antenna ranges from 3.07 GHz to 19.91 GHz.

Dorostkar *et al*., (2013) proposed an antenna that was made of six iterations of hexagonal slot inside a circular shaped radiator, which is asymmetrical toward the substrate to achieve SWB characteristics [29]. The achieved impedance bandwidth ranges from 2.18 GHz to 44.5 GHz.

Singhal *et al*., (2016) presented a SWB antenna with bandwidth dimension ratio (BDR) of 11:1 and fractional bandwidth ranging from 3.4 GHz to 37.4 GHz [30]. A two iterative square slot inside a hexagonal radiator with co-planar waveguide feeding was used to achieve that bandwidth.

Manohar *et al*., (2014) proposed an antenna in which an exponential tapered feed region was incorporated between the main radiating patch and triangular feed-line to achieve good matching, thus making the antenna resonating from 2.5 GHz to 80 GHz [31].

Azari *et al*., (2011) proposed a novel SWB antenna that consists of two iterative octagonal slot loaded in an octagonal radiator fed by a coaxial probe [32]. Even though its impedance bandwidth is huge, i.e., 10-60 GHz, its BDR is very less and it does not operate in UWB range.

Singhal *et al*., (2017) presented a SWB antenna in which a four iterative octagonal slot was loaded inside a octagonal radiator that was fed by a CPW feed-line, and also two rectangular notches were loaded in the modified ground plane to achieve a wide bandwidth, i.e., 3.8-68 GHz [33]. However, it does not cover frequencies from 3.1 GHz to 3.8 GHz in UWB spectrum.

Tran *et al*., (2011) presented a SWB antenna of bandwidth 145 GHz (i.e., 5-150 GHz). Pattern stability over decade bandwidth was achieved [34]. However, its BDR is less and it is not able to operate in the entire UWB range.

Cao *et al*., (2013) proposed a novel compact SWB antenna fabricated on a low cost FR-4 substrate of physical volume 42 mm × 45 mm × 1.5 mm with an impedance bandwidth,

i.e., 2-100 GHz and excess ratio of 50:1. A circular patch with a pair of ears fed by a 50 ohm microstrip line and a rectangular notch loaded top corner rounded ground plane was used to achieve extremely huge bandwidth [35].

Chen *et al*., (2011) proposed a super wideband monopole antenna that has an asymmetrical ground plane embedded with a semi elliptical fractal complementary slot and having an impedance bandwidth, i.e., 1.44-18.8GHz and bandwidth dimension ratio of 2735 [36].

Shahu *et al*., (2015) presented an antenna that comprises two iterations of triangular slot on a hexagonal shaped radiator with tapered strip line feed and a modified ground plane to achieve bandwidth, i.e., 3-35 GHz for SWB applications [37].

Hakimi *et al*., (2014) proposed a CPW-fed transparent antenna with a -10 dB reflection coefficient bandwidth that ranges from 3.15 GHz to 32 GHz [38]. In order to enhance the overlapped resonant frequencies, a staircase technique was provided for the rectangular patch with a modified ground plane.

Wang *et al*., (2014) proposed a dual port antenna that consists of UWB sensing and narrow band dielectric resonator antennas on a ground plane of size 150 × 150 mm^2. UWB sensing and narrow band dielectric resonator antennas operate at 2.4-12 GHz and 2.3-5 GHz, respectively [78]. However, in the frequency range, i.e., 2-4 GHz, mutual coupling of less than -6 dB was achieved between them.

Tawk *et al*., (2011) reported a dual port antenna system in which an UWB sensing antenna and a rotatable narrow band antenna were incorporated on the same substrate [79]. Frequency reconfiguration was achieved by rotating the patches to five different positions; consequently, the rotatable narrow band antenna operates at five different narrow bands in the frequency range, i.e., 2-10 GHz. However, the presence of stepper motor on the back side of the substrate made the printed circuit board bulky.

Jin *et al*., (2011) presented a single port UWB/NB antenna, which operates in an UWB mode and three narrowband modes in which first, second, and third narrowband modes cover 3.55-5.18 GHz, 5.12-6.59 GHz, and 7.10-8.01 GHz, respectively [80]. Frequency reconfiguration was done depending on the statuses of the switches that were controlled optically.

Kumar *et al*., (2016) reported a three port antenna system, which has an UWB sensing antenna and two dual narrow band antennas for the purpose of communication in a compact volume of 30 mm × 30 mm × 1.6 mm [81]. Despite the antenna system is able to perform a maximum of two communication tasks, the two narrow band antennas cover only the high frequency bands (i.e., 6.36-6.63 GHz, 8.78-9.23 GHz, 7.33-7.7 GHz and 9.23-9.82 GHz) in the UWB spectrum are covered.

Nella *et al*., (2018) presented a five-port antenna that comprises one UWB sensing antenna, two dual band communication antennas, and two single band communication antennas [82]. UWB antenna senses the complete UWB spectrum, whereas the dual band and single band antennas cover many frequencies in UWB spectrum in such a way that the complete UWB spectrum is covered. Mutual coupling between any two antennas is less than -16 dB. Also, good match between experimental results and simulated results was achieved.

Pahadsingh *et al*., (2018) proposed an antenna system that consists of UWB sensing antenna that operates at 3-12 GHz and NB cylindrical dielectric resonator communication antenna that operates at 4.93-5.4 GHz, 5.9-6.7 GHz, and 9.28-10.2 GHz [83]. The proposed antenna system has a drawback since the isolation between sensing antenna and communication antenna is just better than 10 dB.

Erfani *et al*., (2012) presented an integrated planar UWB/reconfigurable-slot antenna for CR applications [84]. A slot, which is embedded in the radiator of the disc monopole antenna, acts as resonator. This slot resonator is used to obtain an individual NB antenna. Frequency reconfigurability is achieved by inserting a varactor diode across the slot to tune in 5-6 GHz for communication.

Tawk *et al*., (2009) proposed a novel design of reconfigurable antenna in which an UWB sensing antenna and a reconfigurable communication antenna are integrated [85]. In this work, frequency reconfigurability of the communication antenna is achieved by the rotating part of the antenna. No biasing circuits are required for the activation of switches unlike conventional reconfigurable antennas.

Ebrahimi *et al*., (2011) proposed the concept of integration of antennas for multi-standard antennas [86]. The large area of the ground plane of the CPW fed UWB antenna, which is printed on the top side of the substrate, is utilized by the small antenna. Three different

configurations of integrated WB-NB antenna system in which each antenna system has a matching circuit to tune the antenna to a particular frequency was also demonstrated.

Zheng *et al*., (2014) investigated a new compact optically controlled reconfigurable integrated antenna system [87]. The characteristic of frequency reconfigurability is achieved by using four photoconductive silicon switches that are controlled optically. The antenna system comprises two antennas. One antenna, which operates at 3-11 GHz, is meant for the spectrum sensing and the other antenna, which operates at five different frequency bands in 5.8-9.2 GHz depending on the statuses of the photoconductive silicon switches, is meant for communication.

Mansoul *et al*., (2014) proposed a frequency selective reconfigurable antenna without sensing antenna for CR applications [88]. The proposed antenna consists of an inverted U shaped radiator fed by a fifty ohms microstrip line on the top of the substrate. On the bottom side of the substrate (i.e., ground plane), four horizontal slots, which are integrated with PIN diodes, act as reconfigurable filter to achieve frequency reconfigurability in 2.63-3.7 GHz.

Tawk *et al*., (2011) presented an optically controlled reconfigurable antenna system where laser diodes are integrated on the substrate of the antenna [89]. The proposed antenna system comprises different radiating elements that are connected by photoconductive switches. The laser diodes are utilized to shine light to those switches. The antenna system operates in three different states and a dual band is produced in each state. The three dual bands are produced in 3.2-8.6 GHz.

Augustin *et al*., (2012) proposed a planar antenna that consists of a CPW fed UWB sensing antenna operating at 2.6-11 GHz and a narrow band communication antenna operating at 4.9-6.2 GHz [90]. The narrow band communication antenna is integrated with the sensing antenna by utilizing the space between tapered slots, where surface current density is relatively low.

Aboufoul *et al*., (2012) presented a new UWB monopole antenna that has a reconfigurable multiband functionality. GaAs FET switches, which are used to connect stubs of different lengths to the fifty ohms feed line of the monopole antenna, are incorporated to achieve reconfigurability [91]. Moreover, they do not degrade the antenna gain, antenna efficiency, and radiation patterns since the biasing technique required for them is simple and does not require many biasing components. In UWB mode, all switches are in OFF state, the UWB monopole antenna operates at 2-11 GHz. In communication mode, three states are

investigated. The antenna operates at 2.1-2.6 GHz and 3.6-4.6 GHz in first and second states, respectively. Whereas the antenna operates at 2.8-3.4 GHz and 4.9-5.8 GHz in the third state.

Cheng *et al*., (2015) proposed a three-port MIMO antenna that consists of a wideband sensing antenna with a wide impedance bandwidth ranging from 2.2 GHz to 7 GHz and two identical reconfigurable antennas for communication to cover frequency bands from 2.3 GHz to 6.3 GHz [126]. The reconfigurability is obtained by tuning the capacitance of varactor diodes.

Hussain *et al.,* (2018) proposed an antenna system that consists of a frequency-agile four-element slot based MIMO antenna and an ultra-wideband (UWB) antenna for sensing the spectrum [127]. The impedance bandwidth of the UWB sensing antenna is 6.9 GHz (i.e., 0.75-7.65 GHz) and the frequency-agile four-element slot based MIMO antenna can be tuned in 1.77-2.51 GHz communicating band.

Alam *et al.,* (2018) proposed a four-port polarization diversity MIMO antenna that has two wideband antennas to sense the spectrum in 2.35-5.9 GHz and two reconfigurable NB antennas to tune to the desired frequency band in 2.6-3.6 GHz for interweave CR [128]. Wideband sensing antennas and reconfigurable NB antennas are located on the opposite sides of the substrate. The proposed MIMO antenna is planar and has volume of 80 mm × 80 mm× 1.6 mm. The maximum simulated gain and maximum radiation efficiency are reported as 5 dBi and 92%, respectively.

Zhao *et al.,* (2019) proposed an antenna system that operates either in UWB MIMO mode or reconfigurable MIMO mode by properly selecting the statuses of the varactor and PIN diodes [129]. In UWB MIMO mode, the two antennas sense the spectrum holes in 1-4.5 GHz wideband, while the same two antennas can be tuned in 0.9-2.6 GHz in reconfigurable MIMO mode.

Chacko *et al.,* (2015) proposed a two-element polarization diversity MIMO antenna with a switching capability between the wideband and narrowband modes [130]. The MIMO antenna has wide impedance bandwidth (i.e., 3.4-8.0 GHz) and narrow impedance bandwidth (i.e., 4.7-5.4 GHz) in wideband mode and narrowband mode, respectively. However, the antenna does not have tuning capability in the narrowband mode as the antenna resonates in a single frequency band (i.e., 4.7-5.4 GHz).

Hussain *et al.,* (2018) presented a novel integrated MIMO antenna system, which occupies an area of 50 × 110 mm^2 and comprises two inverted-F shape antennas that operate

at 2.45 GHz and two frequency-agile antennas to cover frequency bands in 1.73-2.28 GHz [131]. The annular slots are responsible for achieving the isolation between two inverted-F shape antennas and are made reconfigurable in 1.73-2.28 GHz with a minimum impedance bandwidth of 60 MHz by using varactor diodes. However, the MIMO antenna system does not have sensing antenna for spectrum sensing.

Hussain *et al.*, (2015) proposed a compact planar two-element reconfigurable MIMO antenna system that comprises wideband sensing antenna, which operates at 0.72-3.44 GHz and two frequency-agile antennas, which cover various frequency bands in 0.72-3.44 GHz with the help of PIN diode and varactor diode [132]. Along with the varactor tuning, the proposed MIMO antenna system reconfigurability uses two modes of selection to cover frequency bands especially below 1 GHz.

Hussain *et al*., (2015) presented four element meandered dual mode meandered F-shaped reconfigurable MIMO antenna for CR applications [133]. By utilizing PIN diodes and varactor diodes, frequency reconfigurability is attained. Moreover, the proposed antenna is compact and can be tuned to many frequency bands that are less than 1 GHz. By means of defected ground structures, isolation among the antenna elements is enhanced significantly. Since the proposed MIMO antenna operates in two modes, it covers frequency bands in 743-1240 MHz in one mode and 2.4 GHz in other mode with a minimum bandwidth of 60 MHz.

Hussain *et al.,* (2018) proposed a novel and compact 4-element reconfigurable CR MIMO antenna system without sensing antenna to cover frequency bands from 1.32-1.49 GHz and 1.75-5.2 GHz [134]. The four antenna elements are designed by etching the pentagonal slots in the ground plane. They are loaded reactively to achieve frequency reconfigurability. Each antenna element operates in three frequency bands due to the proper capacitive reactance loading. Despite the antenna is compact, the mutual coupling is just less than -12 dB.

Alam *et al.,* (2019) proposed a four port CR MIMO antenna that works for overlay and underlay approaches for 5G applications in 2.5-4.20 GHz range [135]. This type of feature of the proposed antenna is obtained by controlling the operating modes of the multifunctional reconfigurable filter since the multifunctional reconfigurable filter, which works in three operational modes such as tunable bandpass filter, tunable band reject filter, and all pass filter, is integrated with UWB sensing antenna.

Riaz *et al*., (2019) proposed a new frequency agile MIMO patch antenna for CR applications [136]. The proposed antenna system comprises two patch antenna elements, which are hexagonal shaped. To achieve compactness and isolation between the antenna elements, hexagonal-shaped defected ground structures are incorporated in the ground plane. The compactness is further attained by utilizing reactive loading. Varactor diodes are employed in the microstrip feedline to achieve frequency reconfigurability. Consequently, frequency tuning is achieved in 1.42-2.27 GHz. However, the proposed MIMO antenna does not have a sensing antenna to sense the spectrum.

Hussain *et al*., (2019) presented a frequency reconfigurable MIMO antenna system for interweave CR applications [137]. The proposed MIMO antenna comprises four reconfigurable antenna elements that are pentagonal slot-based. Varactor diodes are employed to alter the capacitance of the slot. As a result, wide tuning range, which ranges from 3.2 GHz to 3.9 GHz, is achieved with a minimum of 100 MHz bandwidth in each band. However, the proposed MIMO antenna does not have a sensing antenna to sense the spectrum. Also, the mutual coupling among the antenna elements is just less than -10 dB.

2.12. Conclusion

It is obvious from the literature survey that the antenna design for cognitive radio applications and cognitive radio MIMO applications is a well-researched topic. However, it is still in an infant stage since most of the antenna designs in the literature survey are reconfigurable antenna designs, which are complex and difficult to implement in practice. Moreover, all the antenna designs for CR MIMO applications in the literature can perform only one communication task. So, this thesis presents the antenna designs that overcome the above said drawbacks.

Chapter-3

Super Wideband Apollonius Circles Based Fractal Antenna for UWB and SWB Applications

3.1. Introduction

To sense the spectrum holes continuously in a cognitive radio model, a wideband antenna, which is generally an UWB antenna or a SWB antenna, is required. So, this chapter presents a very small printed monopole antenna for UWB and SWB applications as a first contribution of this thesis. An Apollonius fractal with nested Apollonius circles is utilized to generate multiple resonances over the entire bandwidth. The 50 ohm microstrip feed line is tapered to achieve good impedance matching at the low frequencies. Two semi-circular notches and a notch in the ground plane are incorporated to enhance the impedance bandwidth at high frequencies. The antenna's bandwidth ratio is 20:1 and its operating bandwidth ranges from 3 GHz to 60 GHz.

3.2. Antenna Design

Usually, a circle is defined as the group of all points P at a constant distance r (circle's radius) from a fixed point (circle's centre). As per Apollonius's definition, as shown in Fig. 3.1a, it is defined as group of points P that are in accordance with the rate given [67] as

$$\frac{SP}{QP} = \frac{ST}{TQ} \tag{3.1}$$

As shown in Fig. 3.1b, to generate multiband behaviour, three Apollonius circles are made inside of each other by taking their reference triangles satisfying the relation given in [67].

$$\frac{S1P1}{P1Q1} = \frac{S1S2}{S2Q1} \quad \frac{S2P2}{P2Q2} = \frac{S2S3}{S3Q2} \quad \frac{S3P3}{P3Q3} = \frac{S3S4}{S4Q3} \tag{3.2}$$

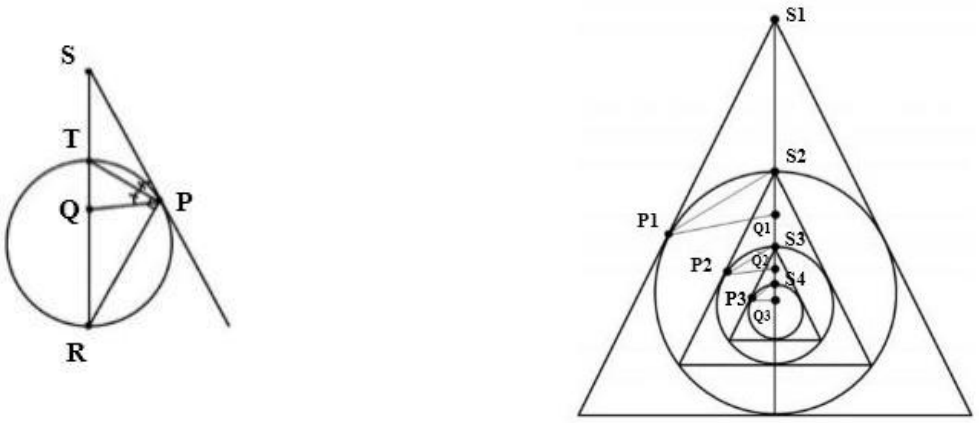

(a) (b)

Fig. 3.1. Apollonius circle (a) Apollonius's definition of circle (b) Generation of Apollonius fractal with nested Apollonius circles

Table 3.1. Optimized dimensions of the designed antenna

Dimension	**mm**	**Dimension**	**mm**
ls	19	ws	31
lg	13	lf	13.87
a	12.67	ln	1
b	6.3	wn	2
c	3.16	d1	2
d	8.5	d2	2
e	4.252	w1	7
f	2.127	w2	7
g	1.06	wf	3.4

The designed antenna's configuration is depicted in Fig. 3.2 and its optimized dimensions are mentioned in Table 3.1. Low cost and lossy FR-4 epoxy substrate that has ε_r of 4.4, loss tangent (Tanδ) of 0.018 and height of 1.6mm is used. In the proposed structure, nested Apollonius circles concept is utilized to get multiband behaviour. As circular radiator is better than any other shaped radiator in terms of bandwidth, it is chosen in this design. As illustrated in Fig. 3.3, the antenna's design process is explained in seven steps. Initially, a circular radiator is fed

by a strip line of impedance 50 Ohms and a triangular slot is made inside the patch. By taking that triangle as reference, three Apollonius circles are nested in the later steps.

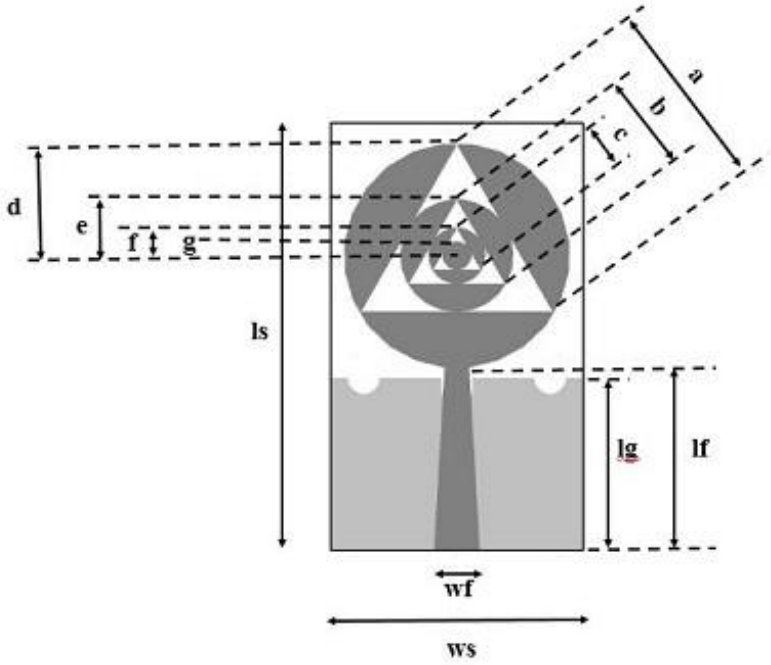

(a)

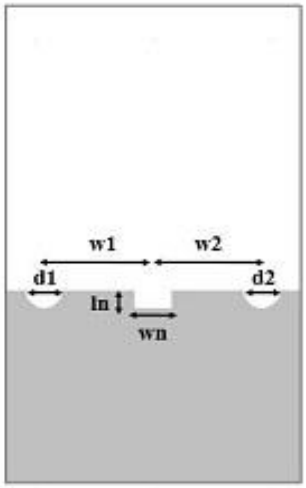

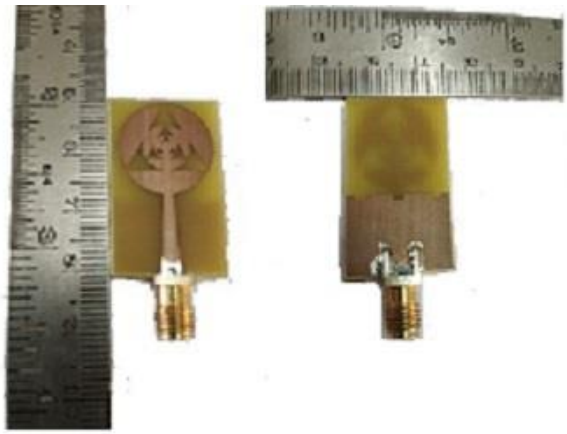

(b) (c)

Fig. 3.2. Geometry of the proposed antenna (a) Front view (b) Back view (c) Prototype of the designed antenna

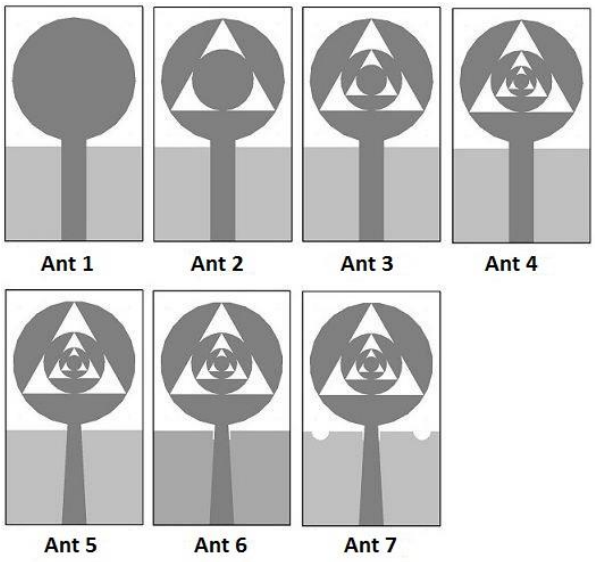

Fig. 3.3. Intermediate steps in the design

3.2.1. Effect of the Increased Number of Iterations

It is generally expected that bandwidth can be improved as iterations are increased. This is due to the self-similarity property of the fractals. However, as iterations are increased, complexity also increases. It is quite evident from the Fig. 3.4 that significant improvement in the bandwidth at high frequencies is observed with the increased number of iterations. However, the reflection coefficient is not less than -10 dB at some frequencies that are below 20 GHz.

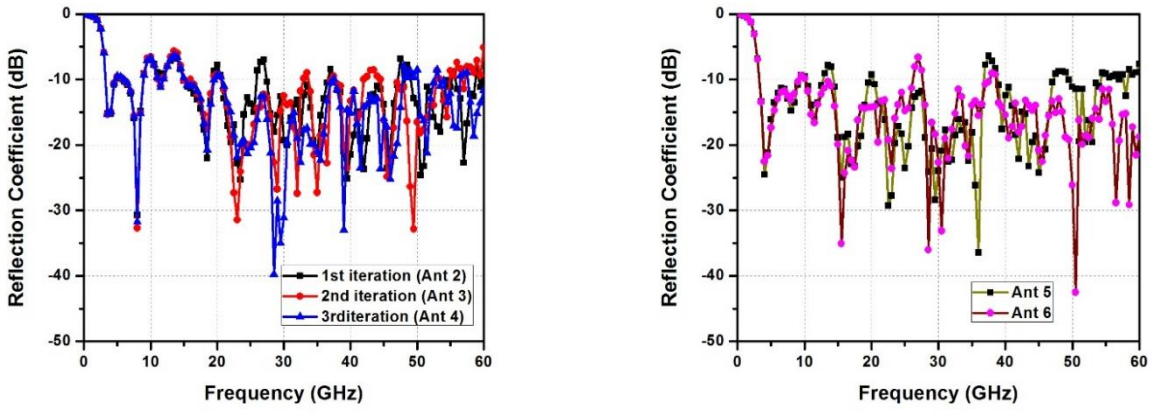

(a) (b)

Fig. 3.4. Reflection coefficient vs frequency in the intermediate steps of the design

As there is no considerable improvement in the reflection coefficient after three iterations and keeping the fabrication difficulties in mind, further iterations are not considered.

3.2.2. Effect of Tapered Strip Line and Notches in the Ground Plane

A tapered strip line is used to achieve impedance matching at 10 GHz and 13.5 GHz. Moreover, a smooth current flow is provided by this tapered feed line. By incorporating a rectangular notch in the ground, some additional resonances are excited at high frequencies, i.e., from 47 GHz to 60 GHz. Capacitive effect is introduced due to the presence of a pair of semicircular notches, thus exciting an additional resonance at 37 GHz. Thus, the mismatch between the radiator and the feed line is eliminated by the modified ground plane, which neutralizes the radiator's inductive effect by producing the capacitive effect. This results in reflecting a pure resistive impedance of 50 ohms approximately at the input terminals. All conductors are considered to be perfect during simulation.

3.3. Results and Discussions

The measured reflection coefficient and VSWR plots shown in Fig. 3.5 and Fig. 3.6 are compared with the simulated results for the experimental validation by using network analyzer which works from 10 MHz to 25 GHz. Since the maximum operating frequency of the network analyzer is 25 GHz, comparison between the simulated and measured results are shown till 25 GHz even though the designed antenna works till 60 GHz. From Fig. 3.5, it is observed that the reflection coefficient is less than -10 dB all over the band except at some frequencies. These discrepancies between the simulated and experimental results could be due to errors in manufacturing, poor quality of SMA connectors, and environmental conditions during measurements.

Resonances occur at 3.8 GHz, 5.4 GHz, 7.4 GHz, 9.4 GHz, 11.4 GHz, and 12.8 GHz in the measured result. Impedance matching is perfect when the feed line's impedance and antenna impedance are of 50 ohms. Wherever the reactive part of the antenna impedance is zero, the real part of the impedance is nothing but the antenna impedance at that resonant frequency.

In Fig. 3.7a, the real and imaginary parts of the reflected impedance at the input terminals of the antenna by considering the radiator as load is plotted. Over the entire operating band, the real part of the impedance fluctuates between 25 Ohms and 77 Ohms. Similarly, the magnitude of the input impedance also varies between 25 Ohms and 77 Ohms, as shown in Fig. 3.7b. As it varies around 50 ohms, good impedance matching is achieved between the

antenna structure and the SMA connector of impedance 50 Ohms. Thus, the reflections are greatly reduced at the input port of the antenna.

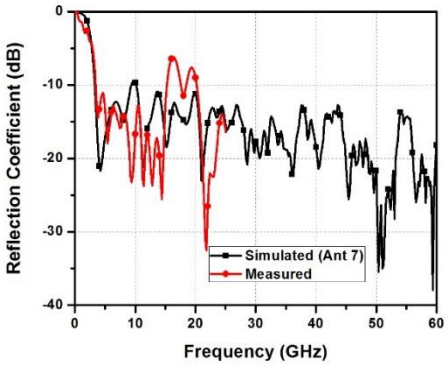

Fig. 3.5. Plot of the simulated and measured reflection coefficient vs frequency

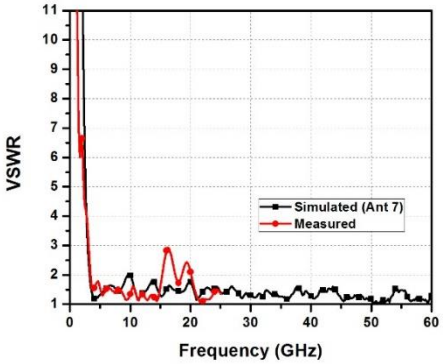

Fig. 3.6. Plot of the simulated and measured VSWR vs frequency

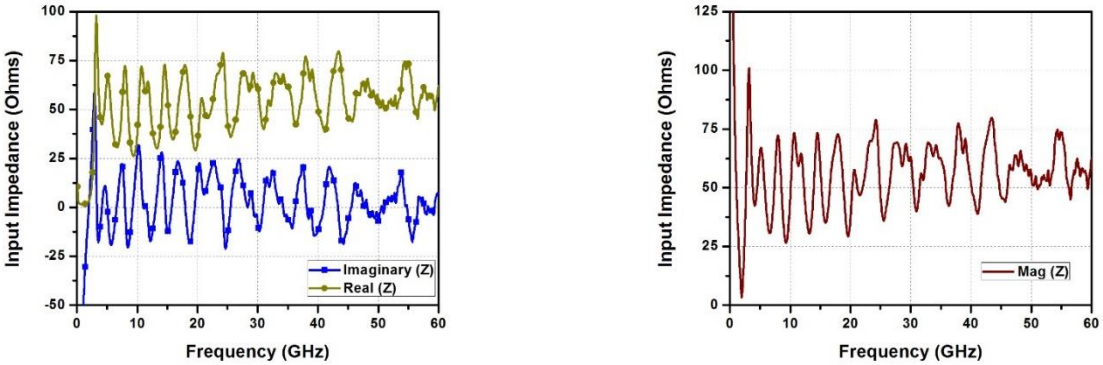

(a) (b)

Fig. 3.7. Input impedance (a) Real and imaginary parts (simulated) (b) Magnitude of the Input Impedance (simulated)

Table 3.2. Comparison between the proposed antenna and other SWB antennas

Antenna	**Dimension**	**Bandwidth**		**BDR**	f_L, **GHz**
		Ratio (:1)	**%**		
[29]	$0.23\lambda \times 0.33\lambda$	20.41	181	2461	2.18
[30]	$0.32\lambda \times 0.34\lambda$	11	166	1531	3.4
[31]	$0.24\lambda \times 0.32\lambda$	32	188	244	2.5
[32]	$2\lambda \times 2\lambda$	5	133	33	10
[33]	$0.23\lambda \times 0.25\lambda$	17.89	179	3015	3.8
[34]	$0.26\lambda \times 0.24\lambda$	30	187	2996	5
[68]	$0.37\lambda \times 0.34\lambda$	34.88	189	1473.1	0.86
[37]	$0.35\lambda \times 0.20\lambda$	11.60	168	2386	3
[69]	$0.35\lambda \times 0.23\lambda$	22.10	183	2168	0.79
[70]	$0.36\lambda \times 0.36\lambda$	34.72	189	1457	0.72
[38]	$0.47\lambda \times 0.31\lambda$	10.16	164	1103	3.15
[71]	$0.55\lambda \times 0.38\lambda$	11.67	168	806	3
[72]	$0.45\lambda \times 0.45\lambda$	19.4	180	891	1
[73]	$0.41\lambda \times 0.29\lambda$	9.11	160	1347.23	3.5
[74]	$0.30\lambda \times 0.23\lambda$	9.81	163	2393.64	2.26
[75]	$0.32\lambda \times 0.27\lambda$	10.66	165	1948.43	2.7
designed	$\mathbf{0.19}\lambda \times \mathbf{0.31}\lambda$	**20**	**181**	**3073**	**3**

A comparison table is provided by comparing the proposed antenna with the previously reported monopole antenna structures designed so far in terms of bandwidth range, dimensions and bandwidth ratio in Table 3.2. The proposed one has many advantages like huge impedance bandwidth, compact in size and good bandwidth ratio over previously reported SWB antennas. Bandwidth Dimension Ratio (BDR) [31] is one of the important parameters for a SWB antenna. It indicates the impedance bandwidth per unit area. Its formula is given below

$$\text{BDR} = \frac{\%\, Bandwidth}{\lambda_{length} \times \lambda_{width}} \tag{3.3}$$

where λ_{length} and λ_{width} are the length and width of the antenna calculated in terms of the wavelength of the lower most frequency in operating bandwidth of the antenna, respectively.

3.3.1. Patterns, Peak Gain, and Efficiency

The setup for measuring radiation patterns of the proposed antenna is shown in Fig. 3.8. As shown in Fig. 3.8, the entire antenna structure lies in x-axis of X-Y plane while pointing in $\emptyset = 0^0$. To measure the radiation patterns in both E-plane (X-Z plane) and H-plane (Y-Z plane), elevation angle (θ) is varied from 0^0 to 360^0.While taking radiation pattern measurements, pyramidal horn antenna is used as a transmitting antenna. The designed antenna in receiving mode is kept in a far-field region and connected to a coaxial detector. At some frequencies, the simulated and measured co-polar and cross-polar radiation patterns in both E-plane and H-plane are illustrated in Fig. 3.9. It is noticed that at low frequencies, i.e., < 10 GHz, co-polar radiation patterns are bidirectional in E-plane and omnidirectional in H-plane. At high frequencies, i.e., > 10 GHz, patterns acquire distorted omnidirectional patterns in both the planes. The reason behind this is higher order modes are excited and radiation due to feed line at high frequencies. At 5 GHz, the maximum cross-polar pattern levels are found to be -38 dB and -34 dB approximately in E-plane and H-plane, respectively.

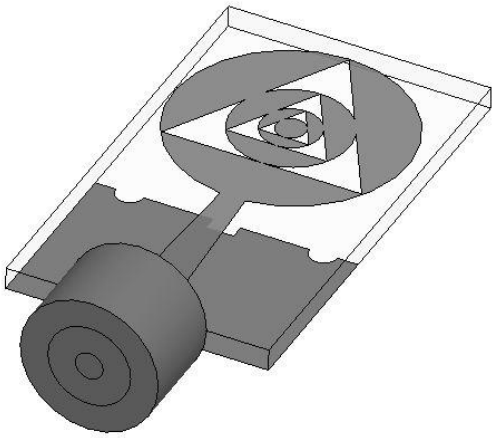

Fig. 3.8. Radiation pattern setup for measurement

However, cross polar level rises significantly at high frequencies (e.g., at 25 GHz) as hybrid modes are excited at those frequencies. From Fig. 10a, a minimum difference of 40 dB is

observed between both simulated and measured co-polar and cross polar radiation patterns at 5 GHz in both the planes. But at high frequencies, the minimum difference level decreases to 0 dB. It can be seen that the magnitude of co-polar patterns are less than the magnitude of cross-polar pattern at some angles.

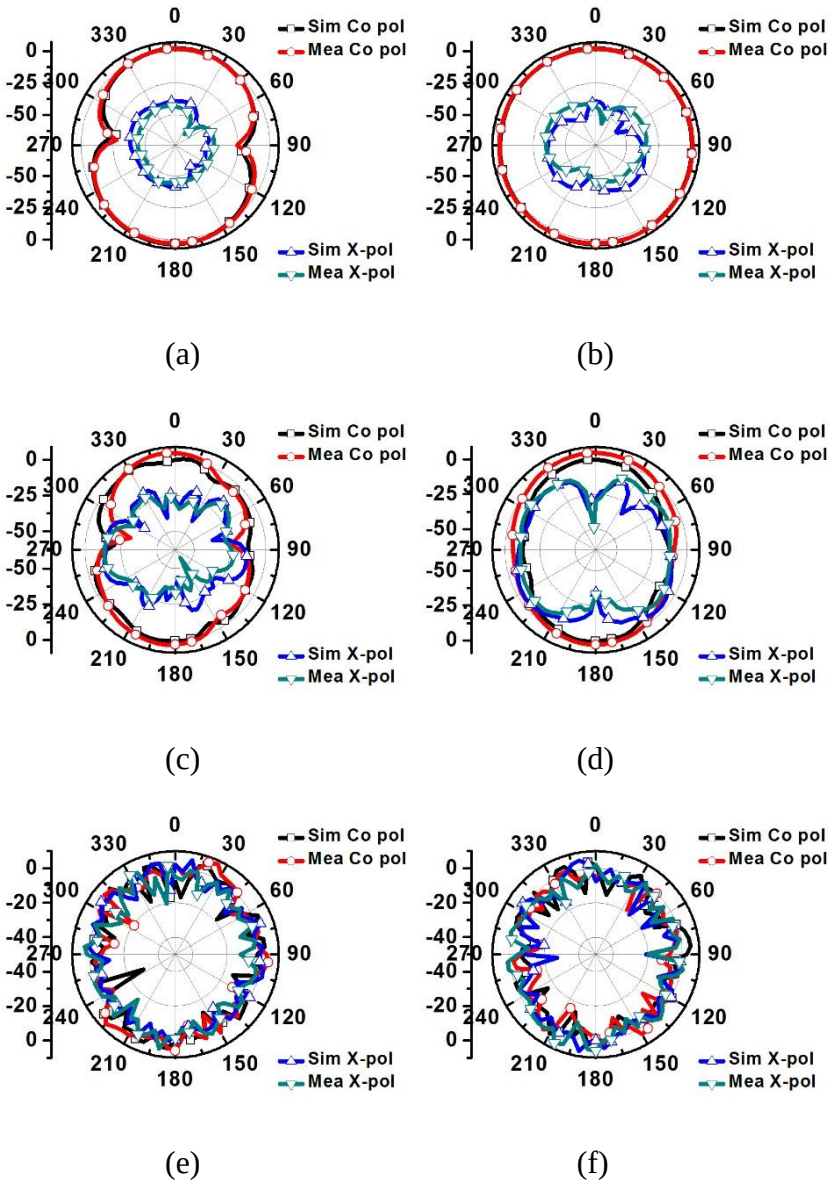

Fig. 3.9. (a) E-plane at 5 GHz (b) H-plane at 5 GHz (c) E-plane at 10 GHz (d) H-plane at 10 GHz (e) E-plane at 25 GHz (f) H-plane at 25 GHz

Fig. 3.10 shows the plot of both simulated and measured peak gain characteristics of the proposed antenna. It demonstrates that peak gain increases with the increase in frequency. The reason for this is the dimensions of the radiator at high frequencies are too larger than their corresponding wavelengths. This results in the enhancement of the peak gain. The measured

maximum and minimum peak gains are 11.5 dBi and 1.5 dBi at frequencies 30 GHz and 3GHz, respectively.

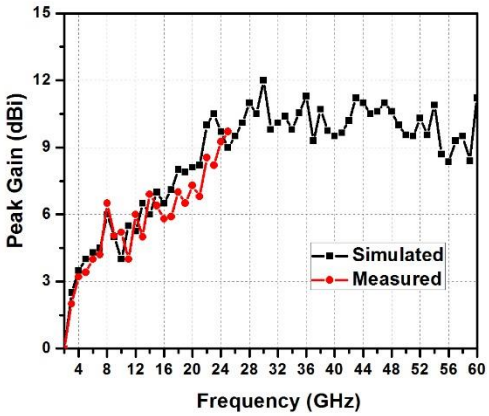

Fig. 3.10. Peak gain (dBi) vs frequency (GHz) of the designed antenna

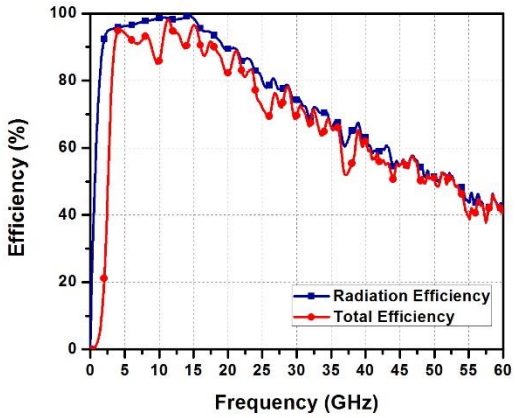

Fig. 3.11. Efficiency plot of the designed antenna

The other parameter to be considered in analysing frequency domain performance is efficiency. A plot containing radiation efficiency and total efficiency of the proposed antenna is depicted in Fig. 3.11. Radiation efficiency is nothing but the efficiency of the antenna without taking the losses in to account. Generally, these losses occur due to the reflections at the input port, dielectric of the substrate and conductors. All these losses are considered while calculating the total efficiency of the antenna.

Throughout the operating band, the efficiencies are greater than 40% as demonstrated in Fig. 3.11, which is acceptable for a small antenna. It can be observed from Fig. 3.11 that

radiation efficiency and total efficiency of the designed antenna become low as frequency increases.

3.3.2. Surface Current Distributions

The surface current density at a few frequencies are shown in Fig. 3.12.

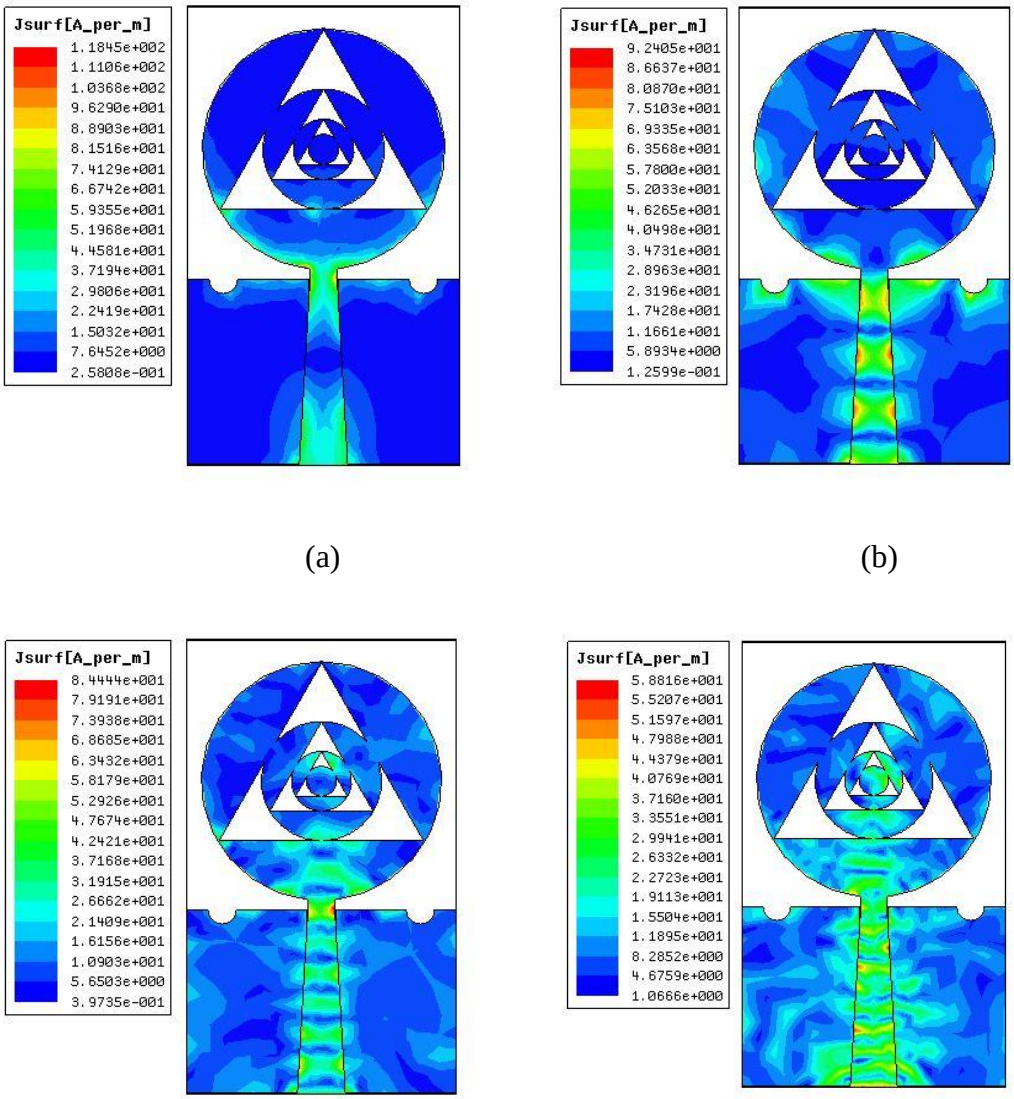

Fig. 3.12. Surface current density of the designed antenna at (a) 5 GHz (b) 20 GHz (c) 34 GHz (d) 50 GHz

As shown in Fig. 3.12, maximum current densities at 5 GHz are observed at the junction of the circular radiator, the feed line, and some portions of the circular radiator, whereas it is uniformly distributed at other portions. At 15 GHz, current density is more concentrated at the

edges of the feed line, edges of the ground plane, and around the semi-circular grooves of the ground plane. Whereas at 34 GHz and 50 GHz, it is more concentrated at some portions on the circular radiator, the ground plane and at the edges of the feed line. Radiation is mainly due to those portions, where the current density is maximum.

3.3.3. Time Domain Analysis

For traditional applications, the characteristics like reflection coefficient, VSWR, radiation patterns and gain are adequate to assess the performance of the antenna in frequency domain. However, for applications like GPR (Ground Penetrating Radar), short range indoor data transmission with high speed, a narrow pulse signal (Gaussian pulse) is used for transmitting and receiving of the signals. Hence, the time domain analysis of the antenna is very crucial and inevitable for UWB and SWB applications. This is carried out by using CST Microwave Simulator software. The designed two identical antennas are placed at a distance of 30 cm in two configurations. The two configurations considered are face to face and side by side. One of the antennas are excited by a normalized Gaussian pulse of duration in hundreds of picoseconds.

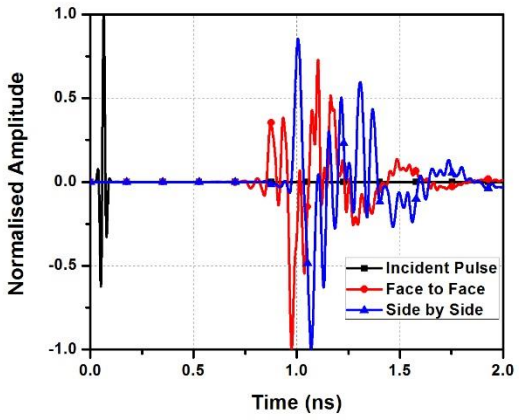

Fig. 3.13. Normalized incident and received pulses in both the configurations

Fig. 3.13 shows the normalized transmitted and received pulses in both the configurations. To compare the similarity between the input signal given to antenna and the received signal in the far-field region, fidelity factor is determined. It is calculated by using the expression [31] given below as

$$\text{Fidelity factor} = \text{maximum}\left[\frac{\int_{-\infty}^{\infty} x_1(t)x_1(t+T)dt}{\int_{-\infty}^{\infty}|x_1(t)|^2 \int_{-\infty}^{\infty}|x_2(t)|^2}\right] \quad (3.4)$$

where $x_1(t)$ and $x_2(t)$ are transmitted and received signals, respectively. T is the delay considered to maximize the numerator. In ideal case, the value of the fidelity factor is equal to 1. It is found that the fidelity factors are 78.03% and 73.25% in face-to-face and side-by-side configurations, respectively. To check the reception of the pulses at the other antenna, the parameters like group delay, isolation between two antennas and phases in the far-field are investigated.

A constant group delay indicates the linearity in the phase which is needed to avoid distortion in the waveform. The mathematical expression to find out the group delay [29] is given as

$$\tau_g = \frac{-d\varphi(\omega)}{d\omega} \tag{3.5}$$

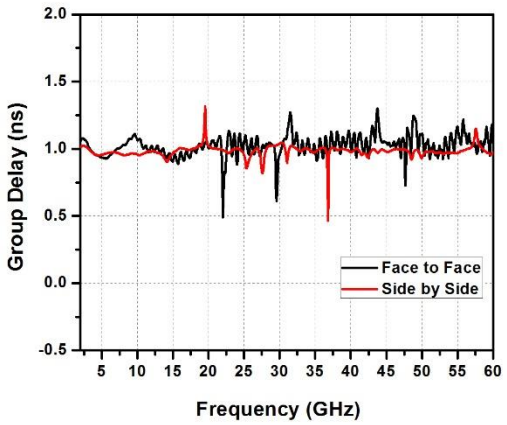

Fig. 3.14. Group delay characteristics of both the configurations

From Fig. 3.14, it is observed that ringing in the tail is a little more in the received pulse when antennas are kept in side-by-side configuration. The reason behind this is the entire radiating surface is open to the receiving signal in face-to-face configuration. As the radiation is in the broadside direction in this case, the signal can be smoothly received in face-to-face configuration. Whereas the radiation exists in end fire direction in side-by-side configuration. It can be seen from Fig. 3.14 that the variations in the group delay are less than 1ns. This ensures the linearity of the phase in the far-field region.

Besides this group delay, the phase responses and transmission loss S_{21} in dB are depicted in Fig. 3.15 and Fig. 3.16, respectively.

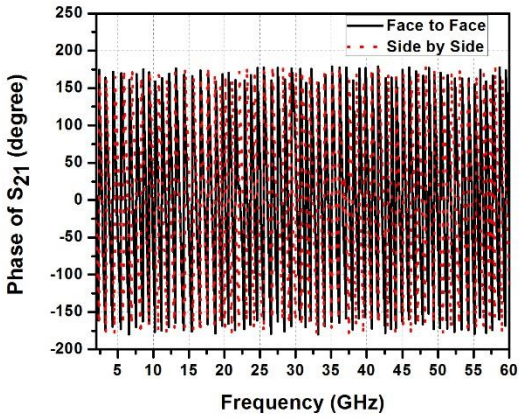

Fig. 3.15. Phase of S_{21} in both the configurations

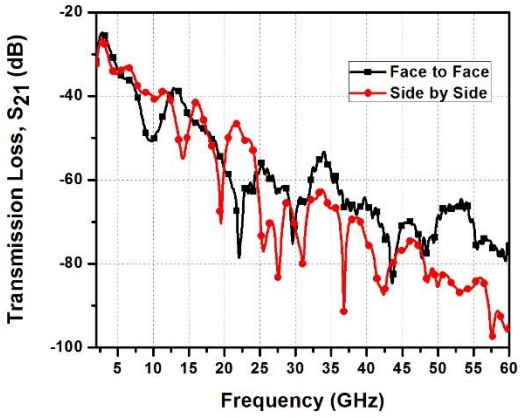

Fig. 3.16. Transmission loss in both the configurations

It is quite evident from the Fig. 3.15 that the phases are linear in the far-field region for both the configurations. As demonstrated in Fig. 3.16, a good isolation of better than 25 dB is noticed in both the configurations. In face to face configuration, the transmission loss varies from -25 dB to -50 dB and -50 dB to -75 dB in 3-18 GHz and 18-55 GHz, respectively except at six peaks of -79 dB, -77 dB, -84 dB, -79 dB, -78 dB and -76.5 dB at 22 GHz, 29.5 GHz, 44 GHz, 47.5 GHz, 48 GHz and 49.5 GHz, respectively. It is less than -75dB at frequencies that are greater than 55 GHz.

While in side by side configuration, the transmission loss varies from -25 dB to -50 dB in 3-22.5 GHz except at two peaks of -55 dB and -70 dB at 14.5 GHz and 19.7 GHz, respectively. It varies from -50 dB to -75 dB in 22.5-47 GHz except at five peaks of -78 dB, -83 dB, -80 dB, -90 dB and -84 dB at 25 GHz, 27.5 GHz, 31 GHz, 36.5 GHz and 42.5 GHz. It is less than -75 dB at frequencies that are greater than 47 GHz.

3.4. Conclusion

In this chapter, by utilizing the Apollonius fractal with nested Apollonius circles, a compact SWB antenna for both UWB and SWB applications has been designed. It has been compared with the other SWB antennas which were presented in the previous literatures in terms of BDR, size, and percentage bandwidth. It covers Ku, K, Ka and V bands in which their applications in communications are not explored so far. Since it covers frequencies from 3 GHz to 60 GHz, it is also useful for spectrum sensing in cognitive radio applications.

Chapter-4

Frequency Reconfigurable Nine Port MIMO Antenna with Polarization Diversity for CR applications

4.1. Introduction

The high data rates wireless devices with efficient spectrum utilization are grabbing more attention as they have become crucial in the present day wireless communication. As MIMO systems provide high data rates and CR technology utilizes the spectrum efficiently, MIMO systems with CR technology are treated as promising systems to attain high data rates and utilize the spectrum efficiently.

In this chapter, a nine port planar antenna, which consists of one wideband antenna for sensing and eight similar reconfigurable antennas for performing communication tasks, is presented for cognitive radio (CR) multiple input multiple output (MIMO) applications. The sensing antenna operates at 1.8-10 GHz, whereas the reconfigurable antenna for communication operates at any one of five frequency bands (i.e., 1.77-1.95 GHz, 1.9-2.15 GHz, 2.19-2.45 GHz, 2.63-3.02 GHz, 3.19-3.84 GHz, and 3.82-5.16 GHz) based on the ON and OFF statuses of the p-type intrinsic n-type (PIN) diodes. In all operating states of the reconfigurable antenna, the isolation between the sensing antenna and any reconfigurable antenna is more than 15dB, while the isolation is more than 14 dB between every two similar reconfigurable antennas. Validation of the proposed cognitive radio MIMO antenna is done by achieving a close match between the simulated and experimental results. The proposed MIMO antenna for CR applications in this chapter not only performs multiple communication tasks concurrently but also acts as a

dynamic n-element MIMO antenna system, where n is a variable that depends on the number of detected spectrum holes. When 1, 2, and 4 spectrum holes are identified, the proposed antenna system acts as 8-element, 4-element, and 2-element MIMO antennas, respectively. When 3 spectrum holes are identified, the proposed MIMO antenna system acts as 2-element with any two of the eight reconfigurable antennas terminated with matched impedance of 50 Ohms. Moreover, polarization diversity is also attained by the MIMO antenna designed on FR-4 substrate as some of the reconfigurable antennas for communication are linearly polarized in +X, -X, +Y, and –Y directions.

The remaining contents of this chapter are structured as follows: The design procedure of the wideband sensing antenna is described in Section 4.2. The design methodology of the reconfigurable antenna that is used in the designed MIMO antenna system is given in Section 4.3. The final design of the nine port MIMO antenna and its measurement results are elucidated in Section 4.4. The conclusion of this chapter is given in Section 4.5.

4.2. Design Procedure of the Sensing Antenna

The sensing antenna, which has a wide bandwidth that ranges from 1.8 GHz to10 GHz, is shown in Fig. 4.1a. As seen in Fig. 4.1b, the design process of the sensing antenna is completed in seven stages. A conventional monopole antenna with partial ground plane (i.e., Ant I), which produces a wide bandwidth (i.e., 2.6-10 GHz), is designed in the first step, as shown in Fig. 4.1b. A circular patch of radius 5.28 mm is merged with the circular patch of radius 8.78 mm in the second stage to shift the lower cut-off frequency to left side, as shown in Fig. 4.1b. Fine impedance matching is attained in two frequency bands (i.e., 2.25-3 GHz and 5.75-10.4 GHz) with the configuration of Ant II, as seen in Fig. 4.1c. In the third stage, another circular patch of radius 4 mm is merged with the radiator of the Ant II to further shift the lower cut-off frequency to left side, as depicted in Fig. 4.1b. It can be noticed from Fig. 4.1c that the good impedance matching is obtained with the geometry of Ant III in the frequency bands, i.e., 2.07-2.55 GHz, 4.3-8.1 GHz, and 8.8-10.8 GHz.

In the fourth stage, another circular patch of radius 3 mm is merged with the radiator of Ant III, as shown in Fig. 4.1b. It is obvious from Fig. 4.1d that a fine impedance matching is attained with the geometry of Ant IV in 2-2.31 GHz, 4-7.65 GHz, and 8.82-10 GHz. To obtain the lower cut off frequency less than 2 GHz, a circular patch of radius 2 mm is merged with the radiator of Ant IV, as shown in Fig. 4.1b. Reflection coefficient curve of Ant V is less than -10

dB in 1.94-2.21 GHz, 3.8-4.67 GHz, 5.25-7.33 GHz, and 8.28-9.61 GHz, as depicted in Fig. 4.1d.

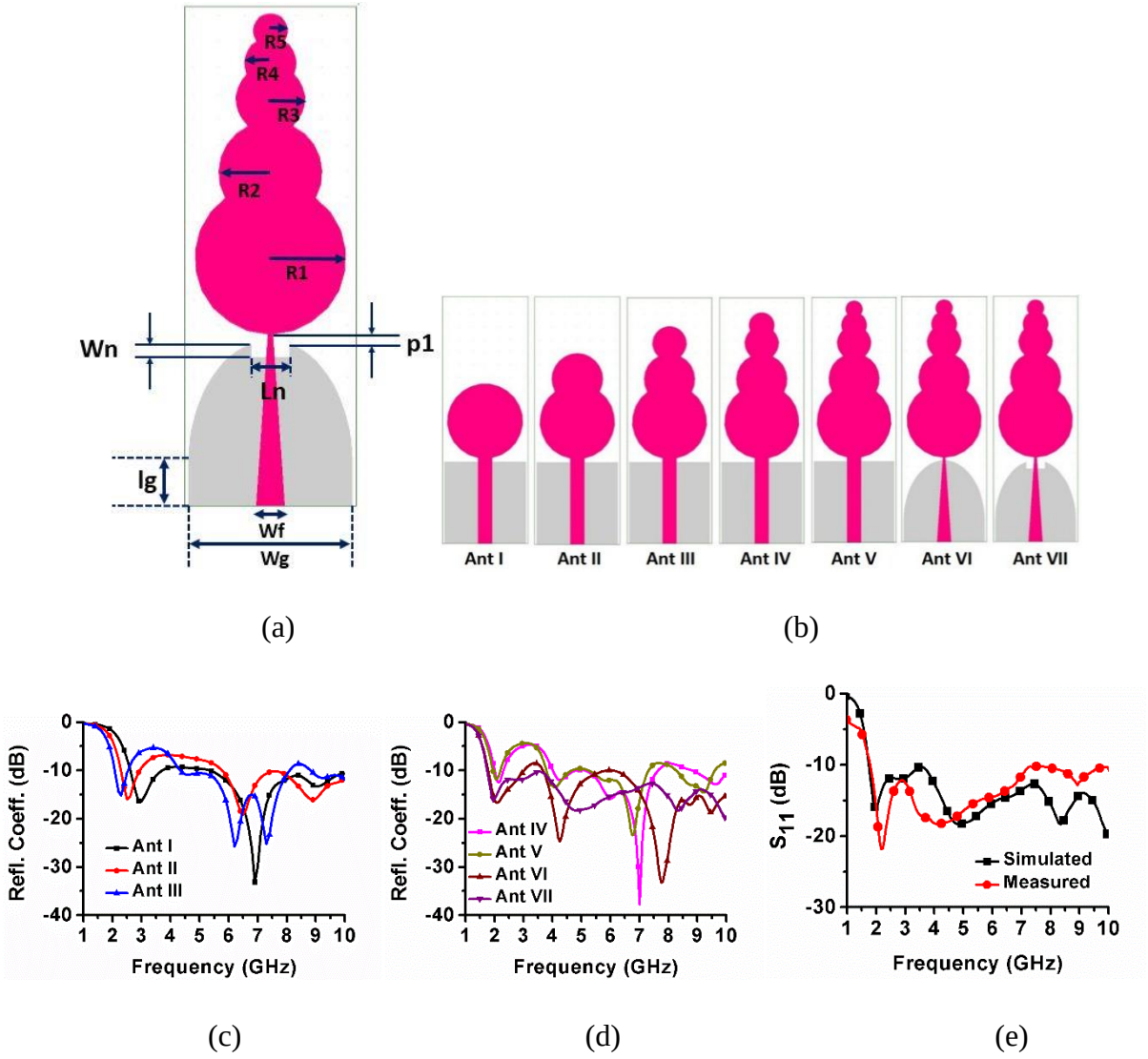

Fig. 4.1. Sensing antenna (a) Geometry of the sensing antenna (b) Evolution of the sensing antenna (c) Reflection coefficients of Ant I, Ant II, and Ant III (d) Reflection Coefficients of Ant IV, Ant V, Ant VI, and Ant VII (e) Plot of S_{11}

Since the sensing antenna should have a wide impedance bandwidth to sense the wide range of frequencies, rectangular shaped ground plane is modified to a semi-elliptic shaped ground plane, as depicted in Ant VI of Fig. 4.1b. Thus, a fine impedance matching is attained from frequencies that are greater than 1.8 GHz except in 3.01-3.68 GHz, as seen in Fig. 4.1d. In the last stage, to achieve good impedance matching in 1.8-10 GHz, a rectangle shaped notch is employed the ground plane, as depicted in Ant VII of Fig. 4.1b. Hence, as shown in Fig. 4.1d,

reflection coefficient of Ant VII is less than -10 dB in the bandwidth that ranges from 1.8 GHz to 10 GHz. The reflection coefficient of the sensing antenna accessed at port 1 is depicted in Fig. 4.1e. The dimensions of the wideband sensing antenna are given in Table 4.1.

Table 4.1. Dimensions of the sensing antenna

Parameter	**mm**	**Parameter**	**mm**
R1	8.78	Lg	5
R2	5.28	Wg	18.98
R3	4	Wf	3.3
R4	3	Ln	4.5
R5	2	Wn	1.57
p1	1.16		

4.3. Design Procedure of the Reconfigurable Antenna

A reconfigurable monopole antenna with bent microstrip line feeding shown in Fig. 4.2a is designed to operate at different frequencies depending on the statuses of the PIN diodes used.

The circuit equivalents in ON and OFF states of BAR64-03w PIN diode in HFSS are shown in Fig. 4.2b. Biasing voltage of 3 V is given to diodes externally. 100 nH is used to choke RF signals and 470 pF capacitor is used to short the RF signals that come from external bias. D1, D2, D3, and D4 are ON and the remaining diodes are OFF in the first operating state, so the current flow mainly occurs in the strips of lengths 4.25 mm, 4.05 mm, 4 mm, and 7.35 mm, thus resulting in a resonance at 1.85 GHz, as shown in Fig. 4.2c. As this structure of the reconfigurable antenna provides the longest current path, the reconfigurable antenna resonates at the lowest frequency. In the second operating state, D2, D3, and D4 are ON and the remaining diodes are OFF, so the current that flows in the strips of lengths 4.05 mm, 4 mm, and 7.35 mm through the diodes generates resonance at 2.05 GHz, as depicted in Fig. 4.2d. In the third operating state, D3 and D4 are ON and the remaining diodes are OFF, so the current mainly flows in the strips of lengths 4 mm and 7.35 mm, thereby generating a resonance at 2.3 GHz, as shown in State II of Fig. 4.2e. Only D4, D5, and D6 are ON in the fourth, fifth, and sixth operating states, respectively.

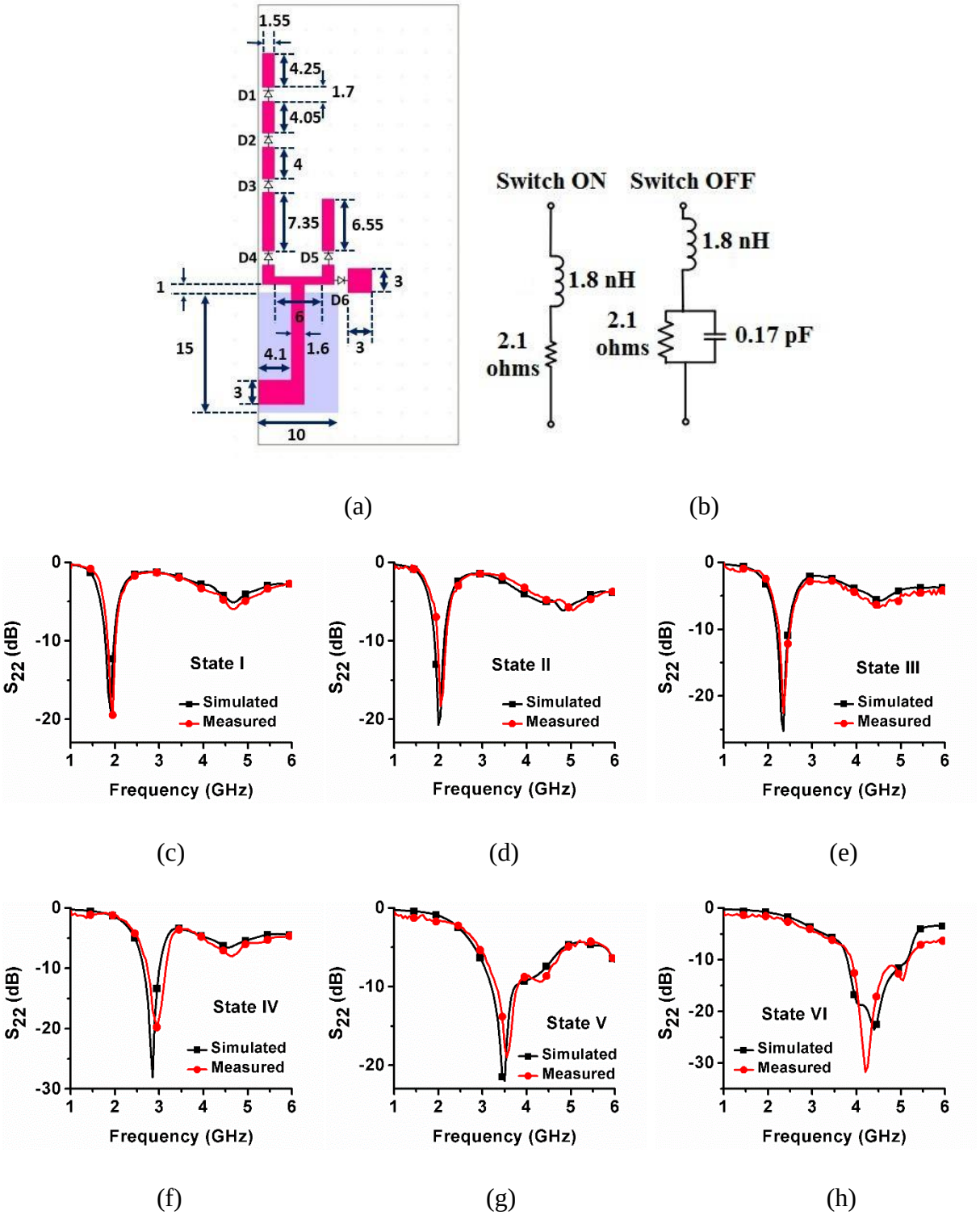

Fig. 4.2. Reconfigurable antenna (a) Geometry of the reconfigurable antenna (b) R-L-C equivalent of the PIN diode (c) Plot of S_{22} in State I (d) Plot of S_{22} in State II (e) Plot of S_{22} in State III (f) Plot of S_{22} in State IV (g) Plot of S_{22} in State V (h) Plot of S_{22} in State VI

The radiating strips of lengths 7.35 mm, 6.55 mm, and 3 mm are alone responsible for the resonances in the fourth, fifth, and sixth operating states, respectively. The impedance bandwidths in the fourth, fifth, and sixth operating states are 0.39 GHz (i.e., 2.63-3.02 GHz), 0.65 GHz (i.e., 3.19-3.84 GHz), and 1.34 GHz (i.e., 3.82-5.16 GHz), respectively, as shown in Fig. 4.2f, Fig. 4.2g, and Fig. 4.2h. The dimensions of the reconfigurable communication antenna are tabulated in Table 4.2.

Table 4.2. Dimensions of the reconfigurable communication antenna

Parameter	**Mm**	**Parameter**	**mm**
L1	4.25	L7	2.5
L2	4.05	L8	6
L3	4	Lg1	15
L4	7.35	Wg1	10
L5	6.55	Wf1	3
L6	3	lf1	4.1
W1	1.55	Wc	1.6
W2	3	p2	1

The surface current densities of the reconfigurable communication antenna are illustrated in Fig. 4.3. The resonating lengths of the reconfigurable communication antenna are assessed from the portions of the antenna, where maximum surface current densities exist since resonances are excited due to those portions. It can be seen from Fig. 4.3 that maximum surface current densities exist on the strips of lengths ($\frac{L1}{2}$ + L2 + L3 + L4 + L7 + L8), (L2 + L3 + L4 + L7 + L8), (L3+ L4 + L7 + L8), (L4 + L7 + L8), and ($\frac{2L5}{3}$ + L7 + L8) in States I, II, III, IV, and V, respectively. So, the resonating lengths of the reconfigurable communication antenna in States I, II, III, IV, and V are expressed as shown in equations 4.1, 4.2, 4.3, 4.4, and 4.5, respectively. They are equal to $\left(\frac{1}{4}\right)^{\text{th}}$ of the guided wavelength at their corresponding resonant frequencies.

$$L_{r\,(\text{State I})} = \frac{L1}{2} + L2 + L3 + L4 + L7 + L8 \tag{4.1}$$

$$L_{r\,(\text{State II})} = L2 + L3 + L4 + L7 + L8 \tag{4.2}$$

$$L_{r\,(\text{State III})} = L3 + L4 + L7 + L8 \tag{4.3}$$

$$L_{r\ (State\ IV)} = L4 + L7 + L8 \tag{4.4}$$

$$L_{r\ (State\ V)} = \frac{2L5}{3} + L7 + L8 \tag{4.5}$$

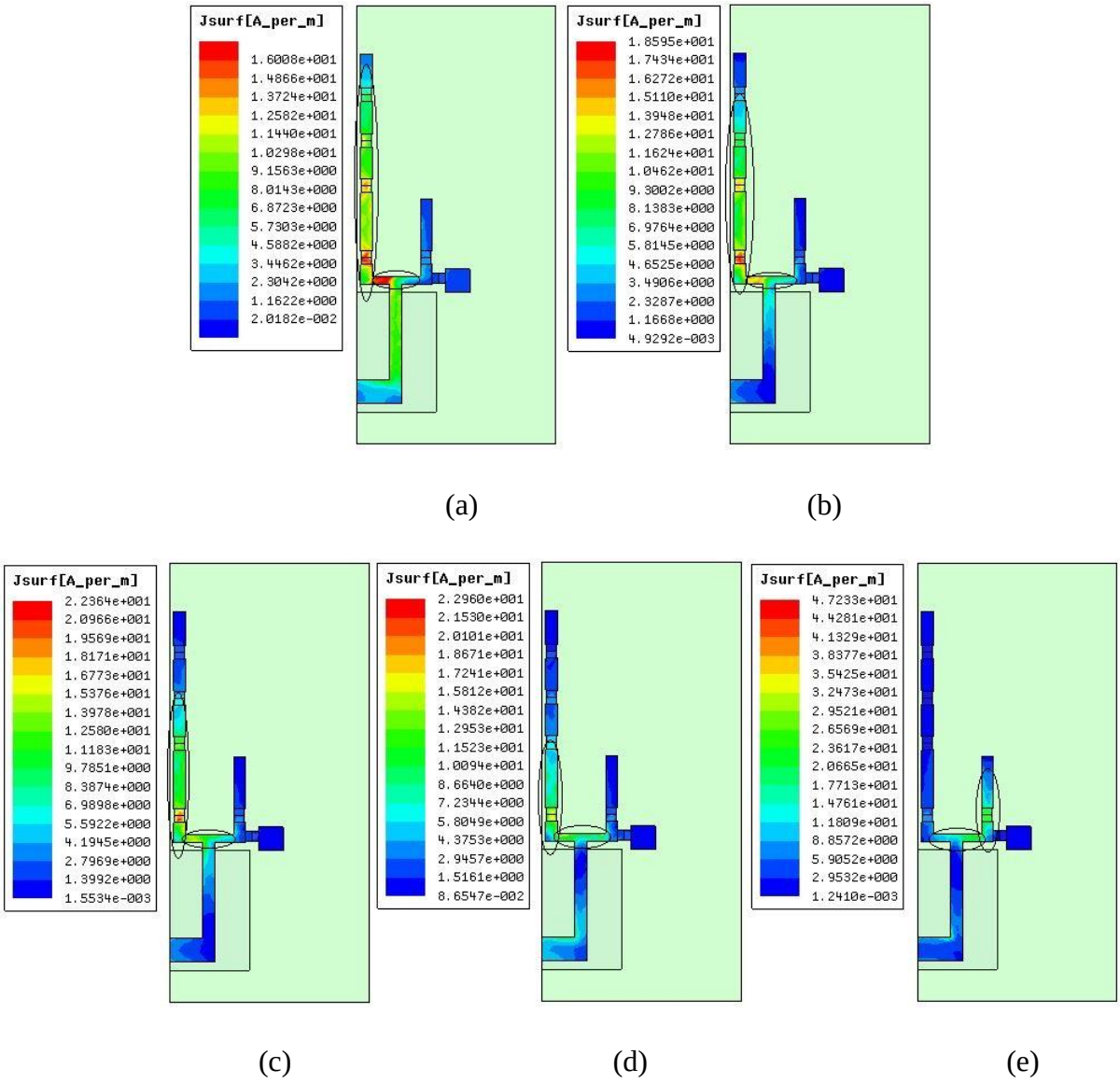

Fig. 4.3. Surface current densities of the reconfigurable communication antenna (a) at 1.85 GHz in State I (b) at 2 GHz in State II (c) at 2.35 GHz in State III (d) at 2.85 GHz in State IV (e) 3.5 GHz in State V

$\frac{L1}{2}$ and $\frac{2L5}{3}$ are considered in equations 4.1 and 4.5, respectively, since strong current densities exist on half portion of strip that has length L1 and two-third portion of strip that has length L5 in State I and State V, respectively, as shown in Fig 4.3a and Fig. 4.3e. As resonating length is

equal to $\frac{1}{4}^{th}$ of the guided wavelength at the corresponding resonant frequency, the resonant frequency can be calculated using equation 4.6.

$$f_r = \frac{c}{4L_r\sqrt{\varepsilon_{eff}}} \tag{4.6}$$

ε_{eff} is taken as the average of ε_r and 1, i.e., $\varepsilon_{eff} = \frac{\varepsilon_r+1}{2}$. The resonant frequencies obtained from equation 4.6 in States I, II, III, IV, and V are 1.75 GHz, 1.91 GHz, 2.29 GHz, 2.87 GHz, and 3.54 GHz, respectively. Whereas the resonant frequencies obtained from HFSS simulation in States I, II, III, IV, and V are 1.85 GHz, 2.00 GHz, 2.35 GHz, 2.85 GHz, and 3.5 GHz, respectively. The percentage differences of the resonant frequencies of the reconfigurable communication antenna obtained from HFSS simulation and design equation are 5.4%, 4.5%, 2.1%, 0.7%, and 1.1% in States I, II, III, IV, and V, respectively.

4.4. Results and Discussions

After designing sensing antenna and reconfigurable monopole antenna, eight similar reconfigurable monopole antennas and one sensing antenna are placed as depicted in Fig. 4.4a. The proposed cognitive radio MIMO antenna's fabricated prototype is depicted in Fig. 4.4b.

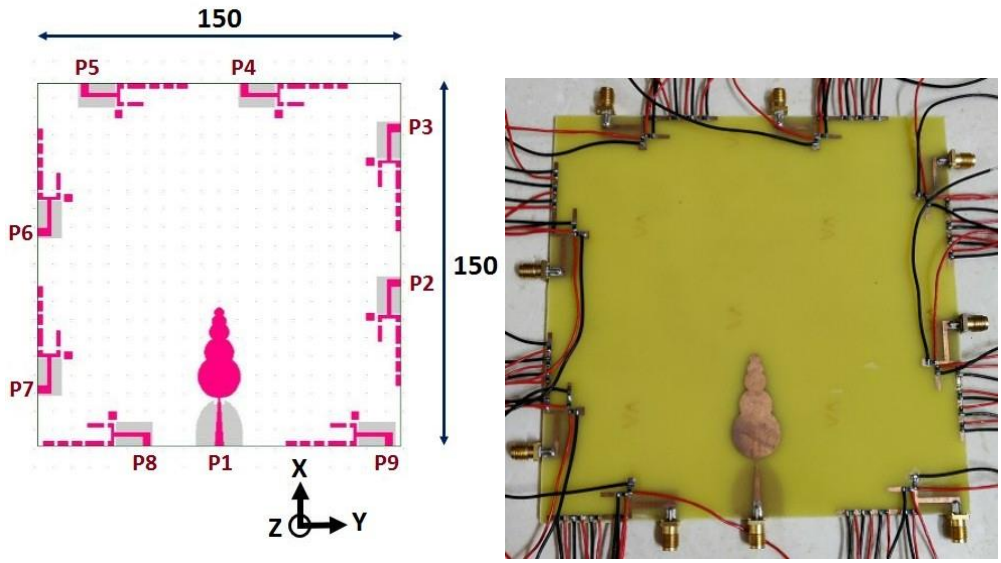

(a) (b)

Fig. 4.4. Nine port reconfigurable CR MIMO antenna (a) Structure of the CR MIMO antenna (b) Photograph of the fabricated prototype

The reflection coefficients of the antennas associated with ports 3, 4, 5, 6, 7, 8, and 9 in the designed CR MIMO antenna system are not shown for brevity since they are also similar to the reconfigurable antenna accessed at port 2. While measuring the reflection coefficient of an antenna, the remaining antennas are terminated with a matched load of 50 ohms.

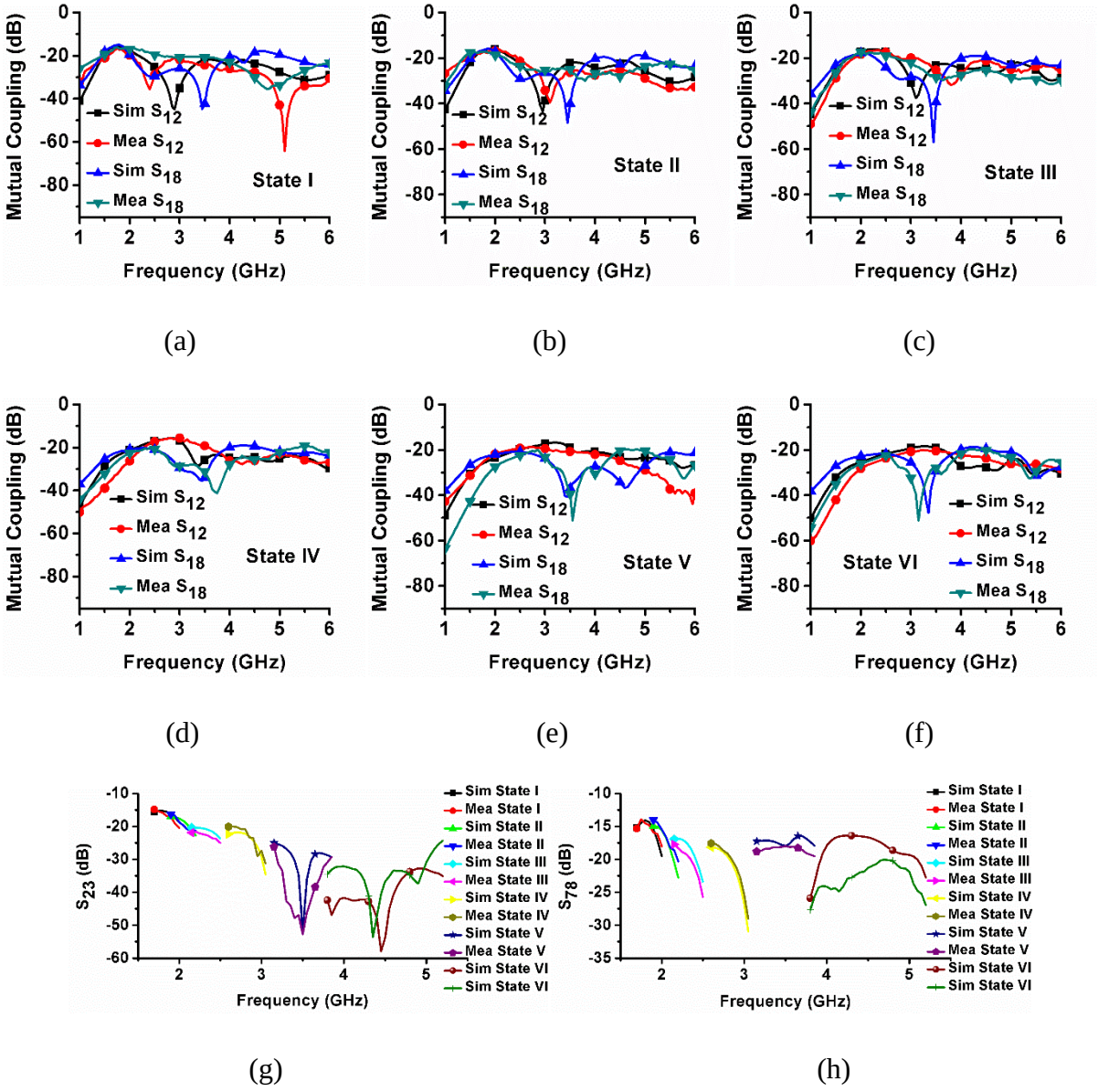

Fig. 4. 5. Mutual coupling between sensing antenna and reconfigurable antennas (a) S_{12} and S_{18} in State I (b) S_{12} and S_{18} in State II (c) S_{12} and S_{18} in State III (d) S_{12} and S_{18} in State IV (e) S_{12} and S_{18} in State V (f) S_{12} and S_{18} in State VI (g) S_{23} in all states (h) S_{78} in all states

The mutual coupling between sensing antenna and reconfigurable antenna accessed at port 2 that is parallel to the wideband sensing antenna, and also the mutual coupling between sensing antenna and reconfigurable antenna accessed at port 8 that is perpendicular to the sensing

antenna in States I, II, III, IV, V and VI are depicted in Figs. 4.5a, 4.5b, 4.5c, 4.5d, 4.5e, and 4.5f, respectively. For brevity, the mutual coupling between sensing antenna and other reconfigurable antennas are not provided as they also follow the similar trend. Also, in all operating states, the mutual coupling between vertically separated reconfigurable antennas (antennas accessed at ports 2 and 3) and the mutual coupling between orthogonally placed antennas that are close to each other (antennas accessed at ports 7 and 8) are illustrated in Figs. 4.5g and 4.5h, respectively. For brevity, the mutual coupling between other reconfigurable antennas are not provided as they also follow the similar trend.

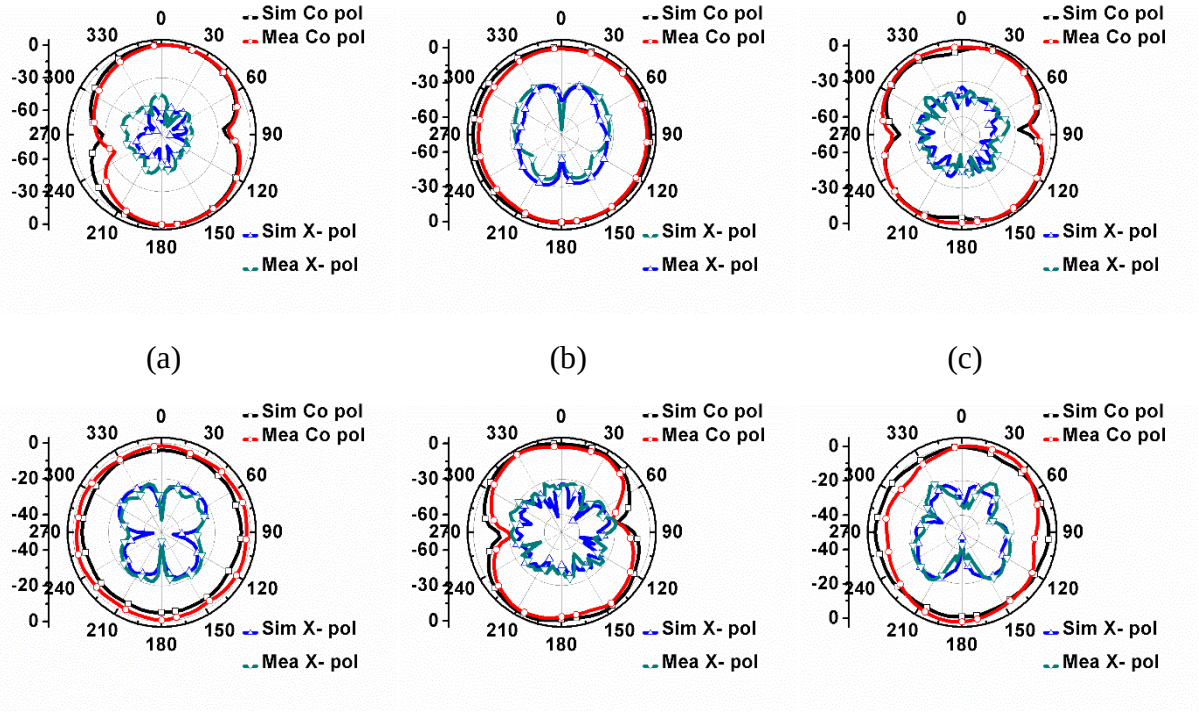

Fig. 4.6. Patterns of the antenna accessed at port 1 at (a) 2.5 GHz-XZ plane (b) 2.5 GHz-YZ plane (c) 4 GHz-XZ plane (d) 4 GHz-YZ plane (e) 5 GHz-XZ plane (f) 5 GHz-YZ plane

It is evident from Figure 4.5 that the mutual coupling between the wideband sensing antenna and any reconfigurable antenna is less than -15 dB, while the mutual coupling between any two reconfigurable antennas is less than -14 dB in all operating states of the reconfigurable antenna. Since some of the reconfigurable antennas are separated at long distances, the mutual coupling between them are not presented for brevity. Good isolation between every two antennas that are separated horizontally is achieved as the distance between them is more than one-fourth of the wavelengths corresponding to their lowest operating frequencies.

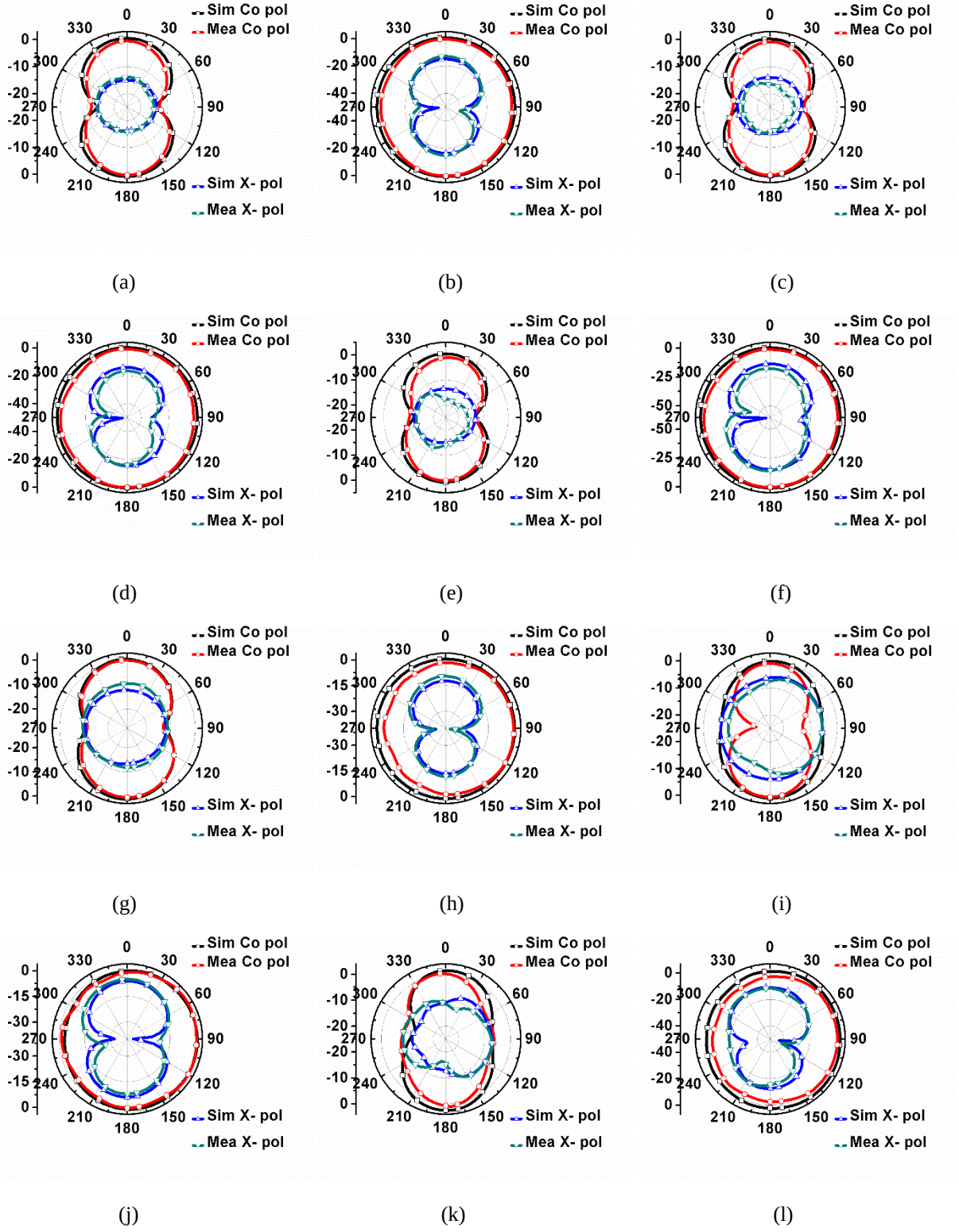

Fig. 4.7. Patterns of the antenna accessed at port 2 at (a) 1.9 GHz-XZ plane (b) 1.9 GHz-YZ plane (c) 2.1 GHz-XZ plane (d) 2.1 GHz-YZ plane (e) 2.3 GHz-XZ plane (f) 2.3 GHz-YZ plane (g) 2.8 GHz-XZ plane (h) 2.8 GHz-YZ plane (i) 3.5 GHz-XZ plane (j) 3.5 GHz-YZ plane (k) 4.5 GHz-XZ plane (l) 4.5 GHz-YZ plane

Even though the every two antennas in four antenna pairs (i.e., antenna accessed at ports 2 and 3, antenna accessed at ports 4 and 5, antenna accessed at ports 6 and 7, and antenna accessed at ports 8 and 9) are separated at distances of less than one-fourth of the wavelengths corresponding to their lowest operating frequencies, good isolation is accomplished between them as the two antennas in each pair of antennas are separated vertically.

Table 4.3. Comparison of the designed MIMO antenna with the other MIMO antennas for CR applications

Ref.	Size (mm^2)	Sensing antenna's range in GHz	Frequency ranges covered for communication	Minimum Isolation attained (dB)	n-element MIMO antenna	Polarization diversity
[131]	50 × 110	-	1.73-2.28 and 2.45	10	2	No
[132]	65 × 120	0.72-3.44	Some frequencies in 0.72-3.44	15.5	2	No
[134]	60 × 120	-	1.32-1.49 and 1.75-5.2	12	4	No
[154]	100 × 120	2.5-4.2	Some frequencies in 2.5-4.2	15	4	No
[163]	60 × 120	-	1.65-2.6	15	2	No
[129]	60 × 120	1-4.5	0.9-2.6	12.5	1	No
[166]	52.2 × 35	1.7-10.6	5.1-5.5, 6.6-7.2, and 9.7-10.2	15	1	No
[135]	109 × 109	2-5.7	2.5-4.2	15	4	Yes
proposed	**150 × 150**	**1.8-10**	**1.77-1.95, 1.9-2.15, 2.19-2.45, 2.63-3.02, 3.19-3.84, and 3.82-5.16**	**14**	**8**	**Yes**

The patterns of the wideband sensing antenna and the reconfigurable antenna connected to port 2 are depicted in Figs. 4.6 and 4.7, respectively. Exact '8' shaped patterns and omnidirectional

patterns are observed at 2.5 GHz in XZ and YZ planes, respectively, whereas a little distorted dipole natured patterns are noticed at 4 GHz and 5 GHz as the sensing antenna operates at higher ordered resonating modes, as illustrated in Fig. 4.6.

As illustrated in Fig. 4.7, stable radiation patterns, which a dipole antenna has normally, are achieved in all operating states of the reconfigurable antenna since reconfigurable communication antenna operates at its first resonating mode in all operating states. In case of sensing antenna, the simulated radiation efficiency varies from 80% to 96%, while the measured radiation efficiency varies from 72% to 87%. In case of reconfigurable antenna, the simulated radiation efficiencies vary from 70% to 75%, 61% to 71%, 66% to 72%, 67% to 87%, 74% to 87%, and 71% to 80% in States I, II, III, IV, V, and VI, respectively. Whereas the measured radiation efficiencies vary from 65% to 71%, 57% to 64%, 61% to 67%, 61% to 81%, 71% to 85%, and 70% to 76% in States I, II, III, IV, V, and VI, respectively.

It is evident from Table 4.3 that the designed CR MIMO antenna can perform communication tasks in 1.77-5.16 GHz and has a feature of polarization diversity. Moreover, the designed MIMO antenna is higher element MIMO antenna over other MIMO antennas for CR applications in literature.

In case of sensing antenna, the simulated peak gain varies from 1.8 dBi to 5.5 dBi, while the measured peak gain varies from 1.1 dBi to 5.2 dBi. In case of reconfigurable antenna, the simulated peak gains vary from 0.75 dBi to 0.89 dBi, 0.12 dBi to 0.52 dBi, 0.59 dBi to 0.92 dBi, 1.46 dBi to 2.01 dBi, 1.62 dBi to 3.21 dBi, and 1.86 dBi to 4.3 dBi in States I, II, III, IV, V, and VI, respectively. Whereas the measured peak gains vary from 0.61 dBi to 0.69 dBi, 0.02 dBi to 0.42 dBi, 0.47 dBi to 0.76 dBi, 1.28 dBi to 1.78 dBi, 1.45 dBi to 3.02 dBi, and 1.72 dBi to 3.82 dBi in States I, II, III, IV, V, and VI, respectively.

4.5. Conclusion

In this chapter, a nine port integrated sensing antenna and reconfigurable communication antennas for CR MIMO applications has been presented. It acts as a dynamic n-element MIMO antenna depending on the number of spectrum holes detected. Moreover, polarization diversity is also attained as some of the reconfigurable communication antennas are polarized in +X, -X, +Y, and –Y directions. The simulated and measured results confirm that the designed antenna is a fine candidate for CR MIMO applications.

Chapter-5

Integrated UWB Sensing and WB/NB Antennas Systems for CR Applications

5.1. Introduction

Most of the reported antennas in the literature are based on reconfigurable mechanisms that have unavoidable drawbacks like slow tuning, power consumption, and negative effects of the biasing lines, which affect the radiation characteristics when switches like PIN diodes, varactor diodes and RF MEMS are embedded into the radiating surface of the antenna. Moreover, it is difficult to implement these reconfigurable mechanisms in practice. So, in this chapter, a low profile and compact three port antenna for cognitive radio applications is presented. The proposed system has a sensing antenna that operates in ultra wideband (3.1-10.6 GHz) approved by FCC and a pair narrowband antennas for communication. Two narrowband antennas have -10 dB reflection coefficient bandwidths of 2.6 GHz (6.8-9.4 GHz) and 1.2 GHz (9.4-10.6 GHz). Isolation of better than 14 dB over the entire bandwidth of the sensing antenna is achieved between any two antennas without decoupling mechanism. The proposed system is realized on a low cost FR-4 substrate in a physical volume of 41 mm × 39 mm × 1.6 mm. An average gain of 3.3 dBi is achieved by sensing antenna in its operating bandwidth. Moreover, the radiation efficiencies of narrowband antennas are greater than 75% in their operating bandwidths and acceptable gains are achieved. More importantly, the proposed antenna system is a good alternative to reconfigurable antennas. Moreover, it is able to perform two communication tasks at a time when the spectrum (6.8-9.4 GHz and 9.4-10.6 GHz) is unutilized by primary users.

In this chapter, a six port antenna for better spectrum utilization efficiency in cognitive radio (CR) applications is also presented. In this six port antenna system, an ultra-wideband

(UWB) sensing antenna and five wideband/narrowband (NB) antennas are integrated on the same substrate in a compact area of 1134 mm^2. Antenna associated with port 1, which is meant for sensing, has -10 dB reflection coefficient bandwidth of 8 GHz (3-11 GHz) and the antennas associated with ports 2, 3, 4, 5 and 6 have -10 dB reflection coefficient in 3.6-5.8 GHz (single band), 2.9-3.6 GHz and 5.4-7.98 GHz (dual band), 7.95-8.38 GHz and 9-9.85 GHz (dual band), 8.38-9 GHz (single band) and 9.7-10.7 GHz (single band), respectively. Minimum isolation of 20 dB is attained between UWB sensing antenna and any narrowband/wideband antenna except between the antennas associated with ports 1 and 2 where minimum isolation of 12 dB is achieved over the operating bandwidth of UWB sensing antenna. Moreover, among all wideband/narrowband antennas, isolation of less than 15 dB is achieved. More importantly, the narrowband and wideband antennas meant for communication cover all frequency bands in UWB and a good match between the simulated and measured results is noticed.

The remaining contents of this chapter are structured as follows: The design of the three port antenna system that comprises one UWB sensing antenna and two WB/NB antennas is described in Section 5.2. The design of the three port antenna system that comprises one UWB sensing antenna and five WB/NB antennas is presented in Section 5.3. The conclusion of this chapter is given in Section 5.4.

5.2. Three Port Integrated UWB and NB Antennas System Design

In this design, cheap and easily available FR-4 substrate is preferred. Initially, an UWB antenna is designed. The intermediate steps in the design process of UWB antenna are illustrated in Fig. 5.1. The final design and its optimized dimensions are shown in Fig. 5.2. Firstly, a traditional rectangular patch is fed by a strip line of width 3.4 mm. With this structure, good impedance matching is achieved at low frequencies. However, it is poor at high frequencies, as depicted in Ant I of Fig. 5.3. By employing a half circular notch in the ground plane, impedance matching is bettered at high frequencies, as shown in Ant II of Fig. 5.3. It is due to the fact that inductive behaviour of the radiator is neutralized by the capacitance produced by the half circular notch. Thereafter, on both sides of the half circular notch, two similar rectangular notches of dimensions 1.5 mm x 8 mm are applied, as shown in Ant III of Fig. 5.1. By inserting the rectangular notches, the reflection coefficient curve shifts a little leftward and matching is also improved, as depicted Ant II of Fig. 5.3.

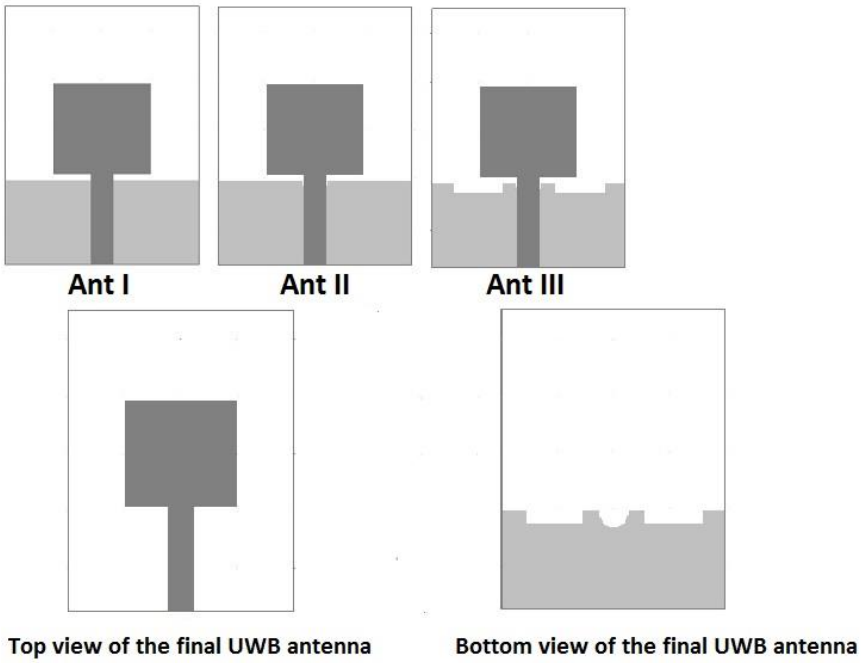

Fig. 5.1. Evolution, top view, and bottom views of the UWB antenna

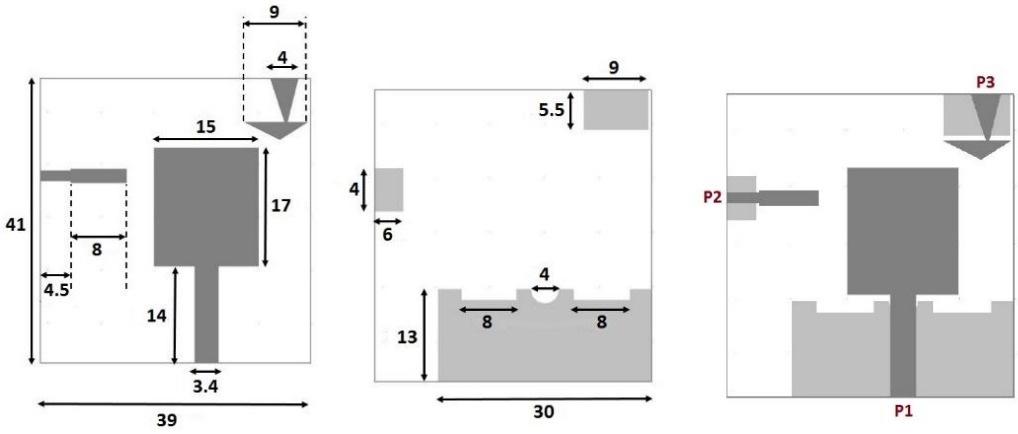

(a) (b) (c)

Fig. 5.2. Three port antenna (a) Top view (b) Bottom view (c) Final design

The simulated and measured reflection coefficients of each antenna in the three port antenna system are displayed in Fig. 5.4. A good agreement between them is observed. While measuring the reflection coefficient of one antenna, the remaining antennas are terminated with an impedance of 50 Ohms. The top and bottom views of the fabricated prototype are shown in Fig. 5.5.

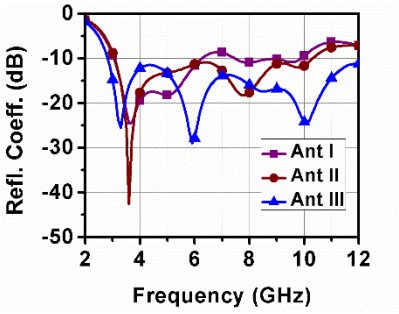

Fig. 5.3. Reflection coefficient of the antennas in the evolution of UWB antenna

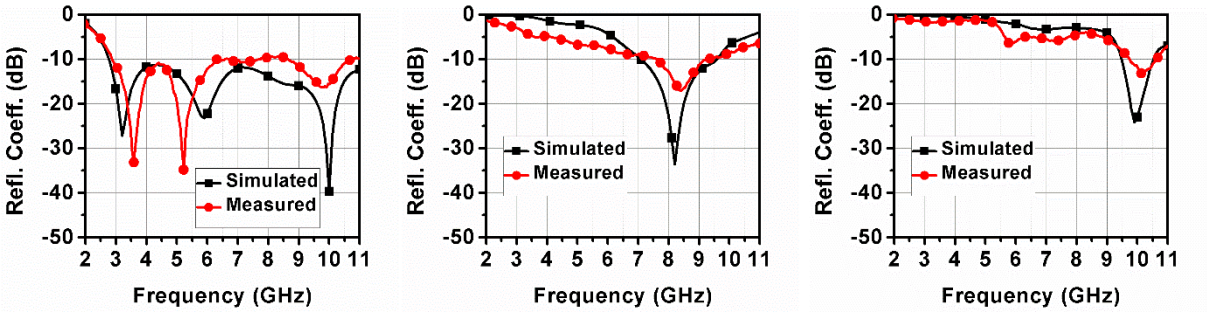

(a) (b) (c)

Fig. 5.4. Reflection coefficients of the antennas accessible at (a) Port 1 (b) Port 2 (c) Port 3

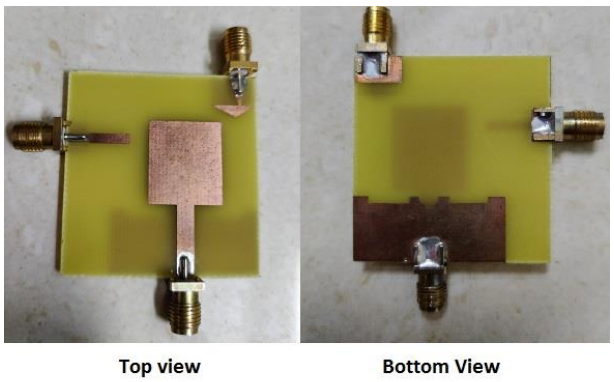

Fig. 5.5. Fabricated prototype of the three port antenna

After designing UWB sensing antenna, two NB antennas are integrated in the same substrate in such a way that a minimum isolation of 14 dB in the UWB between every pair of antennas is attained. Since it is a 3 port antenna, in case of single spectrum hole detection, two cases are possible. In one case, when a spectrum hole in the bandwidth of antenna accessible at port 2 is detected, the other NB antenna is terminated with 50 Ohms load. In this mode, the plot of S_{21} is shown in Fig. 5.6a. It is observed that an isolation of better than 14 dB between UWB antenna and NB antenna accessible at port 2 is achieved. In second case, when a spectrum hole in the

bandwidth of antenna accessible at port 3 is identified, the other NB antenna is terminated with 50 Ohms load. In this mode, the plot of S_{31} is shown in Fig. 5.6b. It is observed that an isolation of better than 15 dB between UWB antenna and NB antenna accessible at port 3 is achieved.

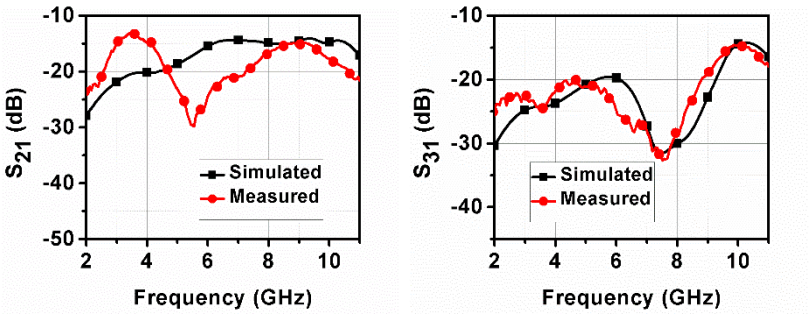

(a) (b)

Fig. 5.6. Isolation between sensing antenna and NB antenna (a) S_{21} in dB (b) S_{31} in dB

Table 5.1. Radiation efficiencies and peak gains of all antennas in the three port antenna system

Antenna	**Radiation Efficiency (%)**		**Peak Gain (dBi)**	
	Simulated	Measured	Simulated	Measured
Antenna accessible at port 1	95-85	87-81	2.3-6.5	1.8-5.8
Antenna accessible at port 2	90-86	84-79	4.4-5.1	4.1-4.7
Antenna accessible at port 3	87-64	81-62	2.1-4.3	1.8-4.1

It can be observed from Table 5.1 that the simulated and measured radiation efficiencies of the antenna accessible at port 1 are greater than 85% and 81%, respectively. In case of antenna accessible at port 2, the simulated and the measured radiation efficiencies are greater than 86% and 79%, respectively. Whereas in case of antenna accessible at port 3, the simulated and the measured radiation efficiencies are greater than 64% and 62%, respectively. Low radiation efficiencies are noticed at low frequencies of the antenna accessible at port 3 since the antenna accessible at port 3 is electrically small.

It can be noticed from Table 5.1 that the simulated and measured peak gains of the antenna accessible at port 1 are greater than 2.3 dBi and 1.8 dBi, respectively. In case of antenna accessible at port 2, the simulated and the measured peak gains are greater than 4.4 dBi and 4.1

dBi, respectively. Whereas in case of antenna accessible at port 3, the simulated and the measured peak gains are greater than 2.1 dBi and 1.8 dBi, respectively.

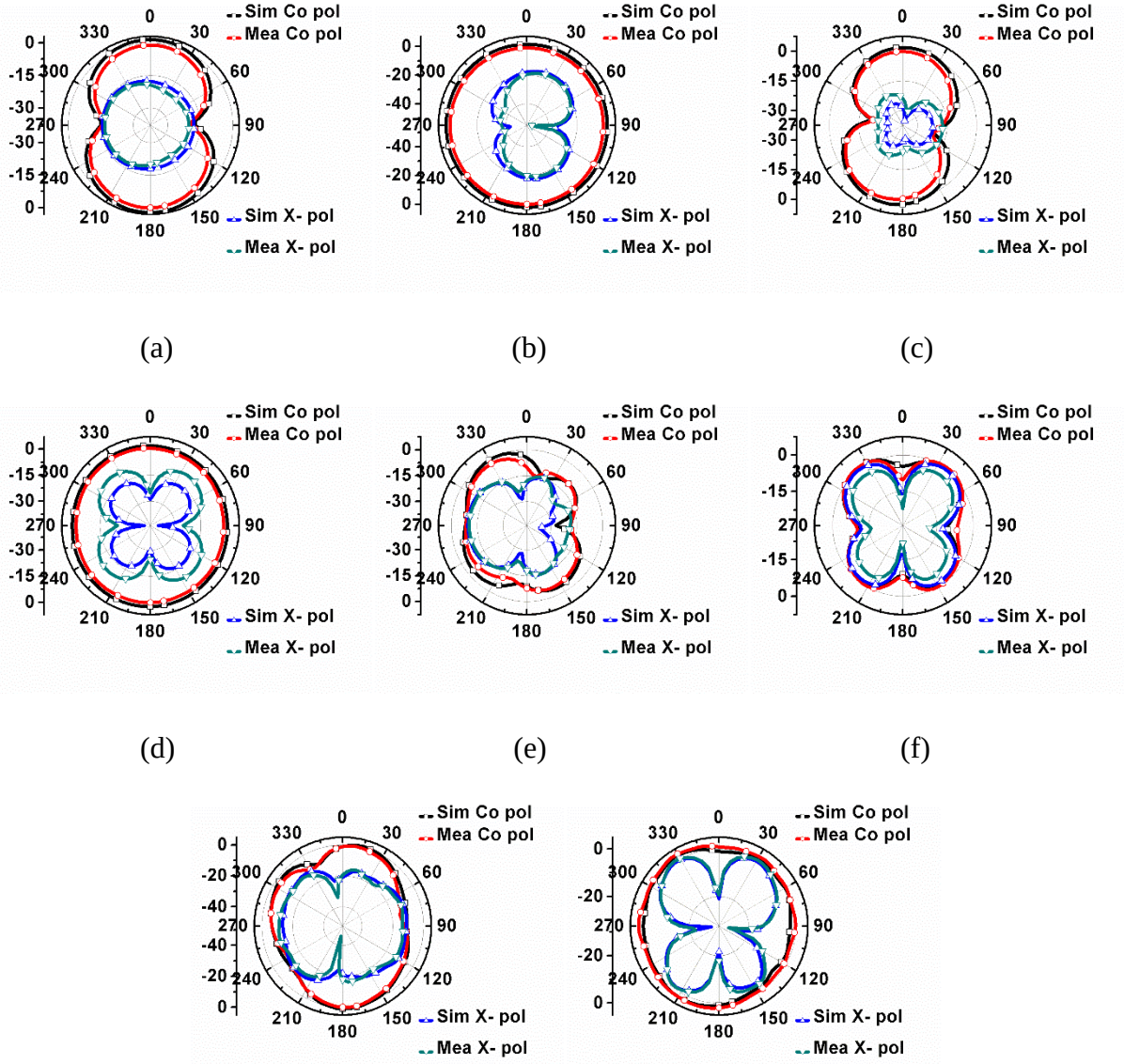

Fig. 5.7. Patterns of the UWB antenna at (a) 3 GHz-XZ plane (b) 3 GHz-YZ plane (c) 5 GHz-XZ plane (d) 5 GHz-YZ plane (e) 7.5 GHz-XZ plane (f) 7.5 GHz-YZ plane (g) 10 GHz-XZ plane (h) 10 GHz-YZ plane

The simulated and measured radiation patterns of the UWB sensing antenna at frequencies 3, 5, 7.5, and 10 GHz, when all other antennas in the six port antenna are terminated with 50 Ohms load, are illustrated in Fig. 5.7. Dipole like patterns and omnidirectional patterns with low cross pol levels are observed at low and high frequencies, respectively. The radiation patterns in

orthogonal planes of the NB antenna accessible at port 2 at 8 GHz are shown in Fig. 5.8. The radiation patterns in orthogonal planes of the NB antenna accessible at port 3 at 10 GHz are shown in Fig. 5.9.

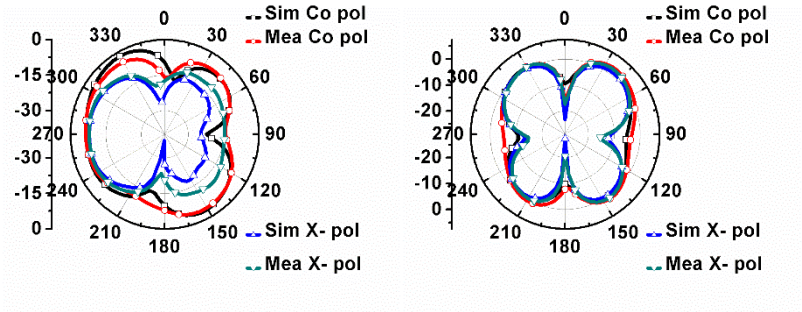

(a) (b)

Fig. 5.8. Patterns of the antenna accessible at port 2 at (a) 8 GHz-XZ plane (b) 8 GHz-YZ plane

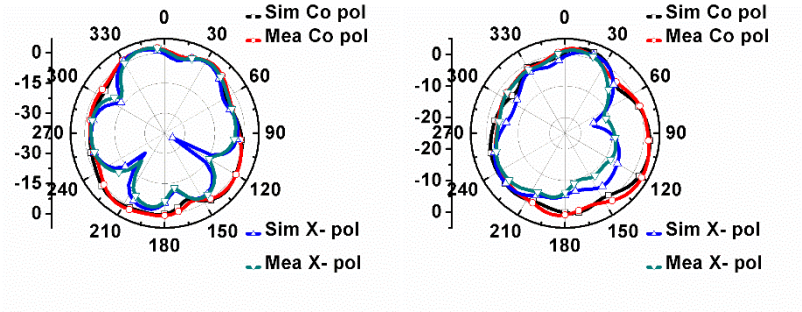

(a) (b)

Fig. 5.9. Patterns of the antenna accessible at port 3 at (a) 10 GHz-XZ plane (b) 10 GHz-YZ plane

5.3. Six Port Integrated UWB and WB/NB Antenna System Design

5.3.1. Design Procedure of the UWB Sensing Antenna

In this section, the step-by-step optimization process of the designed UWB sensing antenna is presented. The configuration of the UWB antenna is illustrated in Fig. 5.10 and all the optimized dimensions of the CPW-fed UWB antenna are reported in Table 5.2. Cheap and easily available FR-4 substrate having thickness of 1.6 mm is chosen in the present design.

CPW feeding technique is highly preferred as it eliminates misalignment between the active patch and ground plane, thus providing easy integration with RF circuits [121-122].

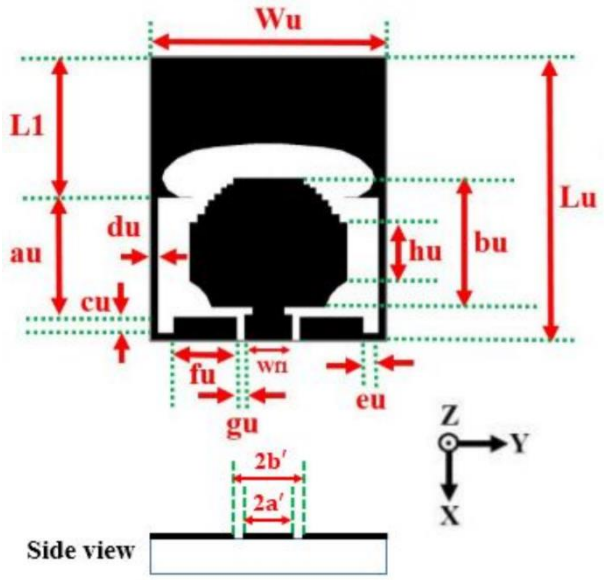

Fig. 5.10. Configuration of the UWB sensing antenna

In order to feed the UWB sensing antenna, a CPW feed line of impedance fifty ohms is designed by using Equations (5.1)-(5.7) that are used to find out a symmetrical double strip CPW line's characteristic impedance. The equations [123] are as follows:

$$k' = \sqrt{1 - k^2} \tag{5.1}$$

$$k_1 = \frac{a'}{b'} \tag{5.2}$$

Here, $a' = wf1$ and $b' = wf1 + gu$. Therefore, k_1 can be expressed in terms of wf1 and gu as shown below.

$$k_1 = \frac{wf1}{wf1+2gu} \tag{5.3}$$

$$k_2 = \frac{\sinh(\frac{\pi a'}{2h1})}{\sinh(\frac{\pi b'}{2h1})} \tag{5.4}$$

$$\frac{K(k)}{K'(k)} = \begin{cases} \dfrac{\pi}{\ln[\frac{2(1+\sqrt{k'})}{1-\sqrt{k'}}]} & 0 \le k \le 0.707 \\ \dfrac{\ln[\frac{2(1+\sqrt{k'})}{1-\sqrt{k'}}]}{\pi} & 0.707 \le k \le 1 \end{cases} \tag{5.5}$$

$$\varepsilon_{eff} = 1 + \left(\frac{\varepsilon_r - 1}{2}\right)\left(\frac{K(k_2)K'(k_1)}{K'(k_2)K(k_2)}\right) \quad (5.6)$$

$$Z_0 = \left(\frac{30\pi}{\sqrt{\varepsilon_{eff}}}\right)\left(\frac{K'(k_1)}{K(k_1)}\right) \quad (5.7)$$

where K(k) and K′(k) are elliptical integrals of the first order with arguments k and complementary argument k^1, respectively, h1 is the thickness of the substrate, wf1 is the width of the feed line (i.e., central conductor), gu is the separation between the central conductor and the ground plane on either side of the conductor, and ε_r is the relative permittivity of the substrate. In this design, wf1 and gu are chosen in such a way that the characteristic impedance of the CPW line is 50 Ohms. The intermediate steps in the design process of UWB antenna are depicted in Fig. 5.11.

Initially, a wide rectangular slot in the ground plane as shown in Ant I of Fig. 5.11 is employed and a rectangular shaped radiator is fed by a 50 Ohms impedance strip line to produce a wide band that ranges from 3.4 GHz to 9.3 GHz, as shown in Ant I of Fig. 5.12. Longest current path is created by reducing the width of strip (du) in the ground plane, which surrounds the wide rectangular slot. By increasing the length L1 in the ground plane, it is observed from Fig. 5.13 that the impedance matching at the low frequencies is significantly improved. At low frequencies, since the current patch is of the ground plane, by properly selecting the value of L1, the capacitive coupling between the ground plane and the rectangular patch neutralizes the inductive behaviour of the ground plane. Hence, the impedance matching is significantly improved at the low frequencies of the UWB sensing antenna. For L1 = 8.9 mm, a minimum reflection coefficient of -42.5 dB at 4.2 GHz is noticed. However, the impedance matching at high frequencies is poor. So, to improve the reflection coefficient characteristics at high frequencies, two circular notches are applied in the both sides of the rectangular patch such that a balance can be achieved between the horizontal and vertical currents, as shown in Ant II of Fig. 5.11. Moreover, a smooth transition from one resonating mode to another resonating mode is achieved; hence, an increment in -10 dB reflection coefficient bandwidth is observed, as depicted in Ant II of Fig. 5.12. But the achieved -10 dB reflection coefficient bandwidth with this structure is 6.6 GHz (3.4-10 GHz), as shown in Ant II of Fig. 5.12. To further increase this bandwidth, as depicted in Ant III of Fig. 5.11, a ‘Ω’ shaped notch is employed in the upper half of the ground plane so that the unwanted coupling between the upper edges of the patch and the upper half of the ground plane is eliminated. Therefore, good reflection coefficient characteristics and radiation characteristics are achieved at high frequencies, as shown in Ant

III of Fig. 5.12. However, the reflection coefficient curve is slightly shifted to right side by employing the 'Ω' shaped notch in the ground plane, as shown in Ant III of Fig. 5.12. Thereafter, modification of the rectangular patch as shown in Ant IV of Fig 5.11 leads to better impedance matching throughout a wide frequency range (i.e., 3.25-11.7 GHz), as demonstrated in Ant IV of Fig. 5.12.

Table 5.2. Optimized dimensions of the proposed UWB sensing antenna

Parameters	**mm**	**Parameters**	**mm**
Lu	18	eu	1
Wu	15	fu	4
au	8.6	gu	0.5
bu	9.13	hu	4
cu	1	L1	8.9
du	0.5	Wf1	3

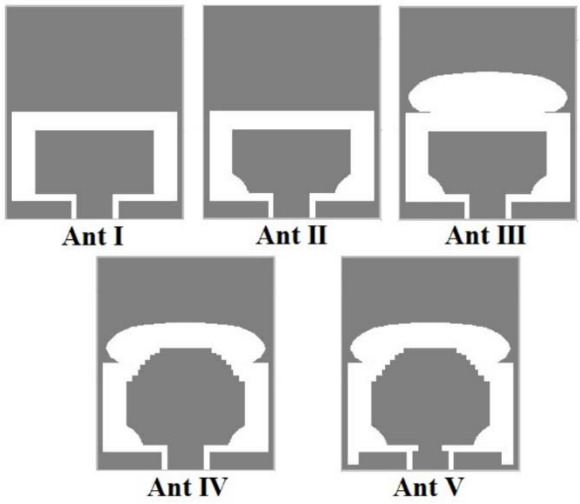

Fig. 5.11. Intermediate steps in the design process of the UWB sensing antenna

To make the antenna resonant from 3 GHz, two rectangular notches in both sides of the ground plane are incorporated and a narrow strip line of 2 mm width is used between the modified rectangular patch and the 50 Ohms feed line, as depicted in Ant V of Fig. 5.11. The presence of these two rectangular notches further helps in providing electrical lengthening. Hence, the reflection coefficient curve of Ant V in Fig. 5.12 shifts a little leftward and is below -10 dB in the entire spectrum of UWB, as shown in Ant V of Fig. 5.12.

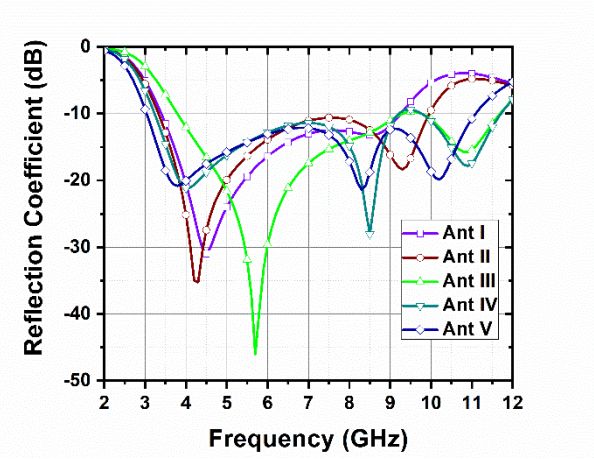

Fig. 5.12. Plot of reflection coefficient vs frequency in the design process of the UWB sensing antenna

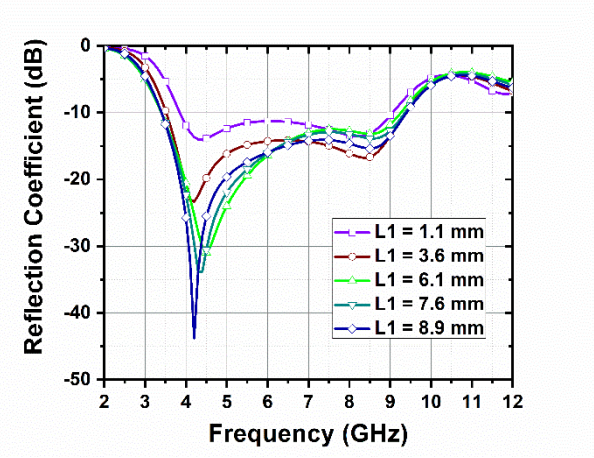

Fig. 5.13. Reflection coefficient's performance of the sensing antenna for different values of L1

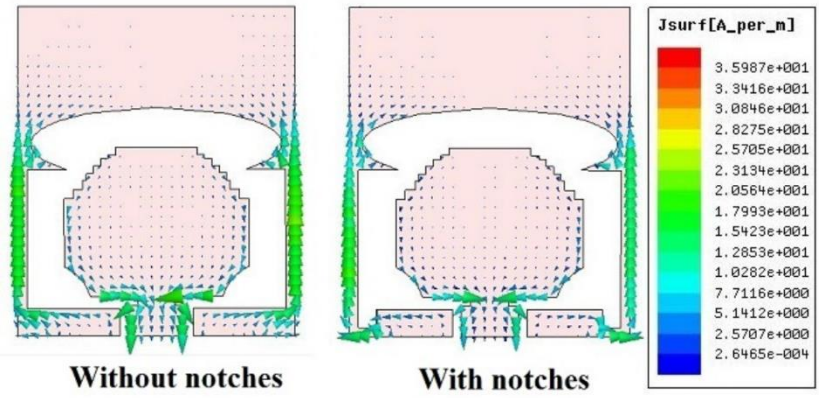

Fig. 5.14. Surface current distributions of the UWB sensing antenna at 3.1 GHz

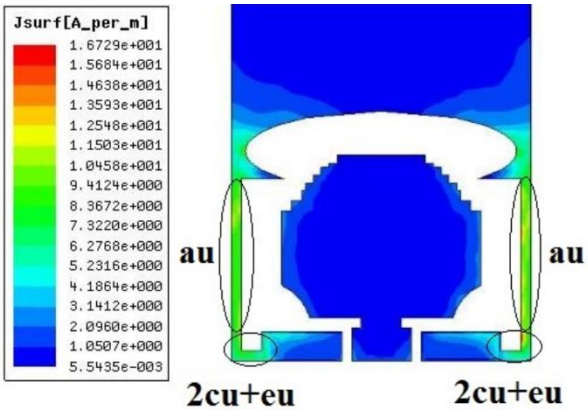

Fig. 5.15. Surface current density of the UWB sensing antenna at 3.79 GHz

The electrical lengthening phenomenon can be understood from Fig. 5.14. As depicted in Fig. 5.14, the surface currents travel additional path due to the presence of rectangular notches. Since the longest current path of an antenna decides the lowest resonant frequency, the first resonant frequency of Ant V decreases slightly compared to the first resonant frequency of Ant IV due to the longer current path provided by the two rectangular notches of Ant V. Therefore, the reflection coefficient curve of Ant V in Fig. 5.12 shifts a little leftward. The first resonance of the UWB sensing antenna is excited due to the some portions of the ground plane where maximum surface current densities exist. As depicted in Fig. 5.15, maximum surface current densities exist at the rectangular notches and also at the narrow elongated strips on the ground plane. Therefore, the length of the ground plane that is responsible for first resonance can be calculated as

$$L_{r_1(P1)} = (au + 2cu + eu) + (au + 2cu + eu) = 2 \times (au + 2cu + eu) \tag{5.8}$$

where au is the length of the narrow elongated strip, cu is the height of the rectangular notch, and eu is the length of the rectangular notch. Normally, the resonating length should be equal to the half of the guided wavelength at a resonant frequency. Therefore, the equation for the first resonant frequency is written as

$$f_{r_1(P1)} = \frac{c}{2L_{r_1(P1)}\sqrt{\varepsilon_{reff}}} \tag{5.9}$$

where ε_{reff} is the effective dielectric constant and c is the velocity of the light in air. Here, ε_{reff} is taken as $\frac{\varepsilon_r+1}{2}$ (i.e., $\varepsilon_{reff} \approx \frac{\varepsilon_r+1}{2}$). So, the value of ε_{reff} is 2.7. From the data given in Table 5.2, $L_{r_1(P1)}$ is found as 23.2 mm. After substituting the values of $L_{r_1(P1)}$, ε_{reff} and c in the Equation (5.9), we get $f_{r_1(P1)}$ as 3.93 GHz (i.e., $f_{r_1(P1)} \approx 3.93$ GHz).

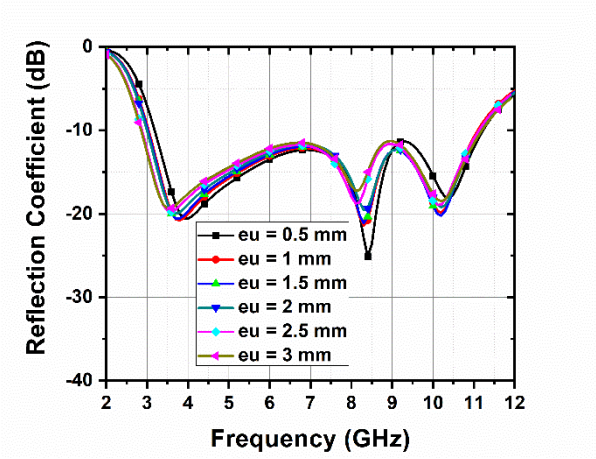

Fig. 5.16. Reflection coefficient plot of the UWB sensing antenna for different values of eu

The reflection coefficient plot of the UWB sensing antenna for different values of eu, while keeping the other parameters (i.e., au and cu) constant, is shown in Fig. 5.16. It can be observed from Fig. 5.16 that the first resonant frequency shifts towards left as eu increases. It is due to the fact that $L_{r_1(P1)}$ increases as eu increases. As a result, $f_{r_1(P1)}$ decreases.

Table 5. 3. Comparison between frequencies obtained from design equation and simulation for first resonance of the UWB sensing antenna

eu (mm)	**$L_{r_1(P1)}$ (mm)**	**Resonant Frequency (GHz)**		**% difference**
		Design Equation	**Simulation (HFSS)**	
0.5	22.2	4.11	4.01	2.49
1	23.2	3.93	3.79	3.69
1.5	24.2	3.77	3.73	1.07
2	25.2	3.62	3.65	0.82
2.5	26.2	3.48	3.57	2.52
3	27.2	3.35	3.51	4.55

In order to show the effectiveness of the design methodology, the percentage differences between the resonant frequencies that are obtained from simulation and the resonant frequencies that are obtained from the design equation are calculated in Table 5.3 for different values of eu that affect $L_{r_1(P1)}$ while keeping all other parameters constant. It can be seen from Table 5.3

that the percentage difference is less than 4.56%, which shows a good agreement between the simulated data and the data obtained from design equation.

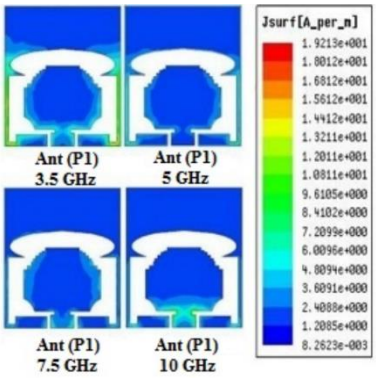

Fig. 5.17. Surface current densities at different frequencies in the UWB spectrum

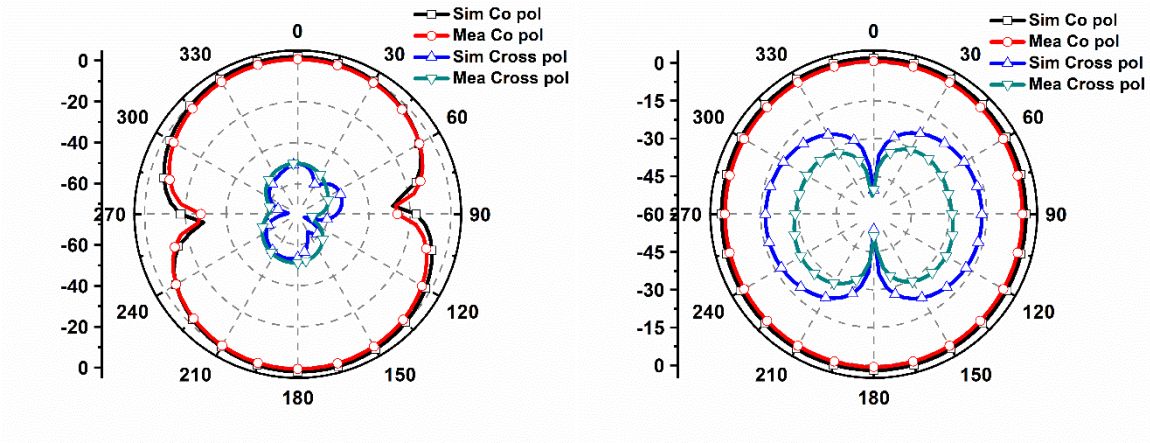

(a) (b)

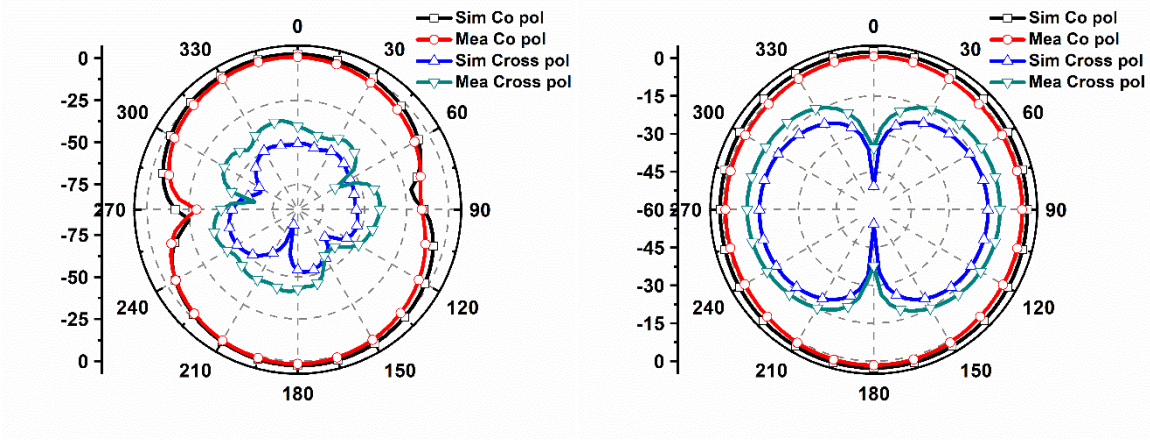

(c) (d)

Fig. 5.18. Radiation patterns of the UWB sensing antenna at low frequencies (a) XZ plane at 3.5 GHz (b) YZ plane at 3.5 GHz (c) XZ plane at 5 GHz (d) YZ plane at 5 GHz

The surface current densities of the sensing antenna at some of the frequencies in UWB are shown in Fig. 5.17. It is obvious from Fig. 5.17 that the elongated ground plane and the rectangular notches are responsible for its good radiation characteristics at low frequencies and the active modified rectangular patch is responsible for its good radiation characteristics at high frequencies in ultra wideband spectrum.

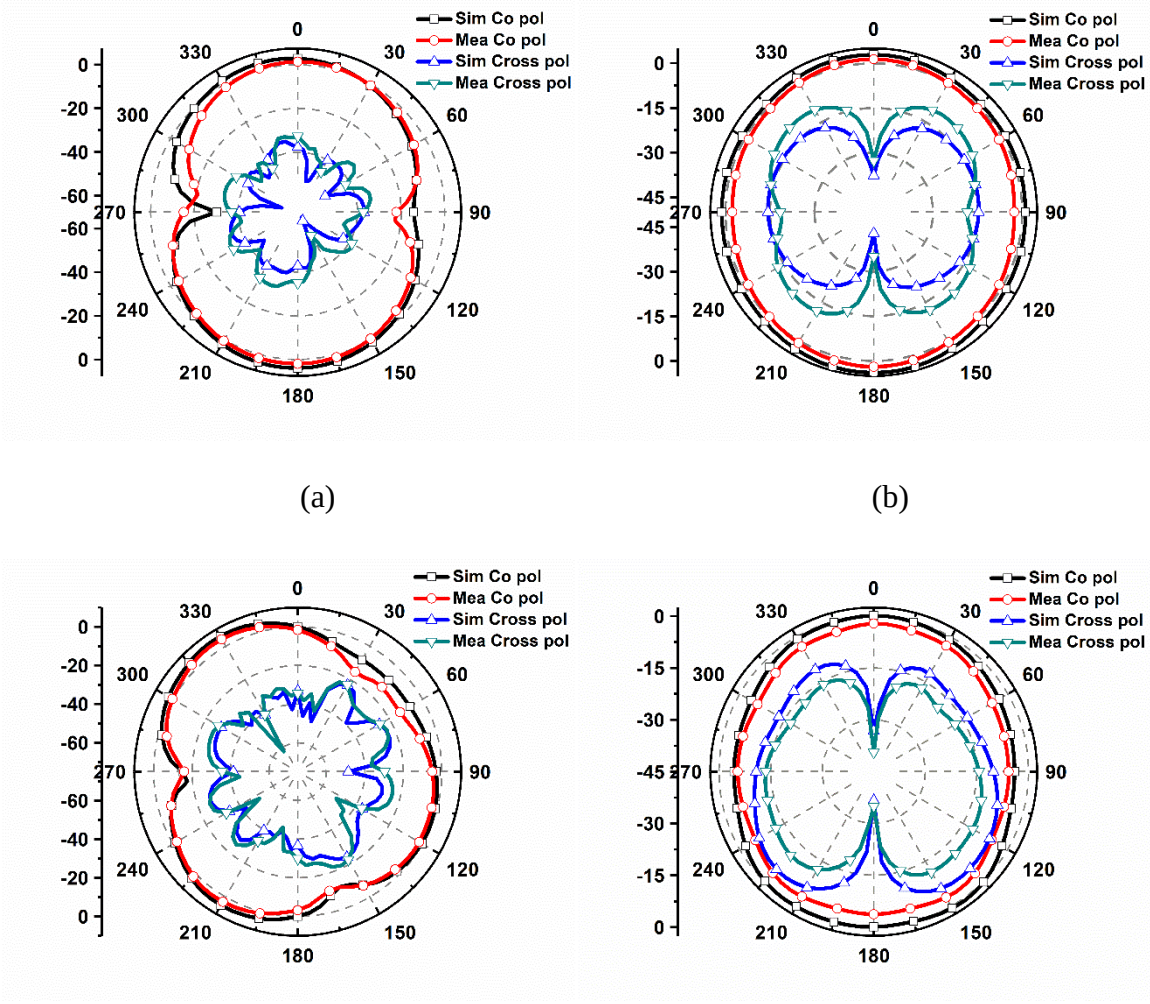

Fig. 5.19. Radiation patterns of the UWB sensing antenna at high frequencies (a) XZ plane at 7.5 GHz, (b) YZ plane at 7.5 GHz, (c) XZ plane at 10 GHz, and (d) YZ plane at 10 GHz

As depicted in Fig. 5.17, since maximum current densities are found at the elongated ground plane and at the rectangular notches at low frequencies (i.e., 3.5 GHz and 5 GHz) and at the active modified rectangular patch at high frequencies (i.e., 7.5 GHz and 10 GHz), the maximum current densities at those portions are responsible for the radiation of the UWB sensing antenna. The simulated and measured radiation patterns at low frequencies (i.e., 3.5 GHz and 5 GHz)

and high frequencies (i.e., 7.5 GHz and 10 GHz), when all other antennas in the six port antenna are terminated with 50 Ohms load, are depicted in Fig. 5.18 and Fig. 5.19, respectively. Dipole like patterns and omnidirectional patterns with low cross pol levels are observed at low and high frequencies, respectively.

5.3.2. Configuration of the Six Port Antenna

The configuration of the six port antenna for cognitive radio applications and the fabricated prototype of the proposed antenna are shown in Figs. 5.20 and 5.21, respectively. The optimized dimensions of the proposed six port antenna are tabulated in Table 5.4. By using HFSS, all dimensions of the antenna are optimized. While optimizing a particular parameter, the other parameters are kept constant during simulation.

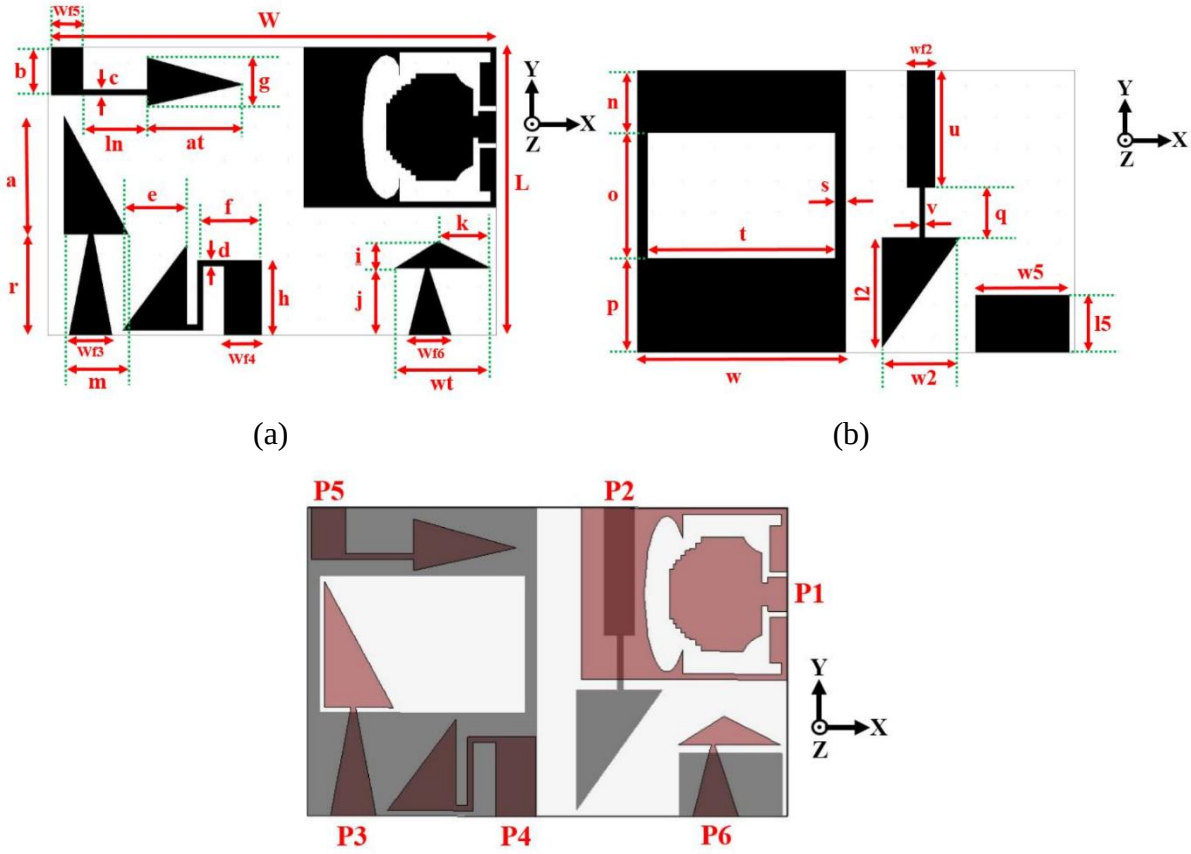

(a) (b)

(c)

Fig. 5.20. Configuration of the proposed six port antenna (a) Top view, (b) Bottom view, and (c) Final structure

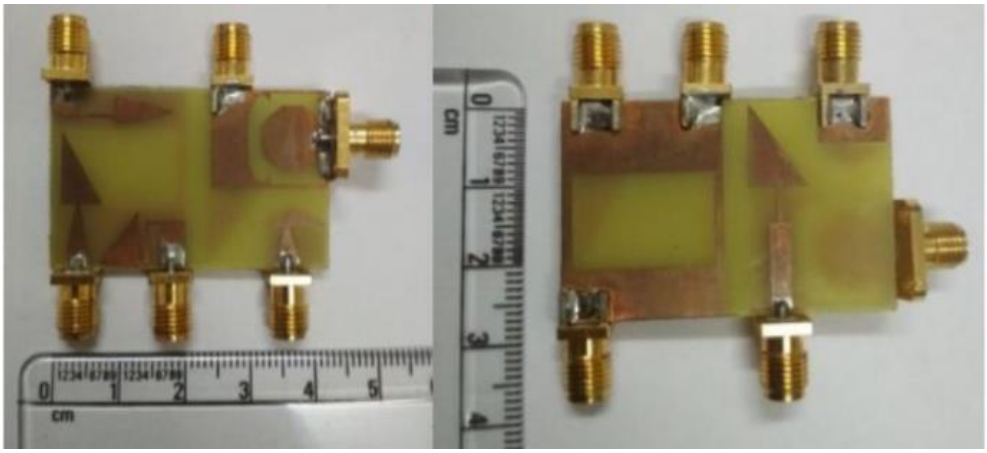

Fig. 5. 21. Top and bottom views of the fabricated prototype of the proposed six port antenna

Table 5.4. Optimized dimensions of the proposed six port antenna

Parameter	Dimension (mm)	Parameter	Dimension (mm)	Parameter	Dimension (mm)
L	27	K	5	q	4.8
W	42	m	6	r	9.5
a	11	ln	6	s	1
b	4.5	wf2	2.65	t	18
c	0.5	wf3	4	u	11.2
d	0.5	wf4	3.5	v	0.5
e	6	wf5	3	l2	10.5
f	6	wf6	4	w2	7.5
g	4.5	wt	9	l5	5.5
h	7	N	6	w5	9
i	2.5	O	12	w	20
j	6.5	P	9	at	9

5.3.3. Design of the Antenna Associated with Port 2

Firstly, a feed line (v) of 2.65 mm width is used to feed a rectangular patch of dimensions 7.5 mm × 10.5 mm at the bottom of the substrate, as shown in Ant I (P2) of Fig. 5.22. It can be

seen from Fig. 5.23 that the impedance bandwidth achieved with this structure lies in 6-7 GHz. However, the first resonance occurs at 4.5 GHz with poor impedance matching. Since the antenna associated with port 2 is mainly targeted to cover the low frequencies of the UWB, a narrow strip line of width 0.5 mm is used in between the rectangular radiator and 2.65 mm feed line to make the antenna resonant at low frequencies, as shown in Ant II (P2) of Fig. 5.22. From Fig. 5.23, it is obvious that good impedance matching is achieved from 4 GHz to 5.6 GHz. In order to find out an approximate calculation of the lower band edge frequency of Ant II (P2) in the evolution of antenna associated with port 2, the Equation (5.10) [124] is used as the Ant II (P2) is a rectangular monopole antenna.

$$f_{L\ Ant\ II\ (P2)} = \frac{7.2}{(L_{p2}+r_{p2}+p_{p2})\times k_{p2}}\ GHz \tag{5.10}$$

L_{p2} in cm is the height of the planar monopole antenna that is considered same as that of an equivalent cylindrical monopole, r_{p2} in cm is nothing but the effective radius of an equivalent cylindrical monopole that is normally determined by equating the areas of cylindrical monopole and planar monopole antennas, p_{p2} is feed gap in cm, and k_{p2} = 1.15, which is a constant, is considered in Equation (5.10) to get lower band edge frequency with an accuracy of 10% approximately. For a rectangular monopole antenna of length L and width W and feed gap p_{p2}, the expressions for L_{p2} and r_{p2} are given below.

$$L_{p2} = L \text{ and } r_{p2} = \frac{W}{2\pi} \tag{5.11}$$

In case of Ant II (P2), L = l2 =1.05 cm, W = w2 = 0.75 cm. p_{p2} = 0.1 cm and k_{p2} = 1.15.

So, L_{p2} = L = 1.05, $r_{p2} = \frac{W}{2\pi} = \frac{0.75}{2\pi}$ = 0.1194 p_{p2} = 0.1 and k_{p2} = 1.15. After substituting the values of L_{p2}, r_{p2}, p_{p2} and k_{p2} in Equation (5.10), we get $f_{L\ Ant\ II\ (P2)} \approx$ 4.93 GHz.

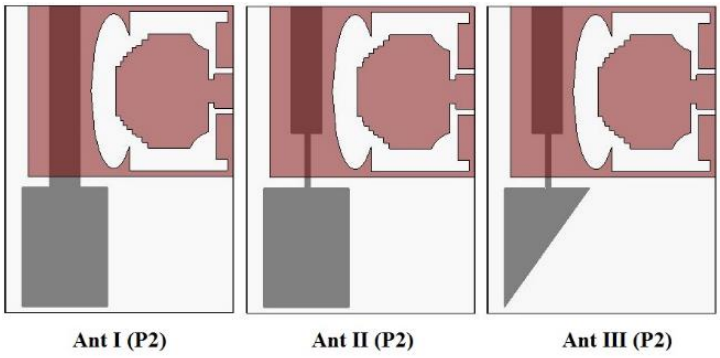

Fig. 5.22. Evolution of the antenna associated with port 2

It is calculated from Equation (5.10) that the lower band edge frequency of Ant II (P2) is 4.93 GHz. However, the lower band edge frequency of Ant II (P2) from simulation is 4 GHz. The mismatch between the lower band edge frequencies of Ant II (P2) is due to the defections in the ground plane. In the last step, the rectangular patch is modified by cutting half triangular part, as depicted in Ant III (P2) of Fig. 5.22. Thus, the antenna is made resonant from 3.6 GHz to 5.8 GHz, as illustrated in Fig. 5.23.

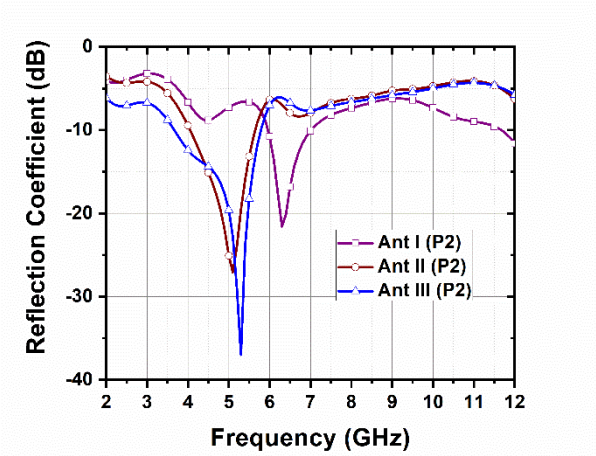

Fig. 5.23. Plot of reflection coefficient vs frequency in the design process of antenna associated with port 2

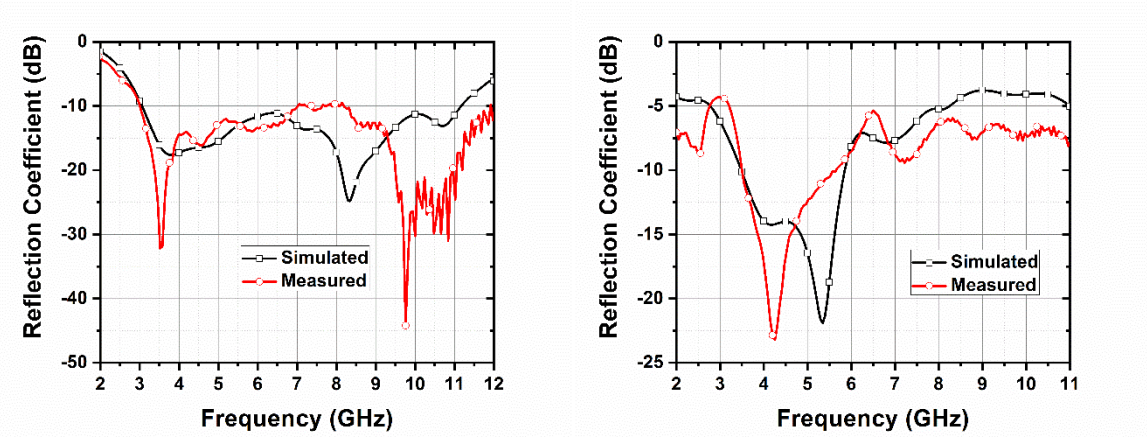

(a) (b)

Fig. 5.24. Plots of reflection coefficient vs frequency (a) UWB sensing antenna and (b) Antenna associated with port 2

Since the feed line part of the antenna associated with port 2 is beneath the ground plane of UWB sensing antenna, much space is saved without occupying extra area. The reflection coefficient performances of the UWB sensing antenna and the antenna connected with port 2,

when only the antennas associated with ports 1 and 2 are excited while the remaining antennas are loaded with 50 Ohms matched termination, are illustrated in Fig. 5.24a and Fig. 5.24b, respectively.

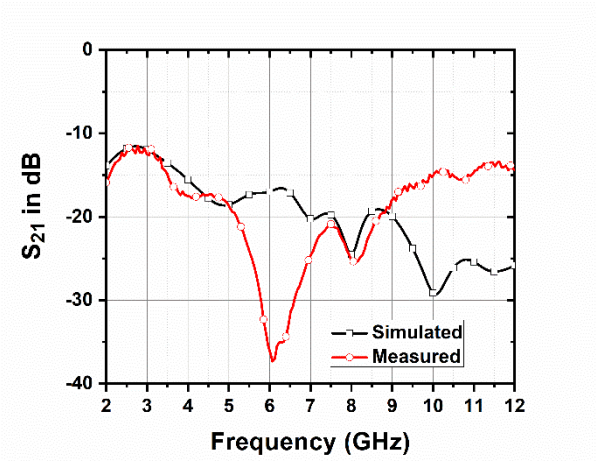

Fig. 5.25. Mutual coupling between antennas associated with port 2 and port 1

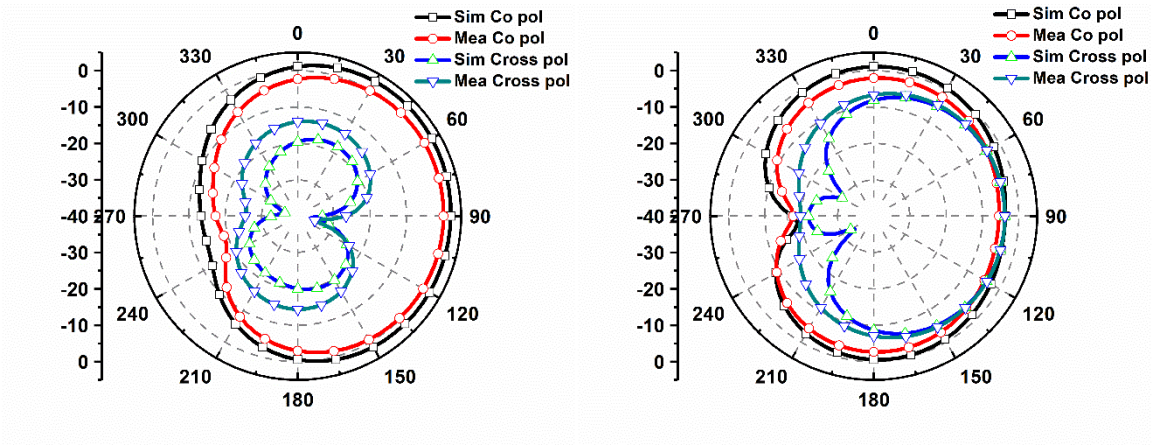

(a) (b)

Fig. 5.26. Radiation patterns of the antenna associated with port 2 at 4 GHz (a) XZ plane (b) YZ plane

From the surface current distributions at various frequencies in UWB, it can be observed that very weak surface currents exist on the enlarged ground plane of antenna associated with port 1, as illustrated in Fig. 5.17. Therefore, although the antenna associated with port 2 and UWB sensing antenna share same ground, a minimum isolation of 12 dB in the operating bandwidth of the sensing antenna is attained, as depicted in Fig. 5.25, which is a welcome factor. It is due to the fact that the feed line portion of the antenna associated with port 2 is located exactly

below the region of the ground plane of the antenna associated with port 1, which has very weak surface currents that exist at all frequencies in 3.1-10.6 GHz when the antenna associated with port 1 is excited. Moreover, the current flow directions of the antennas associated with ports 1 and 2 are also orthogonal in nature.

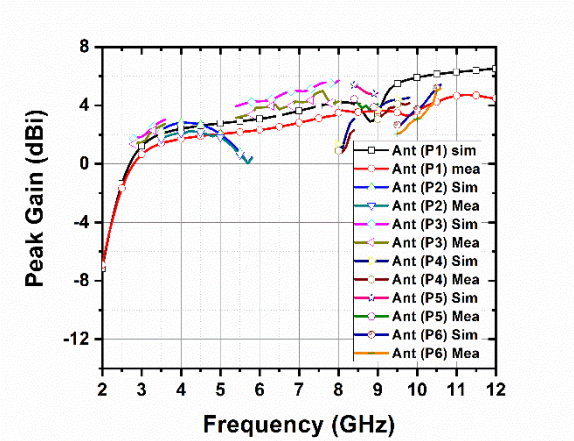

Fig. 5.27. Plot of peak gain vs frequency of all the antennas in their operating bandwidths

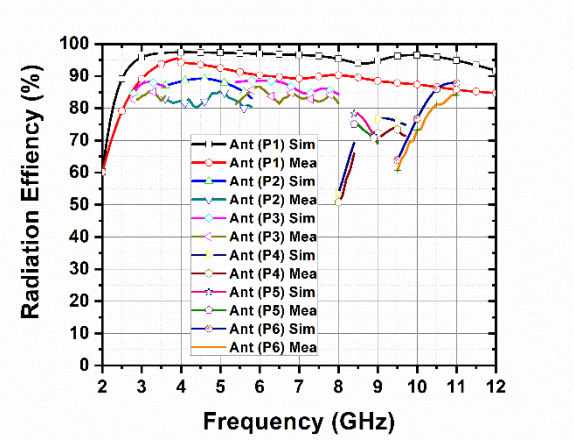

Fig. 5.28. Radiation efficiencies of all the antennas in their operating bandwidths

The simulated and measured radiation patterns of the antenna associated with port 2 in the orthogonal planes when all the other ports of the antenna are terminated with 50 Ohms load are depicted in Fig. 5.26. The antenna associated with port 2 is an asymmetric monopole antenna; however, the radiation patterns of the antenna associated with port 2 are not of dipole natured type radiation patterns due to the defections in the ground plane that are present due to the presence of the rectangular slot, 'Ω' shaped notch and two rectangular notches. At 4 GHz, in XZ plane, simulated gains of 1.1 dBi and 2.13 dBi are achieved in broadside and end fire directions, respectively, as shown in Fig. 5.26a. On the other hand, the maximum cross pol

levels of -9 dB and -4 dB are observed in XZ plane and YZ plane, respectively, due to the horizontal surface currents that exist on the ground plane at 4 GHz. However, the performance of cross pol is not an essential need in indoor communication systems where rayleigh fading is more dominant in the channels [90]. The simulated and measured peak gains and radiation efficiencies of the antennas associated with ports 1, 2, 3, 4, 5, and 6 are depicted in Figs. 5.27 and 5.28, respectively. It can be seen from Fig. 5.28 that the radiation efficiency of the antenna associated with port 2 is greater than 85% in 3.5-5.8 GHz. To further integrate more number of narrowband and wideband antennas, some extra space is utilized. The remaining four wideband and narrowband antennas are designed in such a way that these antennas cover the remaining uncovered spectrum in UWB.

5.3.4. Design of the Antenna Associated with Port 3

Since antenna associated with port 2 has bandwidth that ranges from 3.5 GHz to 5.8 GHz, the antenna associated with port 3 is designed to cover the uncovered low frequencies and frequencies above 5.8 GHz in the spectrum of UWB. Initially, a rectangular patch, which is fed by a tapered feed line to achieve impedance matching in 4.65-8 GHz, is designed, as shown in Ant I (P3) of Fig. 5.27. The lower band edge frequency of Ant I (P3) in the evolution of antenna associated with port 3 can be estimated by Equation (5.12) that is normally used for a rectangular monopole antenna [16].

$$f_{\text{L Ant I (P3)}} = \frac{7.2}{(L_{p3}+r_{p3}+p_{p3})\times k_{p3}}\ \text{GHz} \tag{5.12}$$

In case of Ant I (P3), which is a rectangular monopole antenna of length a, width m and feed gap p_{p3}, the expressions for L_{p3} and r_{p3} are given below.

$$L_{p3} = a \text{ and } r_{p3} = \frac{m}{2\pi} \tag{5.13}$$

In case of Ant I (P3), $L_{p3} = a = 1.1$, $r_{p3} = \frac{m}{2\pi} = \frac{0.6}{2\pi} = 0.0954$, $p_{p3} = 0.05$ and $k_{p3} = 1.15$.

After substituting the values of L_{p3}, r_{p3}, p_{p3} and k_{p3} in Equation (5.12), we get $f_{\text{L Ant I (P3)}} \approx$ 5.02 GHz.

It is calculated from Equation (5.12) that the lower band edge frequency of Ant I (P3) is 5.02 GHz. However, the lower band edge frequency of Ant I (P3) from simulation is found to be 4.66 GHz. The difference between the lower band edge frequencies found from Equation (5.12)

and simulation is 7.95%, which is acceptable as the lower band edge frequency calculated Equation (5.12) ensures an accuracy of 10% approximately. In the next step, a parametric analysis is done by varying the width of the ground plane of the Ant I (P3) of Fig. 5.29 in positive X-direction.

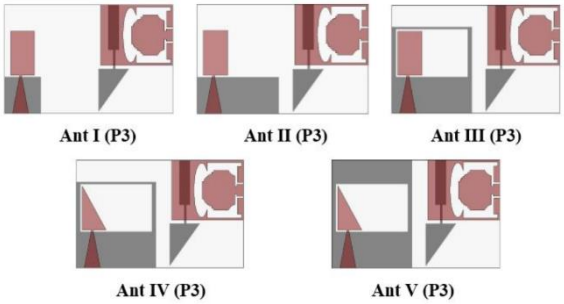

Fig. 5.29. Intermediate steps in the design process of antenna associated with port 3

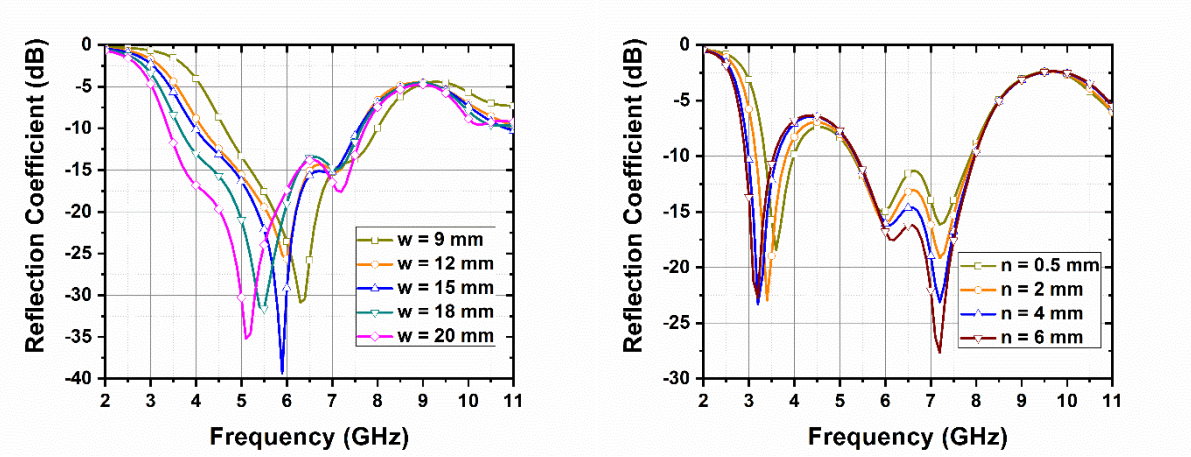

(a) (b)

Fig. 5.30. Reflection coefficient's performance at different (a) widths (w) of the ground plane of Ant I (P3) and (b) heights (n) of the ground plane of Ant IV (P3)

From Fig. 30a, left shift in the reflection coefficient curves is observed when the width of the ground plane increases. An optimal value of 20 mm width is chosen to achieve impedance matching in 3.4-7.7 GHz, thus forming Ant II (P3), as shown in Ant II (P3) of Fig. 5.29. As it is expected to achieve dual band behaviour by elongating the ground plane, the ground plane has been elongated, as depicted in Ant III (P3) of Fig. 5.29. From reflection coefficient curve of Ant III (P3) in Fig. 5.31, it is quite evident that the dual band behaviour of the antenna can be observed. However, it is desired to achieve the left side band at low frequencies of the UWB. Therefore, the rectangular patch is modified by cutting half triangular area, as shown in Ant IV

(P3) of Fig. 5.29. Thereafter, a parametric study is performed by varying the height of the ground plane (n) in positive Y-direction, as depicted in Fig. 30b. As a result, the dual band behaviour is achieved as good impedance matching is achieved in 2.9-3.6 GHz and 5.4-7.98 GHz. The reflection coefficient performances of the UWB sensing antenna and the antenna associated with port 3 when the remaining antennas are terminated with 50 Ohms load are depicted in Fig. 5.32a and Fig. 5.32b, respectively. The mutual coupling between antennas associated with port 1 and port 3 is less than -20 dB, as shown in Fig. 5.33.

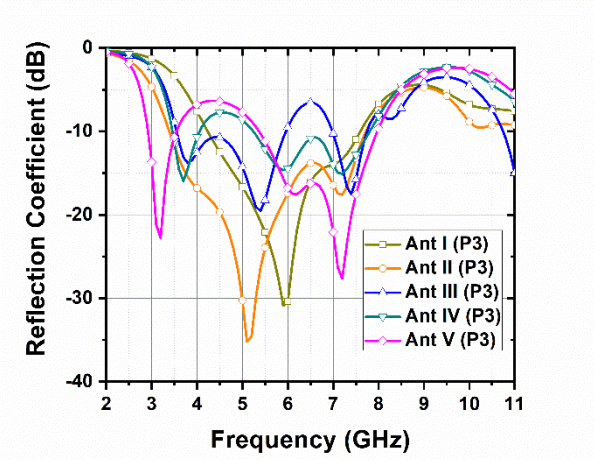

Fig. 5.31. Plot of reflection coefficient vs frequency in the design process of antenna associated with port 3

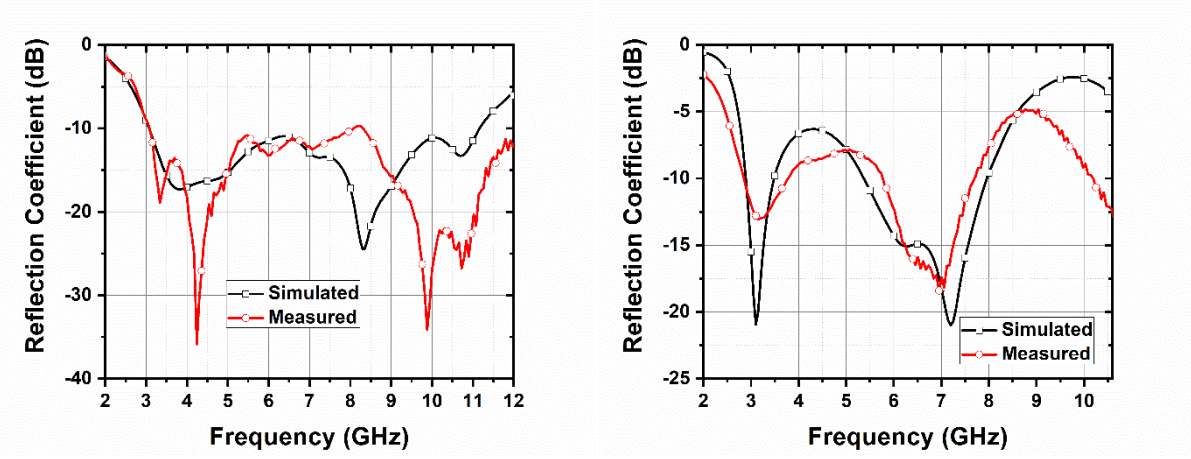

(a) (b)

Fig. 5.32. Plots of reflection coefficient vs frequency (a) UWB sensing antenna (b) Antenna associated with port 3

In all measured results, the slight shifts and some variations in the resonances could be due to the faults in fabrication, imperfections in soldering, material impurities, and connector losses.

However, the measured reflection coefficients of all the antennas in the six port antenna are less than -10 dB in their operating bandwidths.

The first resonance of the antenna associated with port 3 is excited due to the some portions of the ground plane where maximum surface current densities exist. As depicted in Fig. 5.34, maximum surface current densities exist at the narrow elongated strips on the ground plane and at half of the upper portions of the ground plane on either side. Therefore, the length of the ground plane that is responsible for first resonance can be calculated as

$$L_{r_1(P3)} = (o + \frac{n}{2}) + (o + \frac{n}{2}) = 2 \times (o + \frac{n}{2}) \quad (5.14)$$

where o is the length of the narrow elongated strip and n is the upper portion of the elongated ground plane. Normally, the resonating length should be equal to the half of the guided wavelength at a resonant frequency. Therefore, the equation for the first resonant frequency of antenna associated with port 3 is written as

$$f_{r_1(P3)} = \frac{c}{2L_{r_1(P3)}\sqrt{\varepsilon_{reff}}} \quad (5.15)$$

where ε_{reff} is the effective dielectric constant and c is the velocity of the light in air. Here, ε_{reff} is taken as $\frac{\varepsilon_r+1}{2}$ (i.e., $\varepsilon_{reff} \approx \frac{\varepsilon_r+1}{2}$). So, the value of ε_{reff} is 2.7. From the data given in Table 5.4, $L_{r_1(P3)}$ is found as 30 mm. After substituting the values of $L_{r_1(P3)}$, ε_{reff} and c in the Equation (5.15), we get $f_{r_1(P3)}$ as 3.04 GHz (i.e., $f_{r_1(P3)} \approx 3.04$ GHz).

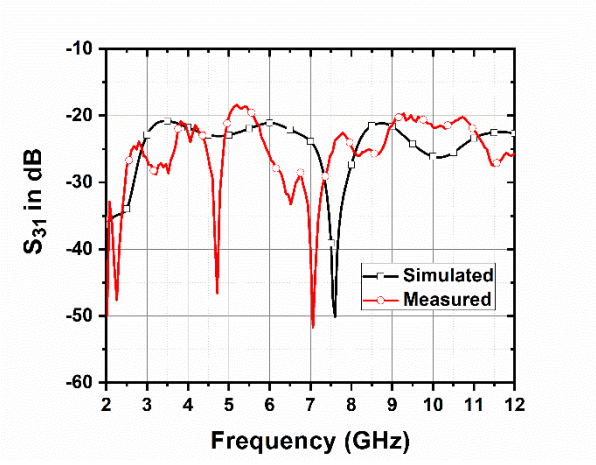

Fig. 5.33. Mutual coupling between antennas associated with port 3 and port 1

The reflection coefficient plot of the UWB sensing antenna for different values of n while keeping the other parameter (i.e., o) constant is shown in Fig. 5.30b. It can be observed from

Fig. 5.30b that the first resonant frequency shifts towards left as n increases. Also, no significant shifts in the resonances of the second frequency band indicate that the first resonance is easily affected by the dimension n. In order to show the effectiveness of the design methodology, the percentage differences between the resonant frequencies that are obtained from simulation and the resonant frequencies that are obtained from the design equation are calculated in Table 5.5 for different values of o that affect $L_{r_1(P3)}$ while keeping all other parameters constant. It can be seen from Table 5.5 that the percentage difference is less than 4.11%, which shows a good agreement between the simulated data and the data obtained from design equation.

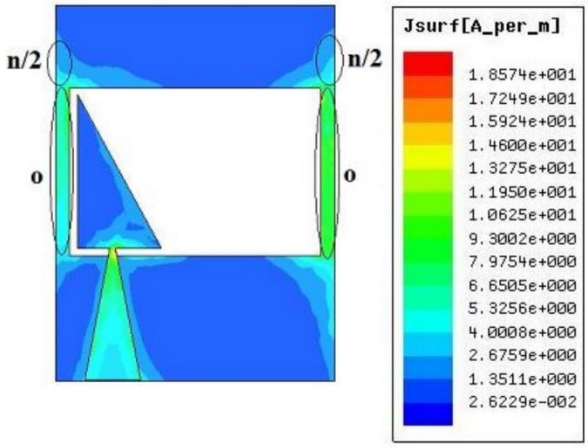

Fig. 5. 34. Surface current density of the antenna associated with port 3 at 3.17 GHz

Table 5.5. Comparison between frequencies obtained from design equation and simulation for first resonance of the antenna associated with port 3

n (mm)	**$L_{r_1(P3)}$ (mm)**	**Resonant Frequency (GHz)**		**% difference**
		Design Equation	**Simulation (HFSS)**	
0.5	24.5	3.72	3.61	3.04
2	26	3.51	3.40	3.23
4	28	3.26	3.20	1.87
6	30	3.04	3.17	4.10

The surface current densities on the dual band antenna associated with port 3 at frequencies 3.2 GHz, 6 GHz and 7.5 GHz are illustrated in Fig. 5.35. It is observed that radiation of the antenna associated with port 3 at 3.2 GHz is mainly because of the strong surface currents at the narrow

elongated strips on the ground plane and at half of the upper portions of the ground plane on either side, as depicted in Ant (P2) at 3.2 GHz of Fig. 5.35. On the other hand, the right angled triangular shaped radiator is accountable for the radiation of the antenna at frequencies 6 GHz and 7.5 GHz, as shown in Ant (P3) at 6 GHz and 7.5GHz of Fig. 5.35.

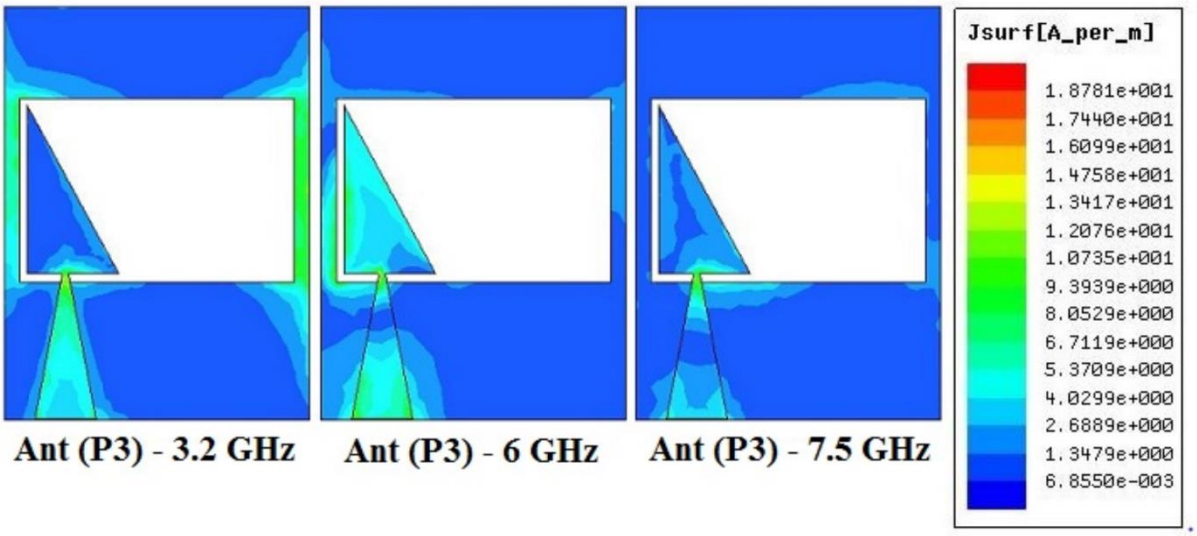

Fig. 5. 35. Surface current densities at frequencies 3.2 GHz, 6 GHz, and 7.5 GHz of the antenna associated with port 3

The simulated and measured radiation patterns of the antenna associated with port 3 when all the other antennas are terminated with 50 Ohms load are illustrated in Figure 5.36. Number '8' shaped pattern and omnidirectional pattern are observed in the orthogonal planes at 3.2 GHz, as illustrated in Fig. 5.36a and Fig. 5.36b, respectively, while slightly omnidirectional natured patterns are achieved in XZ and YZ planes at a frequency of 7.1 GHz, as illustrated in Fig. 5.36c and d. Moreover, the beam maxima in the radiation patterns of UWB antenna and antenna associated with port 3 occurs at $\pm$Z direction, which is much desired when they are employed for simultaneous use [90].

As depicted in Fig. 5.36c and Fig. 5.36d, the cross pol level of the antenna associated with port 3 rises significantly in both the planes. The reason behind this is due to the horizontal surface currents as the antenna associated with port 3 is an asymmetric microstrip fed monopole type antenna. Also, the obtained radiation patterns are very well acceptable for CR applications. As shown in Fig. 5.28, the radiation efficiencies in both the operating bands of the antenna associated with port 3 are greater than 85%.

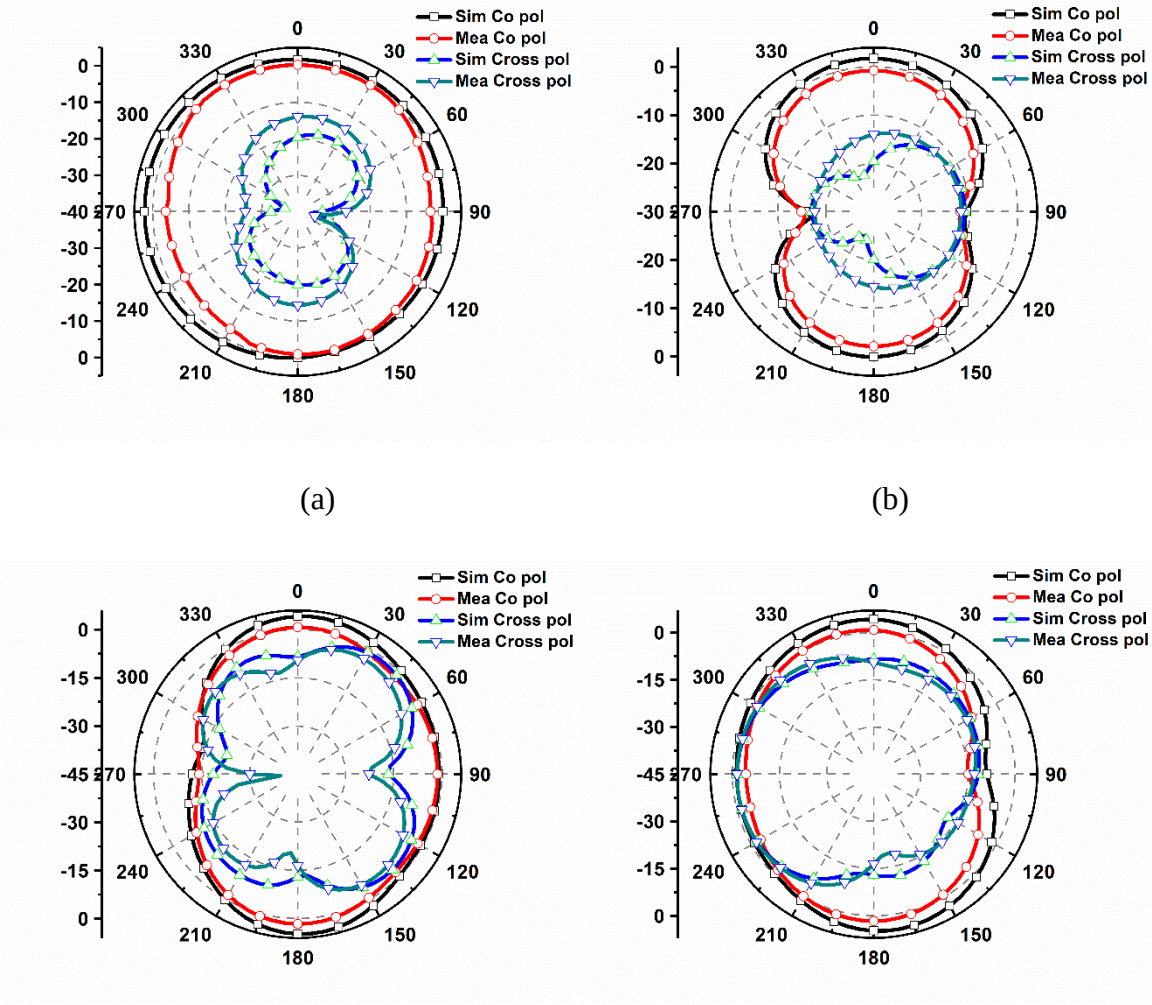

Fig. 5.36. Radiation patterns of the antenna associated with port 3 (a) XZ plane at 3.2 GHz, (b) YZ plane at 3.2 GHz, (c) XZ plane at 7.1 GHz, and (d) YZ plane at 7.1 GHz

5.3.5. Design of the Antenna Associated with Port 4

The uncovered frequencies by the antennas associated with ports 2 and 3 are covered by the remaining narrowband antennas. The remaining antennas (i.e., antennas associated with port 4, 5 and 6) are integrated in the same area occupied by the UWB antenna, antenna associated with port 2, and antenna associated with port 3 without taking any extra space. The reflection coefficient performance of the UWB sensing antenna when only the UWB sensing antenna and the antenna associated with port 4 are excited while the remaining antennas are terminated with 50 Ohms load is depicted in Fig. 5.37a. The antenna associated with port 4, which yields two bands, has -10 dB reflection coefficient bandwidth in 7.95-8.38 GHz and 9-9.85 GHz, as shown in Fig. 5.37b. It uses the same ground plane that is used for antenna associated with port 3.

However, there is no significant current coupling throughout the operating bandwidths of antennas associated with ports 3 and 4. It is because of its location where very weak surface currents that exist at all frequencies in 3.1-10.6 GHz when the antenna associated with port 3 is excited.

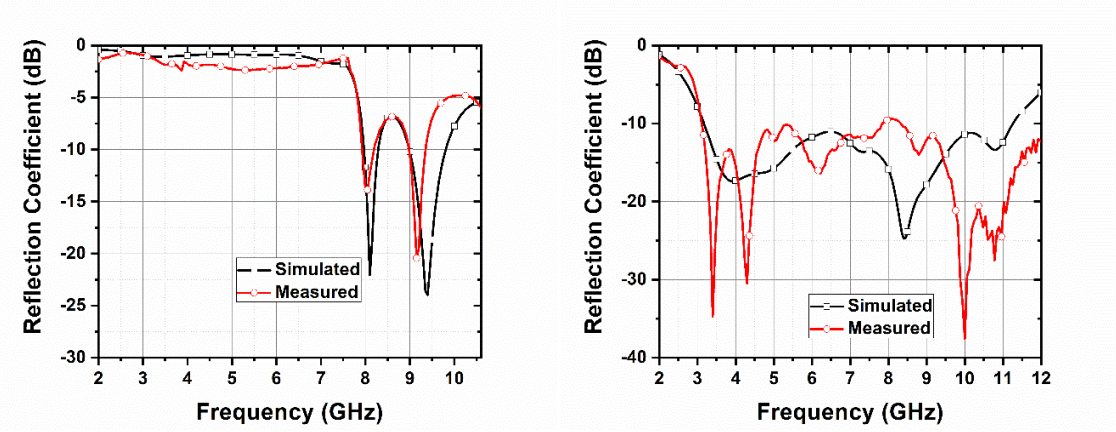

(a) (b)

Fig. 5.37. Plots of reflection coefficient vs frequency (a) UWB sensing antenna and (b) Antenna associated with port 4

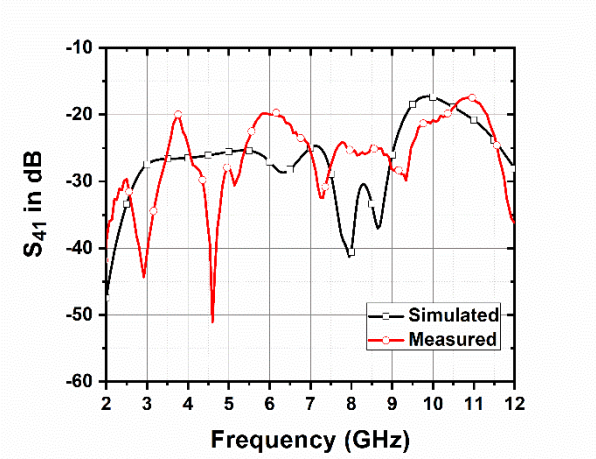

Fig. 5.38. Mutual coupling between antennas associated with port 4 and port 1

Proper impedance matching can be achieved by using a meander line type feed structure to feed the right angled triangular shaped patch, as depicted in antenna associated with port 4 of Fig. 5.20c. The mutual coupling between the antennas associated with ports 1 and 4 is depicted in Fig. 5.38. The radiation patterns in the orthogonal planes of the antenna associated with port 4 when all other antennas are terminated with 50 Ohms load are shown in Fig. 5.39. As the ground

plane of the antenna associated with port 4 acts as defected ground due to the rectangular slot, partly bidirectional and omnidirectional patterns are achieved at 8.3 GHz in XZ plane and YZ plane, respectively, as demonstrated in Fig. 5.39a and Fig. 5.39b. However, partly omnidirectional natured patterns are attained in the both the planes at 9.4 GHz, as seen in Fig. 5.39c and Fig. 5.39d.

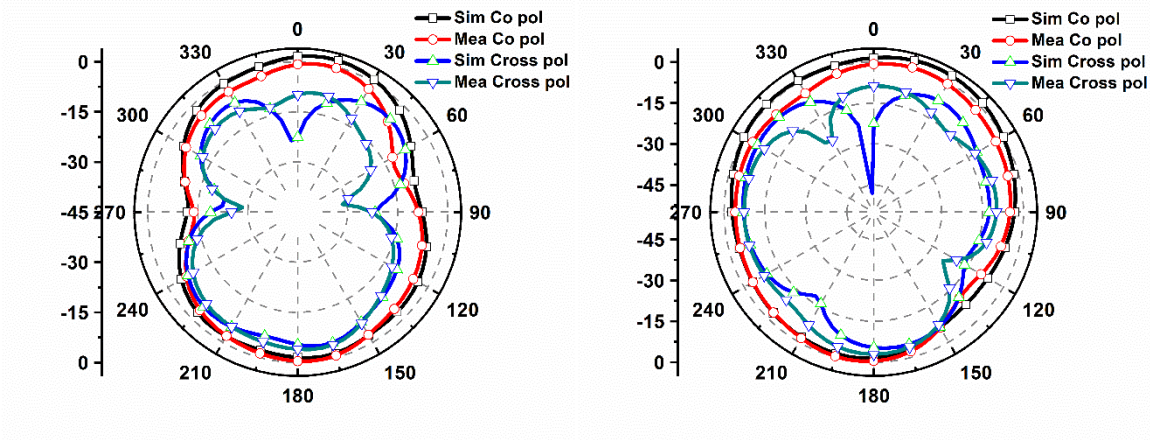

Fig. 5.39. Radiation patterns of the antenna associated with port 4 (A) XZ plane at 8.3 GHz, (B) YZ plane at 8.3 GHz, (C) XZ plane at 9.4 GHz, and (D) YZ plane at 9.4 GHz

As shown in Fig. 5.39a and Fig. 5.39b, simulated gains of 1.52 dBi and 1.53 dBi are achieved in the broadside direction ($\emptyset$=0^0, θ=0^0) in XZ and YZ planes, respectively, at 8.3 GHz. On the other hand, maximum level of cross pol reach -4.5 dB and -5.6 dB in XZ plane and YZ plane, respectively, due to the strong horizontal surface currents in the meander line type structure. From Fig. 5.39c and Fig. 5.39d, it is observed that the simulated gains of 4.12 dBi and 4.03 dBi at 9.4 GHz are achieved in the broadside direction ($\emptyset$=0^0, θ=0^0) in XZ and YZ planes,

respectively. As it can be seen from Fig. 5.28, the simulated radiation efficiency of antenna associated with port 4 is greater than 52% in 7.95-8.38 GHz, whereas it is greater than 74% in 9-9.8 GHz. The reason for its low radiation efficiencies in the low frequency band, i.e., 7.95-8.38 GHz is due to its compact structure. Moreover, as the antenna structure is electrically small, the peak gain in the low frequency band ranges from 1.06 dBi to 3.07 dBi, as depicted in Fig. 5.27.

5.3.6. Design of the Antenna Associated with Port 5

The integration of two more antennas (i.e., two NB antennas associated with ports 5 and 6) are done in such a way that these NB antennas are electrically well isolated from the other antennas. As it is seen in the case of location of the antenna associated with port 4, the location of the antenna associated with port 5 plays a crucial role in achieving the less mutual coupling with the other antennas. The reflection coefficient performance of the UWB sensing antenna when only the UWB sensing antenna and the antenna associated with port 5 are excited while the remaining antennas are terminated with 50 Ohms load is illustrated in Fig. 5.40a. The antenna associated with port 5 has -10 dB reflection coefficient in 8.38-9 GHz, as depicted in Fig. 5.40b. The narrow strip line of width 0.5 mm, which connects the triangular shaped radiator and 50 Ohms feed line depicted in Fig. 5.20c, plays an important role in achieving good impedance matching in the dual band.

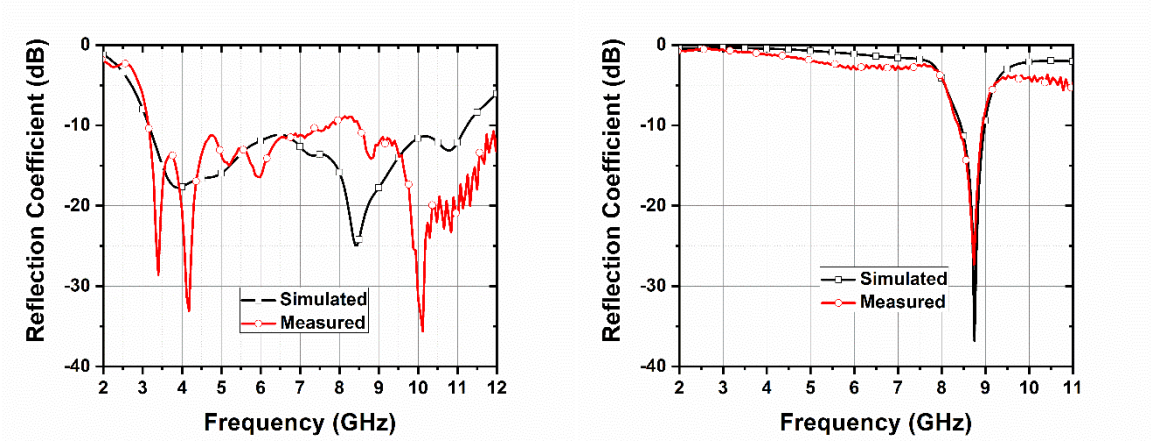

(a) (b)

Fig. 5.40. Plots of reflection coefficient vs frequency (a) UWB sensing antenna and (b) Antenna associated with port 5

Fig. 5.41 depicts the parametric study performed by varying the length (ln) of the narrow strip line of 0.5 mm width. It is observed that as length of the 0.5 mm feed line increases, the

reflection coefficient curve shifts leftward, as illustrated in Fig. 5.41. Base length (g) of the triangular patch has control on bandwidth. Therefore, by properly choosing the base length of the triangular patch and length of the 0.5 mm strip line, impedance matching can be achieved in the desired band, i.e., 8.38-9 GHz. The mutual coupling between antennas associated with port 1 and port 5 is less than -18 dB, as depicted in Fig. 5.42.

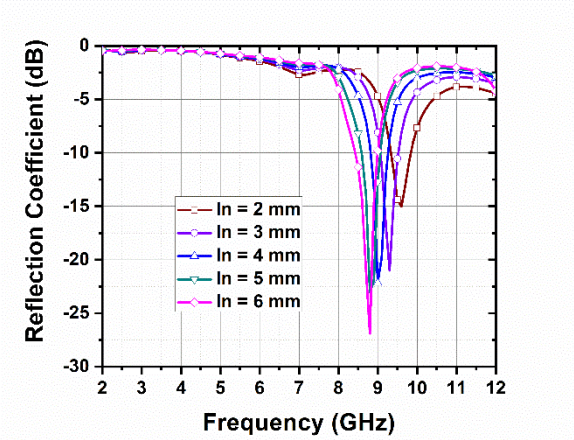

Fig. 5.41. Reflection coefficient's performance of the antenna associated with port 5 at different values of ln

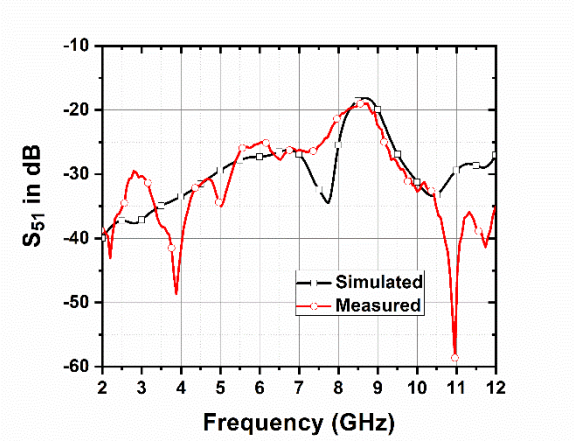

Fig. 5.42. Mutual coupling between antennas associated with port 5 and port 1

It can be observed from Fig. 5.43 that as altitude (at) of the triangular patch increases the resonant frequency of the antenna associated with port 5 decreases due to the electrical lengthening phenomenon. So, the altitude of the triangular patch plays a crucial role in determining the resonant frequency of the antenna associated with port 5. Also, it is noticed from Fig. 5.43 that altitudes of the triangular patch are approximately equal to the half of the guided wavelengths at resonances (i.e., at $\approx \frac{\lambda_g}{2}$).

Therefore, the resonating length that is responsible for resonance of the antenna associated with port 5 (i.e., $L_{r(P5)}$) can be written as given below.

$$L_{r(P5)} = at \tag{5.16}$$

The equation for the resonant frequency of the antenna associated with port 5 is written as given below.

$$f_{r(P5)} = \frac{c}{2L_{r(P5)}\sqrt{\varepsilon_{reff}}} \tag{5.17}$$

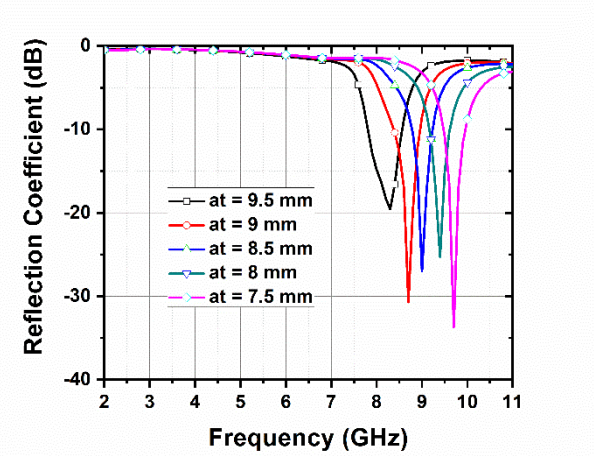

Fig. 5.43. Reflection coefficient of the antenna associated with port 5 for different values of at

Since the antenna associated with port 5 is a microstrip patch antenna with defected ground, ε_{reff} is calculated from the equation that was given in [7]. Its value is found to be 3.91. From Table 5.4, at is 9 mm. So, $L_{r(P5)}$ = 9 mm. After substituting the values of $L_{r(P5)}$, ε_{reff} and c in the Equation (5.17), we get $f_{r(P5)} \approx 8.42$ GHz. To show the effectiveness of the design equation, the percentage differences between the resonant frequencies that are obtained from simulation and the resonant frequencies that are obtained from the design equation are calculated in Table 5.6 for different values of at that affect $L_{r(P5)}$. It can be seen from Table 5.6 that the percentage difference is less than 3.51%, which shows a good agreement between the simulated data and the data obtained from design equation.

The simulated and measured radiation patterns of the antenna associated with port 5 when the remaining antennas are terminated with 50 Ohms load are depicted in Fig. 5.44. Directional patterns are achieved in the orthogonal planes with slight back radiation at 8.8 GHz due to its defected ground plane and the maximum level of cross pol reach -7 dB and -1 dB in

XZ plane and YZ plane, respectively. However, in broadside direction, simulated cross pol levels of -10 dB are observed in both the orthogonal planes, whereas the simulated co-pol levels of 3.9 dB are noticed in both the planes, as shown in Fig. 5.44. As it can be seen from Fig. 5.27, the peak gain of the antenna associated with port 4 is in 4.8-5.4 dBi in its operational bandwidth. Its radiation efficiency ranges from 70 to 80%, as shown in Fig. 5.28.

Table 5.6. Comparison between frequencies obtained from design equation and simulation for first resonance of the antenna associated with port 5

at (mm)	$L_{r(P5)}$ (mm)	Resonant Frequency (GHz)		% difference
		Design Equation	Simulation (HFSS)	
9.5	9.5	7.99	8.28	3.50
9	9	8.42	8.70	3.21
8.5	8.5	8.92	9.02	1.10
8	8	9.48	9.41	0.74
7.5	7.5	10.11	9.71	3.39

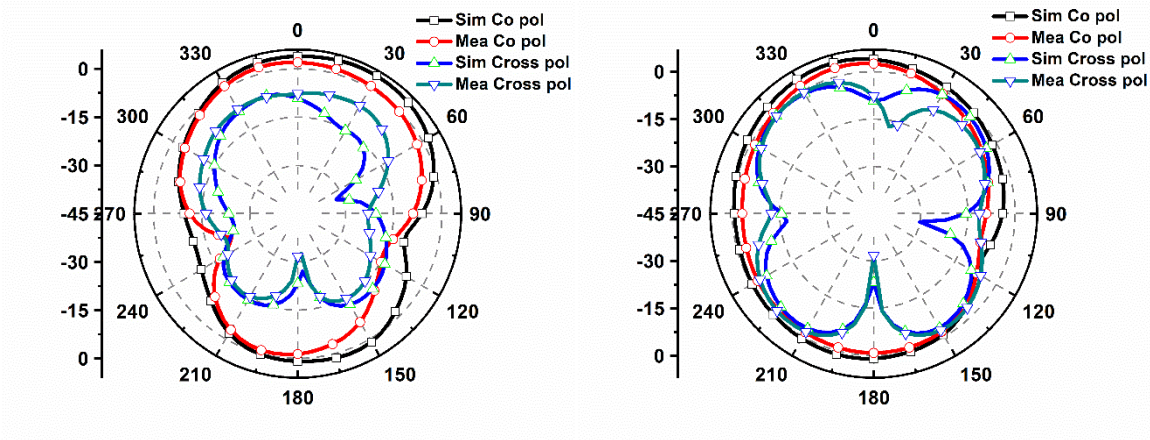

(a) (b)

Fig. 5.44. Patterns of the antenna associated with port 5 at 8.8 GHz (a) XZ plane (b) YZ plane

5.3.7. Design of the Antenna Associated with Port 6

One more NB antenna (i.e., the antenna associated with port 6) can be integrated by utilizing the space adjacent to the antenna associated with port 2 so that the all the frequency bands in

3.1-10.6 GHz are covered by the narrowband/wideband antennas. The reflection coefficient performance of the UWB sensing antenna when only the UWB sensing antenna and the antenna associated with port 6 are excited while the remaining antennas are terminated with 50 Ohms load is illustrated in Fig. 5.45a. The antenna associated with port 6 is an asymmetric fed monopole antenna which has -10 dB reflection coefficient in 9.7-10.7 GHz, as depicted in Fig. 5.45b. By varying the position of the tapered feed line along –ve X direction, impedance matching in 9.6-10.7 GHz is achieved. The measured mutual coupling between antennas associated with ports 1 and 6 is less than -16 dB, as depicted in Fig. 5.46.

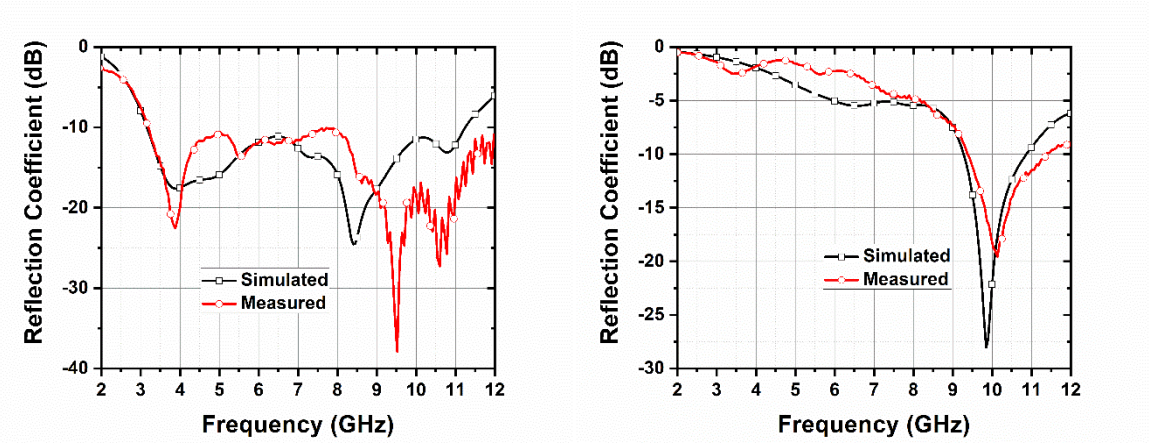

(a) (b)

Fig. 5.45. Plots of reflection coefficient vs frequency (a) UWB sensing antenna and (b) Antenna associated with port 6

The simulated and measured radiation patterns of antenna associated with port 6 when the remaining antennas are terminated with 50 Ohms load are illustrated in Fig. 5.47. In broadside direction, at 10 GHz, it is observed that the cross pol levels (simulated) reach -15.5 dB and -15 dB in XZ plane and YZ plane, respectively, as depicted in Fig. 5.47a and Fig. 5.47b. From Fig. 5.43, a gain of approximately 2.5 dBi is achieved in broadside direction in both the planes. The radiation efficiency is greater than 70% in its operational bandwidth, as illustrated in Fig. 5.28. The peak gain of the antenna associated with port 6 ranges from 3 dBi to 5.5 dBi, as shown in Fig. 5.27.

A special case is considered in which all the frequency bands in the UWB spectrum are unused so that every wideband and narrowband antenna performs a communication task. In such a case, it is necessary to maintain good isolation not only between UWB sensing antenna

and every wideband/narrowband antenna but also between any two wideband/narrowband antennas when all antennas meant for the purpose of communication are in use. The integration of the NB antennas (i.e., antennas associated with ports 4, 5, and 6) are done without disrupting the performances of the antennas associated with ports 1, 2, and 3. It can be seen from Figure 38 that the values of S_{24}, S_{34} S_{45}, S_{46}, S_{25}, S_{35}, S_{56}, S_{26}, and S_{36} are less than -15 dB in the frequency range (i.e., 3-11 GHz), which indicates that there is no significant coupling between the antennas associated with ports 4 and 1, 4 and 2, 4 and 3, 5 and 1, 5 and 2, 5 and 3, 6 and 1, 6 and 2, and 6 and 3. So, the presence of antennas associated with ports 4, 5, and 6 does not affect the performance of the antennas associated with the ports 1, 2, and 3.

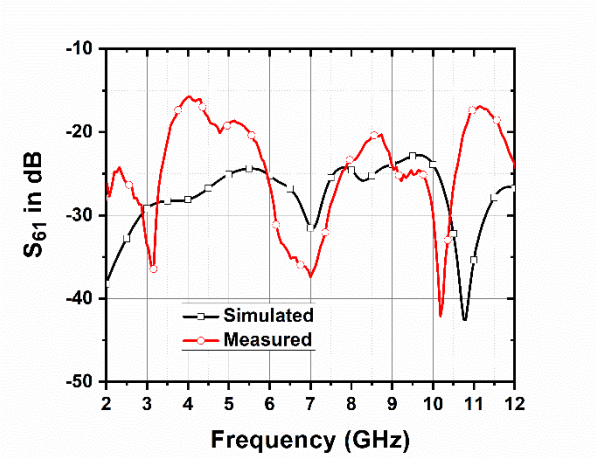

Fig. 5.46. Mutual coupling between antennas associated with port 6 and port 1

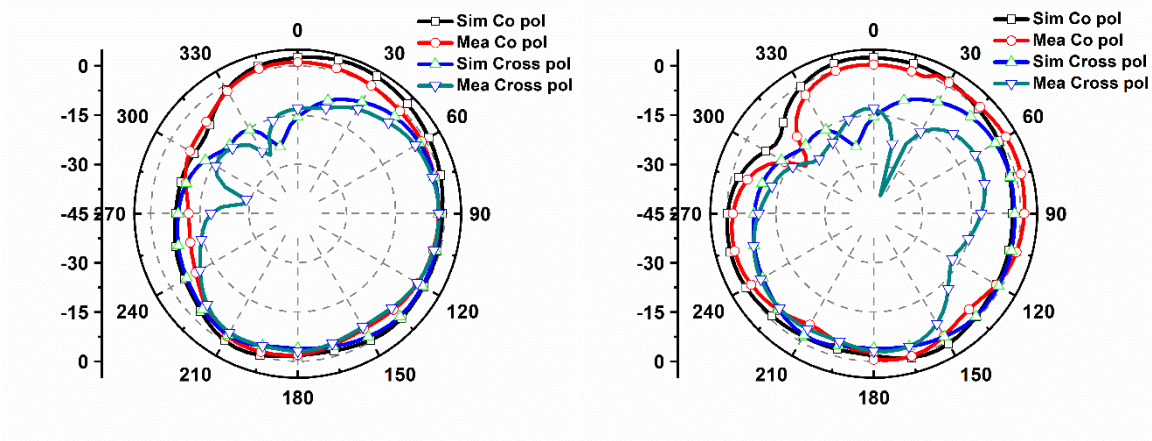

(a) (b)

Fig. 5. 47. Radiation patterns of the antenna associated with port 6 at 10 GHz (a) XZ plane and (b) YZ plane

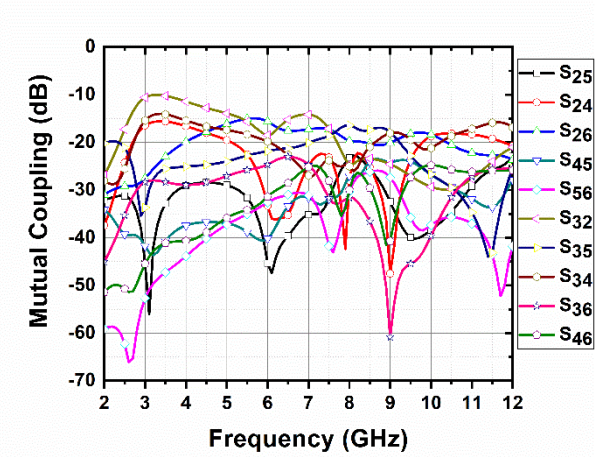

Fig. 5.48. Mutual coupling between the antennas used for communication

From Fig. 5.48, it is quite evident that the simulated inter port isolation between any two NB antennas is less than -15 dB in the spectrum of UWB except between the antennas associated with ports 2 and 3 where inter port isolation is less than -10 dB.

The poor isolation between the antennas associated with ports 2 and 3 is because of the strong surface current densities that exist on the elongated ground plane and on the 0.5 mm width narrow strip feed line of antennas associated with port 3 and port 2, respectively, at low frequencies in UWB of the two antennas. As it is well known that when two antennas having their current directions antiparallel to each other are kept side by side, significant current coupling exists between them.

The reason for good isolation between any other pair of wideband/NB antennas is due to their locations and current flow directions. In Table 5.7, the proposed six port antenna is compared with the other antennas reported in the previous literatures in terms of the dimensions of the substrate, frequency range of the antenna for sensing purpose, and the narrowband frequencies covered for communication purpose.

As shown in Table 5.7, when compared to all the other reported CR antennas in the literature, the proposed six port antenna is very compact and overcomes the difficulties that exist in reconfigurable antennas. Moreover, the proposed antenna can perform more number of communication tasks simultaneously due to the existence of multiple wideband and narrowband antennas for communication purpose. Reasonable peak gains are also achieved by the UWB sensing antenna and all WB/NB antennas for communication. Hence, the proposed six port CR antenna can be useful for CR applications.

Table 5.7. Comparison with the other antennas reported in the literature for CR applications

Ref.	**Dimensions of the substrate (mm^3)**	**Frequency range of the sensing antenna (GHz)**	**Narrowband frequencies (GHz) for the purpose of communication**	**Peak gains (dBi) in narrowband frequency ranges (GHz)**
[79]	70×50×1.6	2-10	Five frequency bands in 2-10	7.77 in 2.1-3, 7.4 in 3-3.4, 6.62 in 3.4-5.56, 6.67 in 5.-6.2, and 8.45 in 6.3-10
[81]	30×30×1.6	3.1-10.6	6.36-6.63, 7.33-7.7, 8.78-9.23, and 9.23-9.82	3.03 in 6.36-6.63, 3.64 in 7.33-7.7, 2.53 in 8.78-9.23, and 3.2 in 9.23-9.82
[83]	40×40×1.6	3-12	4.93-5.4, 5.9-6.7, and 9.28-10.2	Peak gain varies between 1 and 7 in its frequency bands
[82]	40×36×1.6	3.1-10.6	Five frequency bands in the frequency range, i.e., 3.1-10.6	-2.83 in 3.06-4.23, -0.88 in 4-6.37, 0.65 in 6.33-8.83, 5.13 in 8.7-9.92, and 5.61 in 9.82-10.74
[84]	40×36×0.662	3-11	Three frequency bands in 5-6	1.87 in 5-6
[125]	58×65.5×1.6	3.3-11	3.4-4.85 and 5.3-9.15	Not given
[86]	68×54×0.79	3-11	4, 4.9-5.35, 8, and 10	0.2 at 4, 0.6 at 5.15, 1.9 at 8, and 4.4 at 10
[87]	40×38.5×0.5	3-11	Five frequency bands in the frequency range, i.e., 5.8-9.2	-0.1 to 4.5 at four operating bands
Present work	**42×27×1.6**	**3-10.6**	**Five frequency bands cover entire UWB**	**2.7 in 3-3.6, 2.2 in 3.6-5.8, 4.92 in 5.4-8, 2.8 in 8-8.4, 5.28 in 8.4-9, 4.11 in 9-9.8, and 5.04 in 9.7-10.7**

5.4. Conclusion

A 3 port integrated UWB and NB antenna system design has been presented in this chapter as a first contribution. Since two communications are possible at a time, spectrum utilization efficiency is improved significantly. Therefore, the proposed 3 port antenna can be good candidate for CR applications. Also, a compact six port integrated UWB sensing and narrowband/wideband antennas for CR applications has been presented in this chapter. The most distinguishing feature of this design approach is enhancing the utilization of spectrum by performing multiple communication tasks when multiple white spaces are detected. Moreover, all the communication bands in the UWB spectrum are covered by the wideband/narrowband antennas in the proposed designs. Despite being compact in structure, all antennas in the proposed antenna system are electromagnetically well isolated. The obtained radiation patterns are well fit for cognitive radio applications. Hence, the proposed six port antenna is well suitable for cognitive radio applications.

Chapter-6

Integrated Wideband Sensing and WB/NB Antennas Systems for CR MIMO Applications

6.1. Introduction

In the previous chapter, integrated UWB sensing and WB/NB antennas systems for CR applications are presented to eliminate the drawbacks in reconfigurable CR antennas. As a continuation to the previous chapter, integrated wideband sensing and WB/NB antennas systems for CR MIMO applications are presented in this chapter to eliminate the drawbacks in reconfigurable CR MIMO antennas.

In this chapter, to overcome the drawbacks in reconfigurable antennas and maintain all the advantages in planar antennas, a compact twelve port integrated UWB and narrow band (NB)/wideband antenna system for cognitive radio MIMO applications with polarization diversity is presented. The proposed system has one pair of UWB antennas for sensing the spectrum and five pairs of NB/Wideband antennas for communication. Each pair has two identical antennas, which are orthogonal to each other for polarization diversity. Sensing antennas linked with ports (P1 and P7) operate at 3-11 GHz, whereas the antennas linked with ports (P2 and P8), (P3 and P9), (P4 and P10), (P5 and P11), and (P6 and P12) operate at 3.5-5.8 GHz, 2.8-3.5 GHz and 5.6-8 GHz (dual band), 8-8.4 GHz and 9-9.8 GHz (dual band), 8.4-9 GHz, and 9.8-11GHz, respectively. Moreover, the overall volume of the antenna is 58 mm × 50 mm × 1.6 mm and the entire UWB spectrum is covered by narrow band/wideband antennas. Also, without any decoupling network, isolations of better than 20 dB and 15 dB are achieved between every two identical and non-identical antennas, respectively.

This chapter also presents a nine port MIMO antenna for cognitive radio MIMO applications to avoid the complexities involved in reconfigurable antennas and improve the spectrum utilization efficiency. The proposed MIMO antenna system comprises a wideband antenna that operates at 2-12 GHz for sensing the spectrum and four pairs of antennas for communication, which are single and dual-band antennas. Each pair of antennas meant for communication consists of two similar antennas. Moreover, the antennas meant for communication cover 93% of the bandwidth of the sensing antenna. The first pair of antennas accessible at ports P2 and P6 and second pair of antennas accessible at ports P4 and P8, which are dual-band antennas, operate at 3.05-3.85 GHz, 5.8-8 GHz and 2.05-2.55 GHz, 4.7-6.1 GHz, respectively. Whereas the third pair of antennas accessible at ports P3 and P7 and fourth pair of antennas accessible at ports P5 and P9 are single-band antennas and operate at 3.85-4.7 GHz and 8-11 GHz, respectively. Minimum isolations of 20 dB and 15 dB are attained between every two similar antennas for communication and between the sensing antenna and the antennas meant for communication, respectively. The correctness of the proposed antenna is verified with a fine match between the results obtained from simulations and measurements.

The remaining contents of this chapter are structured as follows: The design of the twelve port antenna system that comprises one pair of UWB antennas for sensing the spectrum and five pairs of NB/Wideband antennas for communication is demonstrated in Section 6.2. The design of the nine port antenna system that comprises a wideband antenna that operates at 2-12 GHz for sensing the spectrum and four pairs of antennas for communication is presented in Section 6.3. The conclusion of this chapter is given in Section 6.4.

6.2. Twelve Port Integrated UWB and WB/NB Antennas System Design for CR MIMO Applications

In this design, the antennas, which are designed in six port antenna system for CR applications, are used with slight alterations in their dimensions to get the required frequency band of operation. However, the working principle of the antennas used in this design are presented concisely. In this section, a twelve port MIMO antenna with polarisation diversity for cognitive radio platforms is reported. Among the twelve antennas, two similar UWB antennas are dedicated for sensing purpose and the remaining ten wideband/NB antennas are used for communication. Polarisation diversity and high isolation between the similar antennas are

achieved by placing two identical antennas in each pair perpendicular to each other. The overall area of the proposed MIMO antenna is 58 × 50 mm^2.

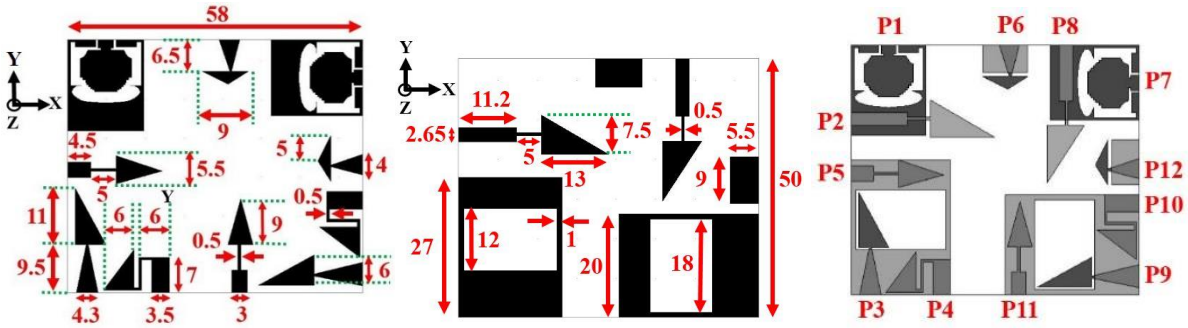

(a) (b) (c)

Fig. 6.1. The proposed twelve port antenna (a) Top view (b) Bottom view (Dimensions in mm) (c) Final structure

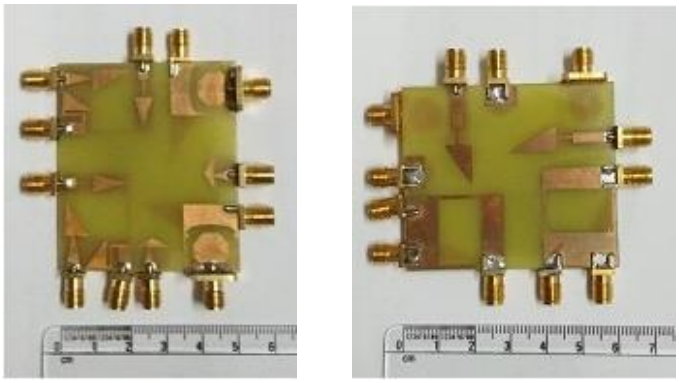

(a) (b)

Fig. 6.2. Fabricated prototype of the twelve port CR MIMO antenna (a) Top view (b) Bottom view

The configuration of the proposed antenna, top and bottom views of the fabricated prototype are depicted in Figs. 6.1, 6.2a, and 6.2b, respectively. Also, the fabricated antenna is tested by using Agilent N5232A PNA-L network analyser to demonstrate its functionality.

6.2.1. Antenna Design

The design process starts with the design of an UWB antenna. Initially, a compact UWB antenna with an area of 15 × 18 mm^2 is designed, as shown in Fig. 6.3. The simulated and measured s-parameters of all the antennas in the twelve port MIMO system are shown in Figs. 6.4, 6.5, and 6.6.

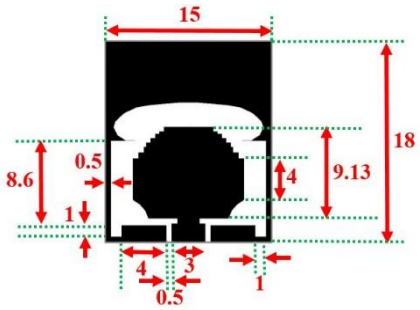

Fig. 6.3. Geometry of the UWB sensing antenna

By properly choosing the dimensions of widths of the wide rectangular slot, two rectangular notches, and ‘ Ω ’ shaped notch in the ground plane, impedance matching at low frequencies is achieved. Later, the rectangular patch is modified to achieve impedance matching at the mid frequencies of UWB and the modified patch is fed by a microstrip line of impedance greater than 50 Ohms added with a strip line of impedance 50 Ohms for impedance matching purpose at high frequencies of the UWB.

The reflection coefficient performance of UWB sensing antenna linked with port 1 is shown in Fig. 6.4a. Thereafter, as illustrated in Fig. 6.1c, beneath the ground plane of the UWB antenna, a very thin strip line of 0.5 mm width is used in between right angled triangular shaped radiator and 50 Ohms strip line to produce a wideband that ranges from 3.5 GHz to 5.8 GHz, which is shown in Fig. 6.4b. The length of 0.5 mm strip line controls the resonance at the low frequencies of the operating bandwidth.

Despite the antenna linked with port 2 shares common ground with UWB sensing antenna, isolation of better than 12 dB is achieved in the entire UWB, as depicted in Fig. 5b. This is due to the fact that current flow directions at all frequencies in the UWB sensing antenna and antenna linked with port2 are orthogonal to each other. Moreover, the other reason is due to the weak surface currents at the ground plane that exists exactly above feed line of antenna linked with port 2 at all the frequencies in UWB when sensing antenna is excited, as depicted in Fig. 6.7.

As illustrated in Fig. 6.4c, the antenna linked with port 3 is a dual band antenna, which covers communication bands, i.e., 2.8-3.5 GHz and 5.6-8 GHz since it has two distinct current paths. From the surface current distribution plots, it is evident that the resonance at the low frequencies of antenna linked with port 3 is due to the long electrical length provided by the

extended ground plane, as shown in Fig. 6.7. Whereas the active right angled triangular patch is responsible for the resonance at high frequencies, as shown in Fig. 6.7.

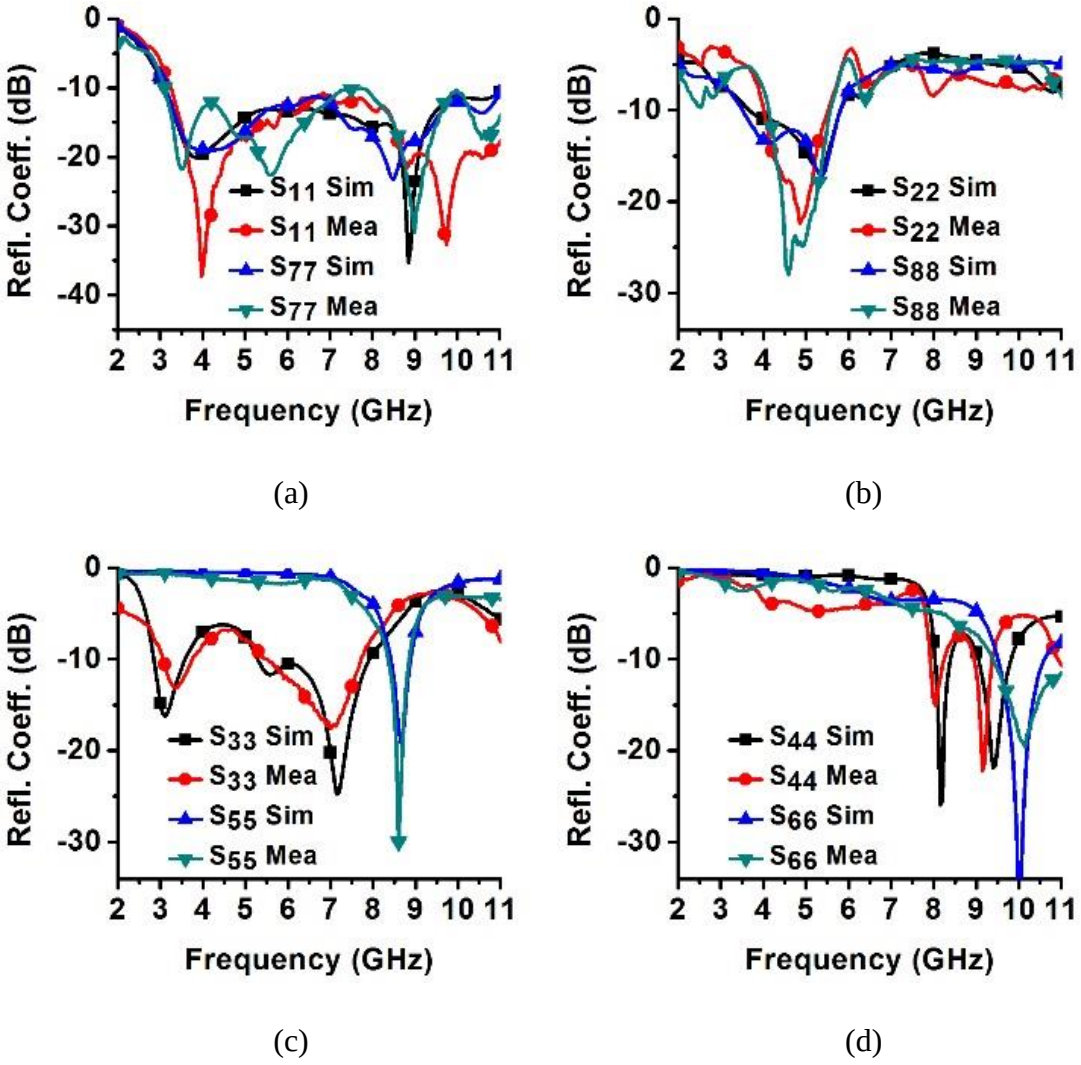

Fig. 6.4. Reflection coefficients of the antennas associated with ports 1, 2, 3, 4, 5, 6, 7, and 8 (a) Plot of S_{11} and S_{77} (b) Plot of S_{22} and S_{88} (c) Plot of S_{33} and S_{55} (d) Plot of S_{44} and S_{66}

Antenna linked with port 4 covers two communication bands, i.e., 8-8.4 GHz and 9-9.8 GHz, as shown in Fig. 6.4d. To achieve impedance matching in these bands, a meander line type feed structure is used, as depicted in Fig. 6.1c. Antenna linked with port 5 is a narrow band antenna, which operates at 8.4-9 GHz, as shown in Fig. 6.4c.

Impedance matching is achieved by selecting the proper length of the 0.5 mm strip line, which is in between the triangular patch and 50 Ohms feed line, as shown in Fig. 6.1c. Although the antennas linked with ports 3, 4, and 5 share common ground, a minimum isolation of better than 15 dB in the entire UWB is achieved among these antennas. Their current flow directions

and placements ensure good isolation among them, which can be understood from the surface current distribution plots shown in Figs. 6.7 and 6.8.

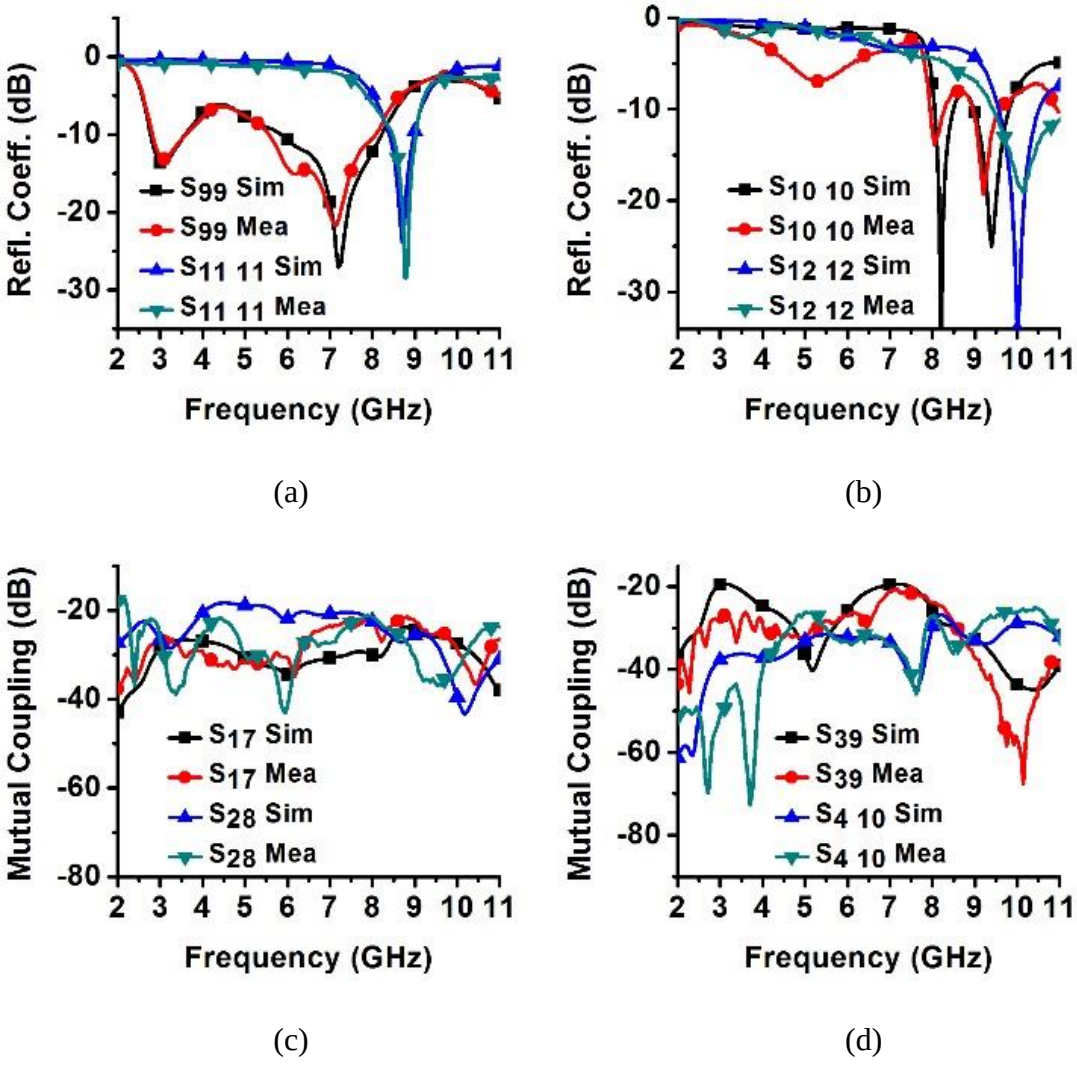

Fig. 6.5. Reflection coefficients of the antennas associated with ports 9, 10, 11, and 12 and mutual coupling (a) Plot of S_{99} and $S_{11\,11}$ (b) Plot of $S_{10\,10}$ and $S_{12\,12}$ (c) Plot of S_{17} and S_{28} (d) Plot of S_{39} and $S_{4\,10}$

For the sake of brevity, isolation plots among the antennas linked with ports 3, 4 and 5 are not presented. Antenna linked with port 6 is an asymmetrically fed monopole antenna with a tapered feed line, which has an impedance bandwidth in 9.8-11 GHz, as shown in Fig. 6.4d. Whenever a spectrum hole is identified, the NB/Wideband antenna that operates in that spectrum is used for communication purpose. Meanwhile, the remaining antennas used for communication are terminated with 50 Ohms load.

For MIMO antenna system with polarization diversity, the identical antennas are placed in such a way that their current flow directions are orthogonal to each other. Moreover, due to their placement, without using any isolation technique, good isolation levels of better than 20 dB are achieved, as illustrated in Figs. 6.5 and 6.6a.

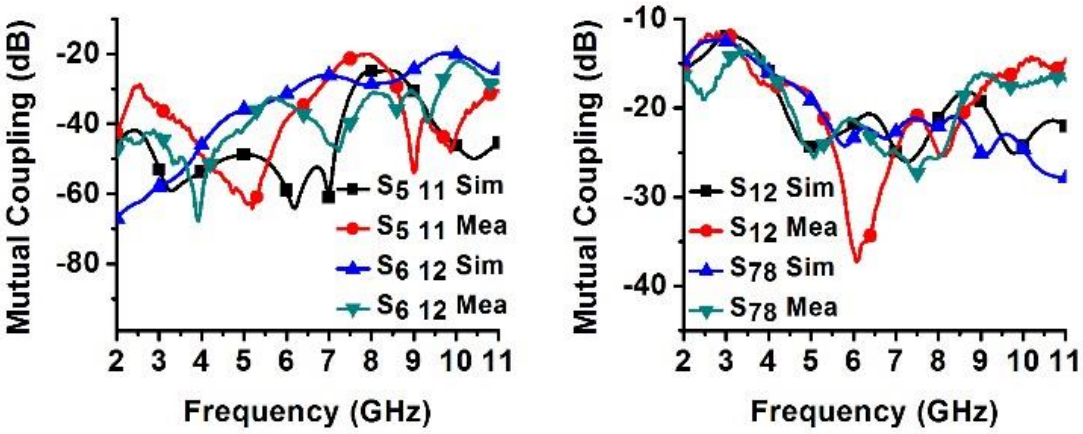

(a) (b)

Fig. 6.6. Mutual coupling between antennas for communication (a) Plots of $S_{5\,11}$ and $S_{6\,12}$ (b) S_{12} and S_{78}

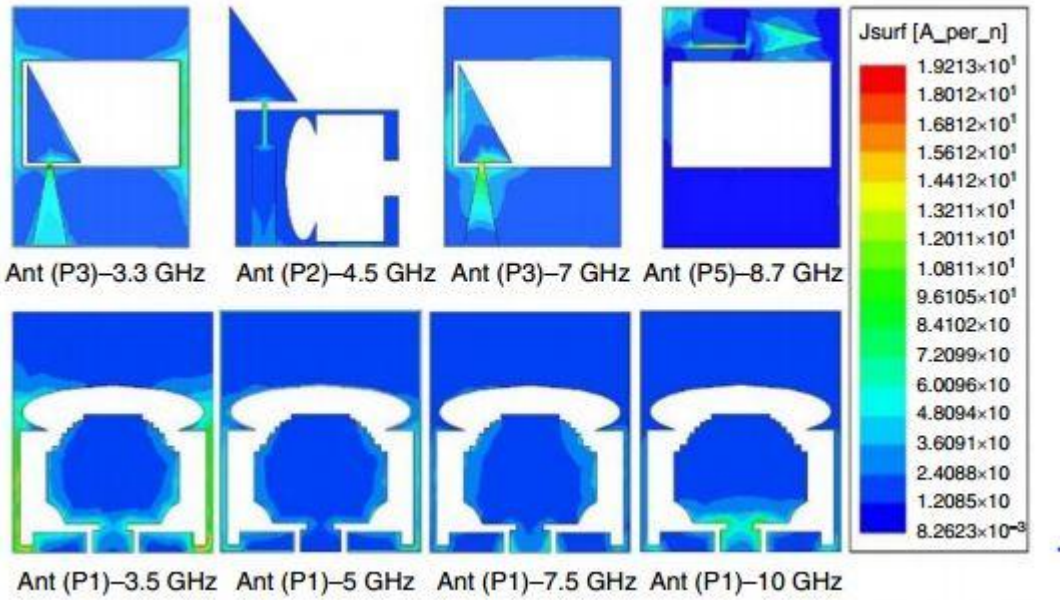

Fig. 6.7. Surface current distributions of the antennas linked with port 3 at 3.3 and 7 GHz, port 2 at 4.5 GHz, port 5 at 8.7 GHz, and port 1 at 3.5, 5, 7.5, and 10 GHz

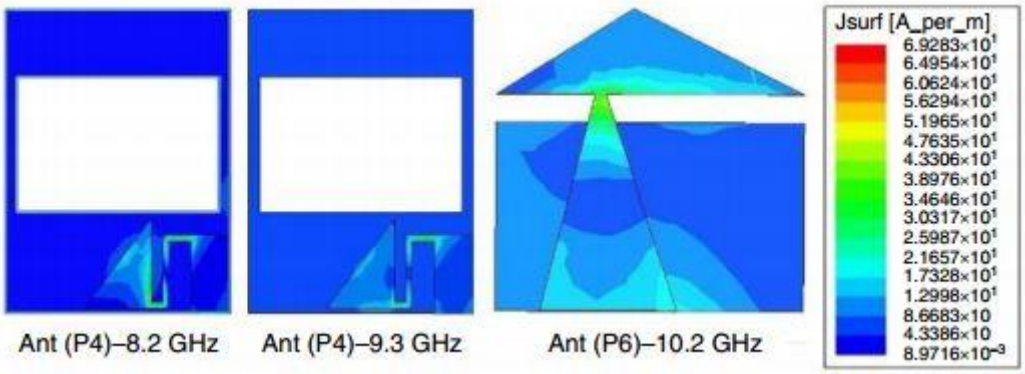

Fig. 6.8. Surface current distributions of the antennas linked with port 4 at 8.2 and 9.3GHz and port 6 at 10.2 GHz

6.2.2. Results and Discussions

The measured radiation patterns of the antennas coupled with port 1, 2, 3, 4, 5 and 6 in orthogonal planes are shown in Figs. 6.9 and 6.10. During measurement time, only one port is excited and the rest of the ports are terminated with 50 Ohms load. At 4.5 GHz, the antenna linked with port 2 has maximum gains of 0.2 dBi and 0.6 dBi in end fire direction in XZ and YZ planes, respectively, as shown in Figs. 6.9a and b.

Since the antenna linked with port 2 is asymmetrically fed monopole antenna, the existence of horizontal surface currents causes maximum cross pol levels to reach -7.3 dB and -4 dB in XZ and YZ planes, respectively, as shown in Figs. 6.9a and b. As illustrated in Figs. 6.9a and b, at 3.3GHz, the antenna linked with port 3 has monopole like radiation patterns in both the planes, whereas nearly omnidirectional patterns are observed in both the planes at 7 GHz.

As depicted in Figs. 6.9a and b, there is a significant rise of cross pol at 7 GHz in both the planes due to its asymmetrically fed monopole like structure of the antenna. However, in indoor wireless communication systems, where channels are influenced by Rayleigh fading, cross pol performance is not a vital requirement.

The antenna linked with port 4 has patterns that are partly bidirectional and directional in nature in both the planes at 8.2 and 9.3 GHz, respectively, as shown in Figs. 6.9c and d. Due to its defected ground structure, the antenna linked with port 5 has directional pattern with a little back radiation in XZ plane, whereas it has nearly omnidirectional pattern in YZ plane at 8.7 GHz, as shown in Figs. 6.9c and d.

At 10.2 GHz, the antenna linked with port 6 has nearly omnidirectional patterns in the orthogonal planes, as shown in Figs. 6.10c and d. From Figs. 6.10a and b, it can be seen that dumbbell shaped patterns in XZ plane and omnidirectional patterns in YZ plane are achieved at three sampling frequencies (3.5, 5, and 7.5GHz) in case of UWB sensing antenna linked with port1.

As illustrated in Figs. 6.10c and d, at high sampling frequency of 10 GHz, nearly omnidirectional patterns in both the planes are achieved and cross polarization significantly grows due to the horizontal current modes.

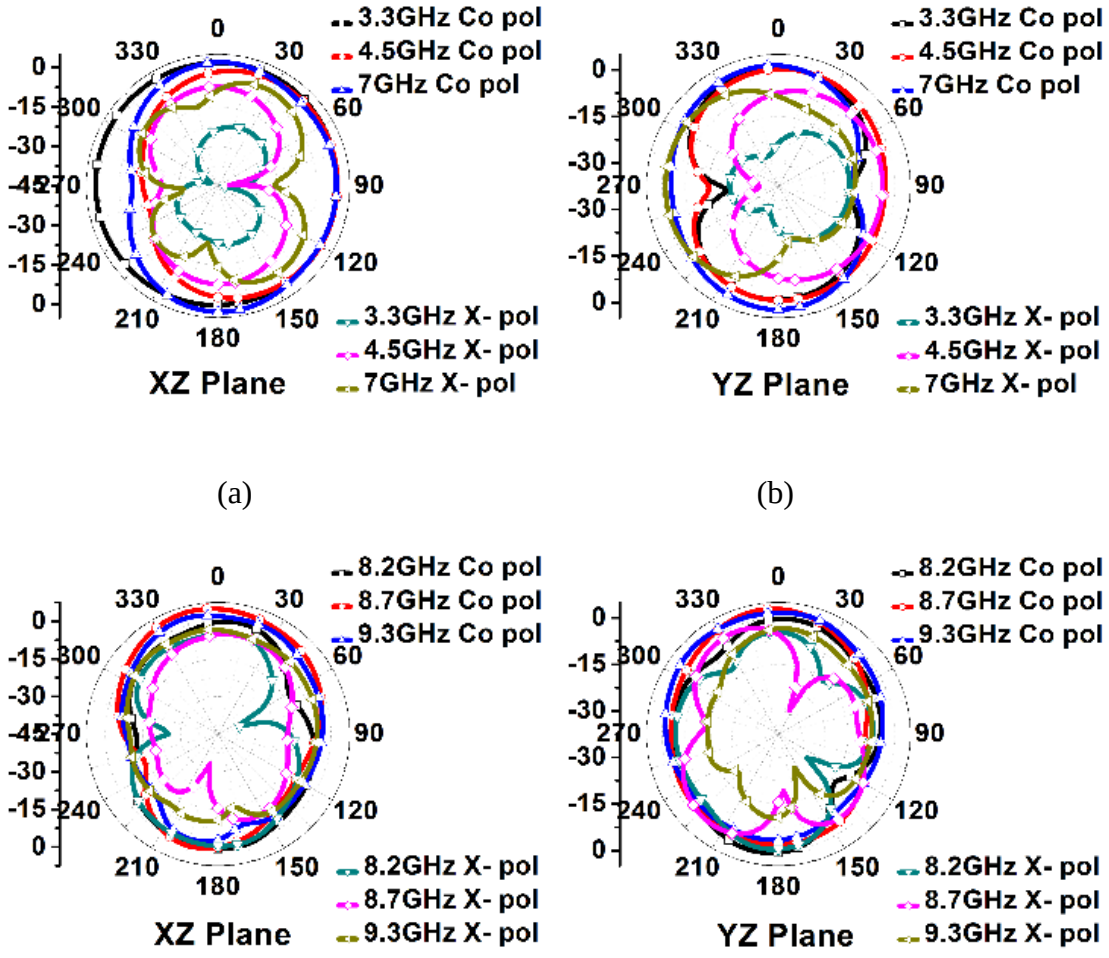

(a) (b)

(c) (d)

Fig. 6.9. Measured radiation patterns of the communication antennas (a) linked with port 2 at 4.5 GHz and port 3 at 3.3 and 7 GHz in XZ plane (b) linked with port2 at 4.5 GHz and port 3 at 3.3 and 7 GHz in YZ plane (c) linked with port 4 at 8.2 and 9.3 GHz and port 5 at 8.7 GHz in XZ plane (d) linked with port 4 at 8.2 and 9.3 GHz and port 5 at 8.7 GHz in YZ plane

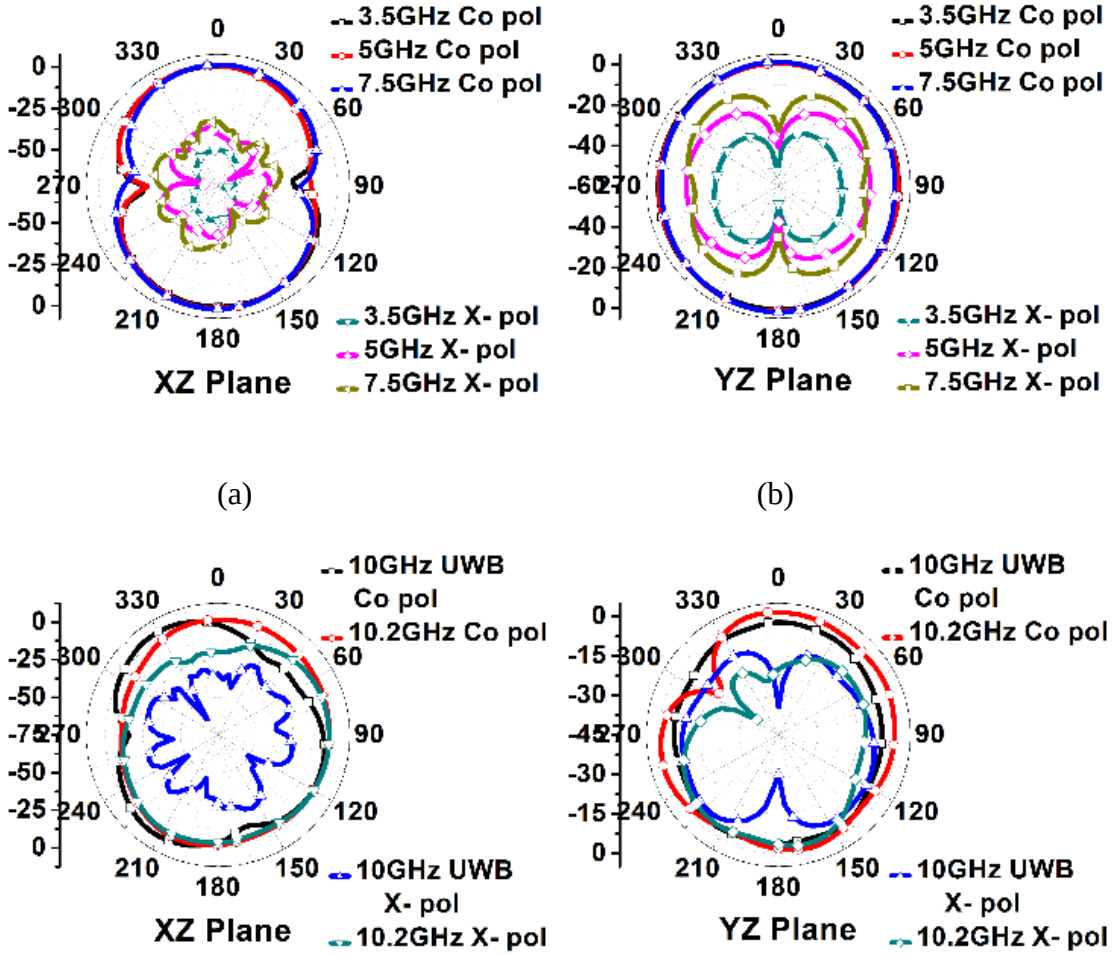

Fig. 6.10. Measured radiation patterns of the linked with port 1 and port 6 (a) sensing antenna linked with port 1 at 3.5, 5, and 7.5 GHz in XZ plane (b) sensing antenna linked with port 1 at 3.5, 5, and 7.5 GHz in YZ plane (c) sensing antenna linked with port 1 at 10 GHz and communication antenna linked with port 6 at 10.2 GHz in XZ plane (d) sensing antenna linked with port 1 at 10 GHz and communication antenna linked with port 6 at 10.2 GHz in YZ plane

The measured peak gains and radiation efficiencies of the UWB sensing antenna and the antennas used for communication purpose are shown in Figs. 6.11a and b, respectively. In order to evaluate the diversity performance of the proposed MIMO antenna, the parameters like Envelope correlation coefficient (ECC) and diversity gain (DG) are calculated using [166]. From Figs. 6.11c and d, it is observed that measured diversity gain between any two identical antennas used for the purpose of communication is approximately 10 dB and Envelope

Correlation Coefficient (ECC) between any two identical antennas used for communication is less than 0.004, which specifies the good diversity performance of the proposed MIMO antenna.

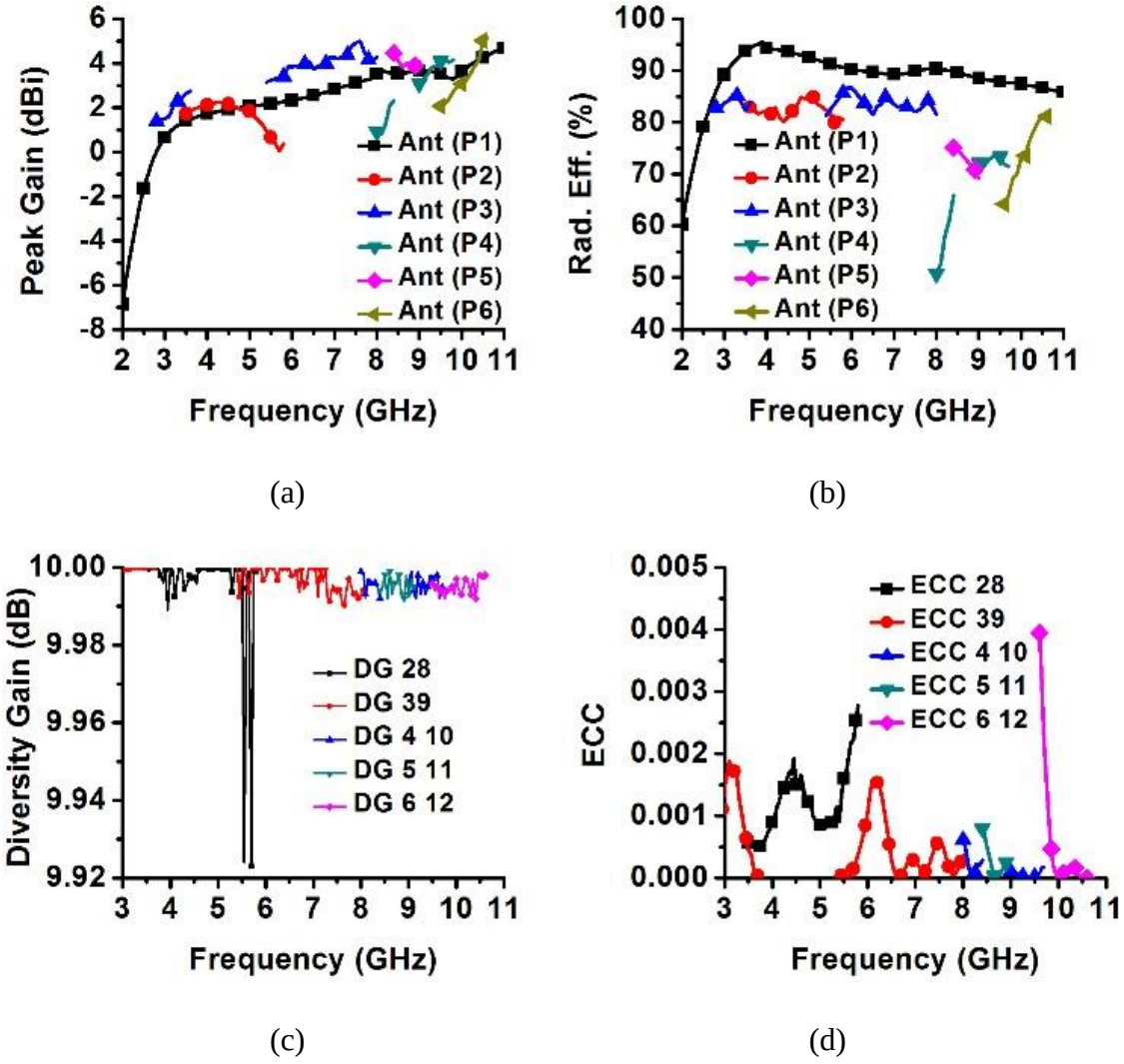

Fig. 6.11. Peak gains, radiation efficiencies, diversity gain, and ECC of the CR MIMO antenna (a) Measured peak gains of the UWB sensing antenna and antennas used for communication (b) Measured radiation efficiencies of the UWB sensing antenna and antennas used for communication (c) Diversity gain of the CR MIMO antenna (d) ECC of the CR MIMO antenna

6.3. Nine Port Integrated WB Sensing and WB/NB Antennas System Design for CR MIMO Applications

The proposed CR MIMO antenna is realized by using an FR4-epoxy substrate, which has a relative permittivity of 4.4, loss tangent of 0.02, and a thickness of 1.6 mm. Its schematic is

illustrated in Fig. 6.12 and the values of the design parameters are listed in Table 6.1. Also, the detailed explanation of each antenna unit in the proposed MIMO antenna is presented in this section. The specifications of the proposed MIMO antenna are tabulated in Table 6.2.

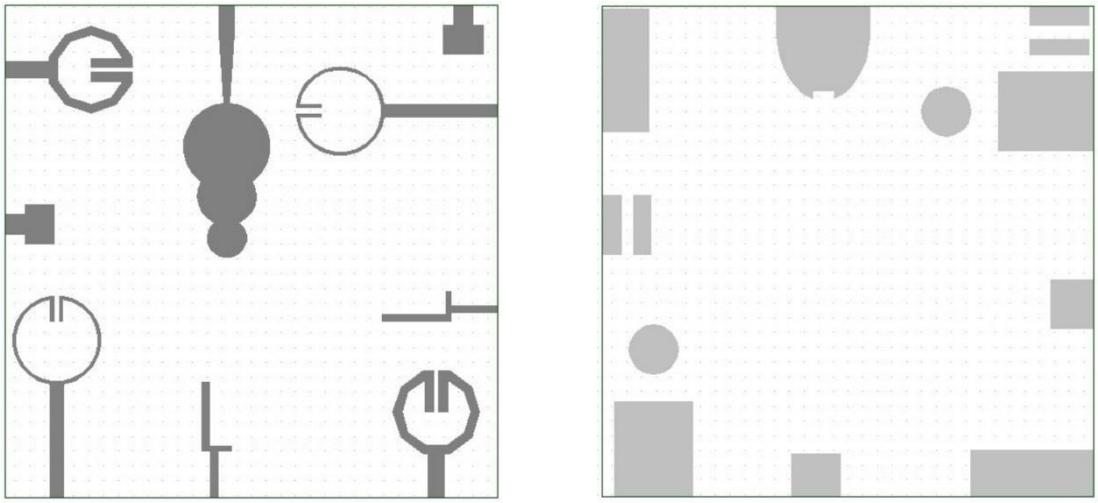

(a) (b)

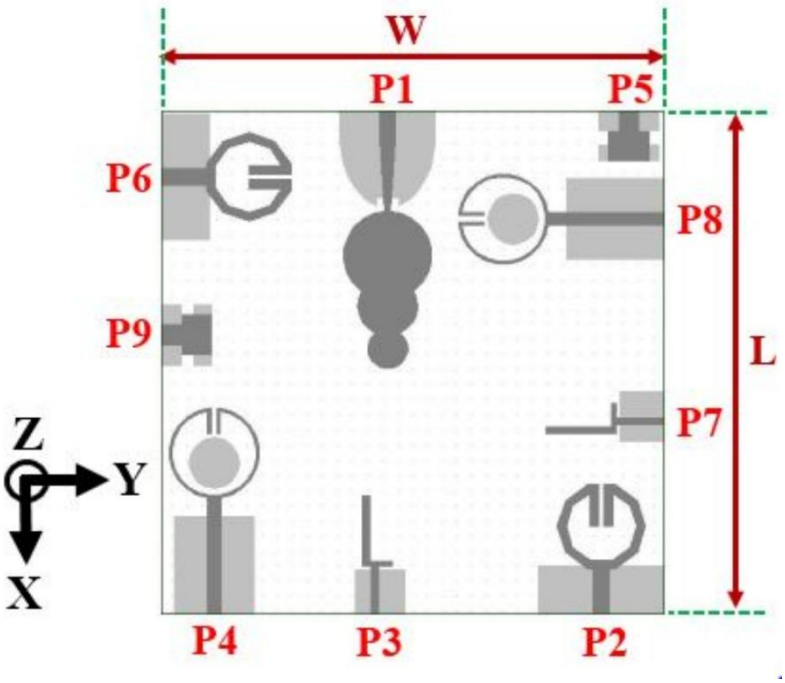

(b)

Fig. 6.12. Geometry of the proposed two-element MIMO antenna (a) Top view (b) Bottom view (c) Antenna structure

Table 6.1. Optimized dimensions of the proposed MIMO antenna

Parameter	Value (mm)	Parameter	Value (mm)	Parameter	Value (mm)
lg_1	5	g3	0.77	W1	1.71
wg_1	18.98	L3	15	W2	1.8
wf_1	3	L4	4.5	g2	1
Ln	1.57	W3	1	lg_3	8.8
Wn	4.5	W4	1.5	wg_3	10
g1	1.16	lg_4	19.5	wf_3	1.5
R1	8.78	wg_4	16	L	100
R2	5.28	wf_4	2.5	wf_5	4
R3	4	L5	4.39	L6	5.8
lg_2	9.5	W5	0.6	L7	4
wg_2	25	D4	16.8	W6	8
wf_2	3.3	D5	10	W7	12
L1	5.43	lg_5	4	W	100
L2	6.5	wg_5	12		

Table 6.2. Specifications of the proposed MIMO antenna

Antenna	Purpose	Operating bandwidths
Ant (P1)	Sensing	2-12 GHz
Ant (P2) and Ant (P6)	Communication	3.05-3.85 GHz and 5.8-8 GHz
Ant (P3) and Ant (P7)	Communication	3.85-4.7 GHz
Ant (P4) and Ant (P8)	Communication	2.05-2.55 GHz and 4.7-6.1 GHz
Ant (P5) and Ant (P9)	Communication	8-11 GHz

6.3.1. Design Procedure of the Wideband Sensing Antenna

The geometry of the wideband sensing antenna is illustrated in Fig. 6.13. The evolution of the wideband sensing antenna (i.e., antenna accessible at port 1) is completed in five steps, as illustrated in Fig. 6.14. In the first step, a simple monopole antenna is designed by feeding a circular patch with a 50 Ohms feed line. This Antenna I yields a wideband that ranges from 2.6 GHz to 10.6 GHz, as depicted in Fig. 6.15. In the second step, to make the antenna resonant at low frequencies, a circle of radius R2 is combined with the top of the circular radiator of radius R1, as shown in Fig. 6.13. As shown in Fig. 6.15, this configuration of Antenna II produces a dual-band (2.25-3 GHz and 5.75-10.4 GHz). In the third step, to further shift the resonant frequencies to the left side, a circle of radius R3 is combined with the top of the radiator of the Antenna II, as depicted in Fig 6.14. It is noticed from Fig. 6.15 that this configuration of Antenna III produces a triple band (2.07-2.55 GHz, 4.3-8.1 GHz, and 8.8-10.8 GHz). But the main purpose of designing this antenna is to produce a 2-11 GHz sensing band. So, in the fourth step, as depicted in Fig. 6.14, a semi-elliptical ground plane is used in Antenna IV instead of the rectangular ground plane and also the upper section of the feed line is tapered for good impedance matching at 2-11 GHz. However, the reflection coefficient of the Antenna IV is slightly greater than -10 dB in the frequency bands, i.e., 2.81-3.58 GHz and 5.57-6.34 GHz, as illustrated in Fig. 6.15. So, a rectangular notch is employed in the semi-elliptical ground plane in the last step to improve the impedance matching in those frequency bands, as shown in Fig. 6.14.

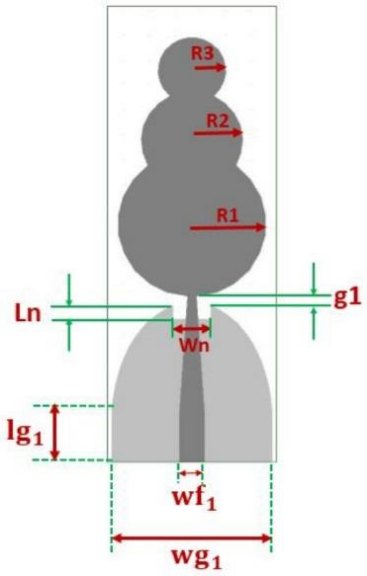

Fig. 6.13. Geometry of the wideband sensing antenna

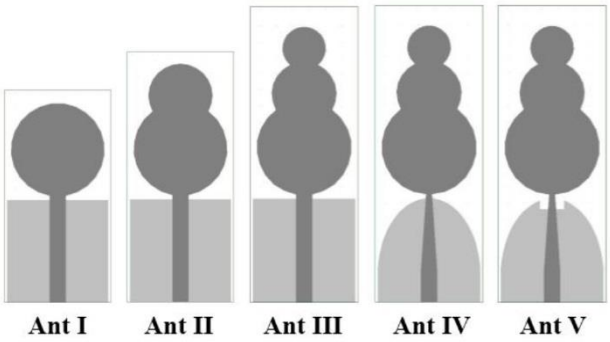

Fig. 6.14. Evolution of the wideband sensing antenna

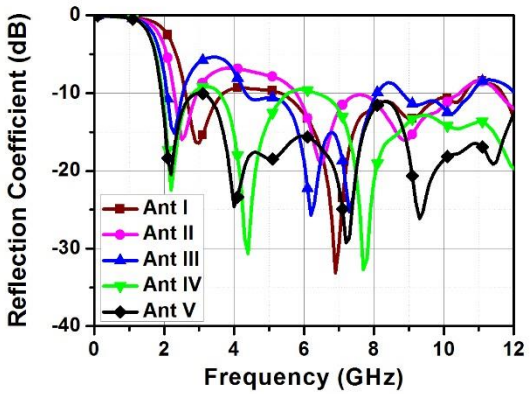

Fig. 6.15. Reflection coefficients of all antennas in the design process of the sensing antenna

6.3.2. Design Procedure of the Antenna Accessible at Port 2

The geometry of the antenna accessible at port 2 is shown in Fig. 6.16.

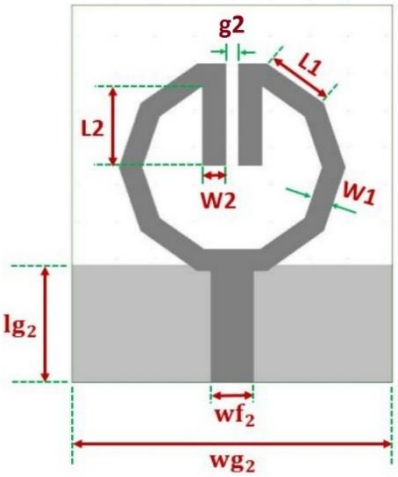

Fig. 6.16. Geometry of the antenna accessible at port 2

The antenna accessible at port 2 is a dual-band antenna, which consists of a decagonal split ring resonator as the radiating element. Split ring resonator (SRR) consists of a single ring in this antenna design, whereas a conventional SRR has two rings. The reason behind choosing this kind of SRR is that the inductance and capacitance of the SRR can be varied by changing its length; hence, the frequency tuning can be done easily.

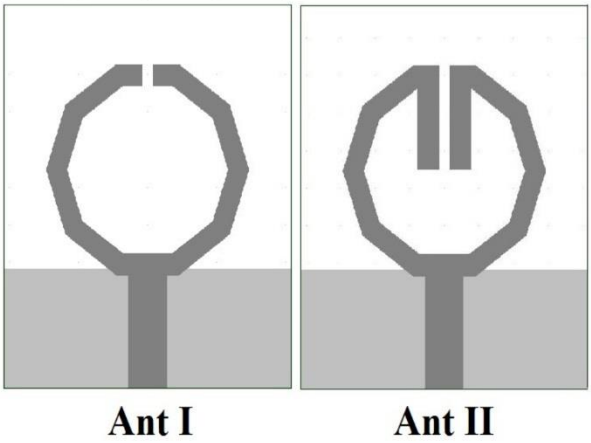

Fig. 6.17. Evolution of the antenna accessible at port 2

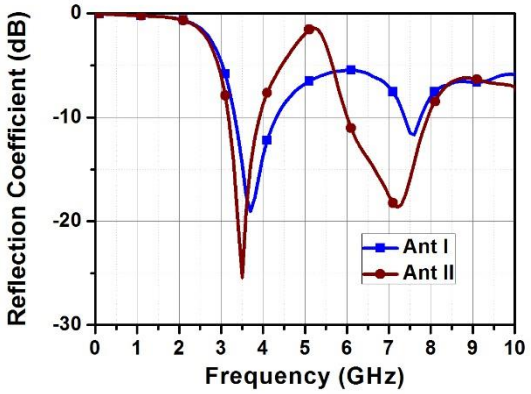

Fig. 6.18. Reflection coefficient performances of the antennas in the design process of antenna accessible at port 2

The total length (2(5L1+L2)-g2) and the split gap (g2) constitute the inductance and capacitance of the decagonal SRR, respectively. Since the resonance characteristics of decagonal SRR are determined by its inductance and capacitance, the desired resonance can be obtained by altering L1, L2, and g2. Initially, a decagonal split ring without the shunt arms is fed by a strip line of 50 Ohms impedance with the partial ground, as shown in Ant I of Fig. 6.17. Two resonances at 3.7 GHz and 7.5 GHz are observed from the reflection coefficient performance of Ant I, as

depicted in Fig. 6.18. However, the antenna accessible at port 2 is mainly targeted to achieve one resonance at 3.5 GHz and other resonance at high frequency with wide bandwidth. So, in the next stage, two shunt arms of equal length L2 are added to the decagonal split ring of Ant I in Fig. 6.17.

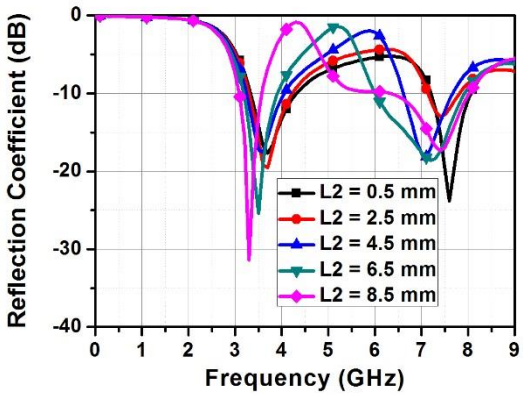

Fig. 6.19. Effect of shunt arms' length L2 on the reflection coefficient performance of antenna accessible at port 2

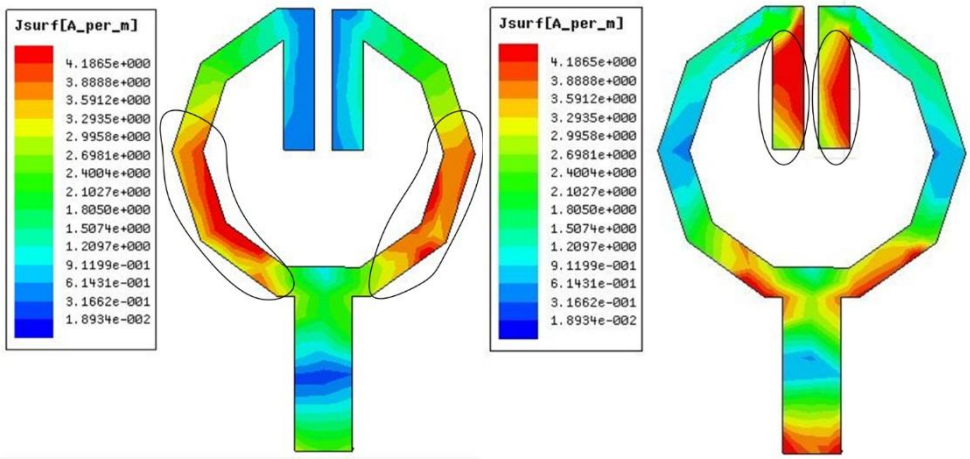

(a) (b)

Fig. 6.20. Surface current densities of the antenna accessible at port 2 at (a) 3.5 GHz (b) 7.15 GHz

As shown in Fig. 6.19, a parametric study is done by varying the length L2 to get the resonance at the desired frequency in the lower frequency band and obtain wide bandwidth in the higher frequency band. As L2 increases, resonant frequency in the lower frequency band shifts to lower frequencies and also -10 dB reflection coefficient bandwidth increases in the upper-frequency

band, as illustrated in Fig. 6.19. An optimum value of L2 (i.e., L2 = 6.5 mm) is taken as it gives the desired performance. Also, it can be observed from Fig. 6.18 that Ant II produces dual-band (3.19-3.90 GHz and 5.8-8 GHz). It is evident from Fig. 6.20 that the maximum surface current densities are located on some portions of the decagonal split ring and shunt arms at first and second resonant frequencies, respectively. The resonating lengths for the first and second resonances can be expressed as

$$L_{1\ \text{res Ant (P2)}} = (L1 + L1 + \frac{L1}{2}) \times 2 = 5L1 \tag{6.1}$$

$$L_{2\ \text{res Ant (P2)}} = (L2 + L2) = 2L2 \tag{6.2}$$

The expressions for the first and second resonating frequencies are as follows:

$$f_{1\ \text{res Ant (P2)}} = \frac{c}{2L_{1\ \text{res Ant (P2)}}\sqrt{\varepsilon_{reff}}} \tag{6.3}$$

$$f_{2\ \text{res Ant (P2)}} = \frac{c}{2L_{2\ \text{res Ant (P2)}}\sqrt{\varepsilon_{reff}}} \tag{6.4}$$

where ε_{reff} (i.e., $\varepsilon_{reff} \approx \frac{\varepsilon_r+1}{2}$) and 'c' are effective dielectric constant and velocity of light in air, respectively. The first resonant frequencies found from the simulation and design equation are 3.5 GHz and 3.36 GHz, respectively. The second resonant frequencies found from the simulation and design equation are 7.15 GHz and 7.02 GHz, respectively.

6.3.3. Design Procedure of the Antenna Accessible at Port 3

The geometry of the antenna accessible at port 3 is illustrated in Fig. 6.21.

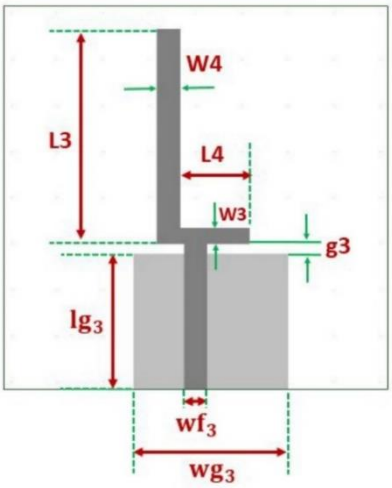

Fig. 6.21. Geometry of the antenna accessible at port 3

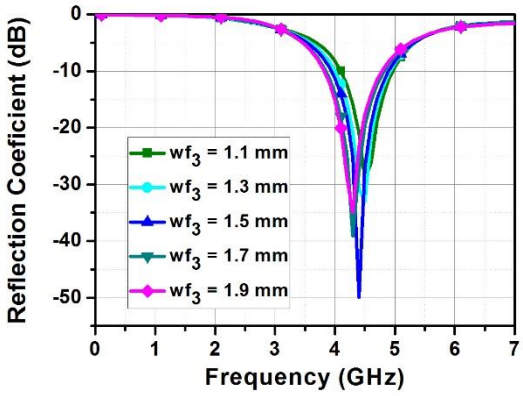

Fig. 6.22. Effect of the width of the feedline on the reflection coefficient performance of the antenna accessible at port 3

The antenna accessible at port 3 is an asymmetric monopole antenna that consists of an 'L' shaped patch fed by a strip-line of 50 Ohms impedance, as shown in Fig. 6.21. It is mainly targeted to cover frequencies above 3.9 GHz that are uncovered by the antenna accessible at port 2.

A parametric study is done by varying the width of the feed line, as presented in Fig. 6.22. It can be seen from Fig. 6.22 that the resonant frequency of the antenna decreases as the width of the feed line increases. Among the different values of width of the feed line, a feed line of width 1.5 mm (i.e., wf_3 = 1.5 mm) is selected since the 10 dB return loss bandwidth starts from 3.9 GHz, as depicted in Fig. 6.22. Thus, a good impedance matching is achieved in the 3.9-4.9 GHz frequency band.

6.3.4. Design Procedure of the Antenna Accessible at Port 4

The geometry of the antenna accessible at port 4 is depicted in Fig. 6.23. The antenna accessible at port 4 is designed with an aim to cover the frequencies that are uncovered by antennas accessible at port 2 and port 3 (i.e., frequencies in 2-3.1 GHz and 4.9-5.8 GHz). The design procedure, which is followed for the antenna accessible at port 2, is used with slight modifications to obtain the desired result. The intermediate steps in the design process of the antenna accessible at port 4 are depicted in Fig. 6.24.

Firstly, a circular split ring monopole antenna (i.e., without the shunt arms), Ant I, is designed, as shown in Fig. 6.24. It yields resonances at 2.6 GHz and 6.8 GHz; however, the impedance matching at 6.8 GHz is very poor, as shown in Fig. 6.25. Since the antenna should

have good impedance matching in the desired frequency band (i.e., 4.9-5.8 GHz), two shunt arms with equal length of 4.5 mm are loaded, as shown in Ant II of Fig. 6.24. Consequently, the second resonance is shifted to a little leftward with a slight betterment in the impedance matching at the second frequency band, as illustrated in Fig. 6.25. In the next step, a circular shaped patch is printed on the backside of the FR-4 substrate to further improve the impedance matching in the second frequency band (i.e., 5.9-6.6 GHz), as depicted in Ant III of Fig. 6.24. Later, a parametric study is done by changing the length (lg_4) of the ground plane to get good impedance matching in the desired frequency band (i.e., 4.9-5.8 GHz).

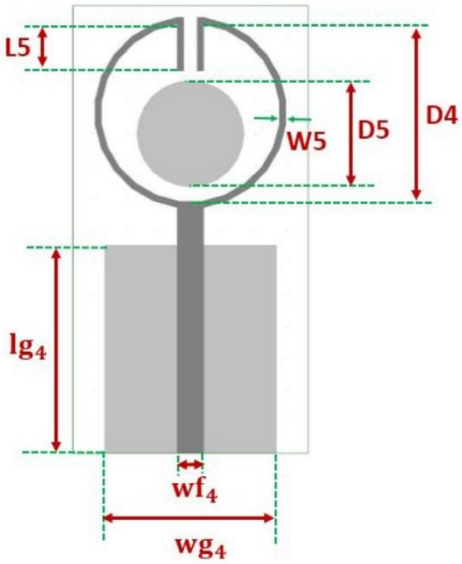

Fig. 6.23. Geometry of the antenna accessible at port 4

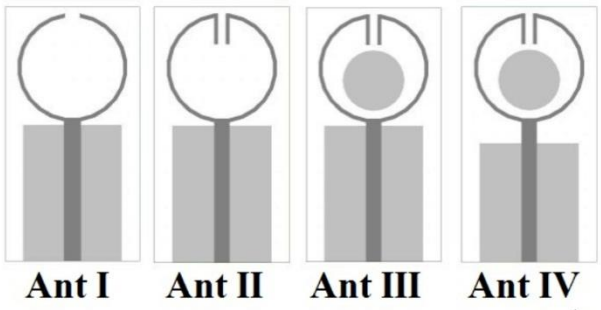

Fig. 6.24. Evolution of the antenna accessible at port 4

It can be seen from Fig. 6.26 that resonant frequency and impedance bandwidth of the second frequency band decrease as lg_4 decreases. Since a good impedance matching in the desired frequency band (i.e., 4.9-5.8 GHz) is achieved with lg_4 of 19.5 mm, a rectangular ground plane of 19.5 mm length is considered finally in the design of the antenna accessible at port 4. Thus,

a good impedance bandwidth is achieved in the two frequency bands, as depicted in Ant IV of Fig. 6.25.

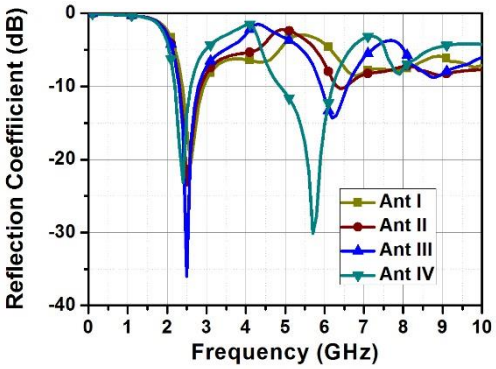

Fig. 6.25. Reflection coefficient performances of the antennas in the design process of antenna accessible at port 4

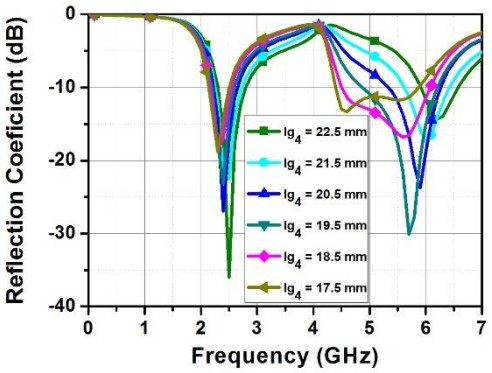

Fig. 6.26. Effect of shunt arms' length lg_4 on the reflection coefficient performance of antenna accessible at port 4

The maximum surface current density exists on two-third of the perimeter of the circular split ring at the first resonant frequency, as depicted in Fig. 6.27a. At the second resonant frequency, it exists on the one-fourth portion of the perimeter of the circular split ring and one-third portion of each of the shunt arms, as shown in Fig. 6.27b. The resonating lengths for the first and second resonances can be expressed as

$$L_{1\ res\ Ant\ (P4)} = 2\pi\left(\left(\frac{D4}{2}\right) + W5\right) \times \frac{2}{3} \tag{6.7}$$

$$L_{2\ res\ Ant\ (P4)} = \left(2\pi\left(\left(\frac{D4}{2}\right) + W5\right) \times \frac{1}{4}\right) + \frac{2}{3} \times L5 \tag{6.8}$$

The expressions for the first and second resonating frequencies are as follows:

$$f_{1\ res\ Ant\ (P4)} = \frac{c}{2L_{1\ res\ Ant\ (P4)}\sqrt{\varepsilon_{reff}}} \tag{6.9}$$

$$f_{2\ res\ Ant\ (P4)} = \frac{c}{2L_{2\ res\ Ant\ (P4)}\sqrt{\varepsilon_{reff}}} \tag{6.10}$$

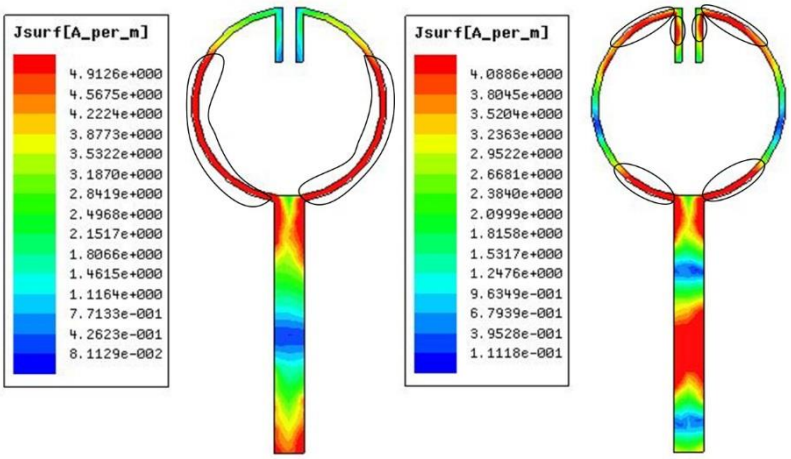

(a) (b)

Fig. 6.27. Surface current densities of the antenna accessible at port 4 at (a) 2.4 GHz (b) 5.7 GHz

The first resonant frequencies found from the simulation and design equation are 2.4 GHz and 2.42 GHz, respectively. The second resonant frequencies found from the simulation and design equation are 5.7 GHz and 5.41 GHz, respectively.

6.3.5. Design Procedure of the Antenna Accessible at Port 5

The geometry of the antenna accessible at port 5 is shown in Fig. 6.28.

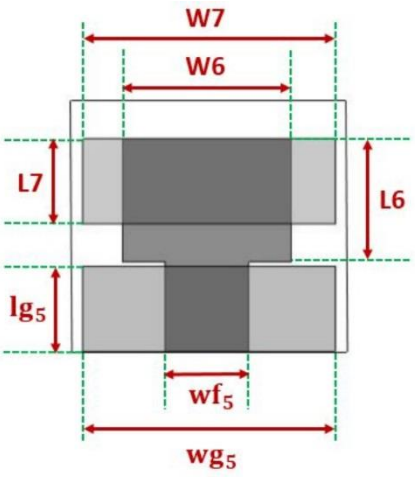

Fig. 6.28. Geometry of the antenna accessible at port 5

The antenna accessible at port 5 is mainly targeted to cover the frequencies that are not covered by antennas accessible at ports 2, 3, and 4 (i.e., above 8 GHz). The evolution of the antenna accessible at port 5 is completed in two steps to achieve the desired response. The design process starts with a conventional rectangular monopole antenna (i.e., Ant I) depicted in Figure 6.29. The lower band edge frequency of the antenna accessible at port 5 is calculated from equation (6.11) [16]. The parameters such as L6, r, and p are expressed in centimetres.

$$f_{\text{L Ant I (P5)}} = \frac{7.2}{(L6+r+p)\times k}\ \text{GHz} \tag{6.11}$$

Here, L6 = 0.58, r = $\frac{W6}{2\pi}$ = $\frac{0.8}{2\pi}$ = 0.1273, p = feed gap = 0.02, k = constant = 1.15

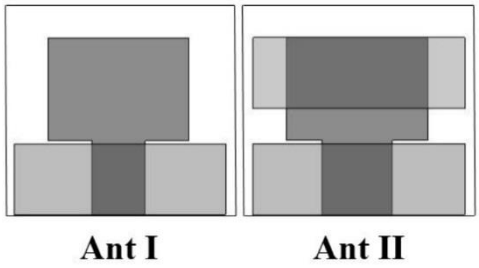

Fig. 6.29. Evolution of the antenna accessible at port 5

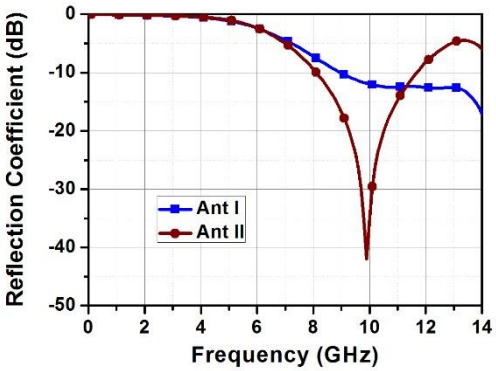

Fig. 6.30. Reflection coefficient performances of the antennas in the design process of antenna accessible at port 5

The lower band edge frequencies found from the equation (6.11) and simulation of Ant I are 8.608 GHz and 8.5 GHz, respectively. The Ant I has a wide impedance bandwidth that starts from 8.5 GHz, as depicted in Figure 6.30. However, to further improve the impedance matching and make the impedance bandwidth to start from 8 GHz, a rectangular shaped patch is printed on the backside of the substrate and a feed line of 4 mm width is chosen in the last stage of the

design process, as illustrated in Fig. 6.29. It is noticed from Fig. 6.31 that the feed line of 4 mm width gives better reflection coefficient performance. Thus, a good impedance matching is achieved in the 8-11.6 GHz frequency band.

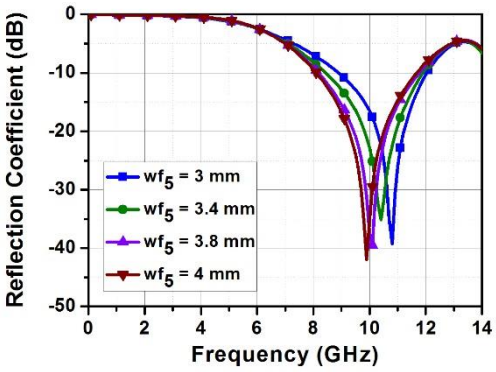

Fig. 6.31. Effect of the width of the feed line on the reflection coefficient performance of antenna accessible at port 5

6.3.6. Inter-Elemental Spacing Analysis

After designing a wideband sensing antenna, two single-band antennas, and two dual-band antennas, the wideband sensing antenna and four pairs of antennas meant for communication in which each pair consists of two identical single/dual-band antennas are placed as illustrated in Fig. 6.12. Generally, it is well known that good isolation is achieved between any two antennas when they are placed perpendicular to each other. As the proposed MIMO antenna comprises nine antennas, some of the antennas are placed parallel. So, the separation between the parallel antennas are maintained in such a way that no antenna's performance deteriorates. Fig. 6.32 shows the inter-elemental spacing of the proposed MIMO antenna.

The lower band edge frequencies of the antennas accessible at ports 1, 2, 3, 4, 5, 6, 7, 8, and 9 are 37.5 mm, 24.59 mm, 19.48 mm, 36.58 mm, 9.375 mm, 24.59 mm, 19.48 mm, 36.58 mm, and 9.375 mm, respectively. Let us consider the antennas that are parallel to the sensing antenna. The sensing antenna (antenna accessible at port 1) is horizontally separated from antennas accessible at ports 2 and 5 at distances of 42.5 mm and 48 mm, respectively, as shown in Fig. 6.32. Since they are horizontally separated at distances that are greater than the $\frac{1}{4}^{\text{th}}$ of the wavelengths corresponding to the lower band edge frequencies of antennas accessible at ports 1, 2, and 5, coupling of currents doesn't occur between them. Similarly, since antennas

accessible at ports 1 and 4 are horizontally separated by a distance of 34.35 mm, which is almost equal to the $\frac{1}{4}^{\text{th}}$ of the wavelengths corresponding to the lower band edge frequencies of antennas accessible at ports 1 and 4, current coupling doesn't exist between them.

Despite antennas accessible at ports 1 and 3 are vertically separated by a distance of 27.49 mm, which is less than the $\frac{1}{4}^{\text{th}}$ of the wavelength corresponding to the lower band edge frequency of antenna accessible at port 1, significant amount of current does not couple from antenna accessible at port 1 to antenna accessible at port 3. It is due to the fact that the vertically separated antennas always give better isolation than the horizontally separated antennas. So, in case of vertically separated antennas, good isolation can be maintained even when the two antennas are placed at short distances.

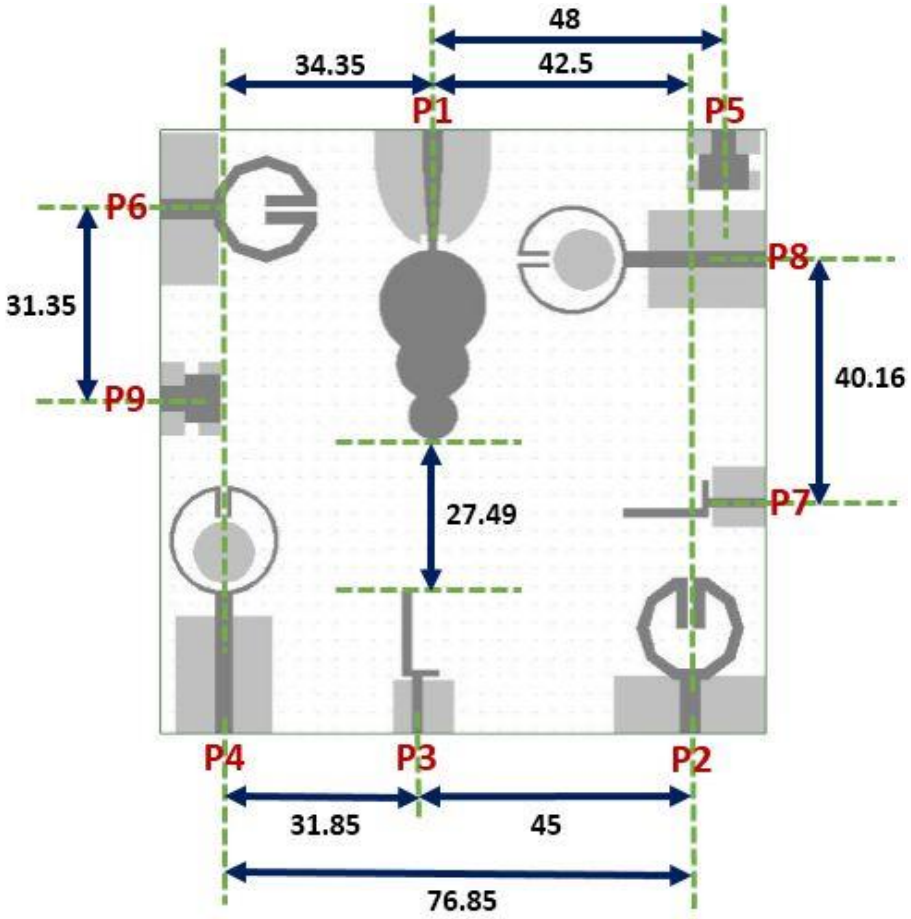

Fig. 6.32. Inter-elemental spacing of the proposed MIMO antenna

Let us consider the antennas that are used for communication. The antennas accessible at ports 2 and 3, antennas accessible at ports 2 and 4, antennas accessible at ports 6 and 9, and antennas

accessible at ports 7 and 8 are horizontally separated at distances of 45 mm, 76.85 mm, 31.35 mm, and 40.16 mm, respectively, as shown in Fig. 6.32. Since they are horizontally separated at distances that are greater than the $\frac{1}{4}^{\text{th}}$ of the wavelengths corresponding to the lower band edge frequencies of both of the antennas in every antenna pair, coupling of currents doesn't occur between two antennas in every antenna pair. Also, as antennas accessible at ports 3 and 4 are horizontally separated by a distance of 31.85 mm, which is almost equal to the $\frac{1}{4}^{\text{th}}$ of the wavelength corresponding to the lower band edge frequency of antenna accessible at port 4 and is greater than the lower band edge frequency of antenna accessible at port 3, coupling of currents doesn't occur between them.

Since the polarization diversity is desired, every two similar antennas are placed in orthogonal fashion. In the proposed MIMO antenna design, the placement of the radiators plays a crucial role in achieving good isolation between every two radiators. In case the antennas accessible at ports 3 and 4 are interchanged, the horizontal separation between antennas accessible at ports 1 and 4 will decrease. Moreover, antennas accessible at ports 1 and 4 are vertically very close to each other. Since the horizontal separation between the antennas accessible at ports 1 and 4 becomes 0 mm and the vertical separation between them is just 7.82mm, which is much less than the $\frac{1}{4}^{\text{th}}$ of the wavelengths corresponding to the lower band edge frequencies of antenna accessible at port 1 and 4, significant current coupling exists between the antennas accessible at port 1 and 4. So, antenna accessible at port 4 should not be placed in the position of antenna accessible at port 3.

Let us consider the antennas accessible at ports 2 and 5. Since antennas accessible at ports 2 and 5 are vertically separated at a long distance, good isolation is guaranteed. In case the antennas accessible at ports 2 and 5 are interchanged, the isolation between them doesn't deteriorate. However, the overall size of the MIMO antenna will increase, which is not desired. Let us consider the antennas accessible at ports 3 and 5. Since antennas accessible at ports 3 and 5 are vertically separated at a long distance, good isolation is guaranteed. In case the antennas accessible at ports 3 and 5 are interchanged, the isolation between them doesn't deteriorate. However, the overall size of the MIMO antenna will increase, which is not desired.

Let us consider the antennas accessible at ports 2 and 3. In case the antennas accessible at ports 2 and 3 are interchanged, the isolation between them remain same. But isolation

between antennas accessible at ports 2 and 4 will deteriorate since the distance between them will become 31.85 mm, which is less than $\frac{1}{4}^{\text{th}}$ of the wavelength at 2.05 GHz, i.e., 36.58 mm. So, if a radiator of specific shape is placed at allocation of different radiator, the isolation between antennas decreases, thus resulting in deterioration of antennas' performances.

6.3.7. Results and Discussions

The simulated and measured reflection coefficients of the wideband sensing antenna, four single-band antennas, and four dual-band antennas are illustrated in Fig. 6.33.

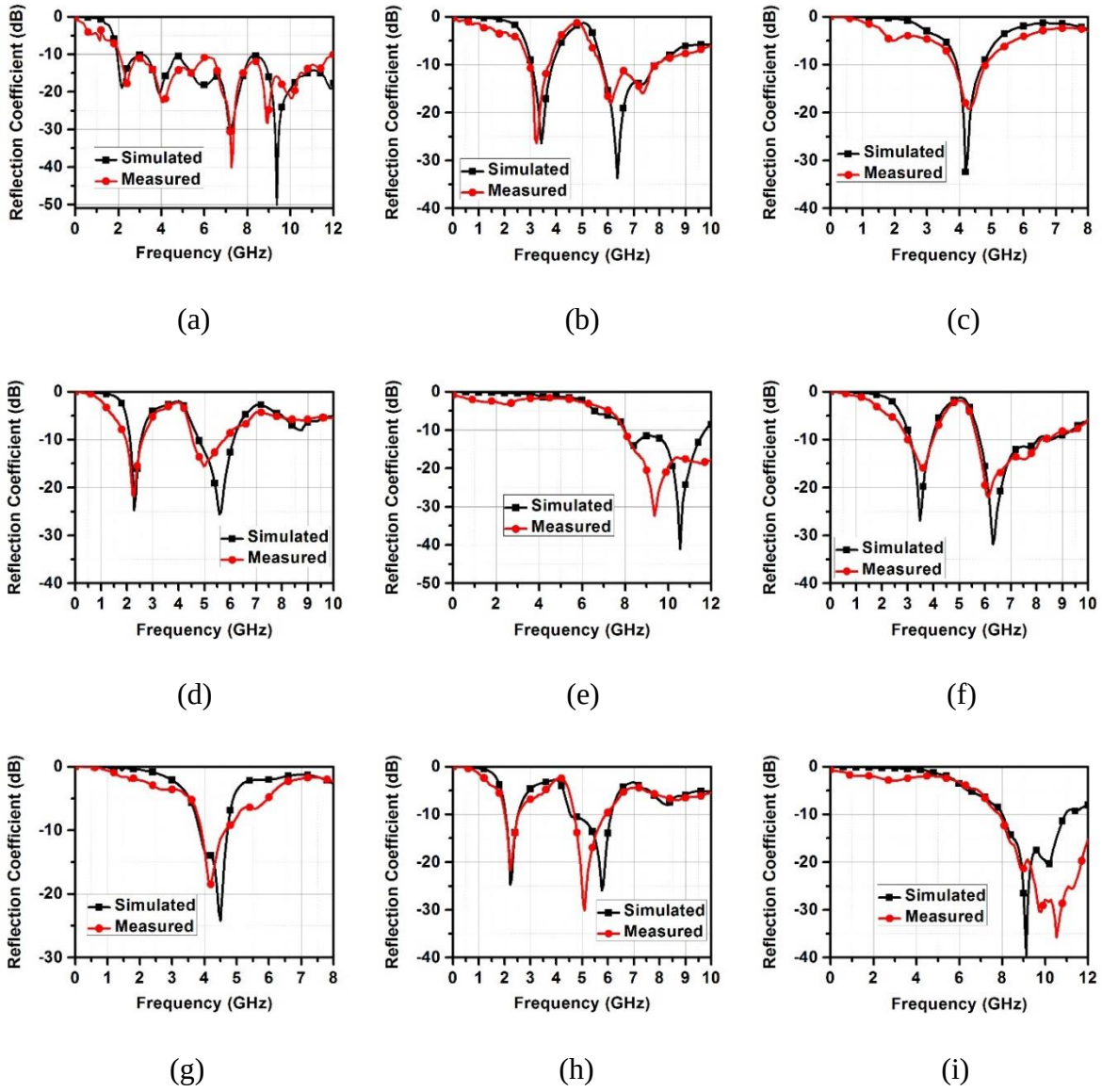

Fig. 6.33. Reflection coefficient performances of all the antennas in the proposed MIMO antenna (a) S_{11} (b) S_{22} (c) S_{33} (d) S_{44} (e) S_{55} (f) S_{66} (g) S_{77} (h) S_{88} (i) S_{99}

The simulated and measured mutual couplings between every two similar antennas when all other antennas are terminated with fifty ohms matched load are illustrated in Figure 6.34.

As illustrated in Fig. 6.34, it is evident that the mutual coupling between every two similar antennas is less than -20 dB. Since every pair of similar antennas meant for communication are placed in orthogonal fashion, good isolation is attained between them.

The simulated and measured mutual couplings between wideband sensing antenna and every single/dual-band antenna for communication when all the other antennas are terminated with fifty ohms matched load are illustrated in Fig. 6.35. Isolation of better than 17 dB is attained between wideband sensing antenna and every antenna meant for communication, as illustrated in Fig. 6.35.

Despite some of the single-band and dual-band antennas are parallel to the wideband sensing antenna, good isolation is attained due to their placement. A fine match between the results obtained from simulations and measurements results are observed, as shown in Fig. 6.33, Fig. 6.34, and Fig. 6.35.

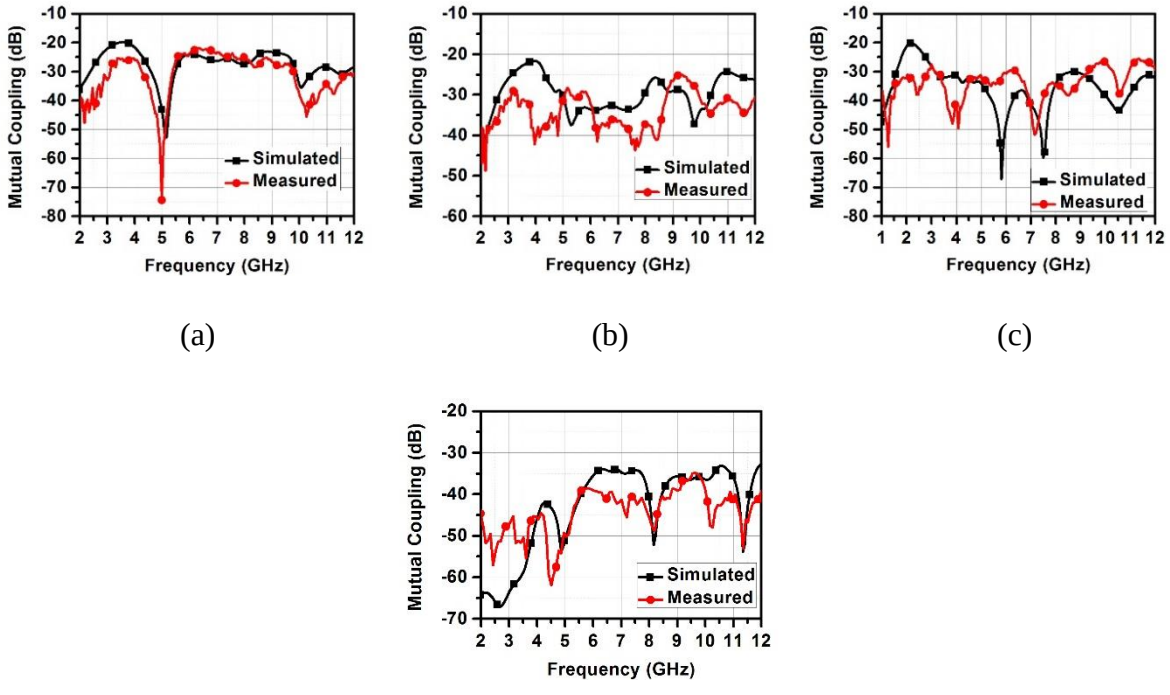

Fig. 6.34. Mutual coupling between similar antennas (a) S_{26} (b) S_{37} (c) S_{48} (d) S_{59}

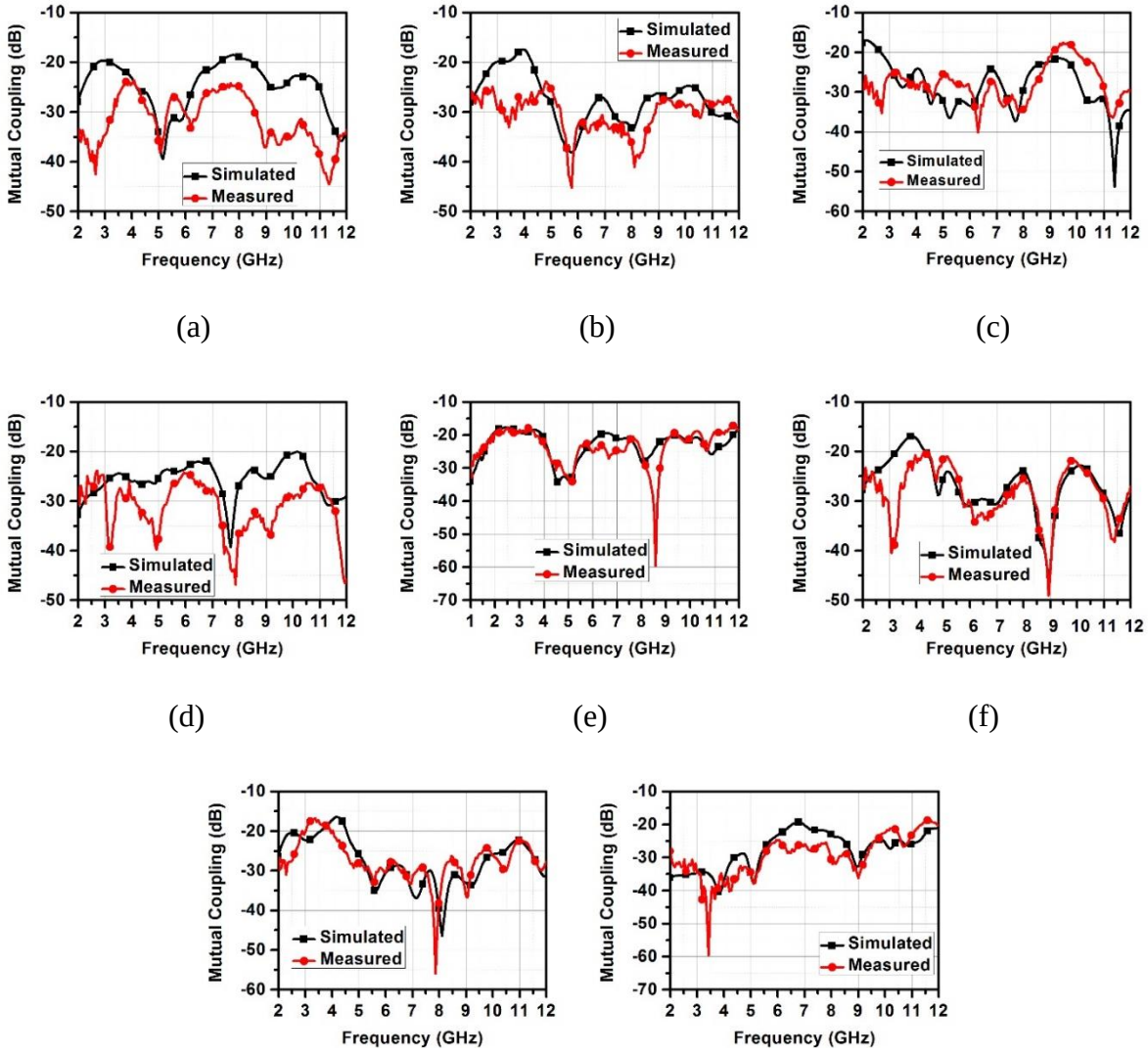

Fig. 6.35. Mutual coupling between sensing antenna and other antennas (a) S_{21} (b) S_{31} (c) S_{41} (d) S_{51} (e) S_{61} (f) S_{71} (g) S_{81} (h) S_{91}

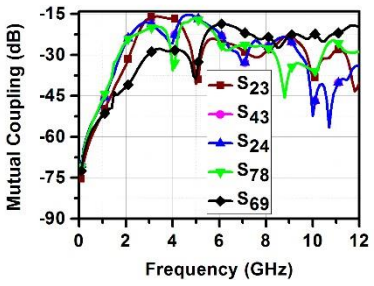

Fig. 6.36. Mutual coupling between every two parallel antennas for communication

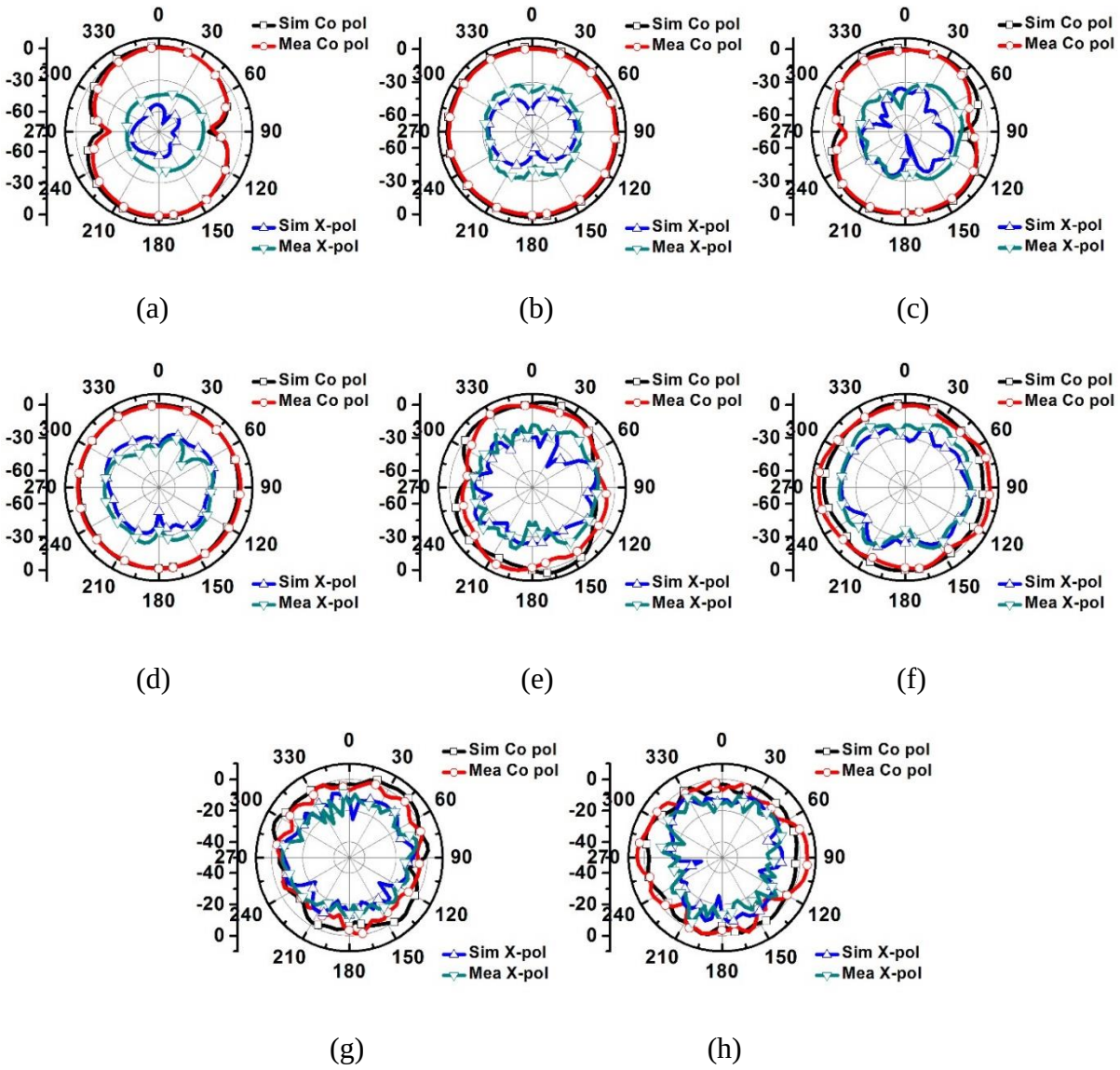

Fig. 6.37. Radiation patterns of the antenna accessible at port 1 at (a) 2.5 GHz-XZ plane (b) 2.5 GHz-YZ plane (c) 5 GHz-XZ plane (d) 5 GHz-YZ plane (e) 7.5 GHz-XZ plane (f) 7.5 GHz-YZ plane (g) 10 GHz-XZ plane (h) 10 GHz-YZ plane

To know the isolation between every two non-similar antennas meant for communication, a special case is considered. In this case, wideband sensing antenna senses all the spectrum holes in the 2-11 GHz frequency band (i.e., primary users do not utilize any frequency bands), so every antenna radiates. Since the mutual coupling between every two similar antennas and the mutual coupling between wideband sensing antenna and antennas that are meant for communication are already shown in Fig. 6.34 and Fig. 6.35, respectively, these are not discussed in this case. When all the antennas radiate simultaneously, the mutual coupling

between any two non-similar antennas that are parallel to each other is less than -15 dB, as illustrated in Fig. 6.36. Despite some antennas are parallel to each other, those antennas are separated in such a way that there exists no coupling between them.

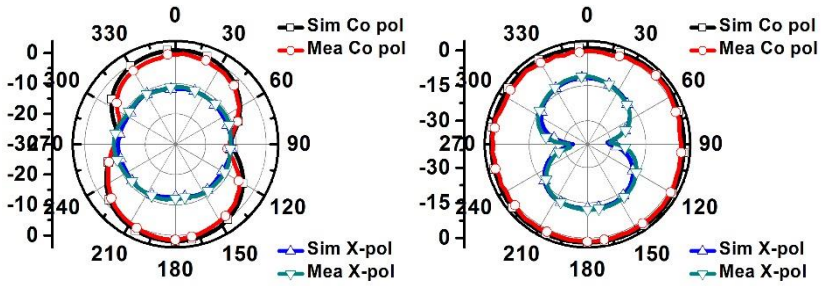

(a) (b)

Fig. 6.38. Radiation patterns of the antenna joined to port 3 at 4.4 GHz in planes (a) XZ (b) YZ

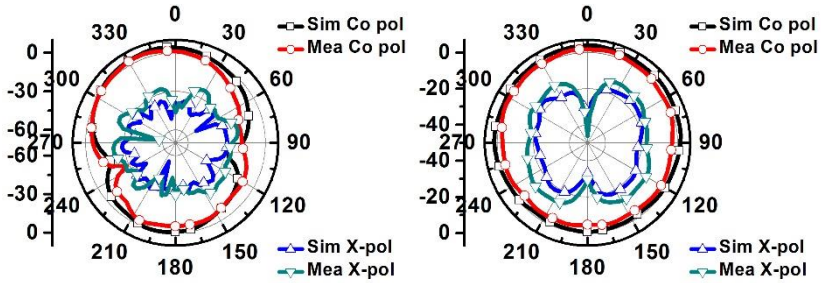

(a) (b)

Fig. 6.39. Radiation patterns of the antenna joined to port 5 at 10 GHz in planes (a) XZ (b) YZ

During the measurement of radiation patterns in an anechoic chamber, pyramidal horn antenna, which is connected to a microwave signal analogue generator, is used as a transmitting antenna, while the proposed antenna is used as a receiving antenna. The proposed antenna is kept in receiving mode in a far-field region and is connected to a coaxial detector. The radiation patterns in the orthogonal planes of the antennas accessible at ports 1, 3, 5, 2 and 4 are shown in Fig. 6.37, Fig. 6.38, Fig. 6.39, Fig. 6.40 and Fig. 6.41, respectively. In the case of antenna accessible at port 1, dipole natured patterns are observed at low frequencies (i.e., 2.5 GHz and 5 GHz) and nearly omnidirectional patterns are observed at high frequencies (i.e., 7.5 GHz and 10 GHz), as depicted in Fig. 6.37. As depicted in Fig. 6.38 and Fig. 6.39, dipole natured patterns are observed in the case of single-band antennas (i.e., antennas accessible at ports 3 and 5).

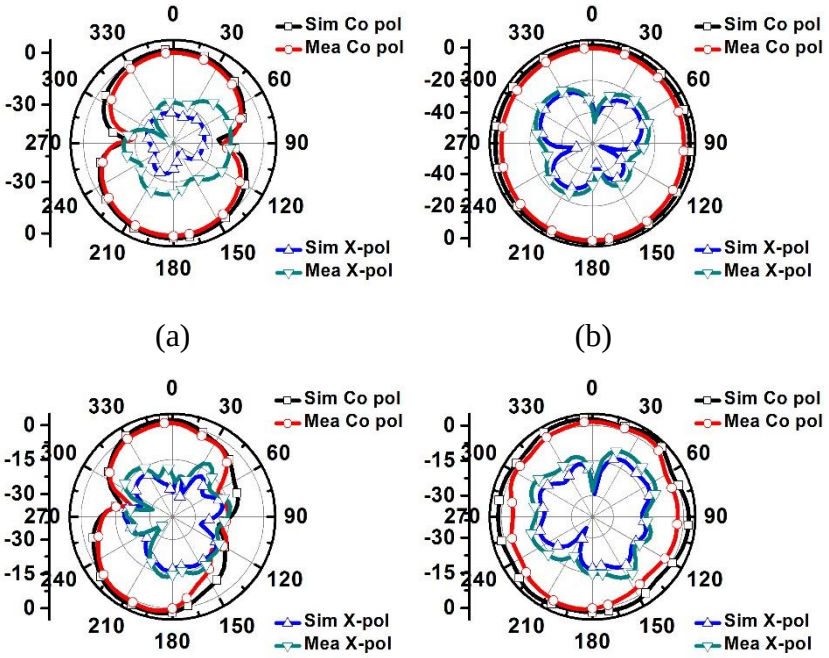

Fig. 6.40. Radiation patterns of the antenna accessible at port 2 at (a) 3.5 GHz-XZ plane (b) 3.5 GHz-YZ plane (c) 7 GHz-XZ plane (d) 7 GHz-YZ plane

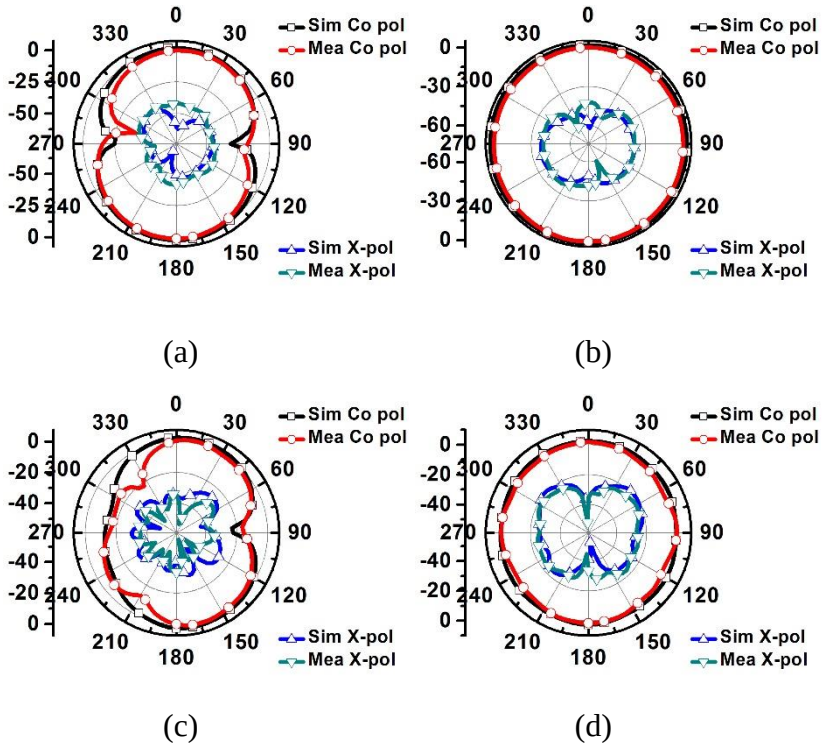

Fig. 6.41. Radiation patterns of the antenna accessible at port 4 at (a) 2.4GHz-XZ plane (b) 2.4GHz-YZ plane (c) 5.4GHz-XZ plane (d) 5.4GHz-YZ plane

In the case of dual-band antennas (i.e., antennas accessible at ports 2 and 4), exact dipole natured patterns and nearly dipole natured patterns are observed at low and high frequencies, respectively, as depicted in Fig. 6.40 and Fig. 6.41. It is well known that a dual-band monopole antenna with two distinct current paths always has dipole natured radiation patterns at lower and higher resonating frequencies [167-169]. So, the reason for the dipole natured patterns at both low and high frequencies is due to the two distinct current paths provided by the split ring structure. As depicted in Fig. 6.20a and Fig. 6.27a, the radiation at low frequencies of antennas accessible at ports 2 and 4 is mainly due to the strong current densities on the decagonal strip and circular strip, respectively. Whereas the radiation at high frequencies of the antennas accessible at ports 2 and 4 is mainly due to the shunt arms of the decagonal split ring and circular split ring, respectively, as depicted in Fig. 6.20b and Fig. 6.27b.

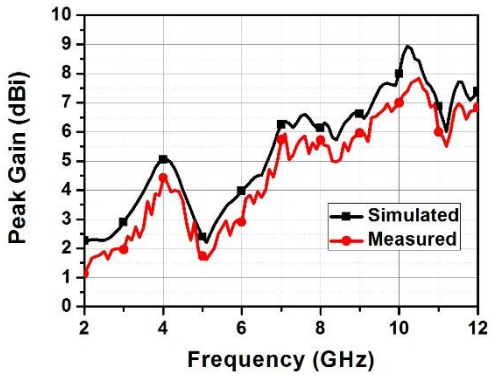

Fig. 6.42. Peak gain of the sensing antenna

The peak gains and radiation efficiencies of the wideband sensing antenna are illustrated in Fig. 6.42 and Fig. 6.43, respectively. As illustrated in Fig. 6.42 and Fig. 6.43, the simulated peak gains and radiation efficiencies of the wideband sensing antenna are more than 2.2 dBi and 81%, respectively. It can be observed from Fig. 6.42 that the maximum difference between the simulated and measured peak gains is approximately 1 dBi, which could be due to the earth's magnetic field, substrate losses, and imperfections in measurement.

The peak gains and radiation efficiencies of the single-band and dual-band antennas for communication in their operating bandwidths are depicted in Fig. 6.44 and Fig. 6.45, respectively. As illustrated in Fig. 6.44 and Fig. 6.45, the simulated peak gains and radiation efficiencies of the single-band and dual-band antennas for communication are greater than 2 dBi and 90%, respectively.

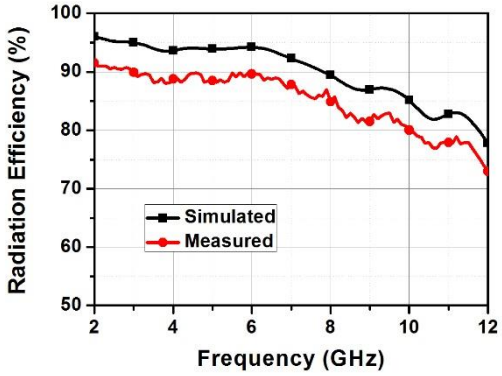

Fig. 6.43. Radiation efficiency of the sensing antenna

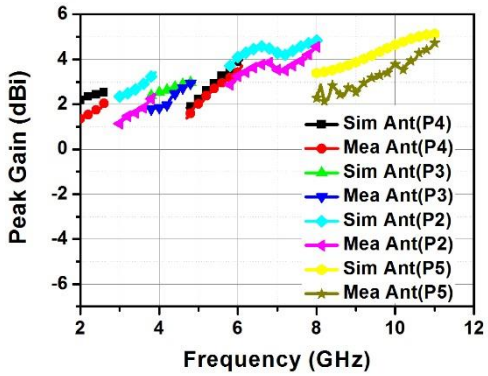

Fig. 6.44. Peak gains of the single and dual-band antennas

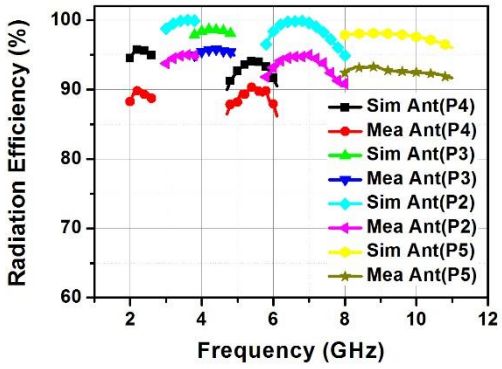

Fig. 6.45. Radiation efficiencies of the single and dual-band antennas

It is seen from Table 6.3 that the proposed MIMO antenna has a salient and novel feature of performing a maximum of four communication tasks simultaneously. Also, no reconfigurable element is incorporated in the proposed MIMO antenna, whereas reconfigurable elements such as PIN diodes, varactor diodes, etc., and lumped elements such as resistance, inductance, and

capacitance were incorporated in the state-of-art CR MIMO antennas. An image of the fabricated CR MIMO antenna is depicted in Fig. 6.46.

Table 6.3. Comparison of the proposed CR MIMO antenna with the CR MIMO antennas

Ref.	**Size (mm^2)**	**Range of wideband sensing antenna (GHz)**	**Covered communic-ation bands**	**Minimum Isolation achieved (dB)**	**Reconfig-urable elements used**	**Maximum number of communic-ations performed at a time**
[126]	60 × 40	2.2-7	2.3-6.3	18	Varactor diodes	1
[127]	60 × 120	0.75-7.65	1.77-2.51	9.5	Varactor diodes	1
[128]	80 × 80	2.35-5.9	2.6-3.6	15	Varactor diodes	1
[129]	60 × 120	1-4.5	0.9-2.6	12.5	Varactor and PIN diodes	1
[130]	63 × 63	3.4-8.0	4.7-5.4	15	PIN diodes	1
[149]	80 × 70	3-6	3.9, 4.21	20	PIN diodes	1
[154]	100 × 120	2.3-5.5	2.5-4.2	15	Varactor and PIN diodes	1
proposed	**100 × 100**	**2-12**	**2.05-2.55 and 3-11**	**15**	**None**	**4**

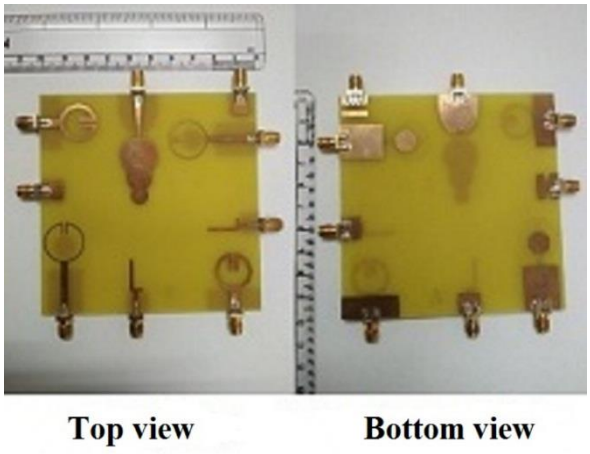

Fig. 6.46. Photograph of the fabricated CR MIMO antenna

6.3.8. Performance Analysis of the Proposed MIMO Antenna

To evaluate the diversity characteristics of the 2-element MIMO antenna, the crucial parameters such as envelope correlation coefficient (ECC) and diversity gain (DG) are calculated.

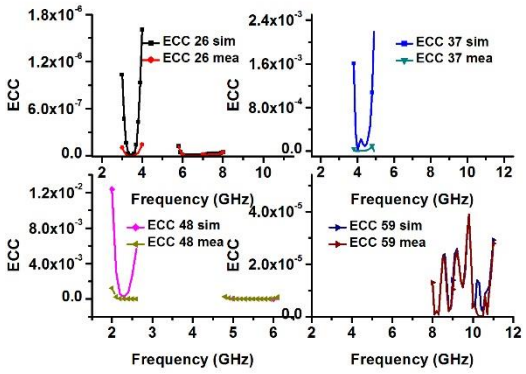

Fig. 6.47. ECCs of the proposed CR MIMO antenna

Normally, the similarity between any two elements is evaluated by correlation. By using the S-parameters, ECC can be found mathematically by using the mathematical relations given in [166]. For a MIMO system with good diversity capability, the value of its ECC should be as low as possible. Ideally, the value of ECC is 0. Fig. 6.47 depicts the simulated and measured ECC of the proposed 2-element MIMO antenna. DG can be calculated by using the ECC given in [166] and its ideal value is 10 dB.

Good inter port isolation ensures better diversity gain. The simulated and measured diversity gains of the proposed antenna are illustrated in Fig. 6.48. A diversity gain of

approximately 10 dB is attained by the proposed antenna. Therefore, the proposed MIMO antenna has good diversity capability in all multipath fading channels.

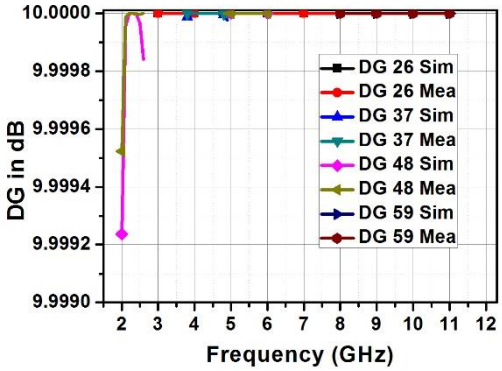

Fig. 6.48. Diversity gains of the proposed CR MIMO antenna

To characterize the quality of the proposed MIMO system, another parameter called capacity loss is calculated. Without increasing the bandwidth or transmitted power, channel capacity increases linearly as the number of antennas used increases under certain assumptions. However, in a MIMO channel, the correlation between the links reduces the MIMO capacity due to the probability of outage, which becomes more significant. Moreover, channel capacity loss (CCL) becomes more with the increase in correlation. It can be calculated by using the equations given in [170].

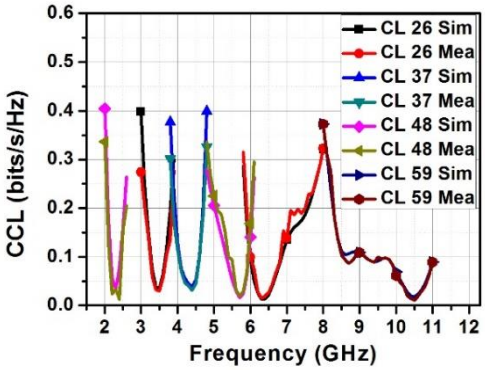

Fig. 6.49. Channel capacity losses of the proposed CR MIMO antenna

Fig. 6.49 shows the variations of capacity loss (bits/s/Hz) of four pairs of antennas used for communication with respect to frequency. It is evident from Fig. 6.49 that the capacity loss of all the NB antennas used for communication does not cross the threshold value of 0.4 bits/s/Hz.

6.4. Conclusion

A twelve port MIMO antenna with polarisation diversity for cognitive radio applications has been presented in this chapter. The five pairs of antennas used for communication have single bands and dual bands to cover entire spectrum of UWB and the two UWB antennas used for sensing purpose cover total spectrum of UWB. Polarisation diversity is achieved by placing every identical pair of antennas orthogonal to each other. Isolation of better than 20 dB is achieved between every two identical antennas. Also, a nine port MIMO antenna without using any reconfigurable elements and lumped elements has been presented in this chapter to improve the spectrum utilization efficiency in CR MIMO applications. Mutual coupling of less than -15 dB has been attained between every two antennas that exist in the proposed CR MIMO antenna. Moreover, 93% of the bandwidth in the 2-11 GHz frequency band has been covered by the single-band and dual-band antennas for communication. The presented CR MIMO antennas have a striking feature of performing multiple operations at a time when all unutilized frequency bands by primary users are detected by sensing antenna. The simulated and measured ECC and DG are in a good match and are within their acceptable limits. Moreover, the proposed CR MIMO antennas are very compact, simple, and inexpensive.

Chapter-7

Conclusions and Future Scope

7.1. Conclusions

In this thesis, the research has been presented on the design of sensing antenna, design of reconfigurable CR MIMO antenna, and design of integrated wideband sensing and WB/NB antennas systems for CR and CR MIMO applications. It contains seven chapters, including this as the last chapter.

In **Chapter 1**, introduction, background, and motivation factor for carrying out this work has been described.

In **Chapter 2**, the literature background of basics of an antenna, different parameters of an antenna, microstrip antenna, printed monopole antenna, UWB technology, SWB technology, CR technology, and types of antenna systems needed for CR MIMO antenna have been provided.

In **Chapter 3**, by utilizing the Apollonius fractal with nested Apollonius circles, a compact SWB antenna for both UWB and SWB applications has been designed. It has been compared with the other SWB antennas which were presented in the previous literatures in terms of BDR, size, and percentage bandwidth. It covers Ku, K, Ka and V bands in which their applications in communications are not explored so far. Since it covers frequencies from 3 GHz to 60 GHz, it is also useful for spectrum sensing in cognitive radio applications.

In **Chapter 4**, a nine port integrated sensing antenna and reconfigurable communication antennas for CR MIMO applications has been presented. It acts as a dynamic n-element MIMO antenna depending on the number of spectrum holes detected. Moreover, polarization diversity

is also attained as some of the reconfigurable communication antennas are polarized in +X, -X, +Y, and –Y directions. The simulated and measured results confirm that the designed antenna is a fine candidate for CR MIMO applications.

In **Chapter 5**, a 3 port integrated UWB and NB antenna system design has been presented as a first contribution. Since two communications are possible at a time, spectrum utilization efficiency is improved significantly. Therefore, the proposed 3 port antenna can be good candidate for CR applications. Also, a compact six port integrated UWB sensing and narrowband/wideband antennas for CR applications has been presented in this chapter. The most distinguishing feature of this design approach is enhancing the utilization of spectrum by performing multiple communication tasks when multiple white spaces are detected. Moreover, all the communication bands in the UWB spectrum are covered by the wideband/narrowband antennas in the proposed designs. Despite being compact in structure, all antennas in the proposed antenna system are electromagnetically well isolated. The obtained radiation patterns are well fit for cognitive radio applications. Hence, the proposed six port antenna is well suitable for cognitive radio applications.

In **Chapter 6**, a twelve port MIMO antenna with polarisation diversity for cognitive radio applications has been presented. The five pairs of antennas used for communication have single bands and dual bands to cover entire spectrum of UWB and the two UWB antennas used for sensing purpose cover total spectrum of UWB. Polarisation diversity is achieved by placing every identical pair of antennas orthogonal to each other. Isolation of better than 20 dB is achieved between every two identical antennas. Also, a nine port MIMO antenna without using any reconfigurable elements and lumped elements has been presented in this chapter to improve the spectrum utilization efficiency in CR MIMO applications. Mutual coupling of less than -15 dB has been attained between every two antennas that exist in the proposed CR MIMO antenna. Moreover, 93% of the bandwidth in the 2-11 GHz frequency band has been covered by the single-band and dual-band antennas for communication. The presented CR MIMO antennas have a striking feature of performing multiple operations at a time when all unutilized frequency bands by primary users are detected by sensing antenna. The simulated and measured ECC and DG are in a good match and are within their acceptable limits. Moreover, the proposed CR MIMO antennas are very compact, simple, and inexpensive.

7.2. Future Scope

In this thesis, design of sensing antenna, design of reconfigurable CR MIMO antenna, and design of integrated wideband sensing and WB/NB antenna systems for CR and CR MIMO applications have been investigated. Based on this work, many future research works may be performed. Some of these are outlined below:

- Higher element MIMO antennas could be designed without using switching elements on the antenna by using novel decoupling schemes.
- CR MIMO antennas with polarization diversity could also be realised by designing right hand circularly polarized communication antennas and left hand circularly polarized communication antennas.
- Also, CR MIMO antennas with pattern diversity could also be designed by using novel techniques.

Bibliography

[1] S. Jayaweera and C. Mosquera, "A Dynamic Spectrum Leasing (DSL) Framework for Spectrum Sharing in Cognitive Radio Networks", in Proceedings of the IEEE Forty-Third Asilomar Conference on Signals, Systems and Computers, pp. 1819-1823, Pacific Grove, California, 2009.

[2] Ahmed Rajaie Raslan, "Metamaterial Antennas for Cognitive Radio Applications", A Thesis Submitted to the Electronics Engineering Department, American University in Cairo School of Sciences and Engineering, May 2013.

[3] M. Al-Husseini, K. Kabalan, A. El-Hajj, and C. Christodoulou, "Cognitive radio: UWB Integration and Related Antenna Design," in New Trends in Technologies: Control, Management, Computational Intelligence and Network Systems, M. J. Er, Ed., INTECH, Rijeka, Croatia, 2010.

[4] Y. Tawk, M. Bkassiny, G. El-Howayek, S. K. Jayaweera, K. Avery and C. G. Christodoulou, "Reconfigurable Front-End Antennas for Cognitive Radio Applications", IET Microwaves, Antennas and Propagation, Vol. 5, no. 8, pp. 985–992, 2011.

[5] FCC 1st report and order on Ultra-Wideband Technology, Feb. 2002.

[6] Available online: http://cdn.arstechnica.net/Gadgets/uwb_tzero_chart.png.

[7] C. A. Balanis, "Antenna Theory Analysis and Design", 3rd edition, John Wiley & Sons, INC, 2005.

[8] Available online: http://images.elektroda.net/65_1330619143.gif.

[9] Marek Bugaj, Rafal Przesmycki, Leszek Nowosielski, and Kazimierz Piwowarczyk, "Analysis Different Methods of Microstrip Antennas Feeding for their Electrical Parameters", PIERS Proceedings, Kuala Lumpur, Malaysia, pp. 27-30, March 27, 2012.

[10] K. Praveen Kumar, K. Sanjeeva Rao, T. Sumanth, N. Mohana Rao, R. Anil Kumar, Y.Harish, "Effect of Feeding Techniques on the radiation Chaaracteristics of Patch antenna: Design and Analysis", International Journal of Advanced Research in computer and communication Engineering, Vol. 2, no. 2, pp. 1276-1281, 2013.

[11] Mahesh M. Gadag, Dundesh S. Kamshetty, Suresh L. Yogi, "Design of Different Feeding techniques of rectangular Microstrip Antenna for 2.4 GHz RFID Applications

Using IE3D", in Proceedings of the International conference on Advances in Computer, Electronics and Electrical Engineering, pp. 522-525, Tamilnadu, March 2012.

[12] Dalia M. Elsheakh, Esmat A. Abdallah, "Different Feeding Techniques of Microstrip Patch Antennas with Spiral Defected Ground Structure for Size reduction and Ultra-Wide band Operation", Journal of Electromagnetic Analysis and Applications, Vol. 4, no. 10, pp. 410-418, 2012.

[13] Alak Majumder, "Rectangular Microstrip patch Antenna Using Coaxial Probe Feeding Technique to operate in S-Band", International Journal of Engineering Trends and Technology (IJETT), Vol. 4, no. 4, April 2013.

[14] V. Mohan Kumar, N. Sujith, "Enhancement of Bandwidth and Gain of a Rectangular Microstrip Patch Antenna", A Thesis Submitted to Electronics and Communication Engineering, National Institute of Technology, Rourkela, 2010.

[15] K.-L. Wong, Compact and broadband microstrip antennas. John Wiley & Sons, 2004.

[16] K. P. Ray, "Design aspects of printed monopole antennas for ultra-wide band applications", International Journal of Antennas and Propagation, Vol. 2008, pp. 1-8, 2008.

[17] Elham Ebrahimi, "Wideband and Reconfigurable Antennas for Emerging Wireless Networks", A Thesis Submitted to the University of Birmingham School of Electronic, Electrical and Computer Engineering, College of Engineering and Physical Sciences, September 2011.

[18] H. Arslan, Z. N. Chen and M. G. Di Benedetto, "Ultra Wideband Wireless Communication", JohnWiley & Sons, New Jersey, United States of America, 2006.

[19] Available online: http://www.peachwire.com/index.php/Faq_quare/che-differenza-ce-tra-lnfc-e-altretecnologie-come-il-bluetooth-e-il-wi-fi/.

[20] Y. Tawk, J. Costantine, C. G. Christodoulou, Cognitive-radio and antenna functionalities: A tutorial [Wireless Corner], IEEE Antennas Propagation Magazine Vol. 56, no. 1, pp. 231-243, 2014.

[21] Available online: http://transition.fcc.gov/pshs/techtopics/techtopic8.html.

[22] Available online: http://cdn.arstechnica.net/Gadgets/uwb_tzero_chart.png.

[23] J. Pourahmadazar, C. Ghobadi, and J. Nourinia, "Novel Modified Pythagorean Tree Fractal Monopole Antennas for UWB Applications", *IEEE Antennas and Wireless Propagation Letters*, Vol. 10, pp. 484-487, 2011.

[24] T. K. Roshna, U. Deepak, V. R. Sajitha and P. Mohanan, “Coplanar Stripline-Fed Compact UWB Antenna,” Electronics Letters, Vol. 50, no. 17, pp. 1181–1182, 2014.

[25] S. Tripathi, A. Mohan, and S. Yadav, “Hexagonal Fractal Ultra-Wideband Antenna Using Koch Geometry with Bandwidth Enhancement,” IET Microwaves, Antennas and Propagation, Vol. 8, no. 15, pp. 1445-1450, 2014.

[26] G. K. Pandey, H. S. Singh, P. K. Bharti, and M. K. Meshram, “Metamaterial-based UWB Antenna,” Electronics Letters, Vol. 50, no. 18, pp. 1266–1268, 2014.

[27] L. Guo, S. Wang, X. Chen, and C. G. Parini, “Study of Compact Antenna for UWB Applications,” Electronics Letters, Vol. 46, no. 2, pp. 115–116, 2010.

[28] M. M. Islam, M. T. Islam, M. Samsuzzaman and M. R. I. Faruque, “Compact Metamaterial Antenna for UWB Applications”, Electronics Letters, Vol. 51, no. 16, pp. 1222–1224, 2015.

[29] M.A. Dorostkar, M.T. Islam, and R. Azim, “Design Of A Novel Super Wide Band Circular-Hexagonal Fractal Antenna”, Progress in Electromagnetics Research, Vol. 139, pp. 229-245, 2013.

[30] S. Singhal, A. K. Singh, “CPW-fed Hexagonal Sierpinski Super Wideband Fractal Antenna”, IET Microwaves, Antennas and Propagation, Vol. 10, no. 15, pp. 1701-1707, 2016.

[31] M. Manohar, R.S. Kshetrimayum, A.K. Gogoi, “Printed Monopole Antenna with Tapered Feed Line, Feed Region and Patch For Super Wideband Applications”, IET Microwaves, Antennas and Propagation, Vol. 8, no. 1, pp. 39-45, 2014.

[32] A. Azari, "A New Super Wideband Fractal Microstrip Antenna, “IEEE Transactions on Antennas and Propagation”, Vol. 59, no. 5, pp. 1724-1727, 2011.

[33] S. Singhal, A. K. Singh, “CPW-fed Octagonal Super-Wideband Fractal Antenna with Defected Ground Structure”, IET Microwaves, Antennas and Propagation, Vol. 11, no. 3, pp. 370–377, 2017.

[34] D. Tran, A. Szilagyi, I. E. Lager, P. Aubry, L. P. Light Art, and A. Yarovoy. “A Super Wideband Antenna”, 5th European Conference on Antennas and Propagation (EuCAP), Italy, 2011, pp. 2656–2660.

[35] P. Cao, Y. Huang, J. Zhang, and R. Alrawashdeh, “A Compact Super Wideband Monopole Antenna”, 7th European Conference on Antennas and Propagation (EuCAP), Gothenburg, Sweden, 2013, pp. 3107-3110.

[36] K. R. Chen, C. Y. D. Sim, and J. S. Row, “A Compact Monopole Antenna for Super Wideband Applications”, IEEE Antennas Wireless Propagation Letters, Vol. 10, pp. 488-491, 2011.

[37] B. L. Shahu, S. Pal, and N. Chattoraj, “Design of Super Wideband Hexagonal-Shaped Fractal Antenna with Triangular Slot”, Microwave and Optical Technology Letters, Vol. 57, no. 7, pp. 1659-1662, 2015.

[38] S. Hakimi, S. K. A. Rahim, M. Abedian, S. M. Noghabaei, and M. Khalily, “CPW-fed Transparent Antenna for Extended Ultra-Wideband Applications”, IEEE Antennas Wireless Propagation Letters, Vol. 13, pp. 1251-1254, 2014.

[39] M. Djaiz, A. Habib, M. Nedil, and T. A. Denidni, “Design of UWB Filter-Antenna with Notched Band at 5.8 GHz”, 3rd IEEE International Symposium on Microwave, Antenna, Propagation and EMC Technologies for Wireless Communications, pp. 1-4, June 2009.

[40] Y. J. Cho, K. H. Kim, D. H. Choi, S. S. Lee, and S. O. Park, “A Miniature UWB Planar Monopole Antenna with 5 GHz Band-Rejection Filter and the Time-Domain Characteristics”, IEEE Transactions on antennas and propagation, Vol. 54, no. 5, pp. 1453–1460, May 2006.

[41] W. S. Lee, D. Z. Kim, K. J. Kim, and J. W. Yu, “Wideband Planar Monopole Antennas with Dual Band-Notched Characteristics”, IEEE Transactions on Microwave Theory and Techniques, Vol. 54, no. 6, pp. 2800–2806, June 2006.

[42] Y. H. Zhao, J. P. Xu, and K. Yin, “Dual Band-Notched Ultra-Wideband Microstrip Antenna Using Asymmetrical Spurlines”, Electronics Letters, Vol. 44, no. 18, pp. 1051–1052, August 2008.

[43] J. Y. Deng, Y. Z. Yin, S. G. Zhou, and Q. Z. Liu, “Compact Ultrawideband Antenna with Tri-Band Notched Characteristic”, Electronics Letters, Vol. 44, no. 21, pp. 1231–1233, Oct. 2008.

[44] Y. Zhang, W. Hong, C. Yu, Z. Q. Kuai, Y. D. Dong, and J. Y.Zhou, “Planar Ultra Wideband Antennas with Multiple Notched Bands Based on Etched Slots on the Patch and/or Split Ring Resonators on the Feed Line”, IEEE Transactions on antennas and propagation, Vol. 56, no. 9, pp. 3063–3068, Sep.2008.

[45] T. N. Chang and M. C. Wu, “Band-Notched Design for UWB Antennas”, IEEE Antennas and Wireless Propagation Letters, vol. 7, pp. 636–640, 2008.

[46] Mohammed Al-Husseini, Youssef Tawk, Ali El-Hajj, Karim Y Kabalan, "A Low-Cost Microstrip Antenna for 3G/WLAN/WiMAX and UWB Applications", in Proceedings of the IEEE International conference on Advances in Computational Tools for Engineering Applications (ACTEA'09), pp. 68-70, Zouk Mosbeh, Lebanon, July 2009.

[47] Mohammed Al-husseini, Ali Ramadan, Youssef Tawk, Ali El-Hajj, Karim Y. Kabalan, "Design and ground plane optimization of a CPW-fed Ultra-Wideband Antenna", Turkish Journal of Electrical Engineering and computer Science, Vol. 19, no. 2, 2011.

[48] Chetan Waghmare and Ashwin Kothari, "Spanner Shaped Ultra Wideband Patch Antenna", in Proceedings of the IEEE students conference on Engineering and Systems (SCES), pp. 1-4, Allahabad, India, May 2014.

[49] N. Anvesh Kumar and A. S. Gandhi, "Small Size Planar Monopole Antenna for High Speed UWB Applications", in Proceedings of the Twenty Second National Conference on Communications (NCC), pp. 1-5, Guwahati, Assam, India, March 2016.

[50] Choi S. H, Park J. K, Kim S. K and Park J. Y, "A new ultra-wideband antenna for UWB applications", Microwave and Optical Technology Letters, Vol. 40, no. 5, pp. 399 - 401, 2004.

[51] Liang J. X, Chiau C. C, Chen, X. D and Parini C. G, "Study of a printed circular disc monopole antenna for UWB systems", IEEE Transactions on Antennas and Propagation, Vol. 53, no. 11, pp. 3500-3504, 2005.

[52] Ooi BL, Zhao G, Leong M. S, Chua K. M and Lu Albert C. W, "Wideband LTCC CPW-fed two layered monopole antenna", Electronics Letters, Vol. 41, no. 16, pp. 889-890, 2005.

[53] Su S, Wong K and Tang C, "Ultra-wideband square planar antenna for IEEE 802.16a operating in the 2–11 GHz band", Microwave and Optical Technology Letters, Vol. 42, no. 6, pp. 463-466, 2004.

[54] N. P. Agrawall, G. Kumar, and K. P. Ray, "Wide-Band Planar Monopole Antennas", IEEE Transactions on Antennas and Propagation, Vol. 46, no. 2, pp. 294-295, 1998.

[55] J. A. Evans and M. J. Ammann, "Planar Trapezoidal and Pentagonal Monopoles with Impedance Bandwidth in Excess of 10:1", IEEE Antennas and Propagation International Symposium (Digest), Vol. 3, pp. 1558-1561, Orlando, FL, 1999.

[56] S. Y. Suh, W. L. Stutaman and W. A. Davis, "A New Ultrawideband Printed Monopole Antenna: The Planar Inverted Cone Antenna (PICA)", IEEE Transactions on Antennas and Propagation, Vol. 52, no. 5, pp. 1361-1364, 2004.

[57] Jianxin Liang, Choo C. Chiau, Xiaodong Chen, and C. G. Parini, “Study of a Printed Circular Disc Monopole Antenna for UWB Systems”, IEEE Transactions on Antennas and Propagation, Vol. 53, no. 11, 2005.

[58] Raj Kumar and Sheetal Gaikwad, “On the Design of Nano-arm Fractal Antenna for UWB Wireless Applications”, Journal of Microwaves, Optoelectronics and Electromagnetic Applications, Vol. 12, no. 1, pp. 158-171, June 2013.

[59] Sameer Kumar Sharma, Ashish Gupta and Raghvendra Kumar Chaudhary, “UWB Ring-shaped Metamaterial Antenna with Modified Phi-shaped SRR”, in Proceedings of the IEEE International Symposium on Antennas and Propagation & USNC/URSI National Radio Science Meeting, pp. 1966 – 1967, British Columbia, Canada, July 2015.

[60] Sherif R. Zahran, Omar H. El Sayed Ahmed, Ahmed T. El-Shalakany, Sherif Saleh and Mahmoud A. Abdalla, “Ultra Wide Band Antenna with Enhancement Efficiency for High Speed Communications”, in Proceedings of the IEEE 31st National Radio Science Conference (NRSC), pp. 65 - 72, Cairo, Egypt, April 2014.

[61] Gopal M. Dandime, Veeresh G. Kasabegoudar, “A slotted circular monopole antenna for wireless applications”, International Journal of Wireless Communications and Mobile Computing, Vol. 2, no. 2, pp. 30-34, 2014.

[62] Shrivishal Tripathi, Sandeep Yadav, Vivek Vijay, Ambesh Dixit, Akhilesh Mohan, “Hexagonal Shaped Fractal UWB Antenna”, in Proceedings of the IEEE Applied Electromagnetics Conference (AEMC), pp. 1-2, Bhubaneswar, India, Dec. 2013.

[63] Mohammed Al-Husseini, Ali Ramadan, Ali El-Hajj and Karim Y. Kabalan, Youssef Tawk and Christos G. Christodoulou, “Design Based on Complementary Split-ring Resonators of an Antenna with Controllable Band Notches for UWB Cognitive Radio Applications”, in Proceedings of the IEEE International Symposium on Antennas and Propagation (APSURSI), pp. 1120 – 1122, Washington, U.S.A, July 2011.

[64] Ronghua Shi, Xi Xu, Jian Dong, and Qingping Luo, “Design and Analysis of a Novel Dual Band-Notched UWB Antenna”, International Journal of Antennas and Propagation, Vol. 2014, pp. 1-10, 2014.

[65] Chaabane Abdelhalim and Djahli Farid, “A Compact Planar UWB Antenna with Triple Controllable Band-Notched Characteristics”, International Journal of Antennas and Propagation, Vol. 2014, pp. 1-10, 2014.

[66] Shilpa Jangid, Mithilesh Kumar, "A Novel UWB Band Notched Rectangular Patch Antenna with Square slot", in Proceedings of the IEEE Fourth International Conference on Computational Intelligence and Communication Networks (CICN), pp. 5 – 9, Uttar Pradesh, India, Nov. 2012.

[67] S. Kuzu and N. Akcam, "Array Antenna Using Defected Ground Structure Shaped With Fractal Form Generated by Apollonius Circle", IEEE Antennas and Wireless Propagation Letters, vol. 16, pp. 1020-1023, 2017.

[68] J. Liu, K. P. Esselle, S. G. Hay, Z. Sun, and S. Zhong, "A Compact Super-Wideband Antenna Pair With Polarization Diversity", IEEE Antennas and Wireless Propagation Letters, vol. 12, pp. 1472-1475, 2013.

[69] S. Barbarino and F. Consoli, "Study on Super-Wideband Planar Asymmetrical Dipole Antennas of Circular Shape", IEEE Transactions on Antennas and Propagation, vol. 58, no. 12, pp. 4074-4078, 2010.

[70] J. Liu, K.P. Esselle, S. G. Hay, and S. Zhong, "Study of nan Extremely Wideband Monopole Antenna with Triple Band-Notched Characteristics", Progress in Electromagnetics Research, Vol. 123, pp. 143-158, 2012.

[71] A. Gorai, A. Karmakar, M. Pal, and R. Ghatak, "A CPW-Fed Propeller Shaped Monopole Antenna with Super Wideband Characteristics", Progress In Electromagnetics Research C, Vol. 45, pp. 125-135, 2013.

[72] J. Yeo and J. I. Lee, "Coupled-Sectorial-Loop Antenna with Circular Sectors for Super Wideband Applications", Microwave and Optical Technology Letters, Vol. 6, pp. 1683-1689, 2014.

[73] M. N. Srifi, S. K. Podilchak, M. Essaaidi and Y. M. M. Antar, "Compact Disc Monopole Antennas for Current and Future Ultrawideband (UWB) Applications", IEEE Transactions on Antennas and Propagation, Vol. 59, no. 12, pp. 4470-4480, 2011.

[74] M. Tang, R. W. Ziolkowski, and S. Xiao, "Compact Hyper-Band Printed Slot Antenna With Stable Radiation Properties", IEEE Transactions on Antennas and Propagation, Vol. 62, no. 6, pp. 2962-2969, 2014.

[75] M. N. Srifi, O. E. Mrabet, F. Falcone, M. S. Ayza, and M. Essaaidi, "A Novel Compact Printed Circular Antenna for very Ultra Wideband Applications", Microwave and Optical Technology Letters, Vol. 51, no. 4, pp. 1130-1133, 2009.

[76] Mohammed Al-Husseini, Joseph Costantine, Christos G. Christodoulou, Silvio E. Barbin, Ali El-Hajj, Karim Y. Kabalan, "A Reconfigurable Frequency-notched UWB

Antenna with Split-ring Resonators", in Proceedings of the IEEE Asia-Pacific Microwave Conference, pp. 618 - 621, Yokohama, Japan, Dec. 2010.

[77] Y. E. Jalil, C. K. Chakrabarty, B. Kasi, "A Compact Ultra Wideband Antenna with Dual Band-Notched Design", in Proceedings of the IEEE 7th International Conference on Signal Processing and Communication Systems (ICSPCS), pp. 1 – 5, Gold coast, Australia, Dec. 2013.

[78] Y. Wang, N. Wang, T. A. Denidni, Q. Zeng and G. Wei, "Integrated Ultrawideband/Narrowband Rectangular Dielectric Resonator Antenna for Cognitive Radio", *IEEE Antennas and Wireless Propagation Letters*, Vol. 13, pp. 694-697, 2014.

[79] Y. Tawk, J. Costantine and C. G. Christodoulou, "A Rotatable Reconfigurable Antenna for Cognitive Radio Applications", in Proceedings of the IEEE Radio and Wireless Symposium (RWS), pp. 158 – 161, Phoenix, Arizona, USA, Jan 2011.

[80] G. P. Jin, D. L. Zhang and R. L. Li, "Optically Controlled Reconfigurable Antenna for Cognitive Radio Applications", Electronics Letters, Vol. 47, no. 17, pp. 948-950, 2011.

[81] N. Anvesh Kumar, A. S Gandhi, "A Compact Novel Three-Port Integrated Wide and Narrow Band Antennas System for Cognitive Radio Applications", International Journal of Antennas and Propagation, Vol. 2016, pp. 1-14, 2016.

[82] A. Nella and A. S. Gandhi, "A Five-Port Integrated UWB and Narrowband Antennas System Design for CR Applications", IEEE Transactions on Antennas and Propagation, Vol. 66, no. 4, pp. 1669-1676, 2018.

[83] S. Pahadsingh, S. Sahu, "Planar UWB Integrated with Multi Narrowband Cylindrical Dielectric Resonator Antenna for Cognitive Radio Application", AEU - International Journal of Electronics and Communications Vol. 74, pp. 150-157, 2017.

[84] E. Erfani, J. Nourinia, C. Ghobadi, M. Niroo-Jazi and T. A. Denidni, "Design and Implementation of an Integrated UWB/Reconfigurable-Slot Antenna for Cognitive Radio Applications", IEEE Antennas and Wireless Propagation Letters, Vol. 11, pp. 77-80, 2012.

[85] Y. Tawk and C. G. Christodoulou, "A New Reconfigurable Design for Cognitive Radio", IEEE Antennas and Wireless Propagation Letters", Vol. 8, pp. 1378-1381, 2009.

[86] E. Ebrahimi, J. R. Kelly and P. S. Hall, "Integrated Wide-Narrowband Antenna for Multi-Standard Radio", IEEE Transactions on Antennas and Propagation, Vol. 59, no. 7, pp. 2628-2635, July 2011.

[87] S. Zheng, X. Liu and M. M. Tentzeris, “A Novel Optically Controlled Reconfigurable Antenna for Cognitive Radio Systems”, in Proceedings of the IEEE Antennas and Propagation Society International Symposium (APSURSI), pp. 1246–1247, Memphis, Tennessee, USA, July 2014.

[88] A. Mansoul, F. Ghanem, M. R. Hamid, and M. Trabelsi, “A Selective Frequency-Reconfigurable Antenna for Cognitive Radio Applications”, IEEE Antennas and Wireless Propagation Letters, Vol. 13, pp. 515-518, 2014.

[89] Y. Tawk, J. Costantine, S. E. Barbin, and C. G. Christodoulou, “Integrating Laser Diodes in a Reconfigurable Antenna System”, In Proceedings of the international microwave and optoelectronics conference (IMOC) (pp. 794–796). Natal, Brazil, 2011.

[90] G. Augustin and T. A. Denidni, “An Integrated Ultra Wideband/Narrow Band Antenna in Uniplanar Configuration for Cognitive Radio Systems”, IEEE Transactions on Antennas and Propagation, Vol. 60, no. 11, pp. 5479-5484, 2012.

[91] T. Aboufoul, A. Alomainy, and C. Parini, “Reconfiguring UWB Monopole Antenna for Cognitive Radio Applications Using GaAs FET Switches”, IEEE Antennas and Wireless Propagation Letters, Vol. 11, pp. 392-394, 2012.

[92] M. Safarpour, P. Rezaei and A. Zarkhoshk, “Compact Multi-Band Reconfigurable Antenna for Cognitive Radio”, in Proceedings of the IEEE International Symposium on Antennas and Propagation & USNC/URSI National Radio Science Meeting, pp. 2397-2398, British Columbia, Canada, July 2015.

[93] H. F. Abu Tarboush, S. Khan, R. Nilavalan, H. S. Al-Raweshidy and D. Budimir, “Reconfigurable Wideband Patch Antenna for Cognitive Radio”, in Proceedings of the IEEE Loughborough Antennas & Propagation Conference (LAPC), pp. 141 – 144, UK, Nov. 2009.

[94] M. G. Aly and Yi Wang, “An Integrated Narrowband-Wideband Antenna”, in Proceedings of the IEEE Loughborough Antennas & Propagation Conference (LAPC), pp. 433 – 435, UK, Nov. 2013.

[95] M. Al-Husseini, A. Ramadan, A. El-Hajj, and K. Y. Kabalan, “A Reconfigurable Antenna Based on an Ultra wide band to Narrowband Transformation”, PIERS Proceedings, pp. 550-553, Moscow, Russia, August 19-23, 2012.

[96] E. J. B. Rodrigues, H. W. C. Lins and A. G. D. Assuncao, “Reconfigurable Circular Ring Patch Antenna for UWB and Cognitive Radio Applications”, in Proceedings of

the 8th European Conference on Antennas and Propagation (EuCAP 2014), pp. 2744-2748, Hague, Netherlands, April 2014.

[97] H. Boudaghi, M. Azarmanesh, and M. Mehranpour, "A Frequency-Reconfigurable Monopole Antenna Using Switchable Slotted Ground Structure", IEEE Antennas and Wireless Propagation Letters, Vol. 11, pp. 655-658, 2012.

[98] C. Gupta, D. Maheshwari, R. K. Saraswat, M. Kumar, "A UWB Frequency-Band Reconfigurable Antenna Using Switchable Slotted Ground Structure", in Proceedings of the Fourth International Conference on Communication Systems and Network Technologies (CSNT), pp. 20-24, Bhopal, India, April 2014.

[99] M. Al-Husseini, A. El-Hajj, Y. Tawk, K. Y. Kabalan, C. G. Christodoulou, "A Simple Dual-port Antenna System for Cognitive Radio Applications", in Proceedings of the IEEE International Conference on High Performance Computing and Simulation (HPCS), pp. 549 – 552, Caen, France, July 2010.

[100] Y. Tawk, J. Costantine, S. Hemmady, G. Balakrishnan, K. Avery, and C. G. Christodoulou, "Demonstration of a Cognitive Radio Front End Using an Optically Pumped Reconfigurable Antenna System (OPRAS)", IEEE Transactions on Antennas and Propagation, Vol. 60, no. 2, pp. 1075-1083, Feb. 2012.

[101] I. Messaoudene, T. A. Denidni, and A. Benghalia, "Ultra-Wideband CPW Antenna Integrated with Narrow Band Dielectric Resonator", in Proceedings of the IEEE International Symposium on Antennas and Propagation (APSURSI), pp. 1308 - 1309, Florida, USA, July 2013.

[102] Y. Wang and G. Wei, T. A. Denidni, Q. Zeng, "Ultra-Wideband Planar Monopole Integrated with Cylindrical Dielectric Resonator Antenna", in Proceedings of the IEEE International Symposium on Antennas and Propagation (APSURSI), pp. 1696 - 1697, Florida, USA, July 2013.

[103] Y. Li, W. Li, R. Mittra, "Integrated Dual-Purpose Narrow/Ultra-Wide Band Antenna for Cognitive Radio Applications", in Proceedings of the IEEE International Symposium on Antennas and Propagation, pp. 1 – 2, Chicago, Illinois, U.S.A, July 2012.

[104] S. H. Zheng, X. Liu and M. M. Tentzeris, "Optically Controlled Reconfigurable Band-Notched UWB Antenna for Cognitive Radio Systems", Electronics Letters, Vol. 50, no. 21, pp. 1502–1504, October 2014.

[105] H. A. Majid, M. K. A. Rahim, M. R. Hamid, and M. F. Ismail, "A Compact Frequency-Reconfigurable Narrowband Microstrip Slot Antenna", IEEE Antennas and Wireless Propagation Letters, Vol. 11, pp. 616-619, 2012.

[106] R. Kumar and R. Vijay, "A Frequency Agile Semicircular Slot Antenna for Cognitive Radio System", International Journal of Antennas and Propagation, Vol. 2016, Article ID: 2648248, pp. 1-11, 2016.

[107] Y. Tawk and C. G. Christodoulou, "A Cellular Automata Reconfigurable Microstrip Antenna Design", in Proceedings of the IEEE Antennas and Propagation Society International Symposium, pp. 1-4, North Charleston, SC, USA, June 2009.

[108] X. Liu, X. Yang, F. Kong, "A Frequency-Reconfigurable Monopole Antenna with Switchable Stubbed Ground Structure", Radio Engineering, Vol. 24, no. 2, 2015.

[109] Chang won Jung and F. De Flaviis, "Reconfigurable Multi-Beam Spiral Antenna with RF-MEMS Capacitive Series Switches Fabricated on Rigid Substrates", in Proceedings of the IEEE Antennas and Propagation Society International Symposium, pp. 421-424, Washington, DC, July 2005.

[110] M. Safarpour, P. Rezaei and A. Zarkhoshk, "Compact Multi-Band Reconfigurable Antenna for Cognitive Radio", in Proceedings of the IEEE International Symposium on Antennas and Propagation & USNC/URSI National Radio Science Meeting, pp. 2397-2398, British Columbia, Canada, July 2015.

[111] H. F. Abu Tarboush, S. Khan, R. Nilavalan, H. S. Al-Raweshidy and D. Budimir, "Reconfigurable Wideband Patch Antenna for Cognitive Radio", in Proceedings of the IEEE Loughborough Antennas & Propagation Conference (LAPC), pp. 141 – 144, UK, Nov. 2009.

[112] M. G. Aly, Yi Wang, "An Integrated Narrowband-Wideband Antenna", in Proceedings of the IEEE Loughborough Antennas & Propagation Conference (LAPC), pp. 433 – 435, UK, Nov. 2013.

[113] M. Al-Husseini, A. Ramadan, A. El-Hajj and K. Y. Kabalan, "A Reconfigurable Antenna Based on an Ultra wide band to Narrowband Transformation", PIERS Proceedings, pp. 550-553, Moscow, Russia, August 19-23, 2012.

[114] N. kumar, P. A. Raju, S. K. Behera, "Frequency Reconfigurable Microstrip Antenna for Cognitive Radio Applications", in Proceedings of the International Conference on Communications and Signal Processing (ICCSP), pp. 370 – 373, Melmaruvathur, India, April 2015.

[115] M. Bitchikh and F. Ghanem, “A Three-Resolution UWB Frequency Reconfigurable Antipodal Vivaldi Antenna for Cognitive Radios”, in Proceedings of the 8th European Conference on Antennas and Propagation (EuCAP 2014), pp. 3665-3668, Hague, Netherlands, April 2014.

[116] H. Nachouane, A. Najid, A. Tribak, and F. Riouch, “Dual Port Antenna Combining Sensing and Communication Tasks for Cognitive Radio”, International Journal of Electronics and Telecommunications, Vol. 62, no. 2, pp. 121–127, 2016.

[117] F. Ghanem, P. S. Hall and J. R. Kelly, “Two Port Frequency Reconfigurable Antenna for Cognitive Radios”, Electronics Letters, Vol. 45, no. 11, pp. 534-536, 2009.

[118] A. Muduli and R. K. Mishra, “Modified UWB Microstrip Monopole Antenna for Cognitive Radio Application”, in Proceedings of the IEEE Applied Electromagnetics Conference (AEMC), pp. 1-2, Guwahati, Assam, Dec. 2015.

[119] Y. Wang, T. A. Denidni, Q. Zeng and G. Wei, “A Design of Integrated Ultra-wideband/Narrow Band Rectangular Dielectric Resonator Antenna”, in Proceedings of the IEEE International Wireless Symposium (IWS), pp. 1-4, Xian, China, March 2014.

[120] P. Tummas, P. Krachodnok and R. Wongsan, “A Frequency Reconfigurable Antenna Design for UWB Applications”, in Proceedings of the 11th International Conference on Electrical Engineering/Electronics, Computer, Telecommunications and Information Technology (ECTI-CON), pp. 1-4, Nakhon Ratchasima, Thailand, May 2014.

[121] Z. P. Zhong, J. J. Liang, M. L. Fan, G. L. Huang, W. He, X. C. Chen, and T. Yuan, “A Compact CPW-Fed UWB Antenna with Quadruple Rejected Bands”, Microwave and Optical Technology Letters, Vol. 61, no. 12, pp. 1-6, 2019.

[122] K. Srivastava, A. Kumar, B. K. Kanaujia, S. Dwari, and S. Kumar, “A CPW-Fed UWB MIMO Antenna with Integrated GSM band and Dual Band Notches”, International Journal of RF and Microwave Computer-Aided Engineering, Vol. 29, no. 1, 2018.

[123] R. Garg, I. Bahl, and M. Bozzi, “Microstrip lines and slotlines” (Microwave &RF, Artech House, 2013, 3rd edition).

[124] A. Kantemur, A. H. Abdelrahman, and H. Xin, “A Novel Compact Reconfigurable UWB Antenna for Cognitive Radio Applications”, 2017 IEEE International Symposiumon Antennas and Propagation & USNC/URSI National Radio Science Meeting, pp. 1369-1370, 2017.

[125] Y. Tawk and C. G. Christodoulou, “A New Reconfigurable Antenna Design for Cognitive Radio”, IEEE Antennas and Wireless Propagation Letters, Vol. 8, pp. 1378-1381, 2009.

[126] S. Cheng and K. Lin, “A Reconfigurable Monopole MIMO Antenna with Wideband Sensing Capability for Cognitive Radio Using Varactor Diodes”, IEEE International Symposium on Antennas and Propagation & USNC/URSI National Radio Science Meeting, pp. 2233-2234, Vancouver, BC 2015.

[127] R. Hussain, M. S. Sharawi, and A. Shamim, “An Integrated Four-element Slot-based MIMO and a UWB Sensing Antenna System for CR Platforms”, IEEE Transactions on Antennas and Propagation, Vol. 66, no. 2, pp. 978-983, 2018.

[128] T. Alam, S. R. Thummaluru and R. K. Chaudhary, “Two-Port MIMO Wide-Band Antenna with Two-Port MIMO Reconfigurable Antenna for Cognitive Radio Platforms”, IEEE Indian Conference on Antennas and Propogation (InCAP), pp. 1-4, Hyderabad, India, 2018.

[129] X. Zhao, S. Riaz and S. Geng, “A Reconfigurable MIMO/UWB MIMO Antenna for Cognitive Radio Applications”, IEEE Access, Vol. 7, pp. 46739-46747, 2019.

[130] B. P. Chacko, G. Augustin and T. A. Denidni, "Electronically Reconfigurable Uniplanar Antenna with Polarization Diversity for Cognitive Radio Applications”, IEEE Antennas and Wireless Propagation Letters, Vol. 14, pp. 213-216, 2015.

[131] R. Hussain, M. U. Khan and M. S. Sharawi, “An Integrated Dual MIMO Antenna System with Dual-Function GND-Plane Frequency-Agile Antenna”, IEEE Antennas and Wireless Propagation Letters, Vol. 17, no. 1, pp. 142-145, 2018.

[132] R. Hussain and M. S. Sharawi, “A Cognitive Radio Reconfigurable MIMO and Sensing Antenna System”, IEEE Antennas and Wireless Propagation Letters, Vol. 14, pp. 257-260, 2015.

[133] R. Hussain and M. S. Sharawi, “4-Element Planar MIMO Reconfigurable Antenna System for Cognitive Radio Applications”, IEEE International Symposium on Antennas and Propagation & USNC/URSI National Radio Science Meeting, pp. 717-718, Vancouver, BC, Canada, 2015.

[134] R. Hussain, M. S. Sharawi and A. Shamim, “4-Element Concentric Pentagonal Slot-Line-Based Ultra-Wide Tuning Frequency Reconfigurable MIMO Antenna System”, IEEE Transactions on Antennas and Propagation, Vol. 66, no. 8, pp. 4282-4287, 2018.

[135] T. Alam, S. R. Thummaluru and R. K. Chaudhary, “Integration of MIMO and Cognitive Radio for Sub-6 GHz 5G Applications”, IEEE Antennas and Wireless Propagation Letters, Vol. 18, no. 10, pp. 2021-2025, 2019.

[136] S. Riaz, X. Zhao and S. Geng, “A Frequency Reconfigurable MIMO Antenna With Agile Feedline for Cognitive Radio Applications”, International Journal of RF and Microwave Computer-Aided Engineering, Vol. 30, no. 3, pp. 1-9, 2019.

[137] R. Hussain, A. Raza, M.U Khan, A. Shammim and M. S. Sharawi, “Miniaturized Frequency Reconfigurable Pentagonal MIMO Slot Antenna for Interweave CR Applications”, International Journal of RF and Microwave Computer-Aided Engineering, Vol. 29, no. 9, pp. 1-12, 2019.

[138] S. S. Zhekov, A. Tatomirescu and G. F. Pedersen, “Compact Multiband Sensing MIMO Antenna Array for Cognitive Radio System”, 2015 Loughborough Antennas & Propagation Conference (LAPC), pp 1-5, Loughborough, U. K., 2015.

[139] R. Hussain and M. S. Sharawi, “A Low Profile Compact Reconfigurable MIMO Antenna for Cognitive Radio Applications”, 9th European Conference on Antennas and Propagation (EuCAP), pp. 1-4, Lisbon, Portugal, 2015.

[140] D. T. Le and Y. Karasawa, “A Simple Broadband Antenna for MIMO Applications in Cognitive Radio”, 2011 IEEE International Symposium on Antennas and Propagation (APSURSI), pp. 806-809, Spokane, WA, USA, 2011.

[141] S. Keerthipriya and C. Saha, “Reconfigurable Multifunctional Vivaldi MIMO Antenna for Cognitive Radio Applications”, IEEE Indian Conference on Antennas and Propogation (InCAP), pp. 1-4, Ahmedabad, India, 2019.

[142] Y. Tawk, F. Ayoub, C. G. Christodoulou and J. Costantine, “A MIMO Cognitive Radio Antenna System”, IEEE Antennas and Propagation Society International Symposium (APSURSI), pp. 572-573, Orlando, FL, USA, 2013.

[143] R. K. Chaudhary and S. R. Thummaluru, “Reconfigurable MIMO Filtenna for Spectrum Underlay Cognitive Radio”, Photonics & Electromagnetics Research Symposium - Spring (PIERS-Spring), pp. 582-586, Rome, Italy, 2019.

[144] B. Bukhari, C. Singh, K. R. Jha and S. K. Sharma, “Planar MIMO antennas for IoT and CR Applications”, IEEE Applied Electromagnetics Conference (AEMC), pp. 1-2, Aurangabad, India, 2017.

[145] S. Riaz and X. Zhao, “An Eight-Port Frequency Reconfigurable MIMO Slot Antenna with Multi-Band Tuning Characteristics”, 12th International Symposium on Antennas, Propagation and EM Theory (ISAPE), pp. 1-4, Hangzhou, China, 2018.

[146] S. Riaz, X. Zhao and S. Geng, “A Compact Frequency Reconfigurable MIMO Antenna with Agile Feedline for Cognitive Radio Applications”, 10th International Conference on Communications, Circuits and Systems (ICCCAS), pp. 176-179, Chengdu, China, 2018.

[147] R. Hussain and M. S. Sharawi, “Frequency Reconfigurable MIMO Slot and UWB Sensing Antennas for CR applications”, IEEE International Symposium on Antennas and Propagation & USNC/URSI National Radio Science Meeting, pp. 1693-1694, San Diego, CA, USA, 2017.

[148] R. Hussain, M. U. Khan and M. S. Sharawi, “Meandered H-Shaped Slot-line Quad-Band Frequency Reconfigurable MIMO Antenna”, 2019 13th European Conference on Antennas and Propagation (EuCAP), pp. 1-3, Krakow, Poland, 2019.

[149] Y. Tawk, J. Costantine and C. G. Christodoulou, “Reconfigurable Filtennas and MIMO in Cognitive Radio Applications”, IEEE Transactions on Antennas and Propagation, Vol. 62, no. 3, pp. 1074-1083, 2014.

[150] R. Hussain and M. S. Sharawi, “An Integrated Slot-Based Frequency-Agile and UWB Multifunction MIMO Antenna System”, IEEE Antennas and Wireless Propagation Letters, Vol. 18, no. 10, pp. 2150-2154, 2019.

[151] J. K. Halpe Gamage, B. Holter, I. A. Jensen, K. Husby and J. Kuhnle, “A Wideband Conformal Antenna Array for Cognitive Radio/MIMO Applications”, Proceedings of the 5th European Conference on Antennas and Propagation (EUCAP), pp. 725-729, Rome, Italy, 2011.

[152] R. Hussain, A. Ghalib and M. S. Sharawi, “Annular Slot-Based Miniaturized Frequency-Agile MIMO Antenna System” IEEE Antennas and Wireless Propagation Letters, Vol. 16, pp. 2489-2492, 2017.

[153] T. Vijetha, U. D. Laxmi, P. Badrinath, G. V. Reddy and K. H. Reddy, “Design and implementation of MIMO antenna for CR applications”, International conference of Electronics, Communication and Aerospace Technology (ICECA), pp. 681-683, Coimbatore, India, 2017.

[154] S. R. Thummaluru, M. Ameen and R. K. Chaudhary, “Four-Port MIMO Cognitive Radio System for Midband 5G Applications”, IEEE Transactions on Antennas and Propagation, Vol. 67, no. 8, pp. 5634-5645, 2019.

[155] R. Hussain and M. S. Sharawi, “Two Element Wide-Band Frequency Reconfigurable MIMO Antenna System for 4G Applications”, IEEE 5th Asia-Pacific Conference on Antennas and Propagation (APCAP), pp. 11-12, 2016.

[156] M. Bouezzeddine and W. L. Schroeder, “Design of a Wideband, Tunable Four-Port MIMO Antenna System With High Isolation Based on the Theory of Characteristic Modes”, IEEE Transactions on Antennas and Propagation, Vol. 64, no. 7, pp. 2679-2688, 2016.

[157] R. Hussain, M. U. Khan and M. S. Sharawi, "Design and Analysis of a Miniaturized Meandered Slot-Line-Based Quad-Band Frequency Agile MIMO Antenna," IEEE Transactions on Antennas and Propagation, Vol. 68, no. 3, pp. 2410-2415, March 2020.

[158] R. Hussain, A. H. Muqaibel, W. Abu-Al-Saud and M. S. Sharawi, “A Low Complexity Direction Finding System Based on a Six-Port Integrated MIMO Antenna System”, IEEE Jordan Conference on Applied Electrical Engineering and Computing Technologies (AEECT), pp. 1-5, Amman, Jordan, 2015.

[159] R. Hussain and M. S. Sharawi, “Reconfigurable Pentagonal Slot Based 4-Element MIMO Antennas”, IEEE International Symposium on Antennas and Propagation & USNC/URSI National Radio Science Meeting, pp. 1151-1152, San Diego, CA, 2017.

[160] R. Hussain and M. S. Sharawi, “Multi-Mode Ground Reconfigurable MIMO Antenna System”, IEEE 4th Asia-Pacific Conference on Antennas and Propagation (APCAP), pp. 144-145, Bali, Indonesia, 2015.

[161] R. Hussain and M. S. Sharawi, “Integrated Reconfigurable Multiple-Input-Multiple-Output Antenna System with an Ultra-Wideband Sensing Antenna for Cognitive Radio Platforms”, IET Microwaves, Antennas and Propagation, Vol. 9, no. 9, pp. 940-947, 2015.

[162] R. Hussain and M. S. Sharawi, “Wide-Band Frequency Agile MIMO Antenna System with Wide Tunability Range”, Microwave and Optical technology Letters, Vol. 58, no. 9, pp. 2276-2280, 2016.

[163] R. Hussain, M. U. Khan, N. Iqbal, E. Almajali, S. S. Alja’Afreh, U. Johar, A. Shamim and M. S. Sharawi, “Frequency Agile Multiple-Input-Multiple-Output Antenna Design

for 5G Dynamic Spectrum Sharing in Cognitive Radio Networks", Microwave and Optical technology Letters, Vol. 63, no. 3, pp. 1-6, 2020.

[164] R. Hussain and M. S. Sharawi, "Planar Meandered-F-Shaped 4-Element Reconfigurable Multiple-Input-Multiple-Output Antenna System with Isolation Enhancement for Cognitive Radio Platforms", IET Microwaves, Antennas and Propagation, Vol. 10, no. 1, pp. 45-52, 2016.

[165] A. Raza, M. U. Khan, F. A. Tahir, R. Hussain and M. S. Sharawi, "A 2-Element Meandered-Line Slot-Based Frequency Reconfigurable MIMO Antenna System", Microwave and Optical technology Letters, Vol. 60, no. 11, pp. 1-8, 2018.

[166] S. Pahadsingh and S. Sahu, "Four port MIMO integrated antenna system with DRA for cognitive radio platforms" AEU - International Journal of Electronics and Communications, Vol. 92, pp. 98-110, 2018.

[167] S. C. Basaran and Y. E. Erdemli, "A Dual-Band Splitring Monopole Antenna for WLAN Applications", Microwave and Optical Technology Letters, Vol. 51 no. 11, pp. 2685-2688, 2009.

[168] V. Rajeshkumar and S. Raghavan, "A Compact Frequency Reconfigurable Split Ring Monopole Antenna for WLAN/WAVE Applications", Applied Computational Electromagnetics Society Journal, Vol. 30 no. 3, pp. 338-344, 2015.

[169] L. M. Si, W. Zhu, and H. J. Sun, "A Compact, Planar, and CPW-Fed Metamaterial-Inspired Dual-Band antenna", IEEE Antennas and Wireless Propagation Letters, Vol. 12, pp. 305-308, 2013.

[170] S. Nandi and A. Mohan, "CRLH Unit Cell Loaded Triband Compact MIMO Antenna for WLAN/WiMAX Applications", IEEE Antennas Wireless Propagation Letters, Vol. 16, pp. 1816-1819, 2017.

List of Publications

International Journals

1. D. Srikar and S. Anuradha, "Twelve port MIMO antenna with polarisation diversity for cognitive radio applications", Electronics Letters, Vol. 55, no. 22, pp. 1165–1168, 2019. (**SCIE-IET**)
2. D. Srikar and S. Anuradha, "A Compact Six port Antenna for Better Spectrum Utilization Efficiency in cognitive radio applications", International Journal of RF and Microwave Computer-Aided Engineering, Vol. 30, no. 10, 2020. (**SCIE-Wiley**)
3. D. Srikar and S. Anuradha, "A New Two-Element MIMO Antenna System for Cognitive Radio Applications", Circuit World, 2021. DOI: 10.1108/CW-06-2020-0101 (**SCIE-Emerald Publishing**)
4. D. Srikar and S. Anuradha, "A Reconfigurable Nine Port MIMO antenna with Polarization Diversity for CR MIMO Applications," Circuit World, 2021. (**SCIE-Under Review**)

International Conferences

1. D. Srikar and S. Anuradha, "A Low Profile and Compact UWB Antenna for Wireless Communication Applications," International Conference on Microwave Integrated Circuits, Photonics and Wireless Networks (IMICPW), NIT Trichy, March 22-24, 2019. (**IEEE Proc.**)
2. D. Srikar and S. Anuradha, "A Compact Super wideband Antenna for Wireless Communications," International Conference on Computing Communication and Networking Technologies (ICCCNT), IISc Bengaluru, Jul 10-12, 2018. (**IEEE Proc.**)
3. D. Srikar and S. Anuradha, "A Compact 3 Port Integrated Wideband Sensing Antenna and Narrow Band Antennas for Cognitive Radio Applications , PIERS, Rome, Italy, 2019. (**IEEE Proc.**)